Effect of Welding Residual Stress and Distortion on Ship Hull Structural Performance

by

Liam Gannon

Submitted in partial fulfillment of the requirements
for the degree of Doctor of Philosophy

at

Dalhousie University
Halifax, Nova Scotia
March 2011

DALHOUSIE UNIVERSITY

DEPARTMENT OF CIVIL AND RESOURCE ENGINEERING

The undersigned hereby certify that they have read and recommend to the Faculty of Graduate Studies for acceptance a thesis entitled "EFFECT OF WELDING RESIDUAL STRESS AND DISTORTION ON SHIP HULL STRUCTURAL PERFORMANCE" by Liam Gannon in partial fulfilment of the requirements for the degree of Doctor of Philosophy.

Dated: March 25, 2011

Supervisor: _____

_____

External Examiner: _____

Readers: _____

_____

_____

_____

Departmental Representative: _____

DALHOUSIE UNIVERSITY

DATE: March 25, 2011

AUTHOR: Liam Gannon

TITLE: Effect of Welding Residual Stress and Distortion on Ship Hull Structural Performance

DEPARTMENT OR SCHOOL: Department of Civil and Resource Engineering

DEGREE: PhD CONVOCATION: May YEAR: 2011

_____

Signature of Author

This thesis is dedicated to my wife, Teresa whose patience and support throughout were beyond measure. Thank you.

Table of Contents

List of Tables

List of Figures

Abstract

The finite element method is used to investigate the effects of welding-induced residual stress and distortion on the strength and behaviour of ship hull structures. A finite element welding simulation consisting of sequentially coupled transient thermal and nonlinear structural analyses is used to predict the three-dimensional residual stress and distortion fields in welded stiffened plates. Three types of stiffener commonly used in commercial and naval applications are considered. The welding simulation is followed by a 'shakedown' analysis to study the possibility of residual stress relief caused by cyclic loads. The strength and behaviour of stiffened plates under axial load is characterized by normalized plots of average axial stress versus axial strain, commonly referred to as load-shortening curves. These curves are used to evaluate the effects of welding-induced residual stress and distortion on stiffened plate behaviour with and without considering stress relief by shakedown. Load-shortening curves generated by finite element analysis are also compared with load-shortening curves produced using analytical methods including those prescribed in ship structural design standards published by the International Association of Classification Societies (IACS). To conclude, a hull girder ultimate strength analysis is carried out using Smith's method with load-shortening curves generated by several different methods.

Results indicate that welding-induced residual stress and distortion decrease the ultimate strength of flat-bar, angle, and tee-stiffened plates investigated in this study by as much as 17%, 15% and 13%, respectively. Stiffened plate ultimate strength values calculated using IACS common structural rules agreed reasonably well with results from numerical models in most cases. There was however, a significant discrepancy between the numerical load-shortening curves and the IACS curves in the post-ultimate regime, where the IACS curves overestimated the post-ultimate strength of stiffened plates by as much as 30%. To investigate stress relief by shakedown, axial stresses of 25% and 50% of the yield stress were applied and residual stresses were reduced by approximately 20% and 40%, respectively. In some cases, these reductions in residual stress led to increases in stiffened plate ultimate strength as high as 7%. Analysis of a box girder using load-shortening curves from a finite element model including residual stresses and distortions predicted by welding simulation predicted a bending moment capacity within 2.7% of the experimentally measured value. Using load-shortening curves from the IACS common structural rules, the ultimate strength was overestimated by 17%.

List of Symbols Used

A: Cross-sectional area

A_e: Effective cross-sectional area

A_{eff}: Effective net area after buckling for deck stiffened panels

$A_{E\text{-}net50}$: IACS stiffener area with attached plating of width $b_{eff\text{-}p}$

A_i: Area of i^{th} element

$A_{net\text{-}50}$: IACS stiffened plate area

A_s: Stiffener area

$A_{s\text{-}net50}$: IACS stiffener area

a: Plate length

b: Plate width

b_e: Effective width of plate

b_e': Reduced effective width of plate

b_t: Half-width of tensile residual stress zone in plate

b_s: Width of tensile residual stress zone in stiffener web

$b_{eff\text{-}p}$: IACS effective width of plate for use in $A_{E\text{-}net50}$

$b_{eff\text{-}s}$: IACS effective height of stiffener web

b_f: IACS width of flange

$b_{x,y,z}$: Element body force components

c: Volumetric specific heat, radius of welding arc heat flux

d_w: IACS depth of web from bottom of flange

$d_{w\text{-}eff}$: IACS effective depth of web

E: Elastic modulus

E_t: Tangent modulus

f_f,f_r: Fraction of total power in front and rear ellipsoid, respectively

I: Current

I_e: Effective second moment of area of stiffened plate cross-section

I_e': Effective second moment of area of stiffener cross-section

$I_{E\text{-}net50}$: IACS moment of inertia of stiffener and effective width of plating

$I_{p\text{-}net}$: IACS stiffener polar moment of inertia

I_{red}: Reduced hull girder moment of inertia

$I_{T\text{-}net}$: St. Venant's moment of inertia of stiffener

L: Column length

l_{stf}: Span of stiffener

M_u: Hull girder ultimate moment capacity

m: Mass

N_i: Polynomial interpolation function

P: Axial load

Q: Volumetric heat generation rate

q: Magnitude of transverse uniformly distributed load, magnitude of heat flow per unit area

q_f, q_r: Power distribution in front and rear ellipsoid, respectively

$q_{x,y,z}$: Applied surface loads

R_r: Factor to reduce plate effective width accounting for residual stress

Ry: Factor to reduce plate effective width accounting for biaxial loading

R_τ: Factor to reduce plate effective width accounting for shear stress

r: Radius of gyration

r_e: Radius of gyration of stiffener and effective plating

s: Breadth of plate

T: Temperature

T_i: Temperature at node i

$T_{\omega\text{-net}}$: IACS sectorial moment of inertia of stiffener about base of stiffener

T_0: Initial temperature, ambient temperature

T_1: Surface temperature

t: Plate thickness, time

t_{net50}: IACS plate thickness

$t_{w\text{-}net50}$: IACS web thickness

U: Strain energy

V: Voltage

v: Welding speed

$\bar{x}$: Position of centroid of hull girder cross-section along x-axis

x_{gi}: Distance of i^{th} element from centroid of hull girder along x-axis

x_i: Distance along x axis of the i^{th} element from the origin

$\bar{y}$: Position of centroid of hull girder cross-section along y-axis

y_{gi}: Distance of i^{th} element from centroid of hull girder along y-axis

y_i: Distance along y axis of the i^{th} element from the origin

Z_c: Distance from neutral axis to extreme fibre in compression

$Z_{dk\text{-}mean}$: Vertical distance to the mean deck height

$Z_{NA\text{-}red}$: Vertical distance to neutral axis of reduced section

Z_{red}: Reduced section modulus of deck

z: Distance from neutral axis

z_c: Distance from neutral axis to extreme fiber in comression

α: Convection heat transfer coefficient, coefficient of thermal expansion

β_0: Plate slenderness

β: Plate slenderness as a function of axial strain

β_p: IACS plate slenderness

β_w: IACS web slenderness

$\delta_{u,y,w}$: Virtual displacements

δ_0: Amplitude of stiffener vertical distortion

δ_{01}: Amplitude of plate vertical distortion half-way between stiffeners

δ_{02}: Amplitude of first linear buckling mode distortion

$\delta\varepsilon_{x,y,z}$: Virtual normal strains

$\delta_{xy,yz,zx}$: Virtual shear strains

ε: Emissivity, strain

$\bar{\varepsilon}$: Strain normalized with respect to yield strain

ε_E: Element strain

ε_i: Strain at the centroid of the i^{th} element

ε_r: Initial residual strain

ε_y: Yield strain

η: Width of tensile residual stress zone at yield stress, welding process efficiency

θ: Angle from main principle axis to moment vector, or predefined end-rotation of beam-column

κ: Thermal conductivity

λ: Column slenderness

π: Pi

ρ: Density

σ: Stress, Stefan-Boltzman constant

$\bar{\sigma}$: Stress normalized with respect to yield stress

σ_{CP}: Ultimate strength of plating attached to stiffener

σ_{C2}: IACS critical buckling stress for lateral torsional buckling of stiffener

σ_{CR1}: IACS compressive resistance against flexural buckling

σ_{CR2}: IACS stiffener lateral-torsional buckling stress

σ_{CR3}: IACS local web buckling stress

σ_{CR4}: IACS local web buckling stress for flat-bar stiffeners

σ_e: Euler column buckling stress

σ_{E1}: IACS euler column buckling stress

σ_{E2}: IACS Euler torsional buckling stress

σ_{E4}: IACS Euler buckling stress

σ_{JO}: Ultimate stress with Johnson-Ostenfeld correction for plasticity

σ_r: Magnitude of uniform compressive residual stress in plate

σ_u: Buckling capacity of stiffened panel or of stiffened plate

σ_y: Yield stress

σ_y: Yield stress of deck material

σ_{yu}: Mean ultimate stress in y-direction

τ: Mean shear stress

τ_0: Ultimate shear stress

Φ: Normalized yield stress

Φ_w: Plate effective width factor

φ: Deviation of stiffened plate element behaviour from perfectly elastic behaviour

Ω: Problem domain

$\mathbf{B}$: Strain-displacement matrix

$\mathbf{b}$: Vector of applied body forces

$\mathbf{C}$: Hull girder curvature vector

$\mathbf{C}_x$: X component of hull girder curvature vector

$\mathbf{C}_y$: Y component of hull girder curvature vector

$\mathbf{c}$: Material constitutive matrix

$\mathbf{d}$: Matrix of nodal displacements

$\mathbf{K}$: Thermal conductivity matrix, stiffness matrix

$\mathbf{k}_T$: Tangent stiffness matrix

$\mathbf{M}$: Hull girder bending moment vector

$\mathbf{M}_x$: X component of hull girder bending moment vector

$\mathbf{M}_y$: Y component of hull girder bending moment vector

$\mathbf{q}$: Vector of heat flow per unit area

$\mathbf{R}$: Vector of applied loads

$\mathbf{R}_b$: Body force vector

$\mathbf{R}_f$: Internal force vector

$\mathbf{R}_q$: Distributed load vector

$\mathbf{r}_\varepsilon$: Vector of loads due to thermal strain

$\mathbf{T}$: Nodal temperature vector

$\mathbf{u}$: Nodal displacement vector

$\Delta\mathbf{d}$: Incremental displacement vector

$\boldsymbol{\varepsilon}_o$: Vector of initial strains

$\delta\boldsymbol{\varepsilon}$: Strain vector

ACKNOWLEDGEMENTS

Sincere thanks to my supervisors, Dr. Yi Liu and Dr. Neil Pegg, who provided valuable guidance throughout the course of this research. I would also like to thank Dr. Malcolm Smith for sharing his expertise and for his thorough review of this work. Thanks also to Dr. Ross Graham and ACEnet for providing the computational resources that made a large part of this research possible.

Chapter 1 - Introduction

1.1 Background

Evaluation of the ultimate longitudinal bending capacity of a hull girder is the most fundamental aspect of ship structural design. Accurate determination of hull girder ultimate strength is essential to ensure a safe and economical design to prevent structural failure, environmental damage and loss of life. The main forces that a hull girder must be able to resist are longitudinal stresses due to bending, therefore the primary structure of the hull is oriented longitudinally. The principle longitudinal load resisting elements are the deck, shell plating and bottom, all of which are in the form of grillages with longitudinally stiffened panels separated by transverse frames. The behaviour of these stiffened panels under axial loads characterizes the response of the hull girder to longitudinal bending.

Several empirical, analytical and numerical methods have been proposed for the determination of hull girder ultimate strength. A number of these methods have been compared in a benchmark study carried out by the International Ship Structures Committee (Ohtsubo & Sumi, 2000) where considerable discrepancy between the results determined by different contributors to the study was observed. This is attributed in part to the fact that accurate assessment of hull girder ultimate strength is sensitive to uncertainties such as residual stress and distortion resulting from fabrication processes. Since these complex, three dimensional stress and distortion fields are difficult to predict,

they are often assumed, simplified or simply neglected in hull girder structural design and analysis.

Analytical and experimental studies have shown that residual stresses may have a significant influence on ultimate strength and behaviour of stiffened panels (Gordo & Guedes Soares 1996, Hansen 1996). Determination of the exact residual stress distribution in a stiffened panel requires costly experiments using specialized equipment or rigorous finite element analysis. For this reason, hull girder design and analysis is usually performed assuming idealized residual stress distributions and distortions. A literature survey revealed that there is little scientific documentation or reported research addressing how the idealized values of these imperfections, or approximate methods of accounting for them, affect the accuracy of hull girder ultimate strength predictions.

Another source of uncertainty in hull girder ultimate strength calculations arises from the fact that there may be a reduction in residual stress in ship structures once they are subjected to cyclic loads while in service (Paik *et al.* 2005). This phenomenon is known as 'shakedown'. Most research on shakedown is concerned with fatigue behaviour of structural connections. There is little information in available literature on the effect of shakedown on residual stresses in stiffened panels and consequently on the ultimate strength of ship hull girders.

The magnitude and distribution of welding-induced residual stress and distortion are affected by many factors including geometry, material properties and welding procedures. Although welding-induced residual stress and distortion may be measured

experimentally using laser measuring devices, x-ray diffraction, neutron diffraction and the method of sectioning (Galambos, Guide to stability design criteria for metal structures, 1998), these methods are time consuming and accuracy is often subject to the precision of the devices and measuring procedures. As an alternative to experimental methods, finite element analysis may be used to predict 3D residual stress and distortion fields produced by welding. In most cases, this is accomplished by a two-step nonlinear finite element analysis performed as follows:

1) Transient thermal analysis in which the time-dependent temperature distribution is determined.
2) Nonlinear structural analysis using the temperature time history from the thermal analysis as a series of loads, giving the three-dimensional residual stress and distortion fields.

Several methods of hull girder ultimate strength analysis are capable of incorporating the effects of welding-induced imperfections. These include Smith's method (Smith, 1977), also referred to as the beam-column method and the idealized structural unit method (ISUM) (Paik & Thayamballi, 2003). Although the ISUM is capable of including residual stress in a hull girder strength analysis, the residual stress distribution is idealized so that it can be more easily included in the specially formulated finite elements employed in the method. Consequently, Smith's method is better suited to include exact three-dimensional residual stress and distortion fields in a hull girder ultimate strength analysis. The

complete process for ultimate strength analysis using Smith's method including exact, 3D residual stress and distortion fields is illustrated in Figure 1.1.

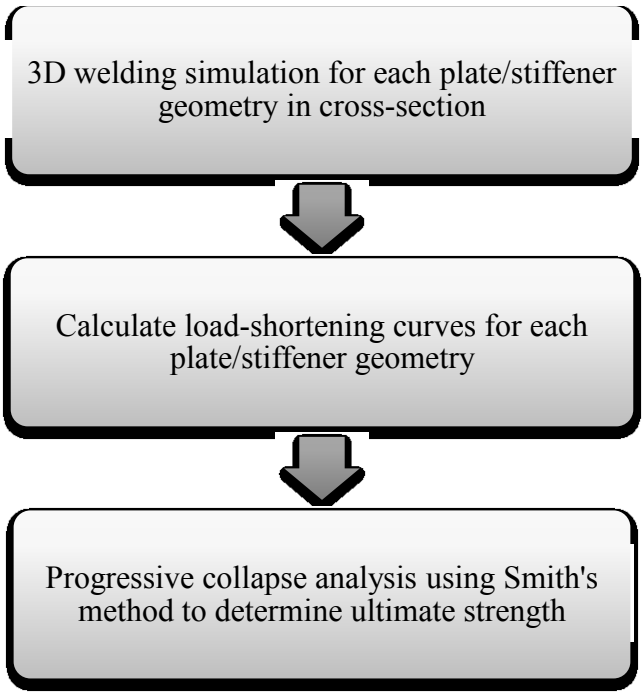

Figure 1.1, Process for ultimate strength evaluation with residual stress and distortion

This document is organized as a series of papers that describe in detail, the process illustrated in Figure 1.1. Following the introduction, Chapter 2 provides a review of literature pertinent to welding simulation by the finite element method, stiffened plate analysis and hull girder ultimate strength analysis. Chapter 3 describes the process of simulating welding using the finite element method to determine the associated 3D residual stress and distortion fields in stiffened plates. The welding simulation is then used to study the effect of welding sequence on residual stress and distortion in flat-bar stiffened plates. If the reader has read Chapter 3, then they may skip the description of the

welding simulation method in subsequent chapters, since much of the information is repeated.

In Chapter 4, residual stress and distortion in welded flat-bar stiffened plates are predicted by the welding simulation developed in Chapter 3. Load-shortening curves describing the behaviour of the stiffened plates under axial load are generated and compared with load-shortening curves derived from formulae provided by IACS (IACS, 2009) for use in hull girder design. Chapter 5 is similar to Chapter 4, however angle and tee-stiffened plates are considered. The introduction and description of analysis methods in Chapter 5 are similar to those in Chapter 4, and so can be skipped by the reader if they have already read Chapter 4.

In Chapter 6, the potential reduction of residual stress in stiffened plates due to shakedown is investigated by application of cyclic axial loads to stiffened plates considering 3D residual stress and distortion fields calculated by welding simulation. The residual stress fields before and after application of cyclic loads are examined and the influence of strain hardening on shakedown is considered. In Chapter 7, the work of the previous papers culminates in a hull girder ultimate strength analysis using Smith's method and including 3D residual stress and distortion fields predicted by welding simulation. The influence of residual stress shakedown on hull girder strength is also examined. The geometry of the hull girder for the numerical model is the same as that used in an experimental program by Akhras *et al.* (1995), so that results from the numerical model can be compared with experimental measurements. The ultimate

strength analysis is also carried out using load-shortening curves from the IACS common structural rules (IACS, 2009) and an approximate method developed by Gordo and Guedes Soares (1993) to assess their accuracy compared to the more rigorous, finite element modelling approach.

1.2 Objectives

The main objectives of this research are to accurately characterize welding-induced residual stresses and associated distortions in typical ship structures; to quantify the potential reduction in residual stress due to shakedown; and to determine the influence of these imperfections on hull girder ultimate strength.

A detailed description of objectives follows:

- Conduct a comprehensive literature review to examine methods of evaluating stiffened plate and hull girder ultimate strength and, to determine the state-of-the-art of finite element welding simulation.
- Create and validate a 3D thermo-elasto-plastic finite element model capable of predicting weld-induced residual stresses and distortions.
- Use the finite element based welding simulation to generate residual stress and distortion fields in stiffened plates typical of commercial and naval ship structures.
- Conduct a shakedown analysis of several stiffened plates to determine the effect of in-service loads on welding-induced residual stress and distortion.

- Generate load-shortening curves for stiffened plates with various stiffener configurations and slenderness incorporating three-dimensional residual stress and distortion fields with and without accounting for the effects of shakedown.
- Evaluate the ultimate strength of a hull girder cross-section using the aforementioned load-shortening curves.
- Compare results of the hull girder ultimate strength analyses with experimental results and the results of ultimate strength analyses using load-shortening curves derived by analytical methods including methods prescribed in the IACS (2009) common structural rules.

Chapter 2 - Literature Review

2.1 Introduction

This chapter begins with an examination of methods used for hull girder ultimate strength analysis. Smith's method is discussed in detail since three-dimensional residual stress and distortion fields can be incorporated in an ultimate strength analysis most easily with this method (Smith, 1977). Smith's method relies on the calculation of load-shortening curves for stiffened plates that represent their behaviour under axial loads in the pre and post-buckling ranges. A review of stiffened plate behaviour is presented and the effective width concept is introduced. This is followed by a discussion of shakedown in welded structures. Although there is relatively little information in available literature on shakedown in stiffened plates in ship structures, some insight into the subject is gained from the study of shakedown as it relates to fatigue analysis. The chapter concludes with a review of welding physics and methods used to calculate residual stress and distortion fields in welded structures. Emphasis is placed on welding simulation using the finite element method which is later used to predict three-dimensional residual stress and distortion fields in welded stiffened plates.

2.2 Hull Girder General Behaviour

The longitudinal strength of a hull girder is a fundamental characteristic of ship strength. It is a measure of the ability of the hull to withstand longitudinal bending under operational and extreme loads without suffering failure. A common means of

representing the behaviour of a hull girder subject to longitudinal bending is a moment-curvature diagram. Several possible moment-curvature relationships are shown in Figure 2.1.

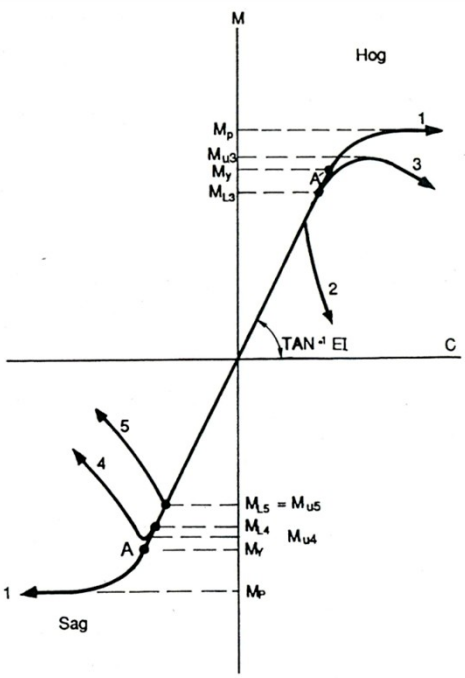

Figure 2.1, Moment-curvature relationships (Rutherford & Caldwell, 1990)

The point at which the slope of the curve becomes zero defines the ultimate moment capacity of the hull girder and is generally different in hogging and sagging. Line 1 represents the behaviour of the girder if its structural members are stocky enough to attain its fully plastic moment before there is any instability of the stiffened plates making up the cross-section. This type of behaviour is unlikely in most ship structures and a plastic analysis of the hull girder cross-section will in most cases result in an overestimate of ultimate strength. The type of behaviour shown by line 2 might result if there is insufficient material ductility and fast fracture occurs. This type of behaviour is also unlikely, since modern material specifications and construction methods are intended to

provide sufficient ductility to prevent this type of sudden failure. Lines 3,4 and 5 show a type of behaviour where buckling of compressed elements in the cross-section initiates failure. These are typical of most ship hull girders.

Current methods of obtaining the moment-curvature relationship for a hull girder require certain assumptions and idealizations that introduce uncertainty in an ultimate strength analysis. These included the possible effects of corrosion, the presence of lateral pressure on some elements of the hull girder, fabrication related imperfections such as residual stress and distortion and a certain amount of error inherent in solution procedures.

It has been shown in several studies that residual stress and distortion due to welding can have a significant influence on hull girder ultimate strength. Since the complicated physics of welding make prediction of residual stress and distortion difficult, the majority of methods used to evaluate hull girder ultimate strength employ simplifying assumptions and idealizations regarding the magnitude and distribution of residual stress and distortion. Many studies assume values based on empirical data and these are often idealized as being two-dimensional (Ohtsubo & Sumi, 2000). Advances in computing technology have now made it possible to predict the three-dimensional distribution of residual stress and distortion in welded structures using numerical methods. This may help to reduce some of the uncertainty in ultimate strength analysis caused by using simplified residual stress and distortion fields.

2.3 Historical Review of Ultimate Strength Analysis

The first evidence of an attempt to evaluate the ultimate strength of a ship hull is from Sir Isambard Kingdom Brunel (Yao, 1999). He carried out longitudinal strength calculations on the Great Eastern, a ship with a loaded displacement of 27,380 tons. He considered the ship to be supported at two points 400ft apart and attempted to provide enough material in the deck and bottom to resist the maximum bending moment. John (1874) was the first to formally introduce classical linear beam theory for ship structural design. He assumed a design wave of length equal to the ship's length and calculated the corresponding bending moments and shear forces. John's method was further refined by subsequent generations of naval architects who extended the theory to account for the following (Rutherford & Caldwell, 1990):

- the influence of superstructure and discontinuities such as hatch openings
- the effects of shear through shear stress and shear lag calculations
- buckling of longitudinal structural elements
- the need to ensure adequate quality of ductile material and of construction to avoid premature failure in longitudinal bending

The first attempt to account for both yielding and buckling in a hull girder ultimate strength analysis was made by Caldwell (1965). He considered failure to occur once overall buckling of the compression zone and yielding of the tension zone had occurred. Caldwell's method allows for plate buckling in longitudinally stiffened hulls before the ultimate strength is reached. This accounts for the fact that following plate buckling, the

plates shed some load to the longitudinal stiffeners and these continue to carry increasing load until they buckle between transverse supporting members. At the ultimate load in the sagging condition, Caldwell assumed that the full yield stress in tension is developed in the structure below the neutral axis and recognized that the effective longitudinal stress in the deck at failure may be less than the yield stress if buckling of the stiffeners occurs. Caldwell proposed replacing the non-uniform distribution of stress in the deck at failure with an equivalent average longitudinal stress in the deck. The side shell stress above the neutral axis was treated similarly. These average ultimate stress values were normalized, giving deck and side strength factors. At the time of the publication, initial buckling behaviour of ship structural elements was well understood, but less was known about post-buckling behaviour and ultimate capacity of complete deck and side shell stiffened panels, so deck and side strength factors had to be estimated from experimental data and then the ultimate moment capacity could be calculated. One shortcoming of Caldwell's method is that it did not account for the post-buckling strength of the structural members which can have a significant effect on the failure load (Rutherford & Caldwell, 1990).

Smith (1977) introduced a method of determining the moment-curvature relationship of a hull girder accounting for the progressive failure and post-buckling capacity of structural elements. Smith considered each stiffened panel in the cross-section to be composed of a number of individually stiffened plates. The stress-strain relationship for each of the stiffened plates making up the cross-section was accounted for by dividing each one into a number of fibers and applying incremental axial stresses. Incremental curvatures were then applied to the hull girder cross-section to obtain the moment-curvature relationship.

The main difference between the application of Smith's method by different researchers is the way in which the stress-strain relationship is determined for the individual beam-columns making up the cross-section.

Dow (1991) divided stiffened plates of a hull girder cross-section into horizontal fibers. Load-shortening curves were derived by finite element analysis where plating between stiffeners was represented by a single fiber whose behaviour was defined by experimental curves. Billingsley (1980) used an analytical approach where a simplified model for each beam-column element was used to derive load-shortening curves for use in Smith's method. Adamchak (1984) developed a simplified model that accounted for flexural-torsional buckling of stiffeners in deriving load-shortening curves for stiffened plates.

The accuracy of Smith's method of analysis was verified by Rutherford and Caldwell (1990), who used the method to calculate the ultimate moment capacity of the hull of the VLCC Energy Concentration that failed while discharging oil at Rotterdam in 1980. The results of their analysis agreed well with values calculated from the known loading condition of the ship at the time of failure. They did not consider post-buckling strength of stiffened panels, but did account for the influence of lateral pressure, initial deformations and corrosion. Gordo *et al.* (1996) also used Smith's method to calculate the ultimate strength of the VLCC Energy Concentration and compared their results with those of Rutherford and Caldwell (1990). The method was used to study the effects of residual stress and corrosion on hull girder behaviour.

An alternative method used to perform progressive collapse analysis is the idealized structural unit method (ISUM) introduced by Ueda and Rashad (1984). This method uses specially formulated finite elements to represent plates with multiple stiffeners. Using single elements to represent large parts of the structure reduces the number of degrees of freedom in the model which reduces solution time. The most important feature of the method is that the structural elements are able to account for buckling and yielding. The ISUM is continually being developed by researchers including Paik *et al.* (1996), Paik (1993), and Fujikubo *et al*. (2000), who have added functionality to the elements including the ability to account for residual stress and distortion. Currently, the ISUM cannot represent localized plastic deformation or stiffener tripping.

It is possible to calculate hull girder ultimate strength by nonlinear finite element analysis of a complete hull girder model. One such analysis was carried out by Kutt *et al.* (1985), but was found to be very time consuming in both model preparation and solution time. The ultimate capacity of the hull girder can also be calculated using a single-step procedure specified by the IACS (2009) which is based on a reduced hull girder bending stiffness to account for buckling of deck elements.

2.4 IACS Single Step Method

The IACS single step procedure for calculation of the sagging hull girder ultimate moment capacity is outlined in the Common Structural Rules for Bulk Carriers (IACS, Common structural rules for bulk carriers, 2009). The method is based on the assumption

that the ultimate hull girder capacity is reached when the ultimate capacity of the stiffened deck panels is reached. The ultimate moment capacity is taken as:

$$M_u = Z_{red}\sigma_{yd} \tag{2.1}$$

where Z_{red} is the reduced section modulus of the deck taken as:

$$Z_{red} = \frac{I_{red}}{Z_{dk-mean} - Z_{NA-red}} \tag{2.2}$$

where I_{red} is the reduced hull girder moment of inertia considering all longitudinally continuous members after deduction of openings using a net thickness not including corrosion allowance, $t_{net\text{-}50}$ for all longitudinally effective members and an effective net area after buckling for each stiffened deck panel given by:

$$A_{eff} = \frac{\sigma_u}{\sigma_{yd}} A_{net-50} \tag{2.3}$$

where σ_u is the buckling capacity of the stiffened deck panel; σ_{yd} is the minimum yield stress of the material used to determine the section modulus; $Z_{dk\text{-}mean}$ is the vertical distance to the mean deck height taken as the mean of the deck at side and the deck at centerline measured from the baseline; A_{net-50} is the area of the stiffened plate and $Z_{NA\text{-}red}$ is the vertical distance to the neutral axis of the reduced section from the baseline. The buckling capacity of stiffened deck panels used in Eqn. (2.3) must consider nonlinear geometric behaviour, inelastic material behaviour, initial distortions, welding residual stress, interactions between adjacent structural elements and simultaneous load types

such as shear, lateral pressure and biaxial moment. The method used to determine the buckling strength is outlined in Appendix D of IACS (2009).

2.5 Smith's Method

Smith's method is a simplified method of hull girder analysis wherein the progressive collapse and post-buckling behaviour of structural elements making up a cross-section are accounted for. The moment-curvature relationship is determined by imposing incremental curvatures on the hull girder cross-section. For each curvature, the average strain in each longitudinally stiffened plate element is calculated based on its position relative to the neutral axis after which the associated stress is determined from a predefined load-shortening curve. The bending moment carried by the cross-section is calculated by summation of the moments of the forces in each individual element about the neutral axis of the cross-section. The main assumptions of the method are (Gordo *et al.*, 1996)

1. The elements into which the cross-section is divided act independently.
2. Plane sections remain plane after bending.
3. Overall grillage failure is prevented by sufficiently stiff transverse frames.

The initial position of the neutral axis passes through the centroid of the cross-section at the point $(\bar{x},\bar{y})$ given by:

$$\bar{x} = \frac{\sum x_i A_i}{\sum A_i}$$
$$\bar{y} = \frac{\sum y_i A_i}{\sum A_i} \tag{2.4}$$

where A_i is the cross-sectional area of the i^{th} element and x_i and y_i are the distances along the x and y axes respectively of the centroid of the i^{th} element from the origin. For the general case of a singly symmetric hull girder cross-section subjected to an unsymmetric bending moment represented by the vector **M**, the associated curvature vector **C**, can be resolved into its components about the major and minor principle axes (x and y axes, respectively) with corresponding curvatures $\mathbf{C}_x$ and $\mathbf{C}_y$, given by:

$$\begin{aligned} \mathbf{C}_x &= \mathbf{C}\cos\theta \\ \mathbf{C}_y &= \mathbf{C}\sin\theta \end{aligned} \tag{2.5}$$

where θ is the angle between the curvature **C**, and the x-axis, shown in Figure 2.2. The strain ε_i, at the centroid of element i is then:

$$\varepsilon_i = \mathbf{C}\left(y_{gi}\cos\theta + x_{gi}\sin\right) \tag{2.6}$$

Where $\langle x_{gi}, y_{gi} \rangle$ is the vector from the centroid of the cross-section to the centroid of the i^{th} element.

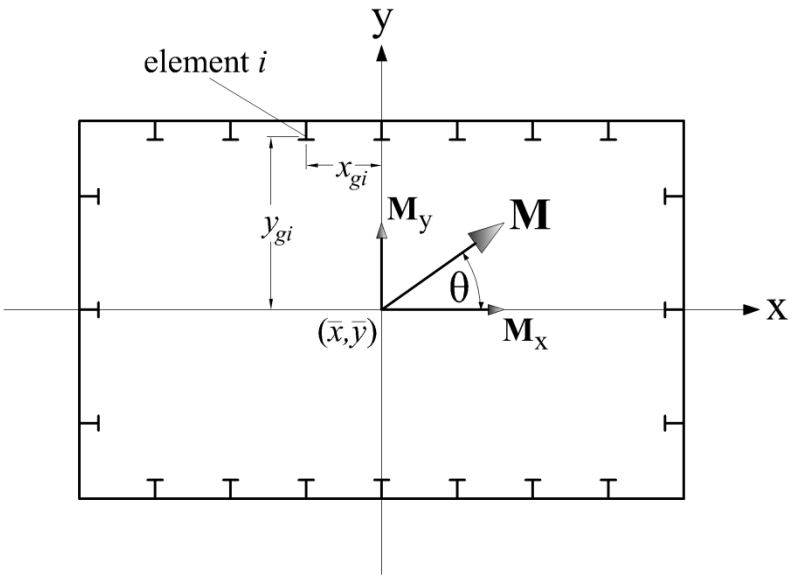

Figure 2.2, Hull girder biaxial bending

With the strain in each element known, the corresponding stresses are determined from the load-shortening curves and the components of the total bending moment about the principle axes, $\mathbf{M}_x$ and $\mathbf{M}_y$, are given by:

$$\begin{aligned} \mathbf{M}_x &= \sum y_{gi} \Phi\left(\bar{\varepsilon}_i\right) \sigma_y A_i \\ \mathbf{M}_y &= \sum x_{gi} \Phi\left(\bar{\varepsilon}_i\right) \sigma_y A_i \end{aligned} \tag{2.7}$$

where $\Phi(\varepsilon_i)$ is the average stress in element i at a strain of ε_i, normalized by the yield stress, σ_y. The bending moment **M**, on the cross-section about the instantaneous center of gravity is then:

$$\mathbf{M} = \sqrt{\mathbf{M}_x^2 + \mathbf{M}_y^2} \tag{2.8}$$

As the curvature increases and the response of the hull girder becomes nonlinear, the location of the centroid changes, making it necessary to calculate the shift in the centroid position between successive curvatures. The new position of the centroid is calculated using the effective area of each element given by:

$$A_{ei} = \varphi A_i \tag{2.9}$$

where φ, represents the deviation of the element from perfectly elastic behaviour, given by:

$$\varphi = \bar{\sigma} / \bar{\varepsilon} = \left(\sigma / \sigma_y\right) / \left(\varepsilon / \varepsilon_y\right) \tag{2.10}$$

The position of the neutral axis is then given by:

$$\begin{aligned} \bar{x} &= \frac{\sum x_i A_{ei}}{\sum A_{ei}} \\ \bar{y} &= \frac{\sum y_i A_{ei}}{\sum A_{ei}} \end{aligned} \tag{2.11}$$

Due to the dependence of A_{ei} on the position of the centroid, Eqns. 2.9 through 2.11 must be applied repeatedly to determine the position of the neutral axis until some convergence criteria is met.

2.6 Stiffened Plates

2.6.1 General Behaviour

The key feature of Smith's method is that a single stiffener and an associated width of attached plating are isolated and treated as a beam-column whose behaviour is representative of a complete stiffened panel. In order to account for nonlinearity in the beam-column response, such as the reduction in effective stiffness of yielded and buckled parts of the member, the equilibrium equation for the beam-column can be solved using an iterative procedure. An effective alternative to analytical methods for the nonlinear analysis of stiffened plates under axial compression is the finite element method. This method has the advantage of being able to consider non-standard stiffened plate geometries, complicated material behavior, and imperfections such as distortion and residual stress.

The analysis of stiffened plates is complicated due to the large number of combinations of plate and stiffener geometry, boundary conditions and loading. Further difficulties are encountered if residual stress and geometric imperfections are to be considered since these vary among manufacturers and geometries. Two main parameters control the load-shortening behaviour of stiffened plates. These are the plate slenderness β_0, and the effective column slenderness λ, that are associated with the geometry of the stiffened plate and its material properties, where

$$\beta_0 = (b/t)\sqrt{\sigma_y / E} \tag{2.12}$$

$$\lambda = (a/\pi r)\sqrt{\sigma_y / E} \tag{2.13}$$

where b and t are the width and thickness of the plate; a is the plate length; r is the radius of gyration and E is the elastic modulus.

Very stocky plates (low β_0) do not suffer significant loss of stiffness in the pre-collapse region and they may sustain the yield stress up to very large plastic strains. Very slender plates loose stiffness at an early stage of loading and show a more pronounced shedding of load to the stiffeners after collapse than stocky plates. The actual distribution of stress in a plate depends on boundary conditions and the length-to-width ratio. In some cases, after buckling, a plate may carry a compressive force many times greater than the load at which buckling begins. Significant savings in weight can be obtained by taking advantage of the additional strength available beyond initial buckling which is important in ship and aircraft structures where reduced weight has great economic value.

The ultimate strength of stiffened plates generally decreases with increasing column slenderness λ. Increasing column slenderness also results in a more sudden loss of load-carrying capacity in stiffened plates after the ultimate load is reached (Smith *et al.*, 1992). Moreover, the reduction in post-ultimate strength is more pronounced when $\lambda > 0.6$. This type of behavior is generally undesirable since there may be little or no warning before collapse of stiffened plates with high slenderness.

The mode of failure and the strength of stiffened plates is largely dependent on the strength of the stiffeners. If the stiffeners have low torsional stiffness, they may fail by lateral-torsional buckling, also referred to as stiffener tripping. Flat-bar stiffeners are particularly susceptible to this type of failure. Tripping of the stiffener is typically followed by flexural buckling of the stiffened panel since the out of plane stiffness of the plate alone is quite low. Failure of the stiffener may also occur as a result of local buckling of the stiffener web or flange. If the stiffeners are relatively strong, the plating between them may buckle into one or more half waves of length approximately equal to the stiffener spacing. Once plate buckling occurs, the stress along the plate edges increase more quickly and the stress in the middle of the plate usually differs little from the critical value. Provided the stiffener is strong enough to continue carrying load after the plate buckles, the stiffener and unbuckled part of the plate will continue to resist load until gross yielding occurs in the remaining effective cross-section, or flexural buckling occurs. A typical stress distribution in a plate between stiffeners following plate buckling is shown in Figure 2.3.

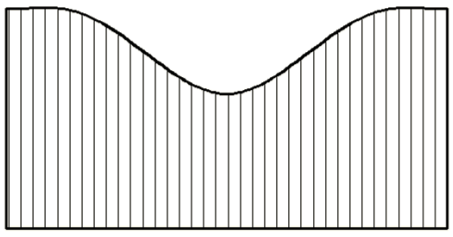

Figure 2.3, Plate post-buckled stress distribution

2.6.2 Ultimate Strength

The ultimate strength of a stiffened plate can be calculated with a high degree of accuracy if progressive yielding of the material and large deformations are tracked throughout the loading history. As an alternative to using incremental iterative methods to determine the complete load-deformation history, simplified analytical and empirical methods can be used to calculate stiffened plate ultimate strength, accounting for nonlinear effects in an approximate manner. These methods are preferable for design because they are not as complicated or time consuming as the former. Two commonly used approximate methods are described in the following.

2.6.2.1 Johnson-Ostenfeld Formulation

The Johnson-Ostenfeld formulation for beam-column ultimate strength may be used to calculate ultimate strength from the elastic buckling capacity (Galambos, 1998). This is an empirical approach used to account for plastic deformation in plates or struts that have a high elastic buckling stress and that develop a certain amount of plasticity before failure (Guedes Soares & Gordo, 1997). When the Euler buckling stress, σ_e is greater than half the yield stress σ_y, the ultimate stress is given by:

$$\sigma_{JO} = \left[1 - \left(\sigma_y / 4\sigma_e\right)\right]\sigma_y \tag{2.14}$$

Faulkner *et al.* (1973) used the Johnson-Ostenfeld formulation to predict the ultimate strength of singly stiffened plates, where an effective width was used to account for the

reduced strength of the plate in the post-ultimate phase. They use the following expression for the ultimate strength of a stiffened plate:

$$\phi_u = \frac{\sigma_u}{\sigma_y}\left[\frac{A_s b_e t}{A_s + bt}\right] \tag{2.15}$$

where:

$$\frac{\sigma_u}{\sigma_y} = \begin{Bmatrix} 1 - \frac{1}{4}\left(\frac{a}{\pi r_e}\right)^2 \frac{\sigma_y}{E}, & \sigma_e \geq 0.5\sigma_y \\ \left(\frac{\pi r_e}{a}\right)^2 \frac{E}{\sigma_y}, & \sigma_e < 0.5\sigma_y \end{Bmatrix} \tag{2.16}$$

$$r_e^2 = \frac{I_e^{'}}{A_s + b_e t} \tag{2.17}$$

where r_e is the radius of gyration of the stiffener and effective attached plating, A_s is the stiffener area, b_e is the effective width of the plate and $EI_e^{'}$ is the flexural rigidity of the stiffener. The reduced effective width of the plate, $b_e^{'}$ represents the contribution of the buckled plate to the flexural stiffness of the beam-column through the reduced moment of inertia and is given by Faulkner (1975) as:

$$\frac{b_e^{'}}{b} = \frac{1}{\beta}\sqrt{\frac{\sigma_y}{E}} \tag{2.18}$$

Recognizing that there is a difference between the load-carrying capacity of the plate and the support given to the stiffener by the plate against buckling, a different effective width is used in calculating the slenderness and is given by:

$$\frac{b_e}{b} = \frac{2}{\beta} - \frac{1}{\beta^2} \tag{2.19}$$

which is derived from experimental data and implicitly accounts for some degree of initial distortion. The factors R_r, R_y and R_τ are used to reduce the effective width to account for the effects of residual stress, biaxial loading and shear stress respectively:

$$R_r = \left\{ \begin{array}{c} 1 - \left(\frac{2\eta}{b/t - 2\eta} \right) \left(\frac{\beta^2}{2\beta - 1} \right) \frac{E_t}{E}, \quad \beta \geq 1 \\ 1, \quad \beta < 1 \end{array} \right\} \tag{2.20}$$

$$R_y = 1 - \left(\frac{\sigma_y}{\sigma_{yu}} \right)^2, \quad \sigma \leq 0.25\sigma_y \tag{2.21}$$

$$R_\tau = \left\{ 1 - \left(\frac{\tau}{\tau_0} \right)^2 \right\}^{1/2} \tag{2.22}$$

where:

$$\frac{E_t}{E} = \left\{ \begin{array}{c} \frac{3.62\beta^2}{13.1 + 0.25\beta^4}, \quad 0 \leq \beta \leq 2.7 \\ 1, \quad \beta > 2.7 \end{array} \right\} \tag{2.23}$$

where σ_{yu} is the mean ultimate stress in the y-direction; τ and τ_0 are the mean and ultimate shear stress respectively; E_t is the tangent modulus and η is the width of the residual tension zone suggested to be from 3 to 4.5 times the plate thickness.

2.6.2.2 Perry-Robertson Formulation

The Perry-Robertson formula is based on the assumption that the beam-column has an initial out-of-straightness, δ_0 at mid-span. Carlsen (1977) used the Perry-Robertson formula along with an effective width approach for the plate to determine the average stress in the plate/stiffener combination at failure given by:

$$\sigma_u = \sigma_y \frac{A_e}{A} \frac{\left(1+\gamma+\varepsilon\right) - \sqrt{\left(1+\gamma+\varepsilon\right)^2 - 4\gamma}}{2\gamma} \tag{2.24}$$

where

$$\gamma = \frac{\sigma_y}{\sigma_e} \tag{2.25}$$

$$\varepsilon = \frac{z_c \delta_0}{r_e^2} \tag{2.26}$$

where z_c is the distance from the neutral axis to the extreme fiber in compression in the plate in the case of plate-induced failure or to the stiffener for stiffener-induced failure, and A_e is the effective area of the stiffened plate using the effective width b_e, of the plate. According to Guedes Soares and Gordo (1997), when calculating the radius of gyration r_e, and the Euler buckling stress, the influence of the plate is negligible, so it can be considered fully effective. Analytical expressions are available (Guedes Soares & Gordo 1997, Hughes 1983) for determining whether failure is initiated by the plate or stiffener. For plate-induced failure, the shift of the neutral axis due to loss of effectiveness of the plate is accounted for by modifying δ_0 as follows:

$$\delta_0 = 0.0015a + z_c\left(1 - \frac{A_e}{A}\right) \tag{2.27}$$

The effective width of the plate used in calculating the reduced cross-sectional area A_e, for plate and stiffener-induced failures respectively is given by (Guedes Soares & Gordo, 1997):

$$\left\{\begin{array}{c} \frac{b_e}{b} = \frac{1.8}{\beta_0} - \frac{0.8}{\beta_0^{\,2}}, \quad \beta_0 > 1 \\ 1, \quad \beta_0 \le 1 \end{array}\right\} \tag{2.28}$$

$$\frac{b_e}{b} = \left\{\begin{array}{c} 1.1 - 0.1\beta_0, \quad \beta_0 > 1 \\ 1, \quad \beta_0 \le 1 \end{array}\right\} \tag{2.29}$$

This formulation includes plate deflections of $0.01b$ and residual stresses of magnitude $0.2\sigma_y$ in the plate. Residual stress in the stiffener is accounted for by reducing the predicted strength by 5%.

2.7 Load Shortening Curves

2.7.1 Rutherford and Caldwell (1990)

Rutherford and Caldwell (1990) carried out retrospective strength calculations on the VLCC Energy Concentration which suffered catastrophic failure of its hull girder while discharging oil at Rotterdam in 1980. The strength of the hull girder cross-section at failure was analyzed using Smith's method. The stiffened plate strength was determined

by two methods; the first relating to plate-induced failure and the second to stiffener-induced failure. The lowest of these values was used to define the failure load and the load-shedding response in the post-buckling region. Two separate possibilities were considered for the post-buckling behaviour for each of the two types of failure. For each type of failure, one theory considers buckling, which was adopted from the work of Murray (1973) while the other represents pure plastic action. Details of these theories are summarized by Rutherford (1982) and Rutherford and Caldwell (1990). The remaining elements of the cross-section such as bilge plating were analyzed in an approximate manner using the Johnson-Ostenfeld correction for plasticity.

The ultimate strength analysis of the failure of the VLCC Energy Concentration considered the sensitivity of the ultimate hull girder moment capacity to material properties, fabrication-related imperfections and corrosion. The influence of increased yield stress on individual elements making up the cross section was evaluated by increasing the yield stress from 0% to 15% above the nominal value. A linear increase in the element ultimate strength was observed with an increase of 8% for a 15% increase in yield stress. Based on the assumption that hull girder strength will increase in proportion to the local element strength, for a 10% increase in yield stress, the authors predicted a 5.4% increase in hull capacity. The influence of residual stress was found to be negligible for the stiffener failure mode predicted since the influence of residual stress in the stiffener was ignored. The authors noted that "further work is needed both with respect to predicting the distribution and magnitude of this component as well as to implementing it in the analytical procedure".

Imperfections used in the stiffened plates were assumed to be sinusoidal in both the longitudinal and transverse directions. Three different magnitudes of imperfection were considered:

1. A square wave with amplitude $(b/200)(\sigma_y/245)^{1/2}$ in the plates.
2. An overall initial deflection of *a*/900 between transverse frames for investigating plate-induced failure.
3. An overall initial deflection of *a*/1200 for investigating stiffener-induced failure.

The slope of the load-shedding portion of the load shortening curve representing individual stiffened plates was found to have a significant influence on hull girder strength. The sensitivity of hull girder strength to this parameter was studied by varying the slope of the load-shedding part of the curve from 0° to 40° from the horizontal as illustrated in Figure 2.4, where a difference in ultimate strength of 10% is observed between the load-shedding curve angles of 0° and 40° to the horizontal.

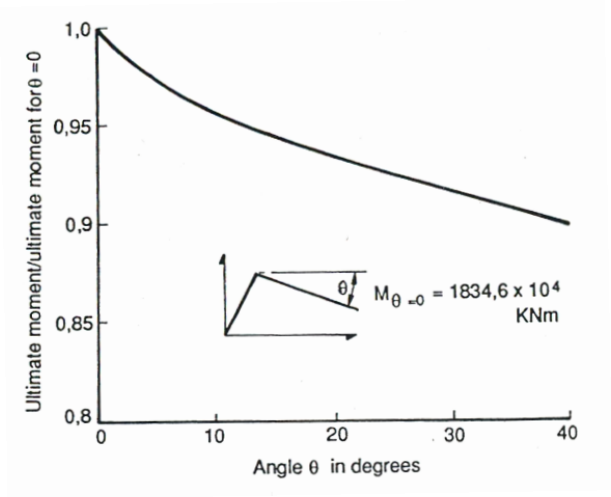

Figure 2.4, Effect of unloading slope on ultimate moment (Rutherford & Caldwell, 1990)

2.7.2 Gordo and Guedes Soares (1993)

Gordo and Guedes Soares (1993) developed an approximate method to define load-shortening curves for stiffened plates accounting for residual stress and initial distortions. The effective width expression derived by Faulkner (1975) was used to model the plate behaviour and it was assumed that the load-shortening behaviour of the plate could be represented by the same expression, where the slenderness is defined at each strain by:

$$\beta = \frac{b}{t}\sqrt{\bar{\varepsilon}} \tag{2.30}$$

where $\bar{\varepsilon}$ is the normalized strain. The effective width b_e, at a given strain is then:

$$\frac{b_e}{b} = \frac{2}{\beta} - \frac{1}{\beta^2} \tag{2.31}$$

Compressive residual stress in the central region of the plate is accounted for by considering an initial strain, ε_r. When the total strain reaches yield, the change in the tangent modulus of the plate is modeled as a straight line between the point of initial yield to twice the yield strain as shown in Figure 2.5. The behaviour of plates using this method of incorporating residual stress was checked against finite element analysis results. Good agreement between the two results was observed.

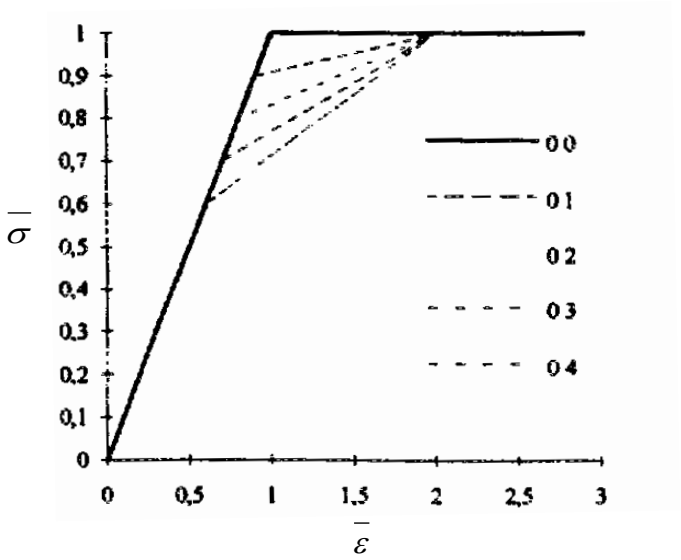

Figure 2.5, Material behaviour incorporating different levels of residual stress (Gordo & Guedes Soares, 1993)

The effect of average initial distortions on the compressive behaviour of the plate was considered implicitly through Faulkner's equation (Eqn. 2.32) for effective width. Although initial distortions do cause a variation in the initial tangent modulus of the plate, this effect was considered small for the usual level of distortions, so the effect of distortions on the tensile behaviour of the plate was neglected. Three collapse modes were considered in the analysis of the stiffened plates: plate-induced failure, stiffener-induced failure and overall flexural buckling. The load-end shortening curve for a beam-column was determined by using the lowest stress, considering each mode of failure for every strain increment of the stiffened plate.

2.7.3 Hansen (1996)

Hansen (1996) presented an analytical method for determining the load-shortening relationship for beam-columns to be used in Smith's method. Eqn. (2.32) was solved iteratively to give the average longitudinal stress in the beam-column, accounting for residual stress in the plate, initial deflection and the effect of lateral load. The associated deflection for any level of load up to the buckling load is given by Eqn. (2.33).

$$\sigma(z) = -\left(\frac{P}{A_E}\right) - \frac{\delta_0 E z P \pi^2}{a^2\left(P - P_E\right)} - \frac{Eqz}{P} + \frac{\alpha E z}{\sin\frac{\alpha a}{2}}\left(\frac{\delta_0 P \pi}{a^2\left(P - P_E\right)} + \frac{aq}{2P} + \theta\right) \tag{2.32}$$

$$\delta = \frac{Pa}{EA_E} \tag{2.33}$$

Where $\alpha = \sqrt{\frac{P}{EI_e}}$; $P_E = EI_e\left(\frac{\pi}{a}\right)^2$; θ is a predefined end rotation; z is the distance measured from the instantaneous neutral axis; q is the magnitude of a lateral line load on the beam-column; I_E is the effective moment of inertia of the cross-section, and P is an axial force applied at the end of the beam-column. The terms A_e and I_e account for the effects of residual stress and are dependent on the loading, therefore they must be determined iteratively. The longitudinal welding residual stress distribution in the plate of the beam-column section is idealized as shown in Figure 2.6, where σ_y is the material yield stress and σ_r is a specified level of compressive residual stress. This distribution of longitudinal residual stress is commonly used and is typical of a plate with welded edges where tensile stresses, often as high as the yield stress of the base metal are present in the

vicinity of the weld. Compressive stresses were prescribed in the middle region of the plate and are of such magnitude that the net force associated with residual stresses on the cross-section is zero. The initial deflection of the beam-column is assumed to have the form of a half-sine wave.

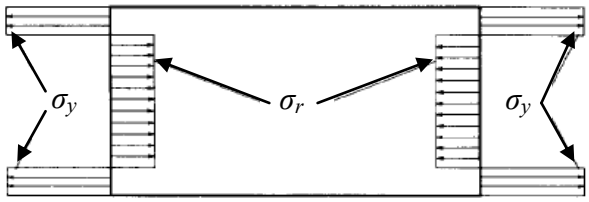

Figure 2.6, Idealized welding residual stress distribution in plate, Hansen (1996)

Hansen (1996) used this analytical method to evaluate the ultimate strength of a 1/3 scale welded steel frigate tested by Dow (1991) and compared his results with experimental findings. The material yield stress was 245MPa and residual stresses ranged from 125MPa to 150MPa. The analytical ultimate moment capacity agreed well with experimental results. Load-shortening curves obtained for analysis of the 1/3 scale frigate with and without residual stress are shown in

Figure 2.7 and Figure 2.8 respectively. A comparison of these figures reveals that the presence of residual stresses has a significant influence on the strength and behavior of stiffened plates. The reduction in compressive strength of the stiffened plates due to residual stress was found to be approximately 25%. Moment curvature relationships derived by Hansen with and without residual stress and distortion for the hull girder of the 1/3 scale frigate are compared against measured values in Figure 2.9. He found that the presence of residual stress caused a reduction in ultimate strength of approximately

15%. Although it seems unusual that the presence of initial deflections resulted in an increase in ultimate strength above that of the perfect structure, the author attributed this to the fact that the assumed initial deflections were not in the shape of the buckling mode, which may have increased the capacity of the deck plating.

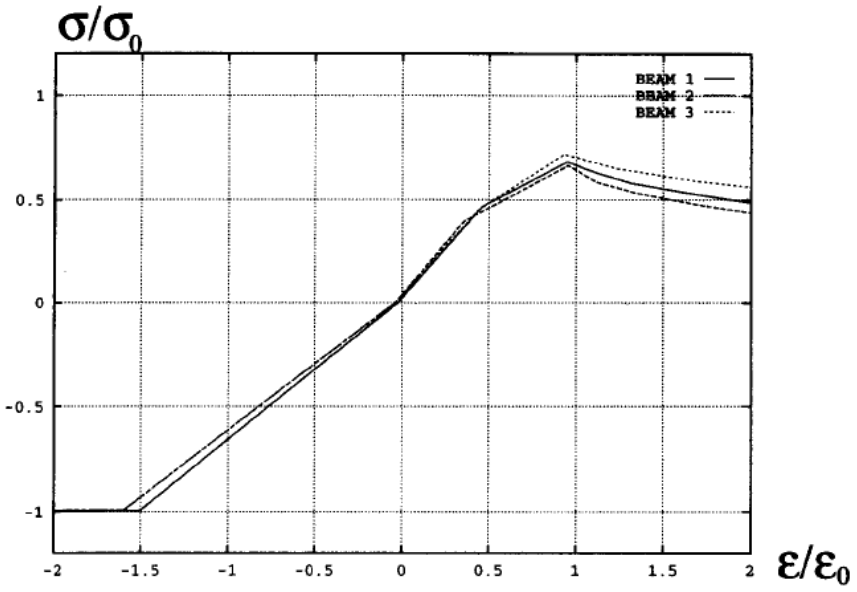

Figure 2.7, Load shortening curves with residual stress, Hansen (1996)

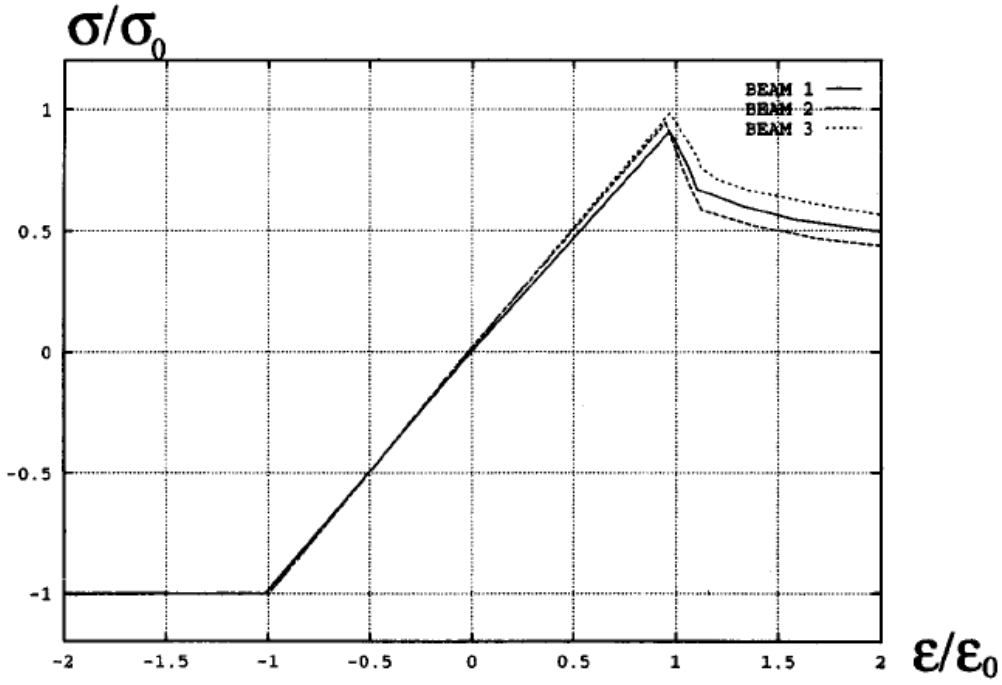

Figure 2.8, Load shortening curves without residual stress, Hansen (1996)

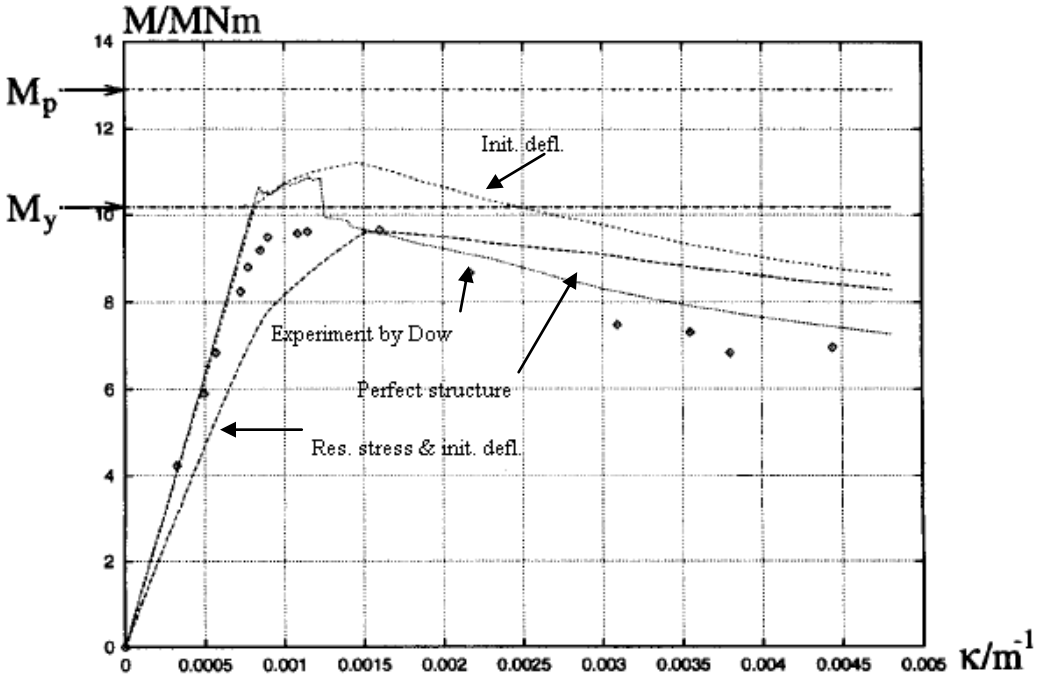

Figure 2.9, Moment-curvature relationships for 1/3 scale frigate, Hansen (1996)

2.7.4 IACS (2009)

IACS provides an analytical method for calculating the load shortening curves for longitudinally stiffened plates used in Smith's method. For each increment in strain, the stress in a stiffened plate is taken as the lowest of the values determined, considering the following possible modes of failure:

1. elasto-plastic failure;
2. flexural buckling;
3. torsional buckling of stiffeners;
4. web local buckling of stiffeners.

2.7.4.1 Elasto-Plastic Failure

The equation describing the load shortening curve for elasto-plastic failure of a structural element is:

$$\sigma = \Phi \sigma_y \tag{2.34}$$

where:

$$\begin{aligned} \Phi &= -1, \quad && \bar{\varepsilon} < -1 \\ \Phi &= \bar{\varepsilon}, \quad && -1 < \bar{\varepsilon} < 1 \\ \Phi &= 1, \quad && \bar{\varepsilon} > 1 \end{aligned} \tag{2.35}$$

$\bar{\varepsilon} = \varepsilon_E / \varepsilon_y$ is the relative strain where ε_E is the element strain and ε_y is the yield strain.

2.7.4.2 Beam-Column Buckling

The equation describing the compression portion of the stress-strain curve for flexural buckling of stiffened plates is:

$$\sigma_{CR1} = \Phi \sigma_{C1} \left(\frac{A_{s-net50} + 10^{-2} b_{eff-p} t_{net50}}{A_{s-net50} + 10^{-2} s t_{net50}} \right) \tag{2.36}$$

where ϕ is the edge function defined by Eqn. (2.35), s is the stiffener spacing; $A_{s\text{-}net50}$ is the area of the stiffener without attached plating in cm^2, t_{net50} is the thickness of the attached plating and σ_{C1} is the critical stress in MPa given by:

$$\begin{aligned} \sigma_{C1} &= \frac{\sigma_{E1}}{\bar{\varepsilon}}, && \sigma_{E1} \le \frac{\sigma_{yd}}{2} \bar{\varepsilon} \\ \sigma_{C1} &= \sigma_y \left(1 - \frac{\sigma_y \bar{\varepsilon}}{4 \sigma_{E1}} \right), && \sigma_{E1} . \frac{\sigma_{yd}}{2} \bar{\varepsilon} \end{aligned} \tag{2.37}$$

where σ_{E1} is the Euler column buckling stress in MPa given by:

$$\sigma_{E1} = \pi^2 E \frac{I_{E-net50}}{A_{E-net50} l_{stf}^2} \tag{2.38}$$

E is the modulus of elasticity taken as 2.06 x 10^5 MPa, $I_{E\text{-}net50}$ is the moment of inertia of the stiffener in cm^4 with an effective width of attached plating and $b_{eff\text{-}s}$ given by:

$$b_{eff-s} = \frac{s}{\beta_p}, \quad \beta_p > 1$$
$$b_{eff-s} = s, \qquad \beta_p \leq 1 \tag{2.39}$$

where:

$$\beta_p = \frac{s}{t_{net50}} \sqrt{\frac{\varepsilon \sigma_0}{E}} \tag{2.40}$$

s is the breadth of the plate in mm, taken as the spacing between stiffeners, l_{stf} is the span of the stiffener in m and $A_{E\text{-}net50}$ is the area of stiffener with attached plating of width $b_{eff\text{-}p}$ given by:

$$b_{eff-p} = \left(\frac{2.25}{\beta_p} - \frac{1.25}{\beta_p^2} \right), \quad \beta_p > 1.25$$
$$b_{eff-p} = s, \qquad \beta_p \leq 1.25 \tag{2.41}$$

2.7.4.3 Lateral-Torsional Buckling of Stiffeners

The equation describing the compression portion of the stress-strain curve for the lateral-torsional buckling of stiffeners is:

$$\sigma_{CR2} = \Phi \frac{A_{s-net50}\sigma_{C2} + 10^{-2} s t_{net50} \sigma_{CP}}{A_{s-net50} + 10^{-2} s t_{net50}} \quad \text{MPa} \tag{2.42}$$

where σ_{C2} is the critical stress in MPa given by:

$$\sigma_{C2} = \frac{\sigma_{E2}}{\bar{\varepsilon}}, \qquad \sigma_{E2} \le \frac{\sigma_0}{2}\bar{\varepsilon}$$
$$\sigma_{C2} = \sigma_0\left(1 - \frac{\sigma_0\bar{\varepsilon}}{4\sigma_{E2}}\right), \quad \sigma_{E2} > \frac{\sigma_0}{2}\bar{\varepsilon} \tag{2.43}$$

σ_{E2} is the Euler torsional buckling stress in MPa calculated using the gross thickness minus half of the corrosion allowance taken as:

$$\sigma_{E2} = \frac{E}{I_{p-net}}\left(\frac{\varepsilon\pi^2 I_{\omega-net}10^4}{l_{stf}^2} + 0.385 I_{T-net}\right) \tag{2.44}$$

where $I_{p\text{-}net}$, $I_{\omega\text{-}net}$, and $I_{T\text{-}net}$ are defined in Figure 2.10 and Table 2.1.

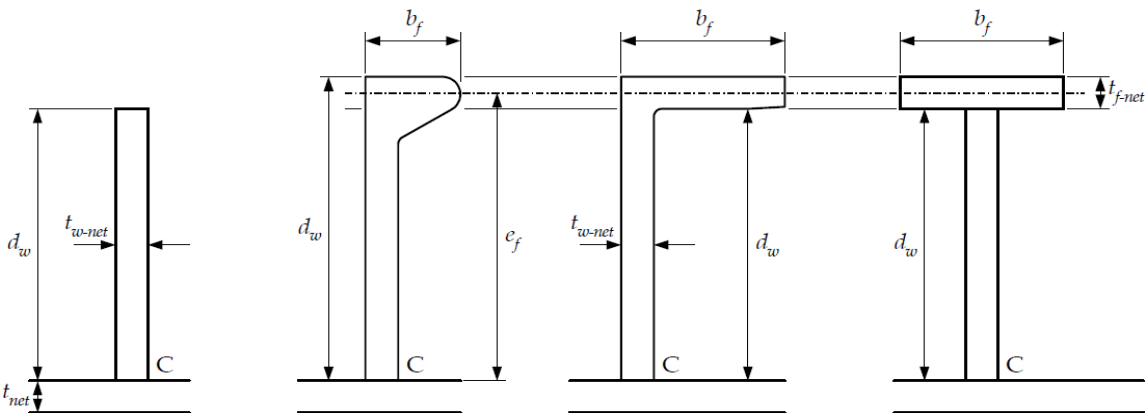

Figure 2.10, Stiffener cross-section dimensions (IACS, 2009)

Table 2.1 Stiffener moments of inertia (IACS, 2009)

Section property	*Flat bars*	*Bulb flats, angles and T bars*
I_{P-net}	$\frac{d_w^3\, t_{w-net}}{3\text{x}10^4}$	$\left(\frac{A_{w-net}(e_f - 0.5t_{f-net})^2}{3} + A_{f-net}\, e_f^2\right)10^{-4}$
I_{T-net}	$\frac{d_w t_{w-net}^3}{3\text{x}10^4}\left(1 - 0.63\frac{t_{w-net}}{d_w}\right)$	$\frac{(e_f - 0.5t_{f-net})t_{w-net}^3}{3\text{x}10^4}\left(1 - 0.63\frac{t_{w-net}}{e_f - 0.5t_{f-net}}\right)$ + $\frac{b_f\, t_{f-net}^3}{3\text{x}10^4}\left(1 - 0.63\frac{t_{f-net}}{b_f}\right)$
$I_{\omega-net}$	$\frac{d_w^3\, t_{w-net}^3}{36\text{x}10^6}$	**for bulb flats and angles:** $\frac{A_{f-net}\, e_f^2\, b_f^2}{12\text{x}10^6}\left(\frac{A_{f-net} + 2.6A_{w-net}}{A_{f-net} + A_{w-net}}\right)$ **for T bars:** $\frac{b_f^3\, t_{f-net}\, e_f^2}{12\text{x}10^6}$

σ_{CP} is the ultimate strength of the plating attached to the stiffener in MPa given by:

$$\sigma_{CP} = \left(\frac{2.25}{\beta_p} - \frac{1.25}{\beta_p^2}\right)\sigma_{yd}, \quad \beta_p > 1.25$$
$$\sigma_{CP} = \sigma_y, \quad \beta_p \le 1.25 \tag{2.45}$$

2.7.4.4 Local Web Buckling of Stiffeners

For the compression part of the load-shortening curve (LSC) for web local buckling of stiffeners, flanged and flat bar stiffeners are considered separately. For stiffeners with flanges, the equation describing the compression portion of the LSC is:

$$\sigma_{CR3} = \Phi\sigma_0\left(\frac{b_{eff-p}t_{net50} + d_{w-eff}t_{w-net50} + b_f t_{f-net50}}{st_{net50} + d_w t_{w-net50} + b_f t_{f-net50}}\right) \text{ MPa} \tag{2.46}$$

where d_w and b_f are the depth of web and width of flange respectively (Figure 2.10), and $d_{w\text{-}eff}$ is the effective depth of the web given by:

$$\begin{aligned} d_{w-eff} &= \left(\frac{2.25}{\beta_w} - \frac{1.25}{\beta_w^2}\right) d_w, \quad \beta > 1.25 \\ d_{w-eff} &= d_w, \qquad\qquad\qquad \beta \le 1.25 \end{aligned} \tag{2.47}$$

$$\beta_w = \frac{d_w}{t_{w-net50}} \sqrt{\frac{\bar{\varepsilon}\sigma_0}{E}} \tag{2.48}$$

For flat bar stiffeners, the equation describing the shortening portion of the LSC is:

$$\Phi_{CR4} = \Phi\left(\frac{st_{net50}\sigma_{CP} + 10^2 A_{s-net50}\sigma_{C4}}{st_{net50} + 10^{-2} S_{s-net50}}\right) \tag{2.49}$$

where

$$\begin{aligned} \sigma_{C4} &= \frac{\sigma_{E4}}{\bar{\varepsilon}}, \qquad\qquad\qquad \sigma_{E4} \le \frac{\sigma_0}{2}\bar{\varepsilon} \\ \sigma_{C4} &= \sigma_0\left(1 - \frac{\sigma_0\bar{\varepsilon}}{4\sigma_{E4}}\right), \quad \sigma_{E4} > \frac{\sigma_0}{2}\bar{\varepsilon} \end{aligned} \tag{2.50}$$

σ_{E4} is the Euler buckling stress given by:

$$\sigma_{E4} = 160000\left(\frac{t_{w-net50}}{d_w}\right)^2 \quad \text{MPa} \tag{2.51}$$

where $t_{w\text{-}net50}$ is the net thickness of the web.

2.8 Shakedown

It has been recognized in literature that there may be a reduction in residual stress in ship structures once they have been subjected to cyclic loads while in service. The extent to which this residual stress relief occurs in stiffened plates making up hull girders is not well documented and consequently, the influence of residual stress relief by shakedown on hull girder ultimate strength has not been considered in available literature. However, shakedown is sometimes considered in determining the state of stress in structures susceptible to fatigue. Those studies provide valuable insight into the potential influence of cyclic loads on the state of residual stress in stiffened plating of ship hull girders.

Shakedown occurs when a structure with elasto-plastic material behaviour is subjected to cyclic loads of magnitude sufficient to cause plastic deformation, but not high enough to cause plastic collapse. The following three types of shakedown are described by Abdel-Karim (2005) according to plastic behaviour:

1. Elastic shakedown: A finite amount of plastic deformation accompanied by a change in residual stress, occurs within the first (or first few) load cycles, after which the response of the structure remains elastic.
2. Plastic shakedown: The structure is subjected to equal, alternating plastic strains over each load cycle such that the net plastic deformation is zero. No plastic strains are accumulated and failure occurs by low cycle fatigue.
3. Ratcheting: A cyclic load causes net increments in plastic strain until gross plastic deformation and plastic collapse occur.

Annealing, uniaxial deformation and cyclic deformation are all processes that may be used convert to elastic residual strains into plastic strains through deformation of the material (Totten *et al.*, 2002). The transformation of elastic strains to plastic strains occurs by dislocation slip between layers of the crystal lattice microstructure of the material. Residual stress relaxation is anisotropic in tension and compression where the relaxation rate of residual stress occurs more rapidly in tension than in compression (Totten *et al*., 2002). Totten *et al*. (2002) show that where a material is subjected to cyclic uniaxial cyclic loading, all residual stress relaxation occurs in the first load cycle unless the magnitude of the load is greater than the yield stress of the material. The level of residual stress in a test speciment for several different magnitudes of applied load is plotted against number of load cycles in Figure 2.11 for AISI 4140 steel which has a yield stress of 400 MPa.

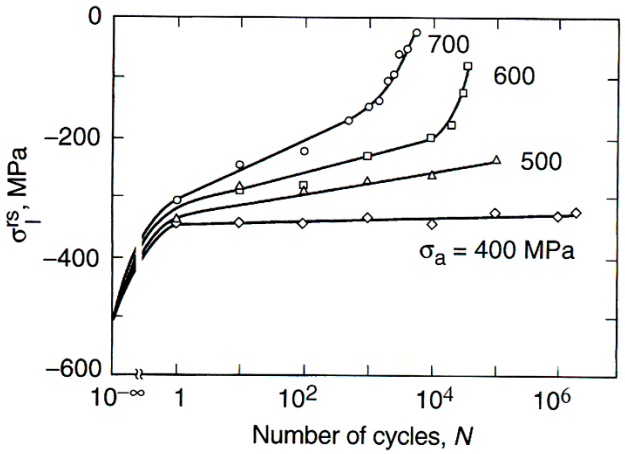

Figure 2.11, Dependence of residual stress relief on number of load cycles for various magnitudes of load (Totten *et al.*, 2002)

In a paper on the structural analysis of an aluminum fast catamaran, Paik *et al.* (2005) reported results of experiments carried out on welded aluminum stiffened panels made

from both 5083 and 8383 aluminum alloys with yield stresses of 236MPa and 244MPa respectively. Residual stresses and initial deflections in the stiffened plates were measured and an average compressive residual stress of approximately 12% of the yield stress was found which is similar to average levels of compressive residual stress in steel plates. Their experimental program included model tests performed to investigate shakedown of residual stress in welded aluminum plates. For each of the two materials, two plates of equal size were joined by a butt weld and subjected to a cyclic three-point load causing both positive and negative bending. The maximum deflection at the center of the plates was 9mm, resulting in extreme fiber stresses of approximately 208 MPa. The specimens made from 5083 and 5383 aluminum alloys were subjected to 3 and 5 load cycles respectively, after which 36% and 33% reductions were in compressive residual stress were measured for the 5083 and 5383 aluminum alloy plates, respectively. The tensile residual stresses were reduced by 21% and 7.6%, respectively. These findings suggest that in-service cyclic loading may result in a significant reduction in residual stresses in stiffened plates and bring to light the need to consider this reduction when incorporating the effects of residual stress in hull girder ultimate strength evaluation.

2.9 The Physics of Arc Welding

Electric arc welding is the most common method of fusion welding. An electric field between the positive anode and negative cathode accelerates a layer of surface electrons towards the anode through a high temperature shielding gas (e.g. argon or helium). The high temperature of the gas causes its atoms to emit electrons, ionizing the gas and

making it electrically conductive. Further ionization is caused as the electrons from the cathode collide with the atoms of the shielding gas imparting more energy to them, causing them to emit more electrons.

The arc is surrounded by a magnetic field that directs the charged particles towards the center of the arc localizing it on a spot on the anode and cathode. At the anode and cathode, temperatures reach 3000 °C to 4000 °C causing the electrode and the workpiece to melt and droplets of the electrode material are deposited on the workpiece. The base metal is fused almost instantaneously and a pool of molten metal forms and expands. The shape of the fusion zone depends on the ratio between current and voltage (Andersen, 2000). A higher current increases the plasma pressure which causes an increased penetration depth as the plasma pushes material on the surface of the weld pool to the rear of the pool where it solidifies.

2.10 Modeling Arc Welding

Rosenthal (1946) was the first to formulate analytical solutions of the heat distribution due to welding during the 1930's and 1940's. He developed solutions for point and line heat sources making it possible to analyze the welding process considering welding parameters such as current, voltage, welding speed and geometry. He assumed quasi steady state conditions meaning that an observer stationed at the heat source sees no change in the temperature around the heat source as it progresses. While Rosenthal's solutions are accurate at locations far removed from the heat source, the assumption of localized point and line heat sources leads to significant error at or near the heat source.

Following Rosenthal's work, several other researchers proposed analytical solutions to the temperature distribution problem using 2D and 3D heat source models that rely on various simplifying assumptions. Wells (1952) considered a 2D moving rectangular heat source with a uniform distribution of heat. Eager and Tsai (1983) considered a 2D heat source with a Gaussian distribution of heat assuming no convective or radiative heat flow, constant thermal material properties and a quasi-steady-state semi-infinite medium. A double ellipsoidal moving heat source considered by Nguyen *et al.* (1999) considering heat transfer by conduction only was found to predict temperatures in good agreement with experimental measurements.

Until the emergence of high speed computer technology, analytical techniques were preferred to numerical methods for the analysis of welding due to the immense amount of calculation required to solve even the most basic problems using numerical methods. The use of numerical methods to analyze welding physics has seen rapid growth since the early 1970's when computer technology made possible the timely numerical solution of complicated problems. Numerical techniques have the advantage that they are able to predict the temperature field during welding and the associated residual stress and distortion without having to make many of the simplifying assumptions used in analytical solutions. The finite element method (FEM) is the most commonly used technique for this purpose. Using the FEM, heat transfer can be simulated accurately, allowing the transient temperature field associated with a moving heat source to be determined. This temperature field can subsequently be applied as a load in a structural analysis from which the associated stresses and deformations are determined.

Welding is a highly nonlinear phenomenon involving several coupled physical processes. A complete simulation involving all of these processes is quite complicated and there are still details that are not fully understood. Furthermore, to include all of the physical processes occurring during welding in a numerical model would require significant computational resources. Fortunately, the couplings between some of the processes are weak enough that they can either be neglected or simplifying assumptions can be made to incorporate their effects in a model with a lesser degree of coupling between fields. Welding is commonly divided into the fields of mechanics, microstructure, heat flow and fluid dynamics. A summary of the various coupled physical processes and the strength of these couplings is presented by Anderson (2000) as follows:

Table 2.2, Coupling of physical processes occurring during welding

Description	Strength
Temperature-dependent microstructural properties	Strong
Thermal properties depend on microstructure	Medium
Latent heat of phase change	Medium
Stress state affects phase change	Weak
Mechanical properties depend on microstructure	Strong
Phase changes yield volumetric strain	Strong
Heat generated by deformation	Weak
Thermal expansion	Strong

The focus of a typical welding simulation is the determination of the temperature field and the associated strain field. With this in mind, the following simplifying assumptions may be made:

1. Microstructural changes are accounted for by specifying temperature dependent material properties.
2. The effect of the stress state on phase change is not included, as it only needs to be considered in a very detailed analysis of the weld pool dynamics.
3. The heat generated by deformation is negligible in comparison to the heat generated by the moving heat source and so may be omitted.

Tall (1964) presented one of the first numerical analyses of welding where the mechanical analysis was one-dimensional and the thermal analysis employed a two-dimensional analytical solution. Since then, research on the mechanical effects of welding using the finite element method has been carried out in many studies. Most early models relied on a number of idealizations and assumptions and initially were fairly crude due to a lack of computational resources. Computational cost in early research was reduced by reducing the problem from three-dimensions down to two or one.

In the early 1970's, the first two-dimensional finite element welding analyses were produced by Iwaki and Masubuchi (1971), Ueda and Yamakawa (1971), Fujita *et al.* (1972), Hibbitt and Marcal (1973) and Friedman (1975). Two-dimensional analysis is typically done under plane strain conditions where the weld is divided into a number of

slices perpendicular to the direction of welding as shown Figure 2.12. A result of the plane strain condition is that the slices are assumed not to interact with each other, therefore longitudinal displacements and heat flow are zero. This assumption results in inaccuracies such as non-zero net longitudinal residual stresses after cooling.

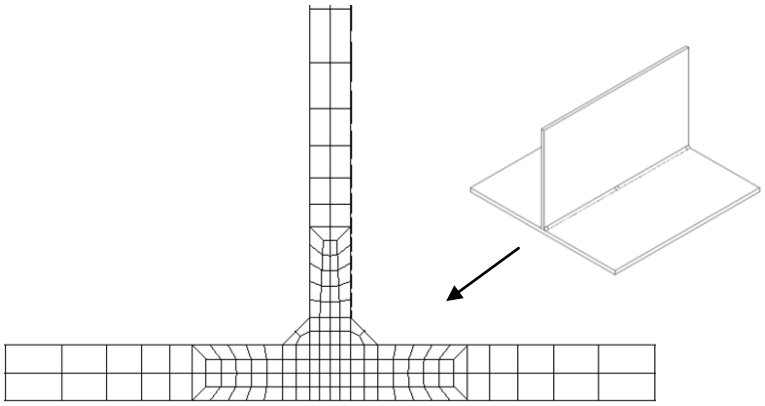

Figure 2.12, 2D finite element model

Full three-dimensional models have been used by several researchers including Deng *et al.* (2007, 2008) and Andersen (2000) to predict welding-induced distortion and residual stress. Solid elements are usually used in the vicinity of the weld where temperature gradients through the thickness are most pronounced. To reduce the number of degrees of freedom in the model and thus to save computing time, shell elements may be used in the far field region where the resolution provided by solid elements is not required. Due to the computationally expensive nature of three-dimensional welding simulations, they are typically limited to the analysis of relatively small structural components. There are several publications such as that by Deng *et al.* (2007) where welding-induced distortions predicted by finite element models are shown to agree well with experimental data.

Many authors have made use of the element birth and death technique in finite element simulations of welding. This typically involves multiplying the stiffness of inactive elements by a severe reduction factor and resetting any strains associated with those inactive elements to zero after the solution so that they are activated in a strain-free state. Recently, Fanous *et al.* (2003, 2003, 2005) introduced the element interaction technique and the element movement techniques. In the element movement technique, the elements of the weld pool are separated from the base plate and gap elements are introduced between the elements of the weld and those of the base plate. As the weld is deposited, the weld elements are moved towards the base plate and the interaction between the elements is controlled by the gap elements which conduct more heat as the elements move closer together. Constraint equations are used in the same manner during the structural analysis to control the structural interaction between the elements. The element interaction technique is used to overcome several shortcomings of the movement technique when simulating a fillet weld. This method uses surface-to-surface interaction between the elements of the weld pool and base metal instead of node-to-node interaction as in the element movement method. For more information on the development of finite element welding simulation, the reader is referred the comprehensive review published by Lindgren (2001, 2001, 2001).

2.11 The Heat Equation

Fourier's law states that the rate of heat flow through a material is directly proportional to both the area of the section orthogonal to the direction of heat flow and to the temperature

gradient in that direction. The heat equation, based on Fourier's law is derived here in one dimension, but can easily be extended to a more general three-dimensional case. Fourier's law for one-dimensional heat flow is expressed by:

$$q(x,t) = -\kappa\left(\frac{dT}{dx}\right) \tag{2.52}$$

where $q(x,t)$ is the heat flow, κ is the thermal conductivity and T is the temperature.

Heat flux is also related to mass, m and temperature by:

$$q(x,t) = cmT(x,t) \tag{2.53}$$

where c is the volumetric specific heat of the material.

Consider a differential length of a homogeneous, insulated rod from x to $x+\Delta x$ with cross-sectional area A. If the density of the material is denoted by ρ the then the mass of the small volume is:

$$\Delta m = \rho A \Delta x \tag{2.54}$$

Substituting Eqn. (2.54) into Eqn. (2.53) gives the equivalent heat for the volume element:

$$q = c\rho A \Delta x T \tag{2.55}$$

For the insulated rod, the rate of change of energy is the difference between the rate of heat input and output:

$$\frac{dq}{dt} = q_{in}\left(x,t\right)A - q_{out}\left(x+\Delta x,t\right)A \tag{2.56}$$

The rate of change of energy can also be found by differentiating Eqn. (2.55):

$$\frac{dq}{dt} = c\rho A\Delta x\frac{dT}{dt} \tag{2.57}$$

which, combined with Eqn. (2.56) gives:

$$\rho cA\Delta x\frac{dT}{dt} = A\left[q\left(x,t\right) - q\left(x+\Delta x,t\right)\right] \tag{2.58}$$

Dividing by Δx and A:

$$\rho c\frac{dT}{dt} = \frac{q\left(x+\Delta x,t\right) - q\left(x,t\right)}{\Delta x} \tag{2.59}$$

The limit as $\Delta x \to 0$ of the right hand side of Eqn. (2.59) is the derivative of q with respect to x, giving:

$$\rho c\frac{dT}{dt} = \frac{dq}{dx} \tag{2.60}$$

Finally, using Fourier's law of heat conduction, Eqn. (2.52), the heat equation is obtained:

$$\rho c\frac{dT}{dt} = \kappa\frac{d^2T}{dx^2} \tag{2.61}$$

which can be generalized to give the three-dimensional heat equation:

$$c\frac{\partial T}{\partial t} = k_x \frac{\partial^2 T}{\partial x^2} + k_y \frac{\partial^2 T}{\partial y^2} + k_z \frac{\partial^2 T}{\partial z^2} \tag{2.62}$$

where $k = \frac{\kappa}{\rho}$.

2.12 Welding Simulation by the Finite Element Method

The magnitude and distribution of welding-induced residual stresses and distortions are affected by many factors including geometry, material properties and welding procedures. Although welding-induced residual stress and distortion may be measured experimentally using laser measuring devices and methods such as x-ray diffraction and the method of sectioning (Galambos, Guide to stability design criteria for metal structures, 1998), these methods are time consuming and the accuracy is often subject to the precision of the devices and measuring procedures. As an alternative to experimental methods, finite element analysis has become an accepted method for predicting 3D residual stress and distortion fields produced by welding. In most cases, this is accomplished by a two-step nonlinear finite element analysis performed as follows:

3) Transient thermal analysis in which the time-dependant temperature distribution is determined.
4) Temperatures from thermal analysis are applied as loads in a structural analysis yielding the three-dimensional residual stress and distortion fields.

2.12.1 Thermal Finite Element Analysis

2.12.1.1 Fundamentals

The thermal analysis is used to determine the temperature distribution within the problem domain Ω. Within this domain, the rate of heat flow per unit area **q,** is written in terms of its Cartesian components as:

$$\mathbf{q}^T = \left[q_x, q_y, q_z \right] \tag{2.63}$$

For a steady state problem continuity requires that:

$$\frac{\partial q_x}{\partial x} + \frac{\partial q_y}{\partial y} + \frac{\partial q_z}{\partial z} + Q = 0 \tag{2.64}$$

where Q is the volumetric heat generation rate. Using the gradient operator ∇, Eqn. (2.64) can be written:

$$\nabla^{\mathbf{T}} \boldsymbol{q} + Q = 0 \tag{2.65}$$

The rate of heat flow is related to the temperature gradient by Fourier's law which is expressed in matrix form as:

$$\boldsymbol{q} = \begin{Bmatrix} q_x \\ q_y \\ q_z \end{Bmatrix} = -\kappa \begin{Bmatrix} \dfrac{\partial T}{\partial x} \\ \dfrac{\partial T}{\partial y} \\ \dfrac{\partial T}{\partial z} \end{Bmatrix} = -\kappa \nabla T \tag{2.66}$$

where κ is a three by three diagonal matrix of thermal conductivities. Substitution of Eqn. (2.66) into Eqn. (2.65) gives the following equation for the temperature distribution over the domain Ω:

$$-\nabla^T \boldsymbol{k} \nabla T + Q = 0 \tag{2.67}$$

which can be rearranged to give the heat equation :

$$k_x \frac{\partial^2 T}{\partial x^2} + k_y \frac{\partial^2 T}{\partial y^2} + k_z \frac{\partial^2 T}{\partial z^2} + Q = 0 \tag{2.68}$$

For a transient thermal problem such as calculation of the temperature distribution during welding, the temperature distribution is not static, but changes with time and an additional term must be added to the right hand side of Eqn. (2.68) giving:

$$k_x \frac{\partial^2 T}{\partial x^2} + k_y \frac{\partial^2 T}{\partial y^2} + k_z \frac{\partial^2 T}{\partial z^2} + Q = c \frac{\partial T}{\partial t} \tag{2.69}$$

Either k or c in Eqn. (2.69) may be a function of T, making the equation nonlinear. Solution of Eqn. (2.69) requires that the initial temperature $T_0(x,y,z)$ be specified. Also, either the natural or essential boundary conditions must be specified. The natural and essential boundary conditions as given by Goldak *et al.* (1984) are respectively:

$$T(x,y,z,t) = T_1(x,y,z,t) \tag{2.70}$$

$$k_n \frac{\partial T}{\partial x} + q + \alpha\left(T - T_0\right) + \sigma\varepsilon\left(T^4 - T_0^4\right) = 0 \tag{2.71}$$

where k_n is the thermal conductivity normal to the surface, q is a prescribed heat flux, α is the convection heat transfer coefficient, σ is the Stefan-Boltzman constant, ε is the emissivity of the material, T_0 is the ambient temperature and T_1 the surface temperature. Eqn. (2.70) represents a prescribed surface temperature and Eqn. (2.71) accounts for heat loss on the surface due to convection and radiation.

Eqn. (2.69) may be solved using the finite element method where the temperature field within each element containing n nodes is approximated by nodal temperatures T_i and polynomial interpolation functions N_i such that:

$$T(x,y,z,t) = \sum_{i=1}^{n} N_i(x,y,z) T_i(t) \tag{2.72}$$

Substitution of Eqn. (2.72) into Eqn. (2.69) results in a system of n algebraic equations. There is some error in the solution referred to as the residual due to the fact that Eqn. (2.72) is an approximation to the exact solution. The residual is minimized using Galerkin's method resulting in a system of nonlinear algebraic equations of the form:

$$\mathbf{KT} = \mathbf{R} \tag{2.73}$$

where **K** is the thermal conductivity or stiffness matrix, **T** is the vector of nodal temperatures (or **U** for displacements) and **R** is the vector of applied loads. The nonlinear system of equations is linearized using the concept of the directional derivative and solved by an iterative numerical algorithm such as the Newton Raphson method to yield the nodal temperatures.

2.12.1.2 Heat Source Modeling

The choice of how to represent the welding heat source in a finite element model is dependent on the type of welding and the scope of the investigation. If the analysis is to be so accurate as to predict the size and shape of the heat affected zone (HAZ) and fusion zone (FZ), a detailed model of the welding heat source must be used. Consequently, the finite element mesh in the vicinity of the heat source must be relatively dense, limiting the size of the model that can be solved in a practical amount of time. In many cases, the heat source model can be simplified allowing for a coarser mesh, hence a larger model. In larger models, it is usually not necessary to predict the size and shape of the FZ. These parameters may be estimated to simplify the heat source model when the objective is to predict the residual stress and deformation of the larger, surrounding structure.

A detailed and comprehensive guide to modeling welding heat sources was published by Goldak *et al.* (1984) who described simple heat source models proposed by Rosenthal (1946) and Rykalin (1974). These are point, line and plane models for which closed form solutions were formulated. These solutions are limited due to the fact that the geometry is idealized (by considering a semi-infinite plate), thermal properties and boundary conditions are constant and heat loss by convection and radiation is ignored. Considerable error exists in the solution in the immediate vicinity of the heat source due to the concentrated heat source model. Solutions are most accurate in regions far from the heat source.

Finite element models can be used to overcome the difficulties associated with analytical solutions and can be used to solve complex, nonlinear problems with various geometries,

nonlinear material properties and boundary conditions. These models are also able to account for the latent heat absorbed or released during phase changes. Models proposed by Westby (1968) and Paley (1975) employed a circular heat source with a constant power distribution. A more accurate model, proposed by Pavelic *et al.* (1969) incorporates a circular heat source with a Gaussian distribution as shown in Figure 2.13. An alternative form of the Pavelic disk suggested by Friedman (1975) and Krutz and Segerlind (1978), is defined relative to a coordinate system that moves with the heat source. The power distribution in this heat source model is given by:

$$q(\xi, y) = \frac{3Q}{\pi c^2} e^{-3\xi^2/c^2} e^{-3y^2/c^2} \tag{2.74}$$

where Q is the heat input and c is the radius of the arc heat flux.

Another heat source model that closely approximates the true distribution of heat during welding is shown in Figure 2.14. This model, developed by Goldak *et al.* (1984) uses a double ellipsoid to represent the volumetric heat from the molten metal droplets and a Gaussian power distribution to represent the heat of the shielding gas plasma on the surface. A Gaussian distribution is also applied to the volumetric heat to represent the distribution of energy by stirring of the molten metal in the weld pool. Although this is an accurate model, it has the disadvantage of requiring a relatively dense mesh in order to represent the more complicated geometry, thus limiting the overall size of the model that can be analyzed.

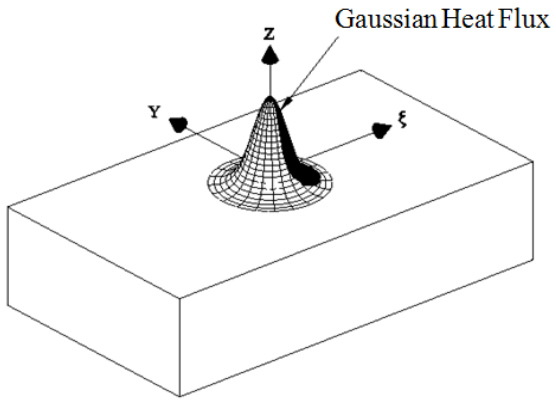

Figure 2.13, Pavelic Disc Heat Source

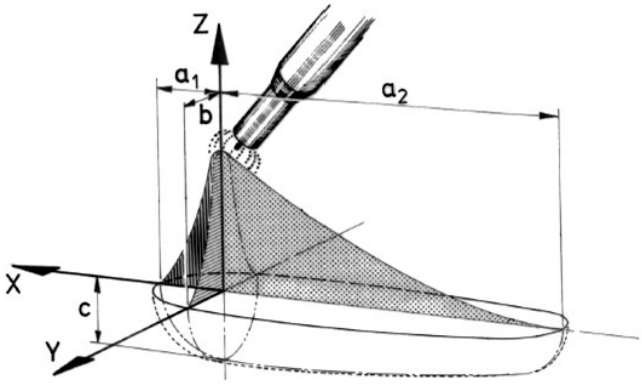

Figure 2.14, Double ellipsoidal power density distribution, Andersen (2000)

The power distribution in the front and rear ellipsoids as given by Andersen (2000) are:

$$q_f(x,y,z,t) = \frac{6\sqrt{3} f_f Q}{a_1 bc\pi\sqrt{\pi}} e^{-3y^2/b^2} e^{-3z^2/c^2} e^{-3\left[x+v(\tau-t)\right]^2/a_1^2} \tag{2.75}$$

$$q_r(x,y,z,t) = \frac{6\sqrt{3} f_y Q}{a_2 bc\pi\sqrt{\pi}} e^{-3y^2/b^2} e^{-3z^2/c^2} e^{-3\left[x+v(\tau-t)\right]^2/a_2^2} \tag{2.76}$$

$$f_f + f_r = 2 \tag{2.77}$$

$$Q = \eta UI \tag{2.78}$$

where q_f and q_r are the power distributions in the front and rear ellipsoids, f_f and f_r are the fraction of total power contained within the front and rear ellipsoids, v,t and τ are the welding speed, time and position of the heat source respectively, η is the welding process efficiency, U is the current and I is the voltage.

2.12.2 Mechanical Finite Element Analysis

2.12.2.1 Fundamentals

The governing differential equations in terms of stresses for a three dimensional solid are:

$$\begin{aligned}
\frac{\partial \sigma_x}{\partial x} + \frac{\partial \tau_{xy}}{\partial y} + \frac{\partial \tau_{xz}}{\partial z} + b_x = 0 \\
\frac{\partial \tau_{yx}}{\partial x} + \frac{\partial \sigma_y}{\partial y} + \frac{\partial \tau_{yz}}{\partial z} + b_y = 0 \\
\frac{\partial \tau_{zx}}{\partial x} + \frac{\partial \tau_{zy}}{\partial y} + \frac{\partial \sigma_z}{\partial z} + b_z = 0
\end{aligned} \tag{2.79}$$

where σ and τ are the normal and shear stress components and $b_x,\ldots$ are body force components. These equations are multiplied by virtual displacements, integrated over the volume and added together to give the weighted residual, which using the Green-Gauss theorem can be written in terms of the principle of virtual displacements as follows (Bhatti, 2005):

$$W = \iiint_V \delta \boldsymbol{\varepsilon}^T \boldsymbol{\sigma} dV - \iint_S \delta \mathbf{u}^T \mathbf{q} dS - \iiint_V \delta \mathbf{u}^T \mathbf{b} dV = 0 \tag{2.80}$$

where $\boldsymbol{\sigma} = (\sigma_x\ \sigma_y\ \sigma_z\ \tau_{xy}\ \tau_{yz}\ \tau_{zx})^T$ are the normal and shear stress components, $\delta\boldsymbol{\varepsilon} = (\delta\varepsilon_x\ \delta\varepsilon_y\ \delta\varepsilon_z\ \delta\gamma_{xy}\ \delta\gamma_{yz}\ \delta\gamma_{zx})^T$ and $\delta\mathbf{u} = (\delta_u\ \delta_v\ \delta_w)^T$ are virtual strains and virtual displacements respectivley, $\mathbf{q} = (q_x\ q_y\ q_z)^T$ are applied surface loads and $\mathbf{b} = (b_x\ b_y\ b_z)^T$ are applied body forces. When the relationship between stresses and strains in Eqn. 2.80 is nonlinear, the right hand side must be linearized using the directional derivative giving a system of algebraic equations of the form:

$$\mathbf{k}_T\Delta\mathbf{d} = -\mathbf{r}_I + \mathbf{r}_q + \mathbf{r}_b \tag{2.81}$$

where $\mathbf{k}_T$ is the tangent stiffness matrix, $\Delta\mathbf{d}$ is the incremental displacement vector, $\mathbf{r}_I$ is the internal force vector for the current solution and $\mathbf{r}_q$ and $\mathbf{r}_b$ are load vectors due to distributed loads and body forces respectively.

2.12.2.2 Thermal Stress

The results of a thermal analysis can be used to specify nodal temperatures in a structural analysis from which the associated strains and stresses are calculated. A change in temperature ΔT within an element results in a uniform strain that depends on the coefficient of thermal expansion, α. Assuming that the material is isotropic, the initial strain vector due to the temperature change in a general 3D solid is expressed as follows (Bhatti, 2005):

$$\boldsymbol{\varepsilon_0} = \begin{Bmatrix} \alpha\Delta T \\ \alpha\Delta T \\ \alpha\Delta T \\ 0 \\ 0 \\ 0 \end{Bmatrix} \tag{2.82}$$

The constitutive relation incorporating initial strain can be written:

$$\boldsymbol{\sigma} = \mathbf{c}\left(\boldsymbol{\varepsilon} - \boldsymbol{\varepsilon_0}\right) \tag{2.83}$$

where **c** is the stress-strain constitutive matrix. The strain energy within an element is:

$$U = \frac{1}{2}\iiint_V \left(\boldsymbol{\varepsilon} - \boldsymbol{\varepsilon}_0^{\mathrm{T}}\right)\mathbf{c}\left(\boldsymbol{\varepsilon} - \boldsymbol{\varepsilon}_0\right)dV \tag{2.84}$$

which can be expanded to give:

$$U = \frac{1}{2}\iiint_V \boldsymbol{\varepsilon}^{\mathrm{T}}\mathbf{c}\boldsymbol{\varepsilon}dV - \frac{1}{2}\iiint_V \boldsymbol{\varepsilon}_0^{\mathrm{T}}\mathbf{c}\boldsymbol{\varepsilon}dV - \frac{1}{2}\iiint_V \boldsymbol{\varepsilon}^{\mathrm{T}}\mathbf{c}\boldsymbol{\varepsilon}_0 dV + \frac{1}{2}\iiint_V \boldsymbol{\varepsilon}_0^{\mathrm{T}}\mathbf{c}\boldsymbol{\varepsilon}_0 dV \tag{2.85}$$

Since the last term of Eqn. 2.85 contains only known terms, it will vanish when the potential energy is minimized and so may be omitted. Also, since the constitutive matrix, **c** is symmetric; the second and third terms are equal and can be combined giving the following expression for the effective strain energy:

$$U_e = \frac{1}{2}\iiint_V \boldsymbol{\varepsilon}^{\mathrm{T}}\mathbf{c}\boldsymbol{\varepsilon}dV - \iiint_V \boldsymbol{\varepsilon}_0^{\mathrm{T}}\mathbf{c}\boldsymbol{\varepsilon}dV \tag{2.86}$$

Making the substitution:

$$\boldsymbol{\varepsilon} = \mathbf{B}^{\mathrm{T}}\mathbf{d} \tag{2.87}$$

Eqn. (2.86) becomes:

$$U_e = \frac{1}{2}\mathbf{d}^{\mathrm{T}} \iiint_V \mathbf{BcB}^{\mathrm{T}} dV\mathbf{d} - \iiint_V \boldsymbol{\varepsilon}_0^{\mathrm{T}}\mathbf{cB}^{\mathrm{T}} dV\mathbf{d} \tag{2.88}$$

$$= \frac{1}{2}\mathbf{d}^{\mathrm{T}}\mathbf{kd} - \mathbf{r}_{\varepsilon}^{\mathrm{T}}\mathbf{d} \tag{2.89}$$

where $\mathbf{k} = \iiint_V \mathbf{BcB}^{\mathrm{T}} dV$ is the element stiffness matrix and $\mathbf{r}_{\varepsilon} = \iiint_V \boldsymbol{\varepsilon}_0^{\mathrm{T}}\mathbf{cB}^{\mathrm{T}} dV$ is the external load vector due to the thermal strain. Once the effective potential energy is minimized with respect to the unknown displacements **d**, Eqn. (2.89) reduces to the familiar form:

$$\mathbf{kd} = \mathbf{r}_{\varepsilon} \tag{2.90}$$

Chapter 3 - Effect of Welding Sequence on Residual Stress and Distortion in Flat-Bar Stiffened Plates

Liam Gannon, Yi Liu, Neil Pegg, Malcolm J. Smith

Published in Marine Structures: Gannon, L. G., Liu, Y., Pegg, N. G., & Smith, M. J. (2010). Effect of welding sequence on residual stress and distortion in flat-bar stiffened plates. *Marine Structures*, *23;* 385-404.

3.1 Abstract

Numerical simulation based on finite element modelling is used to study the influence of welding sequence on the distribution of residual stress and distortion generated when welding a flat-bar stiffener to a steel plate. The simulation consists of sequentially coupled thermal and structural analyses using an element birth and death technique to model the addition of weld metal to the workpiece. The temperature field during welding and the welding-induced residual stress and distortion fields are predicted and results are compared with experimental measurements and analytical predictions. The effect of four welding sequences on the magnitude of residual stress and distortion in both the plate and the stiffener is investigated and their effects on the ultimate strength of the stiffened plate under uniaxial compression are discussed. Appropriate conclusions and recommendations regarding the welding sequence are presented.

3.2 Introduction

The gas metal arc welding (GMAW) process has become a popular method for joining components of steel structures and is the most common joining method used in the shipbuilding industry. Arc welding relies on intense local heating at a joint where a certain amount of the base metal is melted and fused with additional metal from the welding electrode. The intense local heating causes severe thermal gradients in the welded component and the uneven cooling that follows produces residual stresses and distortion. Distortions can be especially problematic in the block assembly method used in shipbuilding. Excessive distortion of welded components results in misalignment of parts and often requires costly remedial measures such as flame straightening and cold bending to reduce distortion to an acceptable level.

In ship construction, where a significant amount of welding is required for the fabrication of stiffened panels, welding-induced residual stresses lead to early yielding in some regions of a stiffened plate reducing the effective cross-sectional area (Deng *et al.*, 2007). For longitudinally stiffened plates subjected to a compressive axial load, the resulting reduction in buckling strength compared to that of the stress free plate may be as much as 25% (Mansour *et al.,* 1990). Smith and Kirkwood (1977) found that residual stresses have a greater influence on the behaviour of slender stiffened panels than in stocky ones and that in extreme cases, they may reduce the compressive strength by nearly 40%. This reduction in capacity of stiffened plates in turn results in a reduction in the overall hull girder ultimate strength. In an analysis of the MV *Energy Concentration,* Gordo *et al.* (1996) found that residual stresses caused a reduction in hull girder ultimate strength of

5.1% and 4.7% respectively in hogging and sagging. The level of longitudinal compressive residual stress in the analysis of MV *Energy Concentration* was taken as 17% of yield stress. Detailed discussion of the influence of residual stress on the strength of stiffened plates is given by Gordo *et al.* (1996), Gordo and Guedes Soares (1993) and Cui *et al.* (2002).

Smith (2008) proposed an idealized welding-induced residual stress distribution used for ultimate strength evaluation of stiffened panels as shown in Figure 3.1, where η usually ranges from 3.0 to 4.5 (Faulkner, 1975). In the region immediately surrounding the weld there are tensile residual stresses equal to the yield stress in both the stiffener and the plate. The remaining portion of the plate is subject to uniform compressive residual stresses. In the stiffener, there is a rapid transition from tensile to compressive residual stress near the base of the stiffener above which the compressive residual stresses decrease linearly to zero at the top of the stiffener.

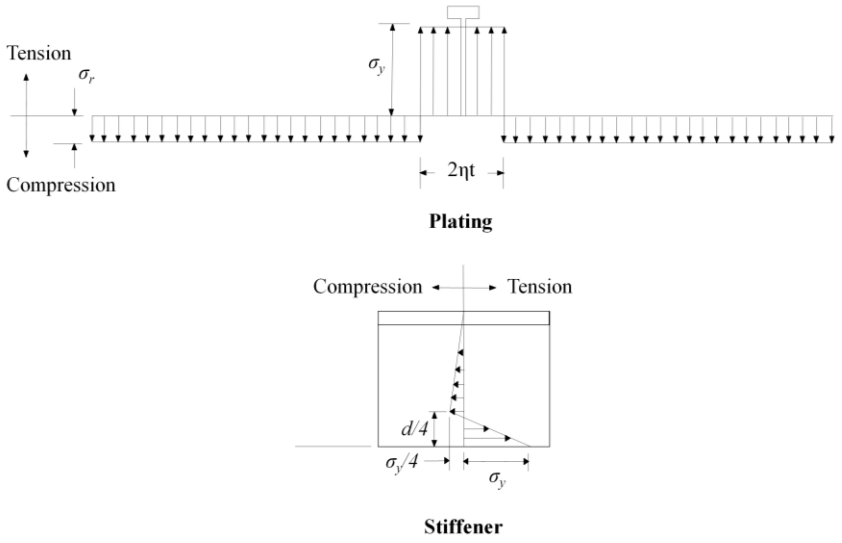

Figure 3.1, Idealized longitudinal residual stress distribution due to welding

Figure 3.2 shows a residual stress distribution suggested by Ohtsubo and Sumi (2000) for use in a benchmark study on the behaviour of stiffened plates under axial compressive load where b_t is the half-width of the tensile residual stress zone in the plate and b_s is the width of the tensile residual stress zone in the stiffener web.

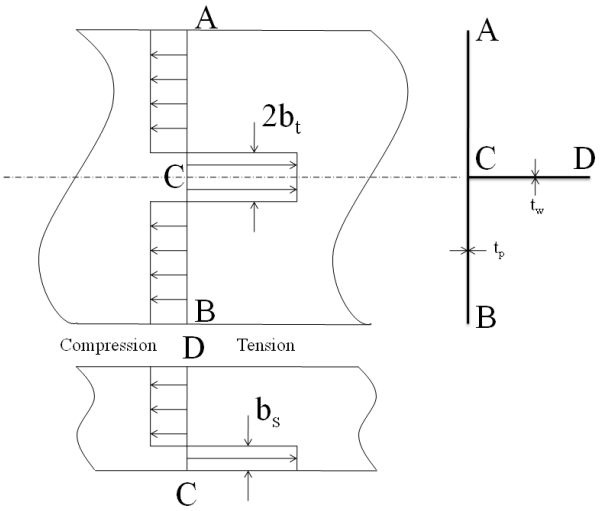

Figure 3.2, Idealized longitudinal residual stress distribution due to welding

Assuming that the residual stresses throughout the complete cross-section are in equilibrium and that the tensile residual stress has reached yield, the compressive residual stress, σ_r is given by:

$$\sigma_r = \frac{2b_t t\sigma_y + b_s t_w \sigma_y}{(b - 2b_t)t + A_s - b_s t_w} \tag{3.1}$$

where:

$$\begin{aligned} b_t &= t_w/2 + 0.26\Delta Q/(t_w + 2t) \\ b_s &= (t_w/t)\times(b_t - t_w/2) \end{aligned} \tag{3.2}$$

$$\Delta Q = 78.8a^2 \tag{3.3}$$

where b is the plate width, t is the plate thickness, t_w is the web thickness, a is the length of the stiffened plate, σ_y is the yield stress and A_s is the stiffener area. All dimensions are in millimeters.

Welding-induced distortions have the potential to reduce the initial stiffness and strength of stiffened plates. ISSC (1979) found that initial deformations reduce the compressive strength of plates and change the failure mode from a sudden event to a more gradual process with a less severe reduction of stiffness in the post collapse regime. Plates of high aspect ratio (a/b) are less sensitive to initial distortions than plates with a low aspect ratio. Based on experimental studies, Dwight and Little (1976) reported that the loss of plate effectiveness due to small initial distortions ($\delta_{o1}/t \leq 0.23$) is negligible for $a/b > 4$ where δ_{o1} is the magnitude of the maximum initial distortion. The strength reduction due to initial distortion is more pronounced when $\delta_{o1}/t > 0.3$ and in severe cases can be as much as 45% (Dwight & Ratcliffe, 1969).

Experimental measurements of fabrication-related distortions in stiffened plate structures have been reported by various researchers (Carlsen & Czujko 1978, Antoniou 1980, Kmiecik *et al.* 1995, Michaleris & DeBiccari 1997). Several empirical formulae based on measured data have been proposed for estimating the maximum magnitude of initial distortion in the plating between stiffeners, δ_{o1} (Paik & Thayamballi 2003, Faulkner 1975, Smith *et al.* 1988). Initial distortions have been categorized as slight, average and

severe by Smith *et al.* (1988) where the maximum vertical deflection between stiffeners is given by:

$$\frac{\delta_{01}}{t} = \begin{cases} 0.025\beta_0^2 & \text{for slight imperfections} \\ 0.1\beta_0^2 & \text{for average imperfections} \\ 0.3\beta_0^2 & \text{for severe imperfections} \end{cases} \tag{3.4}$$

β_0 is the plate slenderness given by:

$$\beta_0 = \frac{b}{t}\sqrt{\frac{\sigma_y}{E}} \tag{3.5}$$

The influence of other parameters such as level of restraint, heat input and plate thickness on the weld-induced residual stress and distortion have also been studied (Cronje, 2005) in an effort to optimize these parameters to minimize distortion. Welding experiments have also been performed with the objective of providing data necessary for validation of numerical models (Deng *et al*. 2007, Deng & Murakawa 2008, Mahapatra *et al.* 2006). Deng *et al.* (2007) welded a flat-bar stiffener to a plate using single pass, continuous fillet welds on both sides of the stiffener. The experimental data was used to validate a finite element welding simulation. The same data is used in the present study to validate the finite element welding simulation.

Numerical models based on the finite element method have been used to supplement experimental investigations, providing insight on welding-induced residual stress fields that are difficult to determine experimentally. One of the earliest numerical predictions of

welding residual stress and distortion used a two-dimensional analytical solution for the thermal analysis and a one-dimensional model for the mechanical analysis where a large number of parallel uniaxial bar elements were used to predict longitudinal residual stress (Tall, 1964). Two-dimensional models were later used by Iwaki and Masubuchi (1971), Ueda and Yamakawa (1971), Fujita *et al.* (1972), Hibbitt and Marcal (1973) and Friedman (1975). The use of 2D models in place of 3D models may affect the accuracy of the solution since the heat flow in the direction of welding is ignored and the plane strain assumption results in non-zero net longitudinal residual stress. Despite the inaccuracy introduced by these assumptions, 2D models are still used for some research due to the reduced computational time compared with 3D models. Neglecting computational considerations, full 3D models are preferred for welding simulation as they allow for consideration of all stress and strain components. Full 3D models often make use of solid elements, however in some cases shell elements are used to reduce the number of degrees of freedom in the model. Lindgren and Karlsson (1988) were among the first to publish numerical predictions of welding residual stress using a 3D model. They used shell elements to model a thin-walled pipe which was later reproduced by Karlsson and Josefson (1990) using solid elements. The results of the two models agreed well with each other, although the predicted residual stresses were higher than experimentally measured values published by Lindgren and Karlsson (1988). A combination of solid and shell elements was first used by Näsström *et al.* (1992). This combination of element types is efficient when through-thickness variations in

temperature and strain are more pronounced in a particular region of the model, such as the region immediately surrounding a weld.

Although three dimensional welding simulations are capable of predicting the complete temperature and strain fields due to welding, the parameters studied in previous research have been limited due to the high computational cost. Extensive parametric studies on welding processes considering heat input, material properties and cross-section dimensions have only recently become practical due to advances in multi-core computing technology (Cronje 2005, Mahapatra *et al.* 2006, Lee & Chang 2007). This paper presents the first known application of three dimensional thermo-elasto-plastic finite element analysis to study the influence of welding sequence on residual stress and distortion in flat-bar stiffened panels.

This paper thus focuses on the influence of welding sequence on residual stress and distortion in flat-bar stiffeners typical in ship hull construction. The welding simulation was carried out using the ANSYS® finite element package and was subsequently validated with experimental results published by Deng *et al.* (2007). The welding simulation consisted of sequential thermal and elasto-plastic structural analyses that were used to evaluate four different welding sequences. The element birth and death feature was used to simulate the addition of molten weld metal as the welding torch progressed along the workpiece. Welding-induced residual stresses and distortions predicted for the four sequences were compared to determine the influence of welding sequence on residual stress and distortion fields.

3.3 Finite Element Modeling

Structural and thermal finite element analyses were performed using ANSYS® (2009) to calculate residual stresses and distortions in a flat-bar stiffened plate resulting from welding the stiffener to the plate. The simulation consisted of two analyses. The first was a transient thermal analysis where the temperature distribution caused by a travelling heat source was determined. The second step consisted of a nonlinear structural analysis that was solved as a series of sequential load steps. Each load step represented an increment in the position of the heat source in the direction of welding. The temperatures from the thermal analysis associated with each load step were applied as loads in the structural analysis. This process was repeated multiple times until the welding was completed.

The plate and stiffener are both made from SM400A shipbuilding steel with a chemical composition given in Table 3.1 (Deng *et al.*, 2007). The plate is 500 mm x 500 mm with a thickness of 9 mm and the stiffener is 300 mm x 500 mm with a thickness of 9 mm. The stiffener is connected to the plate by 6 mm fillet welds deposited on both sides of the stiffener. The geometry of the stiffened plate is shown in Figure 3.3. Four different welding sequences, shown in Figure 3.4, were investigated where the first sequence (Figure 3.4 (a)) is the same as that used in the experiment by Deng *et al.* (2007). Tack welds with a length of approximately 10 mm were first placed on both sides of the stiffener at mid-length and at both ends before the welding procedure. Although the strength of the filler metal has the potential to influence the residual stress distribution, it is assumed in this study that a matching electrode is used. Eight-node, linearly interpolated brick elements were used to mesh the specimen and nonlinear spring

elements were introduced at the interface of the plate and stiffener. These spring elements were assigned a high compressive stiffness and negligible tensile stiffness thus preventing penetration of the stiffener through the plate and allowing sliding and separation at this location.

Table 3.1, Chemical composition of SM400A steel by wt%

Chemical composition (mass %)				
C	Si	Mn	P	S
0.23	-	0.56	<0.035	<0.035

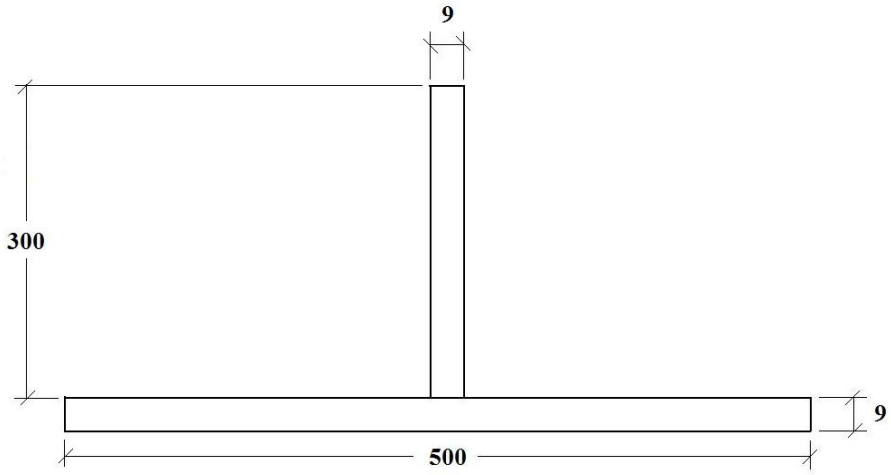

Figure 3.3, Stiffened plate dimensions

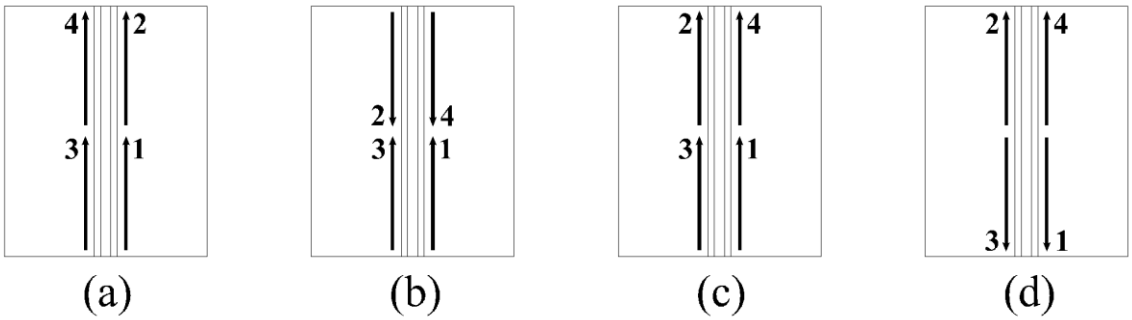

Figure 3.4, Welding sequences

A mesh convergence study revealed that a relatively dense mesh is required through the thickness of the plate in the region surrounding the weld. For the 9 mm plate considered in this study, 12 elements were necessary through the plate thickness at the weld location in order to accurately represent the temperature and strain gradients. In the region away from the location of the weld, the temperature gradient is significantly lower and the mesh was then made less dense in this region to reduce the number of degrees of freedom and thus the time required for solution. A minimum of four elements is used through the thickness of the plate in order to model bending of the plates. The complete model contains approximately 17,000 elements and 19,000 nodes. The finite element mesh is shown in Figure 3.5. The smallest element size used in the mesh was 0.5 mm x 0.75 mm x 10 mm. The specimen was divided into 10 mm long elements along its length. Each model in the present study required 3.5 hrs of computational time using 2 Intel Core i7 920 processors on a 64-bit machine with 6 GB of RAM.

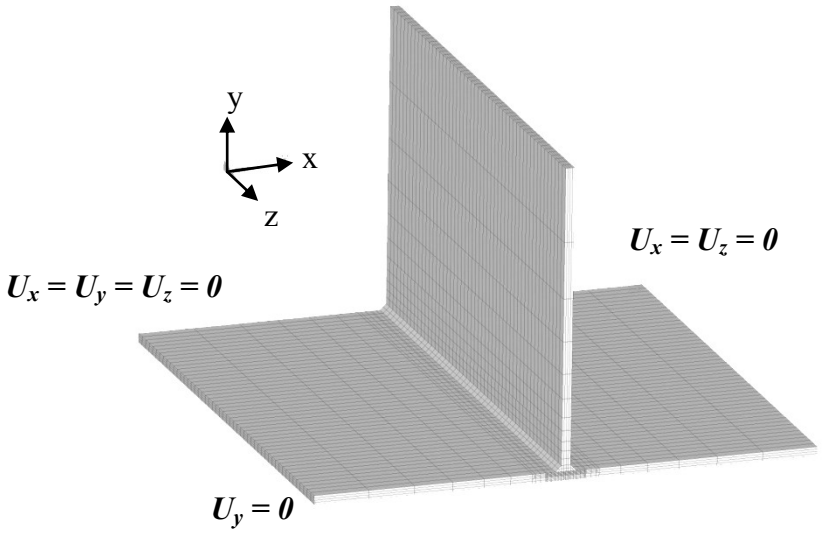

Figure 3.5, Mesh and boundary conditions

3.3.1 Thermal Analysis

A nonlinear transient thermal analysis was conducted to calculate the temperature distribution during welding using the Solid70 eight-node thermal brick element. The heat input was divided into two parts to model the heat flux from the welding torch incident on the surface of the weld and the heat transferred from the molten metal droplets to the workpiece. In this case, 60% of the total heat was considered transferred via the molten metal droplets and 40% by the surface heat flux based on experimentally measured values reported by Allum and Quintino (1985). The surface heat flux was inclined at an angle of 45° so that it was applied normal to the surface of the weld elements. A Gaussian power distribution with an arc radius of 4.24 mm was assumed for the heat flux. The power distribution was defined relative to a coordinate system that was moving with the heat source as shown in Figure 3.6 and is expressed as:

$$q(\xi, y) = \frac{3Q}{\pi c^2} e^{-3\xi^2/c^2} e^{-3y^2/c^2} \tag{3.7}$$

where c is the arc radius and Q is the heat input given by:

$$Q = \eta VI \tag{3.8}$$

where I is the current supplied, V is the voltage across the arc and η is the arc efficiency which is assumed to be 0.8 for CO_2 gas metal arc welding. A summary of welding parameters, adopted from the experimental work of Deng *et al.* (2007) is listed in Table 3.2. User-defined macros were created using the ANSYS® parametric design language to

model the moving heat source and to control the activation of weld elements as the heat source progressed.

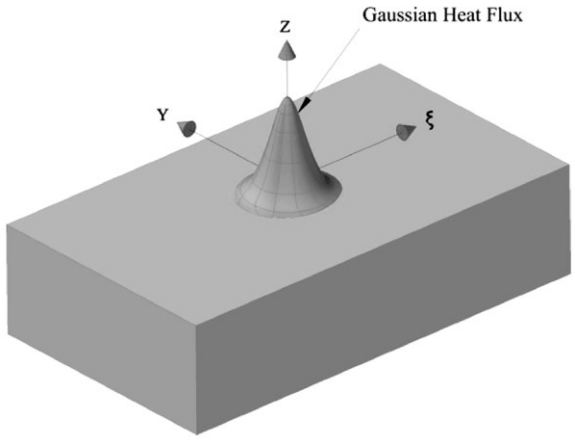

Figure 3.6, Gaussian distributed heat source

Table 3.2, Welding conditions

Weld leg length (mm)	Current (A)	Voltage (V)	Welding speed (mm/min)
6	270	29	400

Heat loss from the surface of the workpiece due to convection and radiation was considered using a temperature dependent film coefficient given by Goldak *et al.* (1984):

$$H = 24.1\times10^{-4}\varepsilon T^{1.61} \tag{3.6}$$

where ε is the emissivity of the surface of the body and is taken as 0.9 for hot-rolled steel (Goldak *et al.,* 1984). In order to account for heat transfer by convection in the weld pool, the thermal conductivity was artificially increased for temperatures above the melting point. The solidification and melting temperatures are 1450°C and 1500°C respectively. The latent heat of fusion is 270 J/g and was incorporated in the material

model by increasing the specific heat at the melting temperature. The thermal material properties, adopted from Deng *et al.* (2008) are shown in Figure 3.7.

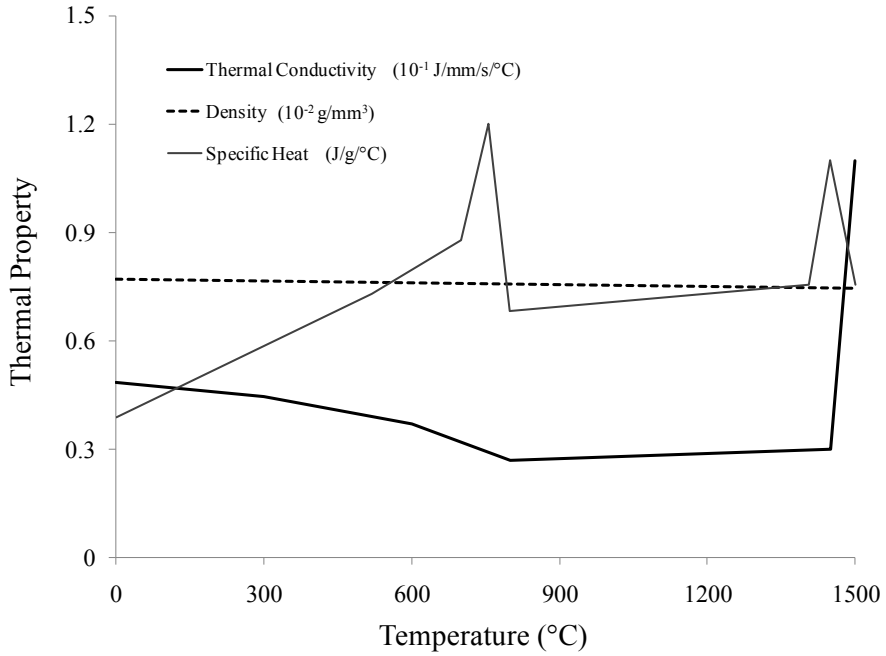

Figure 3.7, Thermal material properties

3.3.2 Mechanical Analysis

The solid model mesh used for the mechanical analysis was the same as that used for the thermal analysis except that the structural element, Solid185, was used for the mechanical analysis in place of the Solid70 thermal element. Since the weld does not fully penetrate the stiffener, the contact between the plate and stiffener was modeled using Combin39 nonlinear spring elements to connect coincident nodes at the plate-stiffener interface. Nonlinear springs were used in place of contact elements to avoid the extensive computation time associated with contact algorithms. The spring elements were given a high compressive stiffness and low tensile stiffness in the direction normal to the plate-

stiffener interface and zero stiffness in the other two orthogonal directions so that sliding and separation were permitted. Temperature dependent mechanical material properties were adopted from Deng *et al.* (2008) as shown in Figure 3.8. An elastic-perfectly-plastic material model is used with von Mises failure criteria and associated flow rule which states that the plastic flow is orthogonal to the yield surface. Nonlinearities due to large strain and displacement are considered. Strain hardening is not included and was also neglected in several past studies (Tall, 1964, Ueda & Yamakawa 1971). Experiments by Karlsson and Josefson (1990) showed a nearly ideal plastic behaviour of material at temperatures above 800 °C. Since most plastic strains during welding occur at high temperature, this indicates that a perfectly plastic behaviour is suitable.

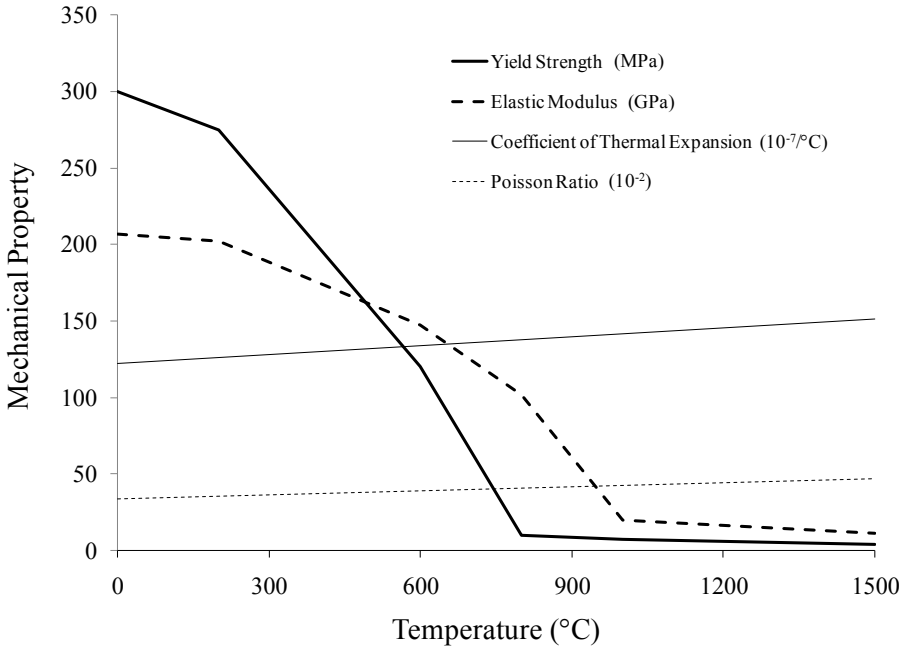

Figure 3.8, Mechanical material properties

The temperature history from the thermal analysis was used as a series of loads in the structural analysis, where each increment of weld deposition made up one load step. All weld elements other than the tack welds were deactivated in the first load step by multiplying their stiffness by a severe reduction factor and re-setting any accumulated strains including plastic strains to zero. This is implemented using the ANSYS® element birth and death feature. In multi-pass welding, this feature can be used to reset the plastic strain to zero for those elements melted during subsequent passes. As the weld progressed, a user-defined subroutine was used to apply loads from the thermal analysis at the corresponding time and to query the average temperatures of the weld elements. Those elements whose average temperature had fallen below the solidification temperature were reactivated, coupling the stiffener to the plate.

The average nodal temperature of each element was applied to that element as a uniform body force. This resolved an inconsistency between the linearly varying strains caused by direct application of the temperature field and the linear shape functions of the structural elements that should permit only constant strain (Lindgren, 2001). The application of constant temperatures to each element also prevented excessive element distortion in areas with a high thermal gradient, thus enhancing solution convergence.

Phase transformations were not considered in the mechanical analysis because the integration point density required to compute phase evolution in the fusion zone and heat affected zone would increase the problem size beyond what can be solved in a reasonable amount of time with currently available computational resources. Furthermore, steels

with low carbon contents have a relatively high martensite start temperature, M_s and as a result the volumetric strain due to the martensitic transformation occurs when the yield stress is low. The result being that for low carbon steels, the volumetric strain due to martensite formation has little effect on the residual stress distribution. This is demonstrated by Deng (2009) who compares two steels with 0.15% C and 0.44% C with martensite start temperatures of 476 °C and 328 °C respectively. He found that there was virtually no difference in the longitudinal residual stress distribution whether or not phase transformation was considered for the low carbon steel. From the chemical composition given in Table 3.1, the steel used in the current study has a martensite start temperature of 423 °C which is relatively close to that of the low carbon steel considered by Deng (2009).

3.3.3 Boundary Conditions

Two different sets of boundary conditions were used for the validation model and the model used to study the effects of welding sequence. For validation of the welding simulation by comparison with published experimental data, boundary conditions consistent with the experimental set-up were used. They were applied such that the plate could deform freely in any direction and rigid body motions were prevented as shown in Figure 3.5. Boundary conditions in the model used to investigate the effects of welding sequence were representative of the level of restraint in stiffened panels in ship hull girders where a panel with multiple evenly spaced stiffeners can be divided into several stiffened plates containing a single stiffener with attached plating. Longitudinal edges

were constrained to remain straight, but free to move in the plane of the plating as suggested by Dow *et al.* (1981). This was achieved by creating a very weak beam element at the mid-span position on the longitudinal edges of the plate. This element introduced a rotational degree of freedom that was used in constraint equations to prevent rotation of the longitudinal edges of the plate about the longitudinal and vertical axes. Simple supports were applied at the ends of the stiffened plate at the centroids of the end cross-sections by constraining displacements along all three coordinate axes at the centroid of one end and the vertical and transverse displacements at the centroid of the opposite end.

3.4 Verification of the Finite Element Model

The finite element model was validated by comparison of predicted deflections with experimental results published by Deng *et al.* (2007). This publication was particularly useful since temperature dependent material properties, essential for accurate welding simulation, were supplied. Although results of several other welding experiments are available, none of these consider flat-bar stiffened plates joined by the GMAW process. The web and flange were first tack welded and then continuous, single pass fillet welds of approximately 6 mm were laid on both sides of the stiffener by a robot welder in the sequence shown in Figure 3.4 (a). During welding, three dimensional photographic measurement was used to measure the deflection of the flange.

In order to ensure that neglecting tack welding in the simulations did not have an overly large influence on the results, the model using welding sequence A was run with and

without simulating tack welding and the resulting out-of-plane distortions in the plate are compared in Figure 3.9. The difference in maximum vertical displacement of the plate at the mid-span cross-section was approximately 3%. There was virtually no difference in the residual stress distribution. A comparison of vertical deflections of the flange at mid-length shown in Figure 3.10 demonstrates good agreement between finite element model predictions using the current model and experimental results. The vertical deflection at the middle of the plate predicted by the finite element model was approximately 6.5 mm. The difference between experimental and predicted angular deflections of the plate to the horizontal was approximately 5.5%. Figure 3.11 shows the deformed shape of the stiffened plate after welding obtained from the finite element model. The residual stress distribution was not reported in the literature and thus the numerical distribution was not compared.

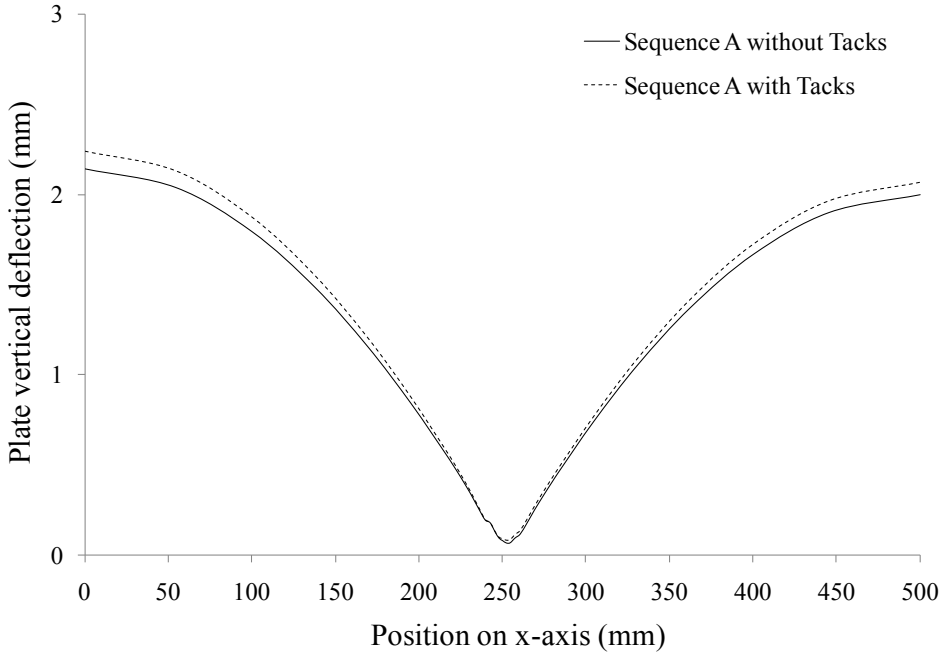

Figure 3.9, Vertical deflection of the plate considering tack welds

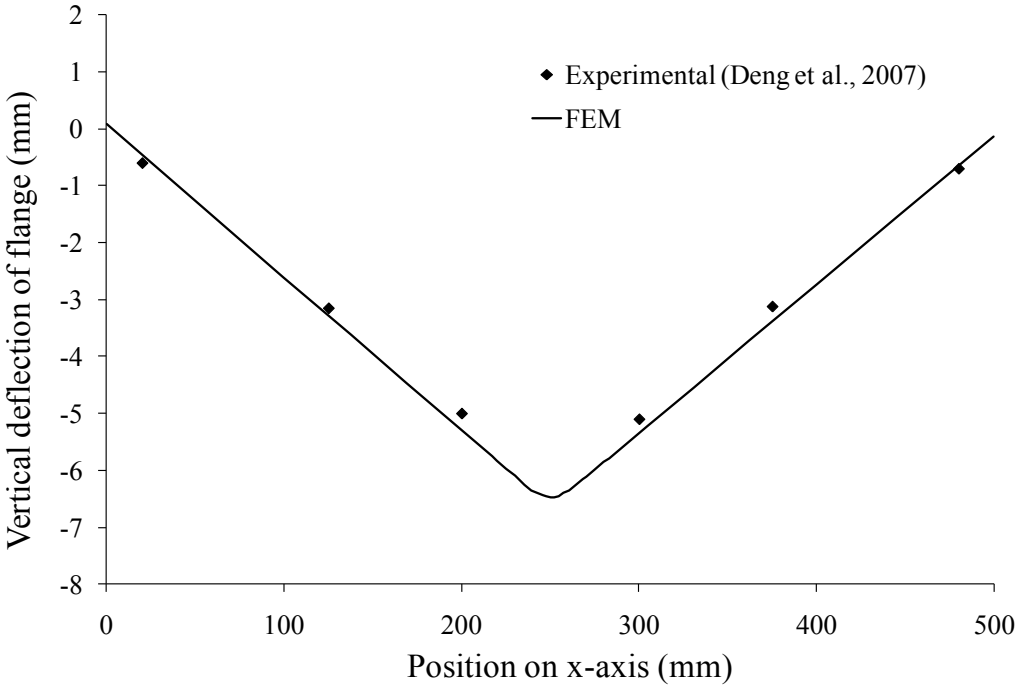

Figure 3.10, Plate vertical deflection distribution at mid-span

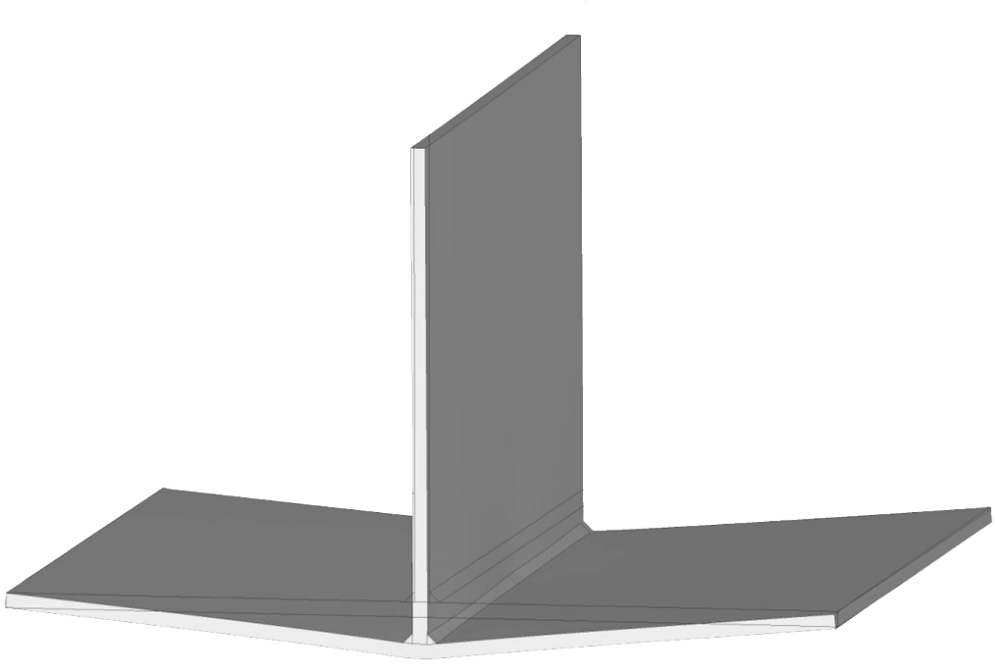

Figure 3.11, Welding deformation predicted by FEM for validation

Figure 3.12 shows the first 250 s of the temperature time-history at points A and B located at the mid-span cross-section as shown in Figure 3.13. Before the heat source reached this section the temperature remained constant at the ambient temperature of 20°C, indicating that the rate of conduction in the direction of welding was low relative to the speed of the moving source. When the heat source reached the cross-section considered, the temperature quickly rose to 1730 °C at point A. The peak temperature at point B was 500 °C and was attained approximately 5 s after the peak temperature at point A. The through-thickness temperature gradient is the mechanism of angular distortion in stiffened plates leading to the familiar hungry horse deformed shape in stiffened panels (Deng *et al.,* 2007). After the maximum temperatures were reached, smaller peaks appeared when the weld was deposited on the other side of the stiffener. The temperature distribution in the stiffened plate (not including the weld) when the heat source first reached the mid-span cross-section is shown in Figure 3.14. The temperature gradient through the thickness of the plate was high near the weld, illustrating the need for a dense mesh in this region. The mesh density through the thickness of the web was made lower than through the thickness of the plate to reduce the number of elements and thus the analysis time. A convergence study showed that the difference in results between using four and eight elements though the web was negligible. Peak temperatures at points A and B predicted by Deng *et al.* (2007) were 1800 °C and 415 °C respectively. The difference in predicted temperatures is attributed to the use of a more dense mesh through the thickness of the plate in the present analysis.

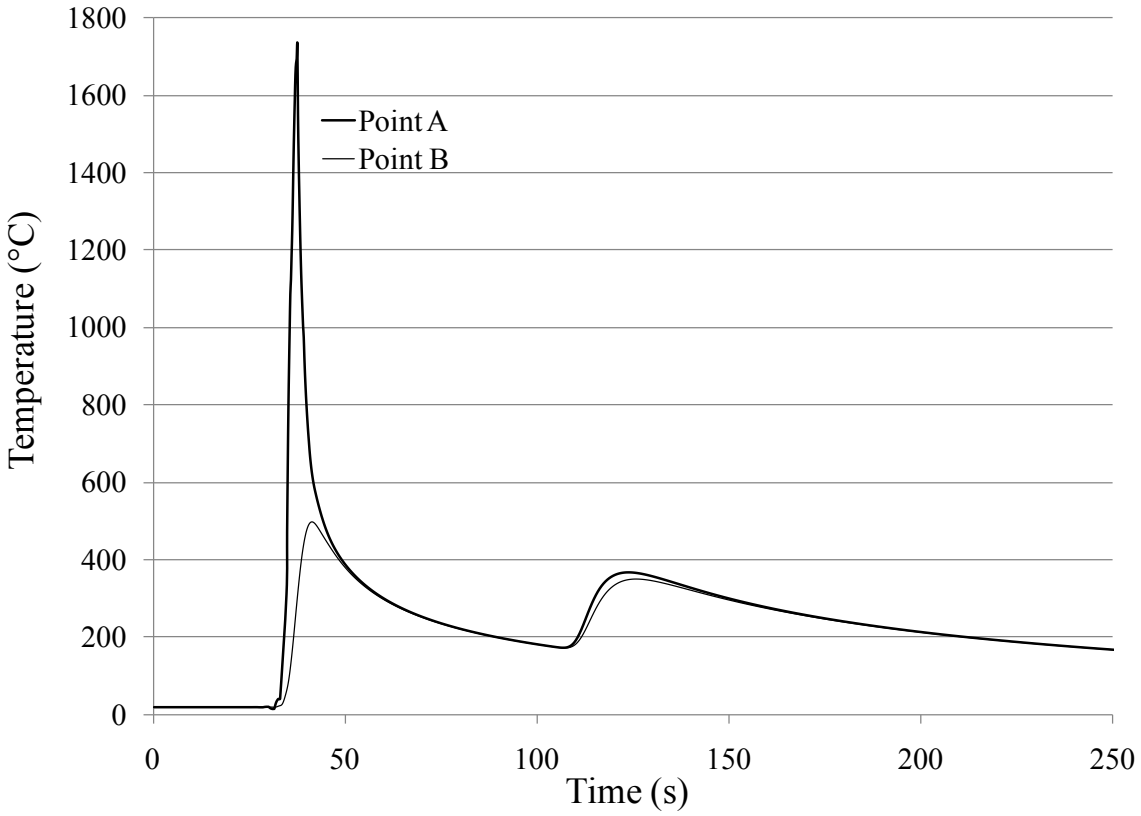

Figure 3.12, Temperature time-histories at points A and B

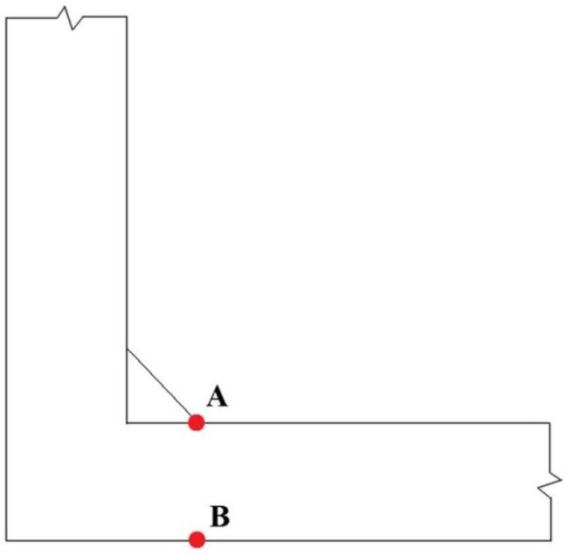

Figure 3.13, Locations for temperature time histories

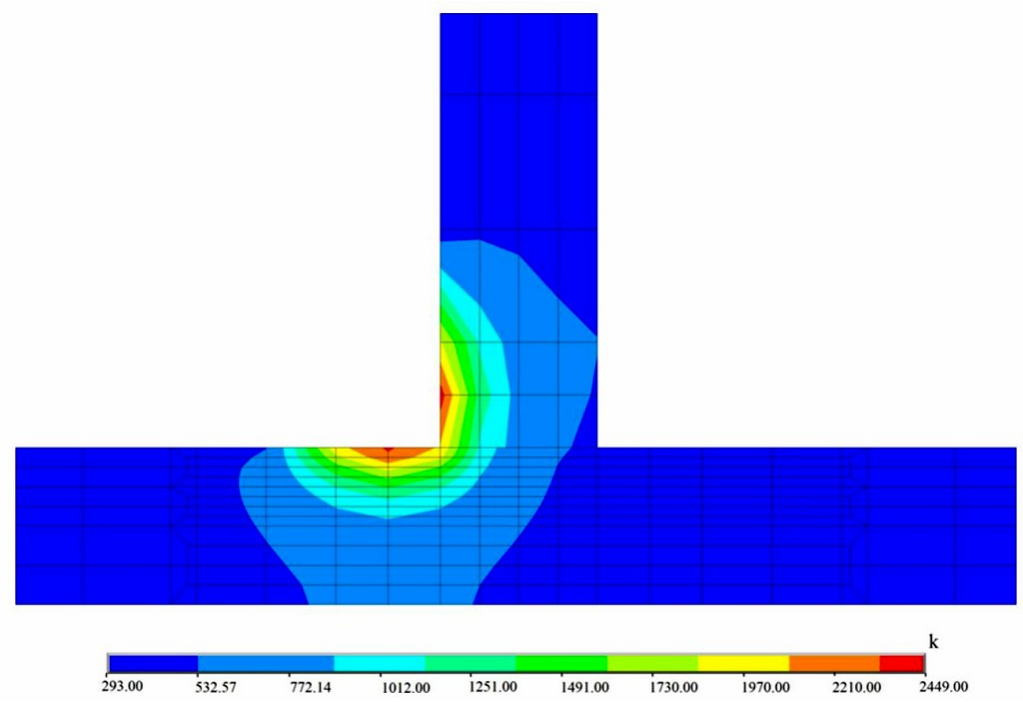

Figure 3.14, Temperature distribution at mid-span cross-section

Overall, the finite element model including both thermal and mechanical procedures has provided simulation results in reasonably good agreement with the experimental measurements. The variations observed between the numerical and experimental results were considered to be within acceptable limits.

3.5 Effect of Welding Sequence on Residual Stress

Although residual stresses caused by welding are three dimensional, the longitudinal component of residual stresses is considered to have the greatest influence on the strength of stiffened plates in ship hulls. Since the load is predominantly applied in a longitudinal direction due to bending of the hull girder, these residual stresses may result in early yielding of some regions of the longitudinally stiffened plates and consequently cause a

reduction in the effective cross-sectional area and moment of inertia leading to the possibility of premature failure.

Figure 3.15 shows the simulated distribution of longitudinal residual stress in the mid-plane of the plate for a transverse section at mid-length for all welding sequences. For comparison, idealized distributions from Figures 3.1 and 3.2 are also plotted. Overall, the numerical results show that high tensile residual stresses equal to the yield stress of 300MPa were present at the location of stiffener attachment acting over a width of approximately three times the plate thickness to each side of the stiffener, corresponding to a value η = 2.8 (Figure 3.1). At this point there is a rapid transition in the residual stress from tension to compression where compressive residual stresses vary in magnitude from -88MPa 30mm from the plate centerline to -36MPa at the plate edges. In general, residual stresses in the plate resulting from welding sequences A and C are of greater magnitude than those resulting from sequences B and D, where the largest difference is approximately 60 percent between maximum compressive residual stresses in the plate at mid-span. The magnitude of residual stresses at other sections along the length are similar to those at mid-span. The longitudinal residual stress distributions used in Figures 3.1 and 3.2 are generally in good agreement with those predicted by the finite element model. Both of these accurately predict the width of the tensile residual stress zone in the plate, giving η = 2.3 and η = 1.9, for the Figure 3.1 and Figure 3.2 distributions, respectively.

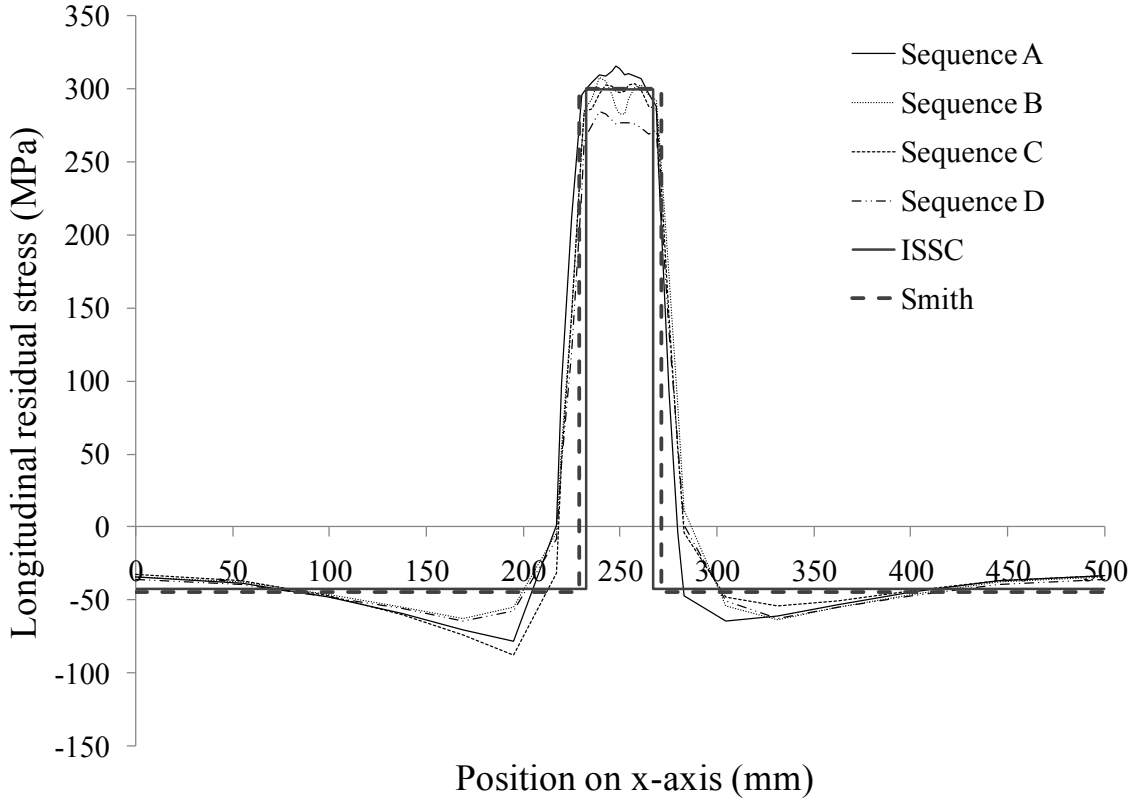

Figure 3.15, Longitudinal residual stress in plate at mid-length

Figure 3.16 shows the distribution of longitudinal residual stress in the mid-plane of the stiffener along with idealized distributions used in Figures 3.1 and 3.2. Numerical results show tensile residual stresses equal to yield near the location of the welds and a rapid transition to compressive residual stress approximately 4 to 5 times the web thickness from the bottom of the web. Welding sequence B resulted in the highest magnitude of both compressive and tensile residual stress in the web. These were -36MPa 70mm from the bottom of the web, and 13MPa at the top of the web, respectively.

The residual stress distributions for the plate and the stiffener were also studied at sections 1 and 3 shown in Figure 3.17. Having distribution patterns similar to section 2, sections 1 and 3 showed that tensile residual stresses at the plate to stiffener junction

reached the yield stress and maximum compressive residual stresses attained values of -97MPa and -60MPa in the plate and web respectively. For all three sections shown in Figure 3.17, welding sequence B was found to result in the highest compressive residual stresses in the web and sequences A and C resulted in the highest residual stresses in the plate. The magnitude and distribution of residual stress predicted by the finite element simulations is consistent with measurements by Nagaraja Rao and Tall (1961) and Nagaraja Rao *et al.* (1961).

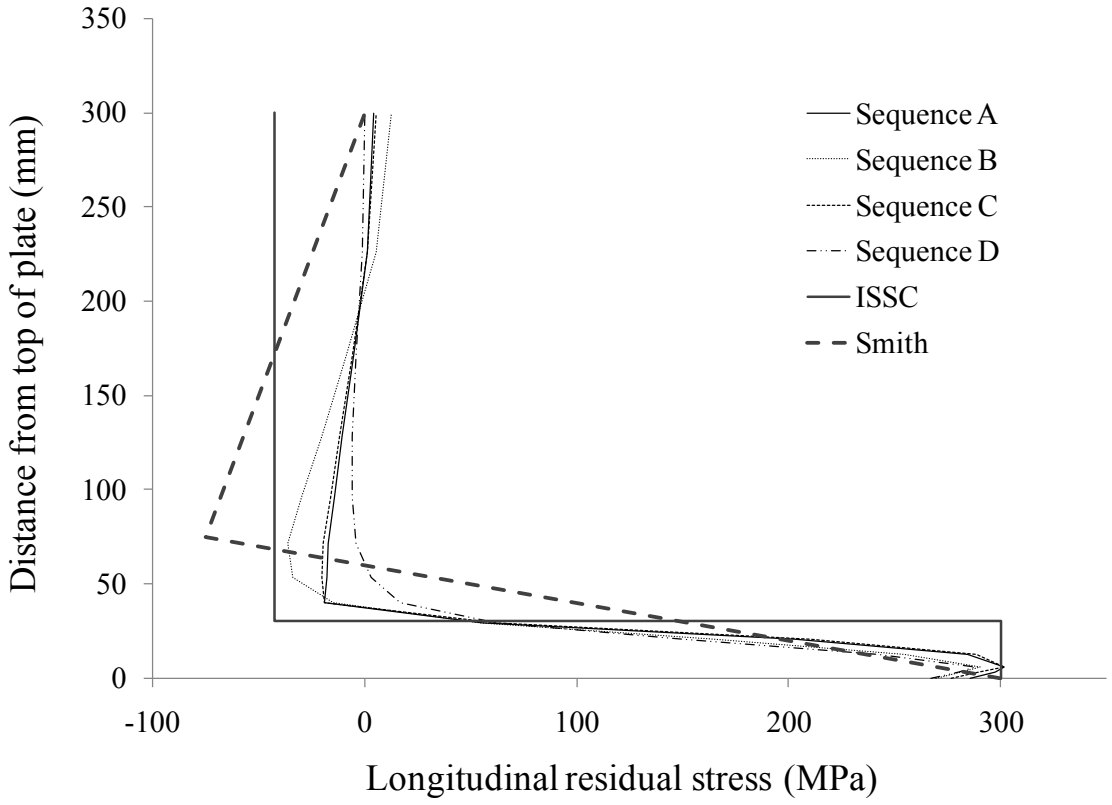

Figure 3.16, Longitudinal residual stress in web at mid-length

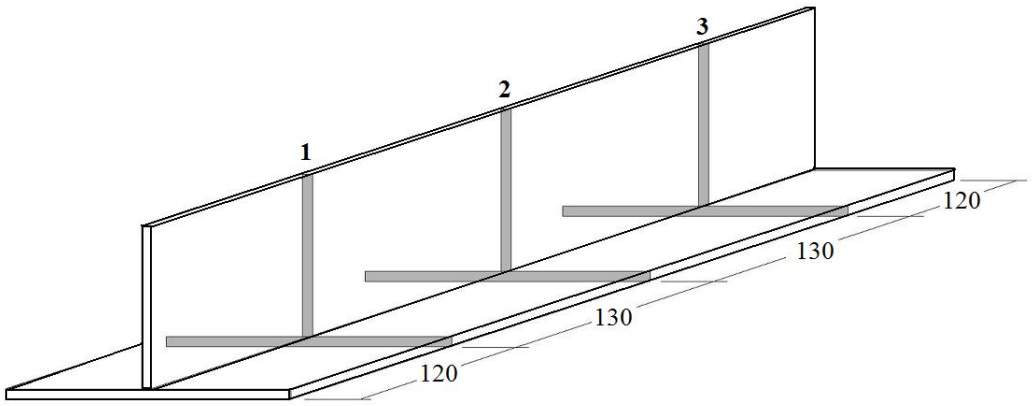

Figure 3.17, Cross-section locations

The residual stress distribution in the web, suggested by Ohtsubo and Sumi (2000) is found to be conservative when compared with the finite element prediction, tending to overestimate the compressive residual stress in the stiffener. The distribution used by Smith (2008) is in better agreement with the finite element prediction. However, the magnitude of maximum compressive residual stress is twice the finite element predicted value. The ideal distribution from Smith (2008) can be made to fit the present finite element residual stress distribution in the web more closely by lowering the maximum compressive residual stress in the web to $\sigma_y/8$ acting at a distance $d/6$ from the bottom of the web. This would also result in an increase in the width of the tension zone in the plate so that it matches numerical distribution of residual stress in the plate more closely, giving $\eta = 2.7$.

3.6 Effect of Welding Sequence on Distortions

Welding of stiffened plates results in distortions in the form of transverse shrinkage, longitudinal shrinkage, longitudinal bending and transverse bending. Bending distortions

are particularly important in this case since they have a significant effect on the ultimate strength of stiffened plates acting as beam-columns.

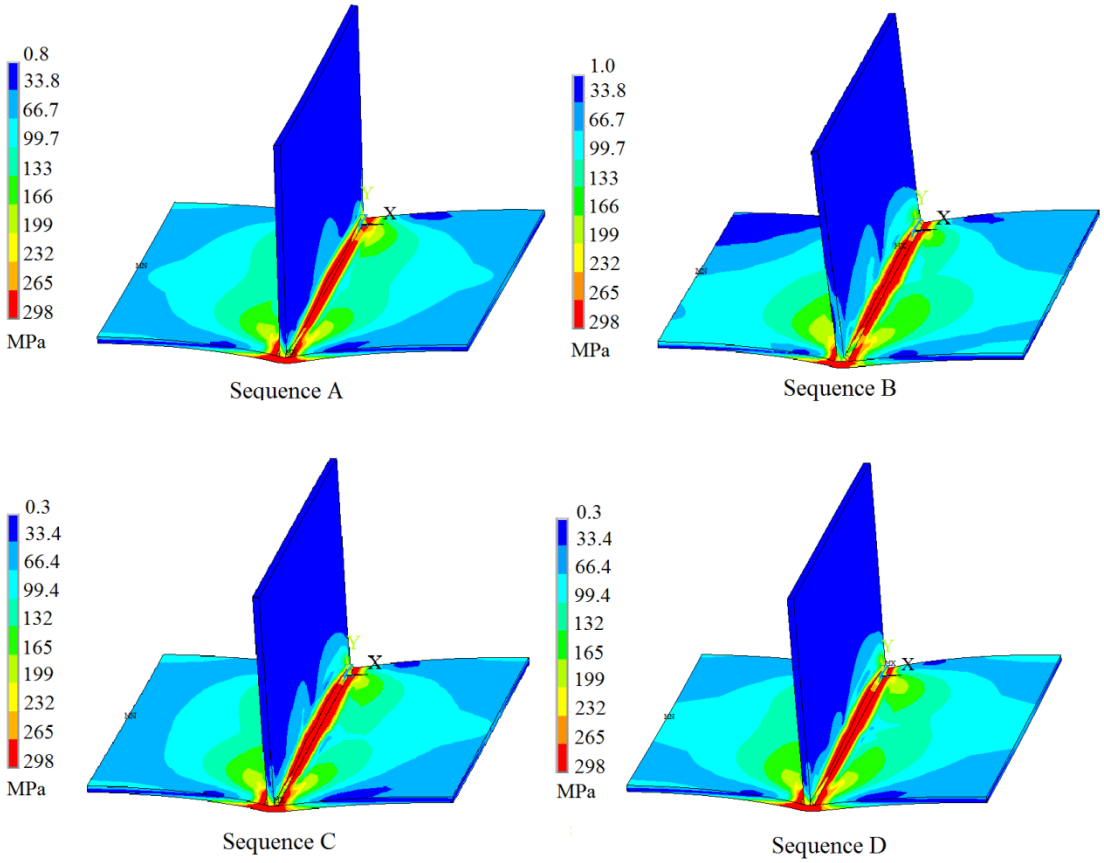

Figure 3.18, Deformed shapes with von-Mises stress contours

Failure of stiffened plates in compression typically occurs in one of four ways: (1) plate-induced failure initiated by buckling of the plate followed by shedding of load to the stiffener, which, depending on the stiffener properties, may result in overall failure soon after plate buckling; (2) stiffener-induced failure due to local buckling of the stiffener web or lateral-flexural buckling of the stiffener. This type of failure is often sudden and followed by a sharp drop in the load-carrying capacity of the stiffened plate due to the

relatively low out-of-plane bending stiffness of the plate acting alone to resist load that is shed onto it following buckling of the stiffener; (3) overall beam-column buckling where the plate and stiffener fail together as a beam-column and (4) failure due to gross section yielding in stocky panels. Figure 3.18 shows an overall view of deformed shapes including Von Mises stress contours after welding for all four welding sequences.

3.6.1 Transverse Bending of the Plate

Mid-plane vertical deflections of the plate at locations 1, 2 and 3 are illustrated in Figure 3.19 for the four welding sequences. For all welding sequences, the plate was deformed such that it assumed the familiar hungry horse shape seen in welded stiffened panels of longitudinally stiffened ship hulls. The different non-symmetric welding sequences resulted in asymmetry of the plate vertical deflection about the stiffener.

Out of plane distortion of the plate contributes to a decrease in the ultimate strength of the plate and consequently, the strength of the stiffened panel (Gordo & Guedes Soares, 1993). The maximum vertical deflection of approximately 2.7mm at the edge of the plate resulted from welding sequence B. This falls between the slight and average levels of imperfection predicted by the empirical relationship of Smith *et al.* (1988). Overall, welding sequence B was found to produce the least favorable vertical distortion in the transverse direction of the plate. The plating vertical deflections predicted by the finite element simulation are similar in magnitude and distribution to those measured by Dow (1991) during the testing of a 1/3 scale frigate cross-section.

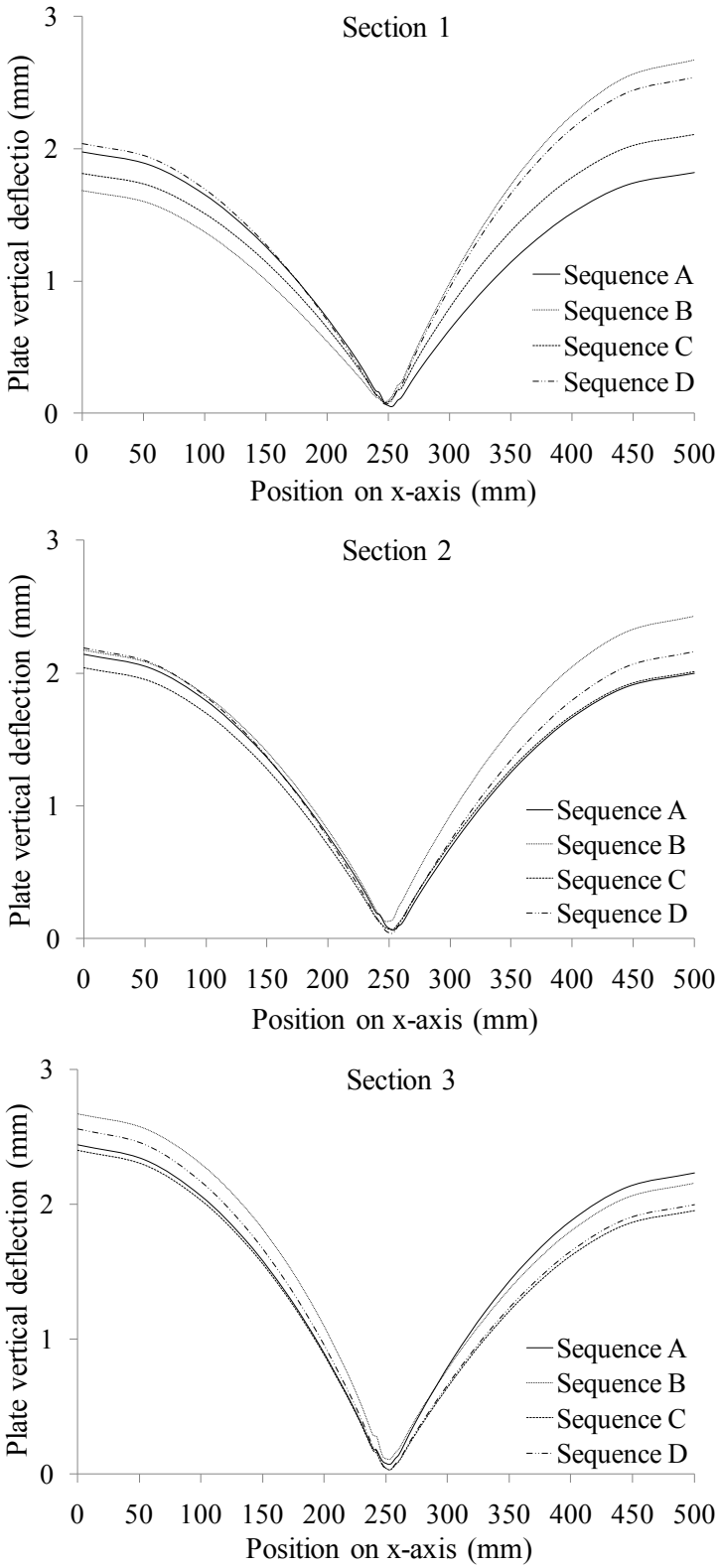

Figure 3.19, Vertical deflection of the plate

3.6.2 Longitudinal bending of the plate

The vertical deflection at the mid-plane of the plate along the axis of the stiffener is plotted in Figure 3.20. All four welding sequences caused the plate to deform out-of-plane in the vertical direction towards the stiffener with maximum deflections, δ_{01} ranging from 0.11 mm to 0.14 mm. These deflections are less than typical values of maximum out of plane deflection given by analytical expressions in literature. Paik *et al.* (2003) give δ_0=0.0015a (0.75mm for the current geometry) for an average level of imperfection, where a is the length between supports. The predicted distortions are also less than those suggested by Ohtsubo and Sumi (2000) for use in a benchmark study where δ_0=0.001a, giving 0.5mm for the panel geometry considered here. It is possible that the numerically predicted distortions are smaller than typical values because the stiffener in the present model is relatively tall with high bending stiffness which suppresses deflection of the plate. Sequences A and B resulted in out-of-plane deformations of the plate in a single lobe whereas deformation patterns for sequences C and D displayed two distinct lobes with close to zero deformation around 280mm along the longitudinal axis. Deformations from sequences A and B may cause a greater reduction in the buckling strength of stiffened panels than deformations from patterns C and D since they have a distribution similar to an overall buckling mode (Faulkner, 1975). The out-of-plane deformation along the stiffener due to welding sequence B was of the highest magnitude, with a somewhat sinusoidal distribution. This shape of initial deflection has the potential to reduce the resistance of the stiffened plate to overall

flexural buckling compared with that of a plate with imperfections in the form of random ripples.

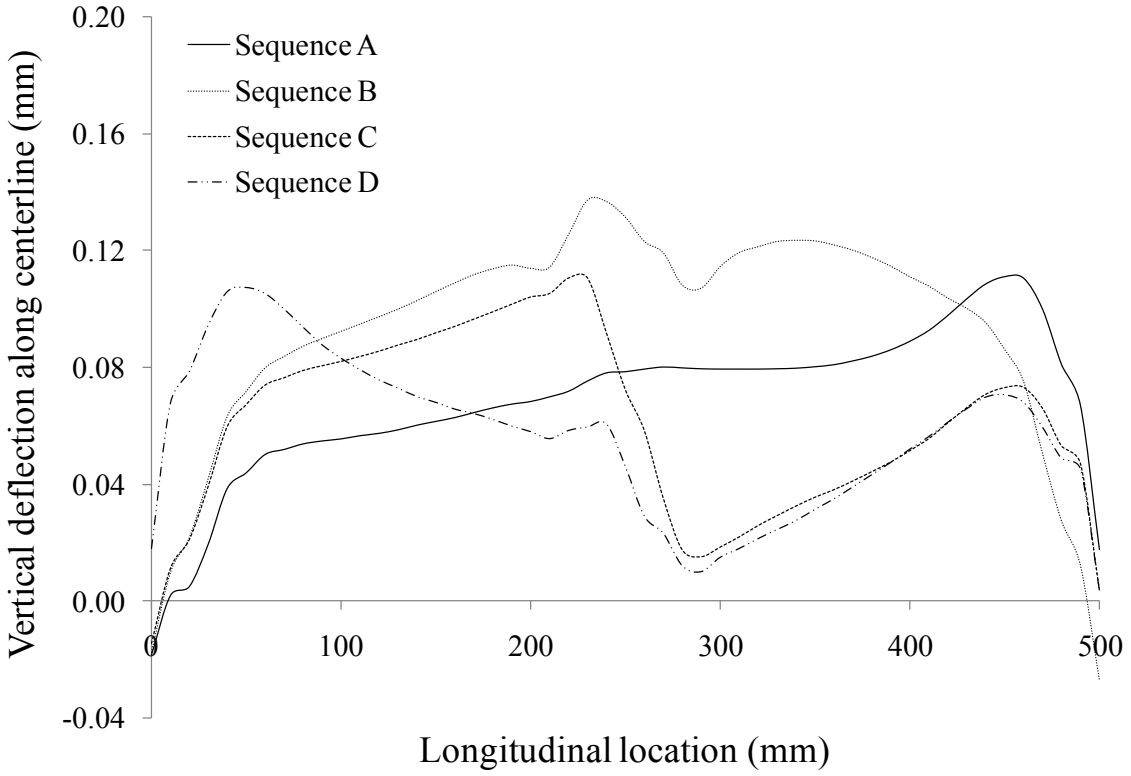

Figure 3.20, Mid-plane vertical deflection of plate along the stiffener

3.6.3 Lateral deflection of the stiffener

Lateral deflection of the stiffener can have a significant effect on ultimate strength of stiffened panels susceptible to stiffener-induced failure (Gordo & Guedes Soares, 1993). Flat-bar stiffeners are sensitive to this type of imperfection due to their low out-of-plane stiffness. Furthermore, failure due to lateral torsional buckling of the stiffener, referred to as stiffener tripping, is often sudden and provides little warning before failure (Paik & Thayamballi, 2006). Figure 3.21 shows lateral deflections of the stiffener for four

welding sequences where negative and positive values indicate that the stiffener deformed towards either the positive or negative x-axis.

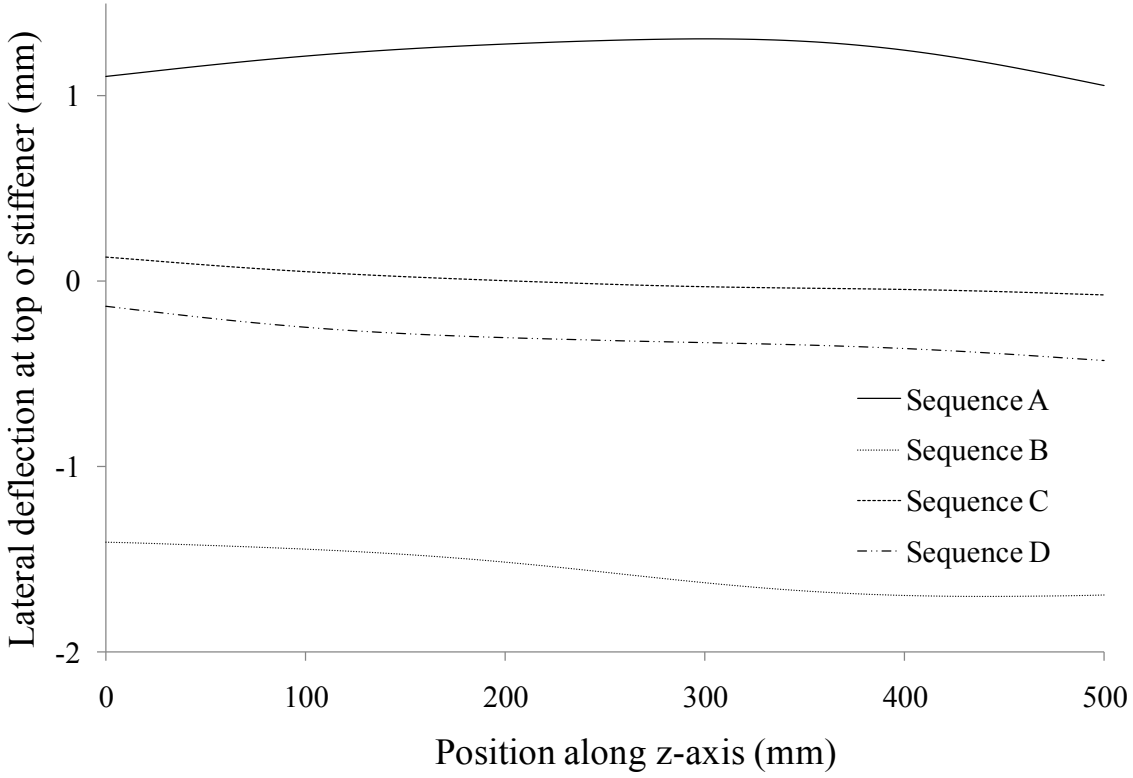

Figure 3.21, Lateral deflection of stiffener

The figure shows that lateral deflections of the stiffener for welding sequences C and D were significantly less than for sequences A and B. Maximum lateral deflections of the stiffener for sequences C and D were 0.42mm and 0.13mm respectively. For welding sequences A and B, maximum lateral deflections of the stiffener were 1.3mm and 1.7mm respectively.

3.7 Conclusions

A finite element model capable of simulating the thermo-mechanical welding process was developed and validated by comparison with experimental data. It has been shown that distortions predicted by the finite element model agree well with measured data and that the numerically obtained residual stress distribution is similar to the idealized distributions used in practice. The finite element simulation was then used to examine the distortion and residual stresses generated during welding for four different welding sequences and their possible effect on the ultimate strength of the stiffened plate under uniaxial compression was discussed. It is noted that many other factors besides residual stresses and distortions determine the ultimate strength of stiffened panels, such as plate and column slenderness, boundary conditions and multi-span versus single-span modeling assumptions. The discussions presented in the paper pertain to the effect of welding sequences on the residual stresses and distortions of a specific stiffened panel. The following conclusions are drawn from this study.

In the case of longitudinal residual stresses, welding sequence did not show a significant influence on the distribution pattern of the stress; however it did affect the peak values. Sequence A and C caused notably higher compressive residual stresses in the plate than sequences B and C. In the stiffener, the maximum compressive residual stress due to sequence B was approximately 3.5 times greater than the next lowest value. The distribution and peak values of residual stress were similar to measured values and predictions used in literature. Maximum tensile residual stresses equal to the material yield strength were predicted in the vicinity of the weld and maximum compressive

residual stresses from -97MPa to -58MPa were predicted in the plate and stiffener respectively.

In the case of welding induced distortion, welding sequence B resulted in the largest out-of-plane deflection of the plate, which may result in a reduced plate effectiveness. Sequence B resulted in the largest out-of-plane deformation of the plate along the axis of the stiffener. These distortions predicted by the numerical model were of lower magnitude than typical values suggested in literature. Welding sequences A and B resulted in the largest lateral deflections of the stiffener. Sequences C and D resulted in the least distortion of both plate and stiffener for the panel geometry considered. Considering both residual stress and distortion as a result of welding, welding sequence D is identified as the preferred welding sequence with the lowest welding induced residual stress and distortion.

Chapter 4 - Effect of 3D Welding-Induced Residual Stress and Distortion Fields on Strength and Behaviour of Flat-Bar Stiffened Plates

Liam Gannon, Yi Liu, Neil Pegg, Malcolm J. Smith

Submitted for publication in Marine Structures

4.1 Abstract

Numerical simulation based on finite element modeling is used to study the influence of welding-induced residual stress and distortion on the behaviour of welded, flat-bar stiffened plates under uniaxial compression. Residual stresses and distortions due to welding are simulated by 3D thermo-elasto-plastic finite element analysis, and the behaviour of stiffened plates under compressive axial loads is evaluated considering various stiffened plate geometries. Welding-induced residual stress and distortion distributions are examined, and the behaviour of stiffened plates under compressive axial loads with and without welding-induced residual stress is compared with IACS design formulas. Results of the numerical analyses reveal that welding-induced residual stresses reduce the ultimate strength of flat-bar stiffened plates by as much as 18%. Comparison of load-shortening curves generated by finite element analysis with curves derived from design formulae shows good agreement among ultimate strength values predicted by the two methods. There is, however, some discrepancy between the post-ultimate capacities

of stiffened plates predicted by the two methods, which may influence the accuracy of ultimate strength calculations for ship hull girders.

4.2 Introduction

The ability to accurately predict the strength of stiffened panels is important for the safe design of ship structures. Evaluating the strength and behaviour of stiffened panels is a complicated problem due to the various combinations of geometry, loading, boundary conditions and collapse modes that are possible. Furthermore, residual stress and geometric imperfections introduced during fabrication are difficult to predict, leading to uncertainty in calculating stiffened plate behaviour. The primary source of residual stress and distortion in ship structures is uneven cooling and plastic deformation induced by welding during fabrication. Welding-induced distortion and residual stresses have been found to reduce the strength of welded stiffened panels typical of ship structures (Gordo & Guedes Soares, 1996). The primary load for which stiffened panels in ships are designed is axial compression caused by wave-induced longitudinal bending. Analytical expressions are often used to evaluate the behaviour of stiffened plates under axial compressive load in design (IACS, 2009). Alternatively, the behaviour of stiffened plates can be studied in greater detail using numerical procedures such as the finite difference and finite element methods. Stiffened plate analysis is often carried out with the goal of calculating a load versus end shortening curve that describes the response of the member to axial load (Gordo & Guedes Soares, 1993). This average axial stress versus axial strain

curve can then be used to characterize the behaviour of a stiffened plate in a ship hull girder.

The first rational method for determining the ultimate moment capacity of a hull girder was proposed by Caldwell (1965). His method relied on assumed strength factors to describe the ultimate strength of stiffened plates. These values were assumed because little was known about the nonlinear behaviour of stiffened plates before collapse and even less was known about post-collapse behaviour at that time. Experimental programs carried out to study the behaviour of stiffened plates considering various loading and boundary conditions contributed substantially to the understanding of nonlinear plate behaviour (Moxham, 1971, Smith 1975, Faulkner 1977, Horne *et al.* 1977). With the availability of experimental data to validate numerical models, computer programs based on finite difference and finite element methods were used in parametric studies to investigate the large deflection, elasto-plastic behaviour of plates under lateral and in-plane loads (Moxham 1971, Chrisfield 1975, ISSC 1979).

Previous research has found that plating between stiffeners is not always fully effective in resisting axial compression or in providing support to the section against flexural buckling. This is a result of shear lag effects and of reduced plate stiffness due to initial distortion and buckling. A review of research on stiffened plates subject to compressive loading by ISSC (1979) concluded that initial distortions reduce the compressive strength of plates and change the failure type from a sudden event to a more gradual process with a less severe reduction of stiffness in the post collapse regime. Plates of high aspect ratio

a/b, are less sensitive to initial distortions than plates with a low aspect ratio when load is applied along the longer axis. From experimental studies, Dwight and Little (1976) found that the loss of plate effectiveness due to small initial distortions ($\delta_{o1}/t \leq 0.23$) is negligible for $a/b > 4$. The strength reduction due to initial distortion is more pronounced when $\delta_{o1}/t > 0.3$ and in severe cases can be as much as 45% (Dwight & Ratcliffe, 1969).

From surveys of ship plating and civil engineering structures, it was found that maximum plate imperfections δ_{o1}, expressed as a fraction of plate thickness t, relate approximately to the plate slenderness β_0, given by:

$$\beta_0 = \frac{b}{t}\sqrt{\frac{\sigma_y}{E}} \tag{4.1}$$

where b is the plate width, σ_y is the yield stress and E is the elastic modulus. It was found that δ_{o1}/t typically lies in the range of $0.05\beta_0^2$ to $0.15\beta_0^2$ with extreme values up to $0.4\beta_0^2$ for heavily welded plates. Smith *et al.* (1992) defined typical levels of welding-induced out-of-plane distortion of plates in the transverse direction considering slight, average and severe levels of distortion as expressed by:

$$\frac{\delta_{01}}{t} = \begin{cases} 0.025\beta_0^2 & \text{for slight imperfections} \\ 0.1\beta_0^2 & \text{for average imperfections} \\ 0.3\beta_0^2 & \text{for severe imperfections} \end{cases} \tag{4.2}$$

where δ_{01} is the maximum initial deflection of the plate between stiffeners. These distortions are the source of the familiar "hungry horse" shape seen in many welded ship hulls.

It is commonly accepted that welding-induced residual stresses have the potential to decrease the ultimate strength of stiffened plates under axial compression. Researchers have reached different conclusions regarding the extent to which these residual stresses affect the strength and behaviour of welded stiffened plates. This ambiguity is attributed to the various assumptions and idealizations that are made with regard to the magnitude and distribution of welding residual stress in the analysis of stiffened plates. Hansen (1996) used an approximate method to calculate load shortening curves for the purpose of assessing the influence of initial imperfections on the ultimate strength of a 1/3 scale frigate model tested by Dow (1991). An idealized, two dimensional welding residual stress distribution was used in the plate, where tensile residual stresses equal to yield were assumed in the heat affected zone and uniform compressive residual stresses acted over the rest of the plate so that the longitudinal residual stresses in the plate were in equilibrium. Residual stresses in the stiffener were not considered. He found that welding residual stresses decreased the ultimate strength of the stiffened plates by roughly 25%. Another approximate method to describe the load shortening curves of stiffened panels was proposed by Gordo and Guedes Soares (1993). They used the Johnson-Ostenfeld correction to account for the influence of inelastic effects on stiffened plate behaviour. It was found that residual stresses only decreased the load-carrying capacity near the collapse load, smoothing the load shortening curve in that region. Compressive residual

stress σ_r, of magnitude $0.2\sigma_y$, in the plate were found to decrease stiffened plate ultimate strength by 10%. Once again, residual stresses in the stiffener were not considered.

A typical longitudinal residual stress distribution in a welded stiffened panel consists of a zone of tensile stress in the plate of width $2\eta t$ at the stiffener to plate intersection. Faulkner (1975) suggested that the value of η normally ranges from 3 to 4.5, depending on the stiffened plate geometry and welding conditions. The maximum tensile residual stress is often equal to the yield stress of the base metal and is balanced by a nearly uniform compressive residual stress across the rest of the plate. In a benchmark study on the behaviour of stiffened plates, Ohtsubo and Sumi (2000) suggested the longitudinal residual stress distribution shown in Figure 4.1 for use in the analysis of stiffened plate behaviour. This distribution is consistent with measured values with the exception that residual stresses in the stiffener typically decrease towards the tip of the stiffener (Nagaraja Rao & Tall, 1961). Figure 4.2 shows the longitudinal residual stress distribution used by Smith (2008) in a parametric study on the strength of stiffened plates under axial compression. Although the residual stress distribution in the plate is similar to that shown in Figure 4.1, the distribution of stress in the stiffener is in better agreement with experimentally measured values determined by Nagaraja Rao *et al.* (1961) than that of Ohtsubo and Sumi (2000).

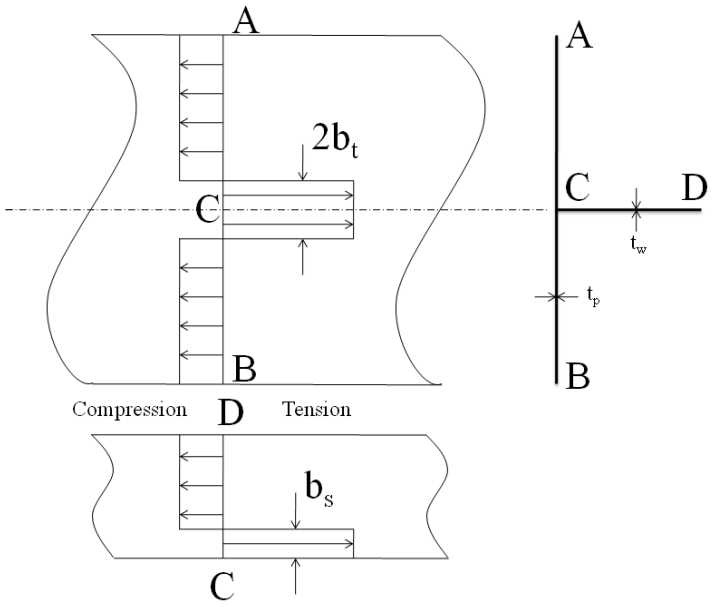

Figure 4.1, Longitudinal residual stress distribution in welded stiffened plates

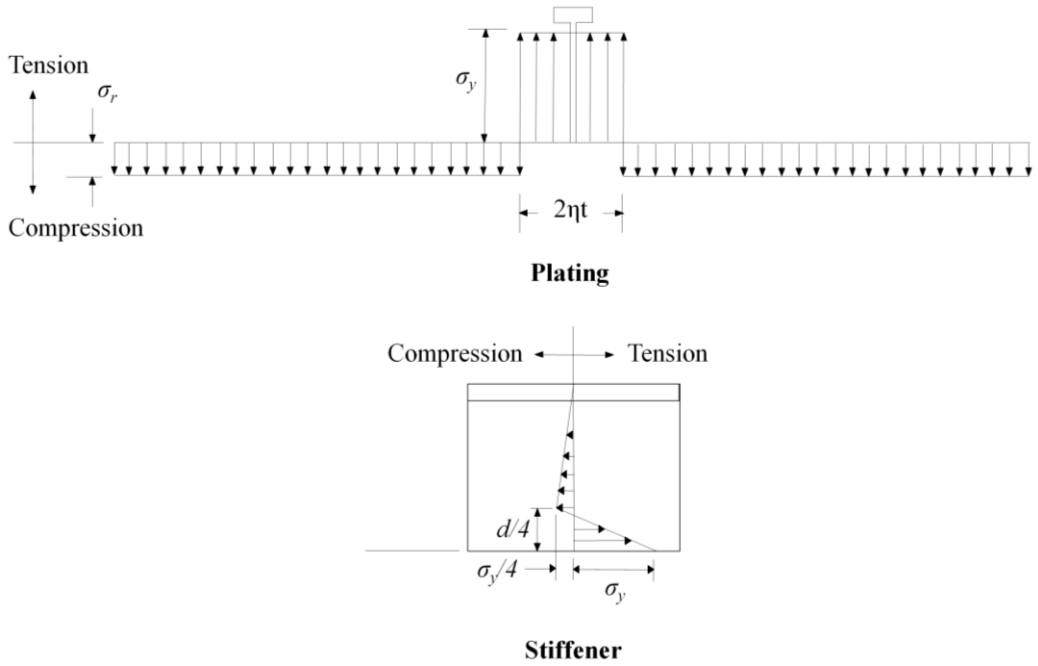

Figure 4.2, Longitudinal residual stress distribution in welded stiffened plates

The objectives of this study are to evaluate the influence of welding-induced residual stress on stiffened plate behaviour and to assess the accuracy of design methods for predicting stiffened plate behaviour proposed by the IACS (2009) common structural rules considering three-dimensional welding-induced residual stress and distortion fields. Welding residual stress and distortion are predicted by 3D thermo-elasto-plastic nonlinear finite element simulations. The accuracy of the finite element welding simulation is verified using experimental results from welding a flat-bar stiffener to a plate. The verified model is then used to generate load versus end shortening curves for seven flat-bar stiffened plate geometries by application of an axial compressive load. The effect of residual stress and distortion on the load versus end shortening curves is discussed and a comparison between these numerically simulated curves and those suggested by IACS (2009) common structural rules is presented. To the authors' knowledge, this is the first time that three dimensional finite element welding simulation has been used to characterize the complete welding-induced residual stress and distortion fields in longitudinally stiffened plates typical of ship hull girders prior to a collapse analysis.

4.3 Finite Element Modeling

4.3.1 Welding Simulation

Residual stress and distortion caused by welding were simulated by three-dimensional, nonlinear finite element analysis using ANSYS® (2009). The finite element simulation consisted of two sequential analyses. The first of these was a nonlinear thermal analysis

where the transient temperature field created by a moving heat source was calculated. The temperature field time history from the thermal analysis was then applied as a series of thermal loads in the structural analysis where each load step represented an increment in the position of the heat source in the direction of welding.

The stiffener was initially attached to the plate by 10 mm long tack welds evenly spaced at 250 mm intervals along the axis of the stiffener on both sides of the stiffener base. Continuous, 7 mm fillet welds were deposited sequentially on both sides of the base of the stiffener. The stiffened plate was allowed to cool for 30 min following the deposition of the first weld and cooled to the ambient temperature of 20°C after deposition of the second weld. The welding process considered was CO_2 gas metal arc welding where the heat input was divided into two parts. Sixty percent of the total heat input was applied as a volumetric heat generation rate within the weld elements, representing the heat transferred to the workpiece by the molten weld metal droplets. The remaining 40% was modeled as a Gaussian distributed heat flux over a circular area, representing the heat transferred to the surface of the weld elements from the plasma around the tip of the welding torch. The welding heat input and corresponding speed of welding was consistent with values recommended in the Canadian Welding Standard, CSA W59-03 (Canadian Standards Association, 2003) for the 7 mm fillet weld used in the welding simulation. The plate and stiffener were both considered to be made from AH36 shipbuilding steel with temperature dependent material properties adopted from Michaleris and DeBiccari (1997). The yield strength and elastic modulus at room temperature were taken as 360 MPa and 210 GPa, respectively. An elasto-plastic material

model using von Mises failure criteria and associated flow rule was used as was done by Michelaris and Debicarri (1997). Geometric nonlinearities associated with large strains and displacements were also included.

4.3.2 Mesh and Boundary Conditions

Figures 4.3 and 4.4 show a typical finite element mesh used for the flat-bar stiffened plate models along with the welding sequence that was used in the simulation. For each model, the same mesh was used for both steps of the welding simulation and the ultimate strength analysis. A mesh convergence study revealed that a relatively fine mesh with 12 elements through the thickness was necessary in the plate near the weld in order to accurately characterize the high thermal gradient at this location. A coarser mesh was used in regions away from the weld to reduce computational time with a minimum of four elements through the thickness. For the thermal analysis, the Solid70 hexahedral element was used whereas the structural equivalent Solid185 element was used in the ultimate strength analysis. Both element types are 8-node, bi-linearly interpolated isoparametric hexahedrons. For the thermal element, only the temperature degree of freedom is considered at each node, whereas the three displacements along the Cartesian coordinate axes are used as degrees of freedom at each node for the structural element. Beam elements with high bending stiffness and low axial stiffness were used to connect all nodes in the end cross-sections of the models to the centroid of the cross-section so that these sections remained plane when a displacement was applied at the centroid during the ultimate strength analysis. These elements were deactivated during the

welding simulation and then activated at the beginning of the ultimate strength analysis using the ANSYS® element birth and death feature.

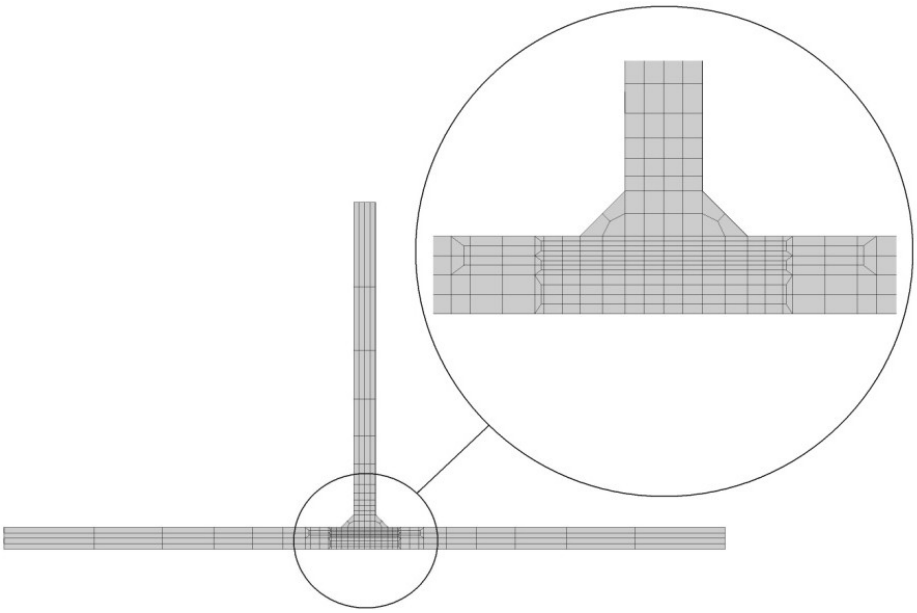

Figure 4.3, Typical finite element mesh

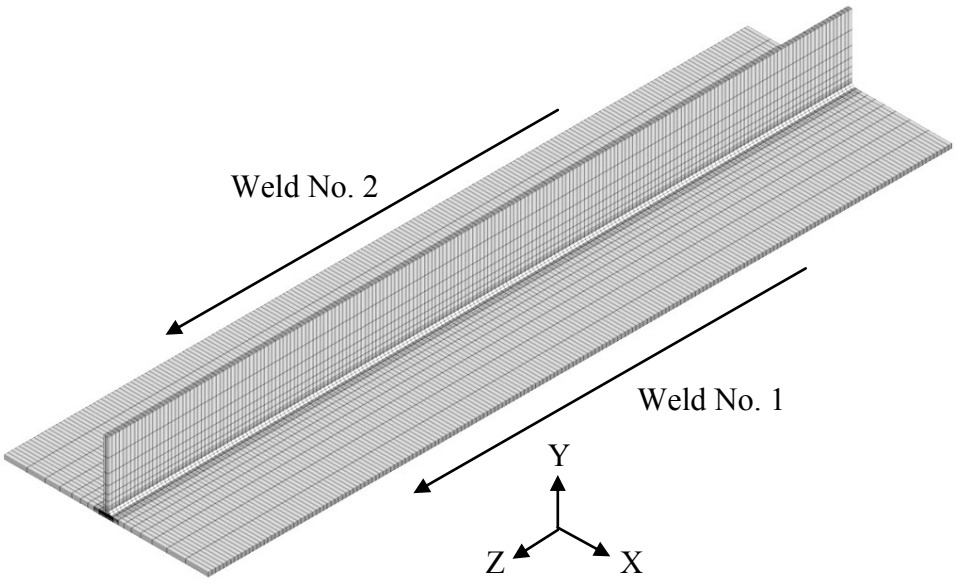

Figure 4.4, Stiffened plate coordinate system and welding sequence

Boundary conditions implemented at the transverse edges of the plates are representative of the level of restraint in stiffened panels in ship hull girders. Transverse edges were constrained to remain straight when moving in the plane of the plating and free to move out of the plane of the plating as suggested by Dow *et al.* (1981). This was achieved by creating a very weak beam element at the mid-span position on the transverse edges of the plate. This element introduced a rotational degree of freedom that was used in constraint equations to prevent rotation of the transverse edges of the plate about the longitudinal and vertical axes. Simple support conditions were applied at the ends of the stiffened plate at the centroids of the end cross-sections by constraining displacements along all three coordinate axes at the centroid of one end and the vertical and transverse displacements at the centroid of the opposite end.

4.4 Verification of the Model

The accuracy of the simulation method was verified by comparing the results of a welding simulation using this method with experimental results from welding a flat-bar stiffener to a steel plate. While the detailed verification is available in Gannon *et al.* (2010), the salient information is provided as follows for reference. A 300 x 500 x 9 mm mild steel flat-bar stiffener was welded to a 500 x 500 x 9 mm plate with sequential, continuous 6 mm fillet welds. The welding process used was CO_2 gas metal arc welding, where a robot welder was used for welding and the test specimen was supported in such a way that it was free to deform in any direction. Figure 4.5 shows the vertical deflection of the plate at mid-span predicted by finite element analysis along with experimentally

measured values (Deng *et al.*, 2007). Both the magnitude and distribution of welding-induced distortion predicted by the finite element model were in good agreement with measured values. Although measurements of residual stress were not available, longitudinal residual stresses predicted by the finite element model were consistent with other measurements available in the literature (Nagaraja Rao & Tall, 1961).

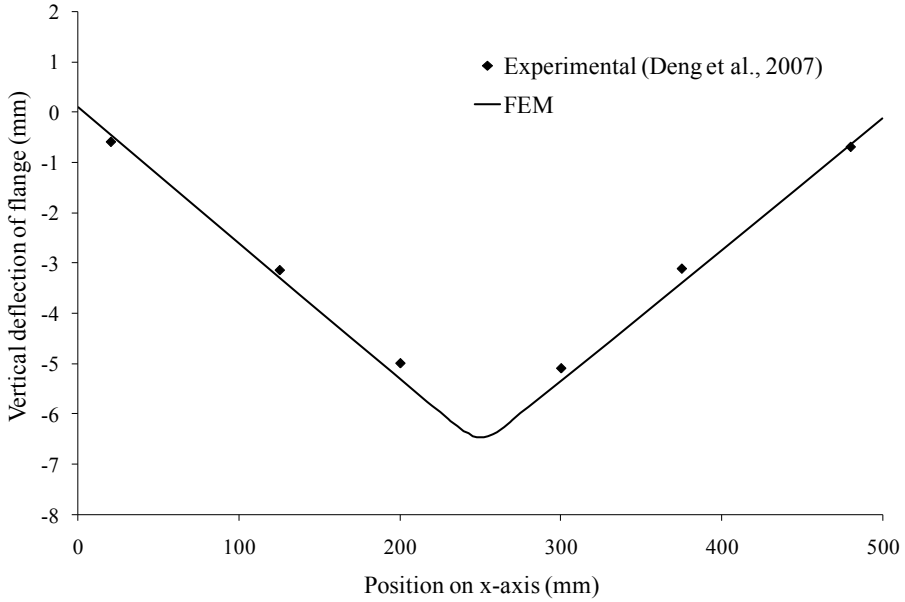

Figure 4.5, Plate vertical deflection comparison for finite element model validation

4.5 Parametric Study

A parametric study was conducted to study the behaviour of flat-bar stiffened plates under compressive axial load, accounting for welding-induced residual stress and distortions determined using the welding simulation method described in the previous section. The load versus end-shortening curves for each model were obtained by applying an axial displacement at the centroid of one end of each stiffened plate and the reaction at the centroid of the opposite end was calculated for each increment in displacement during

the ultimate strength analysis. The stiffened plate geometries, summarized in Table 4.1, were chosen to include a relatively wide range of plate slenderness β_0 (Eqn. (4.1)), and column slenderness λ, values given by:

$$\lambda = \frac{a}{\pi r}\sqrt{\frac{\sigma_y}{E}} \tag{4.3}$$

where E is the elastic modulus, and r is the radius of gyration. In Table 4.1, a, is the length of the stiffened plate. All other dimensions given in the table are illustrated in Figure 4.6. In calculating the radius of gyration, the effective width b_{em}, given by Eqn. (4), and the reduced effective width of the plate b_{em}', given by Eqn. (5), as derived by Faulkner (1975), were used to calculate the effective area and moment of inertia of the stiffened plates, respectively.

Table 4.1, Stiffened plate model dimensions

Section ID	a (mm)	b (mm)	t (mm)	d (mm)	t_w (mm)	β_0	λ
F1	2000	400	12	180	12	1.380	0.504
F2	2000	550	12	180	12	1.898	0.530
F3	2000	700	12	180	12	2.415	0.544
F4	2000	850	12	180	12	2.933	0.553
F5	2000	550	12	140	12	1.898	0.714
F6	2000	550	12	220	12	1.898	0.419
F7	2000	550	12	260	12	1.898	0.346

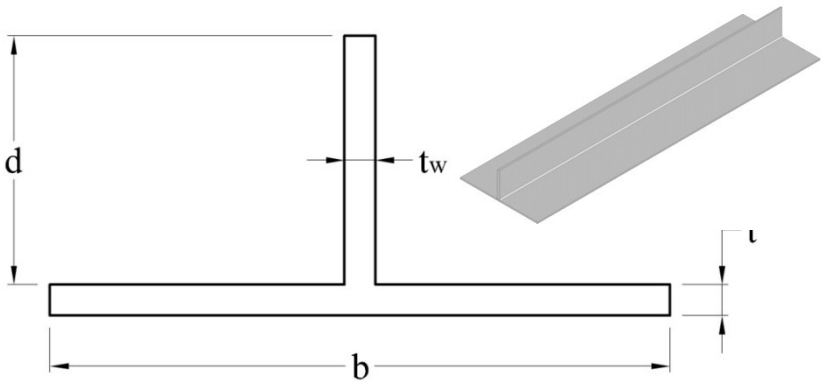

Figure 4.6, Flat-bar stiffened plate dimensions

$$\frac{b_{em}}{b} = \begin{Bmatrix} \frac{2.25}{\beta_0} - \frac{1.25}{\beta_0^2} & \beta_0 > 1 \\ 1 & \beta_0 \le 1 \end{Bmatrix} \tag{4.4}$$

$$\frac{b'_{em}}{b} = \begin{Bmatrix} \frac{1}{\beta_0} & \beta_0 > 1 \\ 1 & \beta_0 \le 1 \end{Bmatrix} \tag{4.5}$$

4.6 Residual Stress and Distortion

4.6.1 Residual Stress

Longitudinal residual stresses in the plate and web of flat-bar stiffened plates, predicted by finite element welding simulation are shown in Figure 4.7 and Figure 4.8, respectively. The residual stresses shown in these figures were taken at the mid-plane of the plate and stiffener at the mid-span cross-section. Residual stresses varied along the length and through the thickness of the stiffened plates. Residual stress distributions shown in Figures 4.7 and 4.8 are typical of residual stress distributions in regions away from discontinuities such as tack welds and the ends of the stiffened plates. The

magnitude and distribution of longitudinal residual stress predicted by the numerical models is consistent with both measured values and numerical predictions (Nagaraja Rao & Tall 1961, Yuan & Ueda, 1996). For all seven studied geometries, a zone of tensile residual stress equal to the yield stress was predicted in the plates near the weld location with widths ranging from 32.5 mm to 59.3 mm (η = 2.7 to 4.9), indicating the distribution is more or less trapezoidal rather than rectangular as suggested by some researchers.

For the plate residual stress distributions shown in Figure 4.7, there was little variation in the magnitude and distribution of the tensile residual stress among the different models. For the compressive residual stress, the magnitude and distribution were almost identical for models F5 through F7 that have the same plate slenderness β_0. For models F1 to F4, with varying plate slenderness, the distribution of compressive residual stress was similar, however the plates of lower slenderness had higher compressive residual stresses than those of higher slenderness. Compressive residual stresses in the plate were highest in model F1 with a value 70 MPa and lowest in model F4 where compressive residual stresses had a magnitude of 27 MPa. In the stiffener, as shown in Figure 4.8, tensile residual stresses near yield were predicted at the weld location for all models. These quickly changed to low tensile or compressive residual stress in the stiffener 35 mm to 40 mm (η = 2.9 to 3.3) from the base of the stiffener. Peak compressive residual stresses in the stiffeners ranged from -9 MPa to -35 MPa for all models, with model F1 again attaining the highest value.

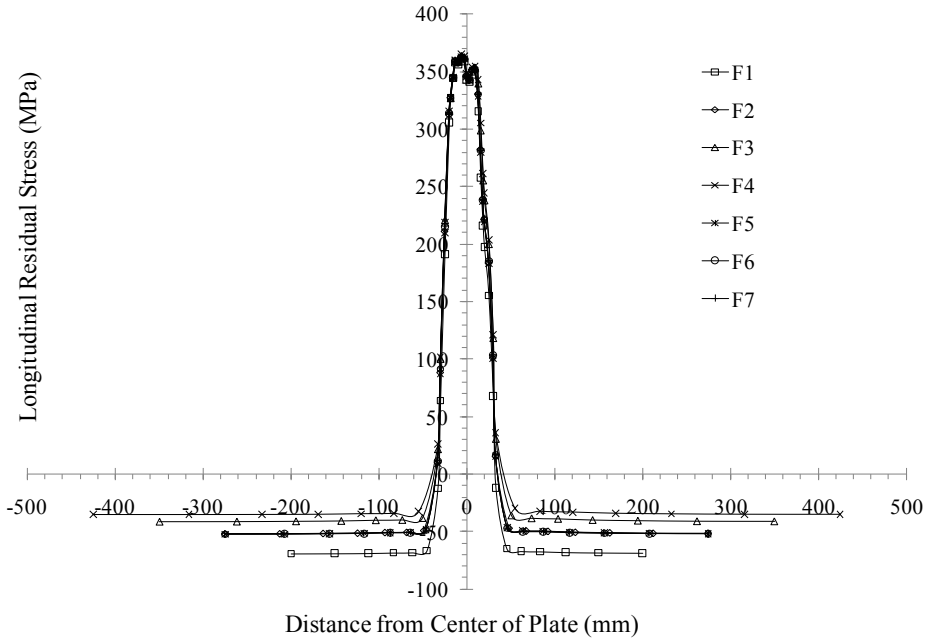

Figure 4.7, Longitudinal residual stress distribution in the plate of flat-bar stiffened plates

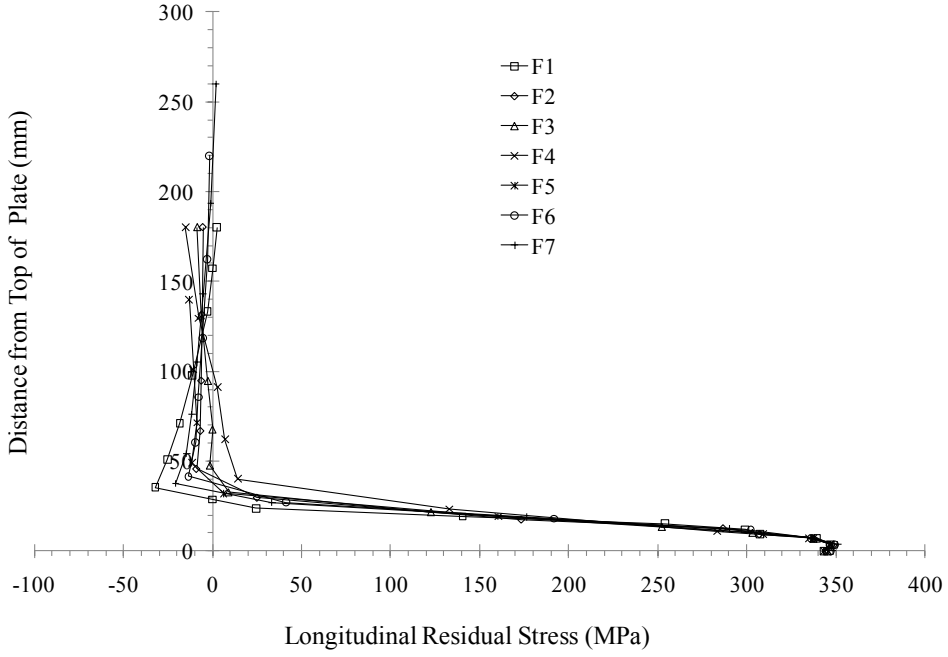

Figure 4.8, Longitudinal residual stress distribution in the web of flat-bar stiffened plates

Faulkner (1975) considered equilibrium of residual stress in the plate separately from the stiffener. The magnitude of compressive residual stress in the plate was calculated based on η and assumed a nearly uniform distribution of compressive residual stress. This idealization is reasonably accurate considering the residual stress distributions shown in Figure 4.7 when the width of the yielded tension zone is assumed constant and taken as the full width of the tensile stress zone in the plate. However, an examination of Figure 4.8 shows that residual stresses were not in equilibrium considering the stiffeners alone. This suggests that equilibrium of residual stress over the complete stiffened plate cross-section should be considered, and that the idealized shape of the tensile residual stress zone in the plate should be better defined to avoid inaccurate prediction of residual stress in the stiffener. The idealized residual stress distributions used by Ohtsubo and Sumi (2000) (Figure 4.1) and Smith (2008) (Figure 4.2) both provide relatively accurate representations of residual stress in the plate, but Smith's distribution characterizes the distribution of residual stress in the stiffener more accurately when compared with results from numerical analysis in this study. In both cases, the distribution of tensile residual stress in the plate could be more accurately represented by a trapezoidal distribution of tensile residual stress near the weld. Yuan and Ueda (1996) measured residual strains in flat-bar stiffened plates for use in the inherent strain method of predicting welding-induced distortions. Their measured residual strains and associated residual stresses in the plate near the weld indicated more or less a trapezoidal distribution, which is consistent with finite element results in this study. It should be pointed out that the exact shape of

the welding-induced residual stress distribution depends on heat input and thermal and mechanical material properties.

4.6.2 Distortion

Figure 4.9 - Figure 4.11 show welding-induced distortions in the flat-bar stiffened plates predicted by finite element analysis. Figure 4.9 shows the vertical distortion of the plate along the x-axis at mid-span whereas Figure 4.10 shows distortions of the plate and stiffener at the mid-plane along the z-axis. Positive and negative distortions are consistent with the coordinate axes shown in Figure 4.4. Figure 4.9 shows that the plates of all models deformed in a "hungry horse" pattern between stiffeners where the deformation was toward the stiffener with an approximate half sine wave distribution. The "hungry horse" type distortions predicted by numerical analysis in this study have maximum values between the slight and average levels of distortion defined by Smith *et al.* (1992) (Eqn. (4.2)).

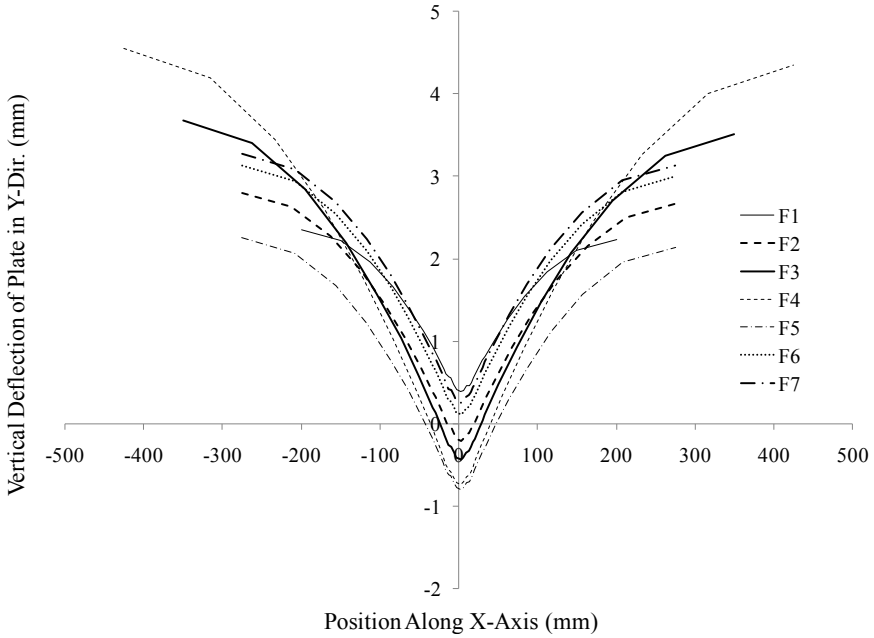

Figure 4.9, Vertical distortion of plate at mid-span

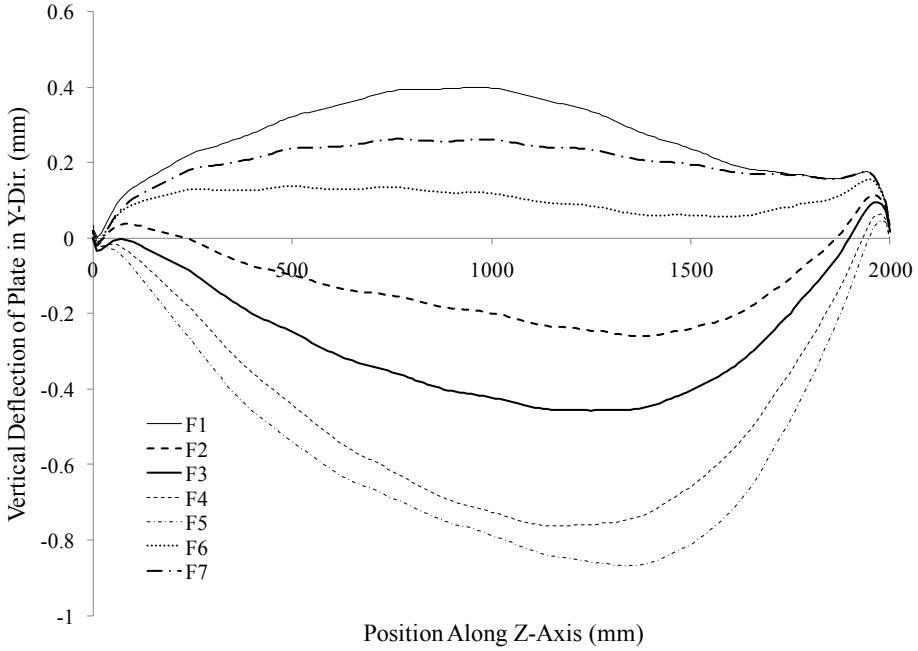

Figure 4.10, Stiffened plate vertical distortion along Z-axis

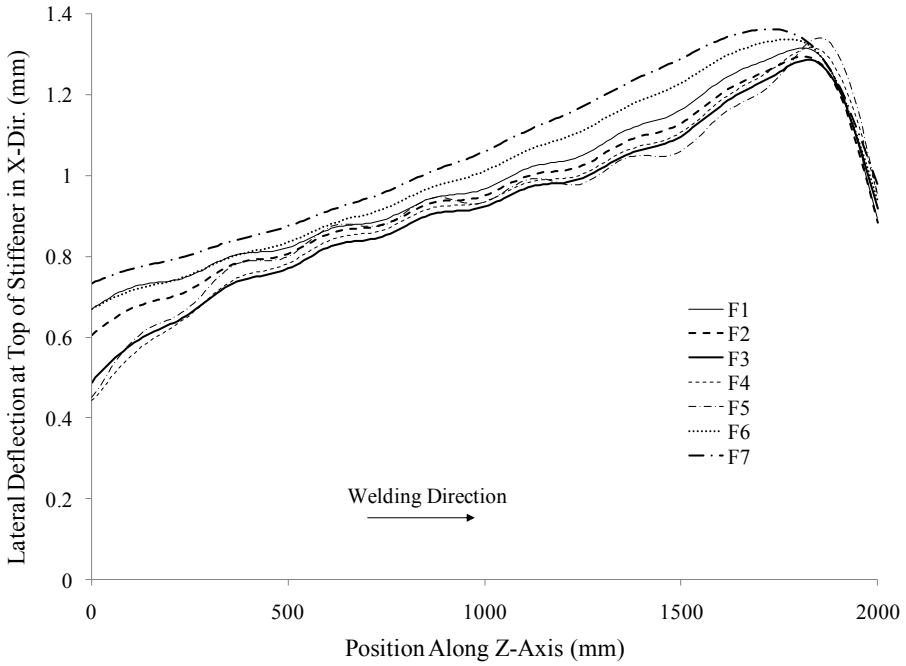

Figure 4.11, Lateral distortion at top of stiffener

For design purposes, welding-induced longitudinal distortion is often assumed to vary in a half sine wave between supports where the maximum distortion δ_0, is taken as 0.001a (Faulkner, 1977) or 0.0015a (Paik & Thayamballi, 2003). For the geometries considered in the current study, these would estimate maximum distortions of 2 mm to 3 mm. These values are conservative in comparison with the distortions predicted by finite element analysis in this study, shown in Figure 4.10 where the maximum out-of-plane distortions correspond to the slight level of longitudinal distortion defined by Smith *et al.* (1992). The magnitude of distortions varied for all stiffened plate geometries, and it was found that for those stiffened plates with the same plate slenderness, the column-type vertical distortion changed from being towards the stiffener to towards the plate as the distance from the bottom of the plate to the neutral axis decreased. This is attributed to the change

in internal bending moment resulting from the sum of longitudinal residual stresses acting about the neutral axis of the stiffened plate cross-section.

In a benchmark study on the behaviour of stiffened plates under axial compressive load, Ohtsubo and Sumi (2000) suggested that lateral distortion at the top of the stiffener be distributed in a half sine wave between supports and that the maximum value be taken as $0.001a$, giving a value of 2 mm for the stiffened plates considered in the present study. The numerical distribution of stiffener lateral distortion shown in Figure 4.11 was not distributed in a sinusoidal pattern. This distortion appeared to accumulate along the axis of the stiffener in the welding direction. The maximum distortion values are however, comparable to those used in the benchmark study.

4.7 Behaviour Under Axial Compressive Load

Following the welding simulation with residual stress and distortion included in the model, a displacement controlled analysis was conducted to obtain the load versus end-shortening curves of the stiffened plates. Incremental displacement instead of load was used in the analysis so that the post-buckling behaviour of the stiffened plates could be observed. For comparison, each stiffened plate was analyzed a second time with the same welding-induced distortion, but with no residual stress, in order to assess the influence of welding-induced residual stress on the stiffened plate behaviour. Table 4.2 provides the normalized ultimate stress values determined by finite element analysis of the models described in Table 4.1, along with ultimate stress values predicted using the analytical methods prescribed by the IACS Common Structural Rules for bulk carriers (IACS,

2009). In addition to the normalized ultimate strength, Table 4.2 indicates the direction in which buckling occurred in the numerical models. In cases where buckling occurred toward the plate, lateral buckling of the stiffener also took place.

Table 4.2, Ultimate strength predictions

ID	1) FEM σ_u/σ_y without residual stress	Buckling direction of 1)	2) FEM σ_u/σ_y with residual stress	Buckling direction of 2)	% Strength reduction from 1) to 2)	3) IACS σ_u/σ_y	% Difference between 2) and 3)
F1	1.027	P	0.980	S	4.6	0.935	4.6
F2	0.997	S	0.818	S	18.0	0.839	-2.6
F3	0.788	S	0.706	S	10.4	0.740	-4.8
F4	0.696	S	0.630	S	9.5	0.656	-4.1
F5	1.002	S	0.831	S	17.1	0.838	-0.8
F6	0.980	P	0.820	S	16.3	0.824	-0.5
F7	0.893	P	0.808	P	9.5	0.801	0.9

P: Buckling towards the plate

S: Buckling towards the stiffener

4.7.1 Ultimate Strength

Figure 4.12 illustrates the variation in ultimate strength determined by the numerical models relative to plate slenderness β_0 for models F1 to F4, showing that ultimate strength decreases with increasing plate slenderness. Also shown in the figure are ultimate strength predictions obtained using the IACS Common Structural Rules for bulk carriers (IACS, Common structural rules for bulk carriers, 2009). Ultimate strength values predicted using IACS analytical methods agreed with those predicted by finite element analysis within acceptable limits where welding residual stresses and distortions were included. Ultimate strength predictions varied from 4.6% to -4.1% between the

analytical and numerically determined values. Figure 4.13 shows the relationship between ultimate strength and column slenderness λ, for models F2, and F5 to F7, with similar plate slenderness. No significant variation in the ultimate strength is observed among the four models in Figure 4.13. This is consistent with results of Smith *et al.* (1992), who found that λ does not affect the ultimate strength of stiffened plates with slight imperfections until $\lambda \geq 0.8$, which is greater than the largest column slenderness value used in this study.

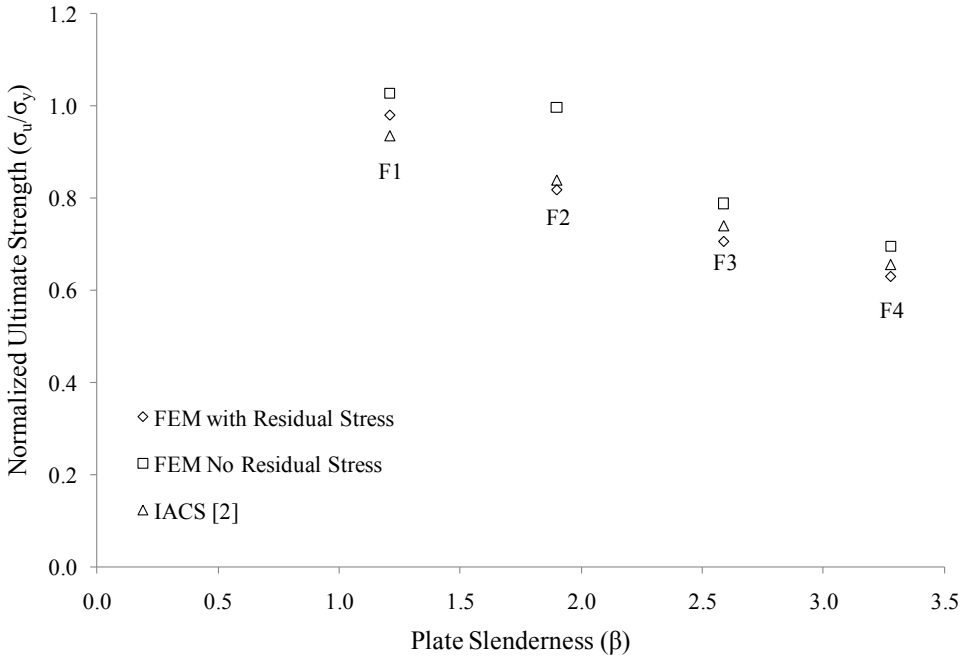

Figure 4.12, Variation in ultimate strength with plate slenderness

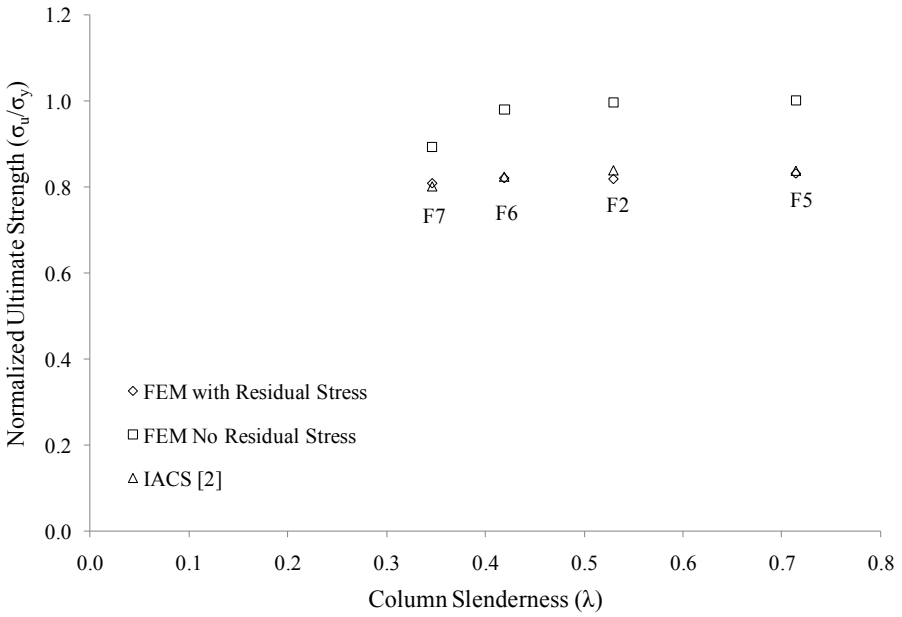

Figure 4.13, Variation in ultimate strength with column slenderness

Table 4.2 shows that the reduction in ultimate strength of flat-bar stiffened panels due to welding-induced residual stress varied from approximately 5 - 18% for all models. Most models failed by flexural buckling towards the stiffener (S) when welding-induced residual stress was considered, except for model F7 which failed by buckling towards the plate. It is noted that the presence of residual stress resulted in a change in failure mode for models F1 and F6. For those stiffened plates that failed by flexural buckling towards the stiffener (S), welding residual stresses were found to cause a greater reduction in ultimate strength as plate slenderness decreased. This is attributed to the higher magnitude of compressive residual stress in plates of lower plate slenderness as illustrated in Figure 4.7. Examples of the buckled shape of flat-bar stiffened plates that failed towards the stiffener and that failed towards the plate are shown in Figure 4.14 and Figure 4.15 for models F3 and F7, respectively. Failure of model F7 towards the plate,

accompanied by lateral buckling of the stiffener is attributed to the height and consequent high slenderness of the stiffener.

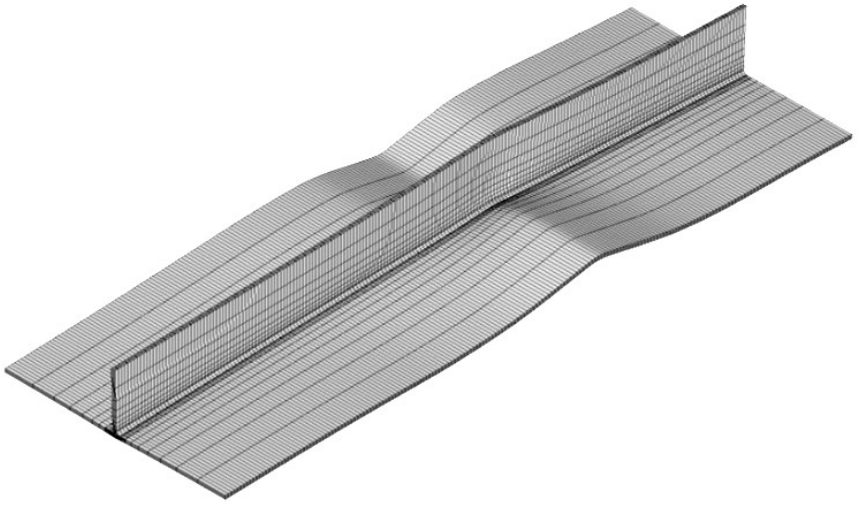

Figure 4.14, Buckled shape of model F3 (S)

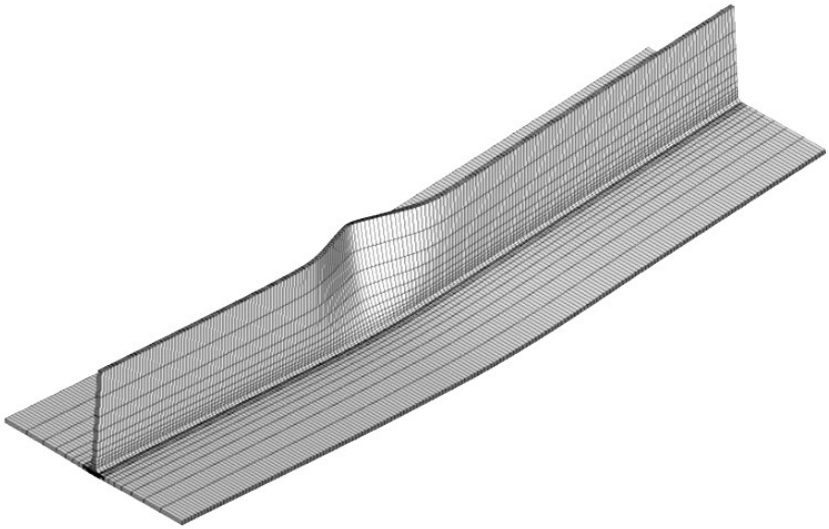

Figure 4.15, Buckled shape of model F7 (P)

4.7.2 Load-Shortening Curves

Load-shortening curves for flat-bar stiffened plates including welding-induced residual stress and distortion predicted by finite element analysis are shown in Figure 4.16 and Figure 4.17. Both figures show that the numerical models generally predicted a stiffer response in the pre-collapse region than curves calculated using the IACS common structural rules where the IACS curves showed non-linearity at lower strains than the numerical curves. The nonlinearity shown in the IACS curves in the pre-collapse response of stiffened plates is a result of the Johnson-Ostenfeld correction for plasticity applied in the IACS analysis. The Johnson-Ostenfeld formulation is an empirically-based approach to account for plastic deformation in the ultimate strength analysis of columns loaded in axial compression. On the other hand, the nonlinearity shown in the numerical load shortening curves was observed at higher load levels, in some cases, up to 95% of the ultimate load. Figure 4.18 compares the load shortening curves for model F2 with and without residual stress. The presence of residual stresses caused an 18% reduction in the ultimate load and smoothed the load-shortening curve near the ultimate load, compared with those models that did not include residual stresses. Those stiffened plates with no residual stress exhibited a more sudden, bifurcation-type failure when the ultimate load was reached as shown in Figure 4.18 for model F2. These results are consistent with the behaviour of stiffened plates observed by Gordo and Guedes Soares (1993).

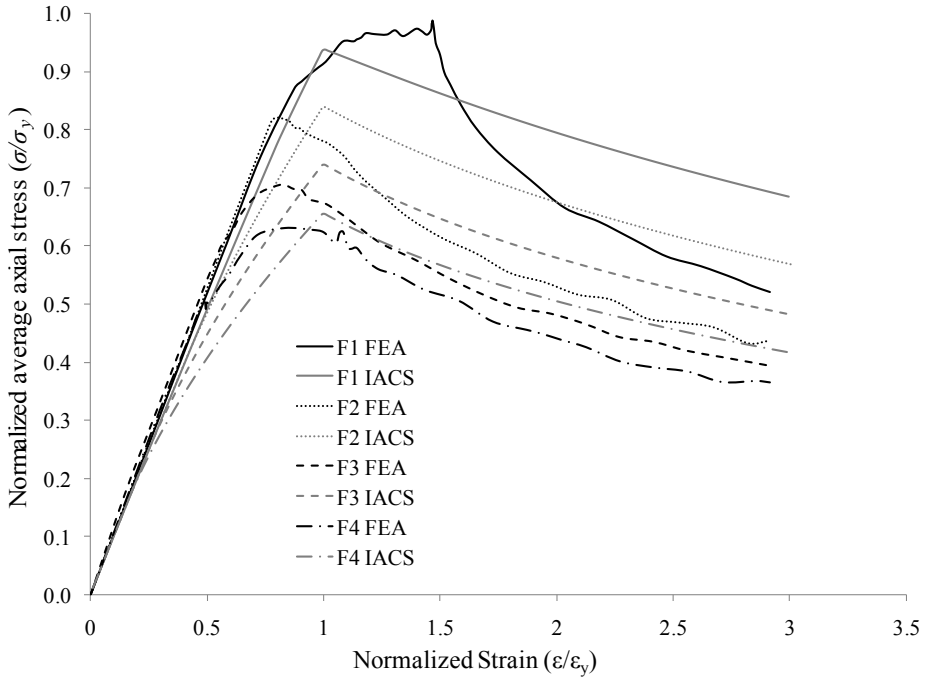

Figure 4.16, Load-end shortening curves for models F1 through F4

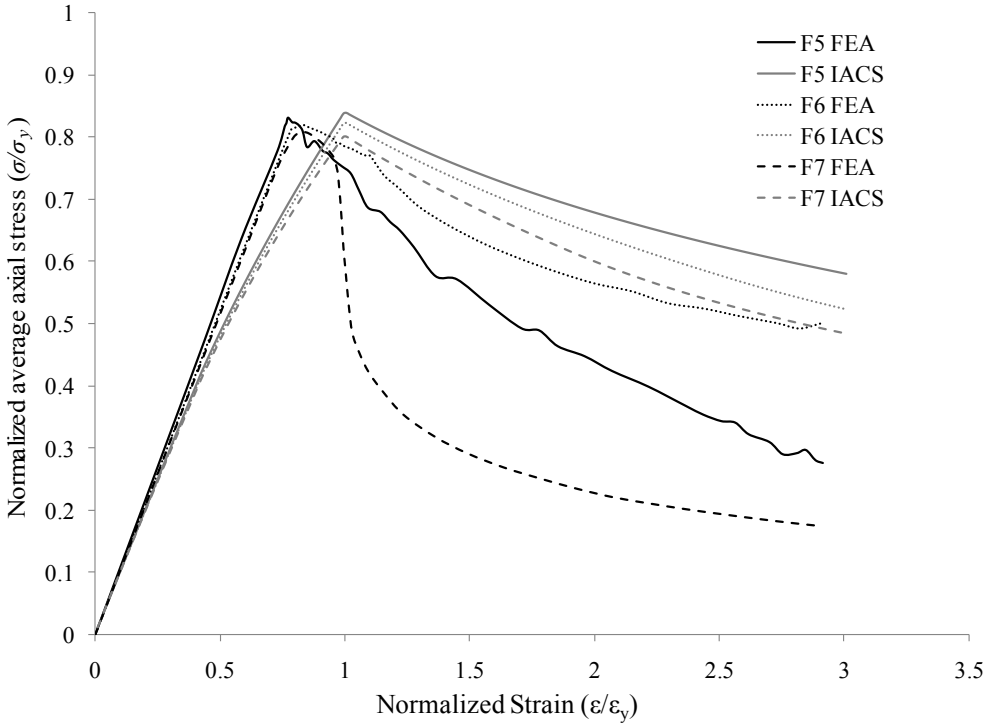

Figure 4.17, Load-end shortening curves for models F5 through F7

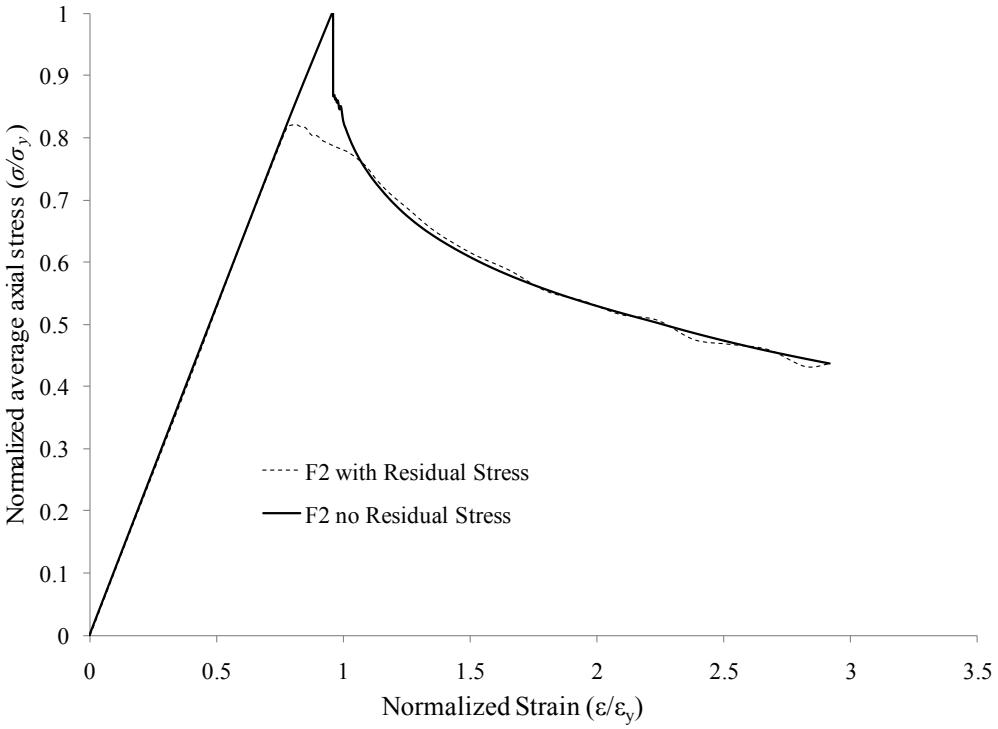

Figure 4.18, Effect of welding-induced residual stress on load shortening curve (F2)

Figure 4.16 and Figure 4.17 show that although the ultimate load and pre-collapse behaviour predicted by the IACS method agrees reasonably well with numerical results, the IACS load shortening curves overestimated the post-collapse capacity of flat-bar stiffened panels by a significant margin. The overestimate of post-ultimate capacity in the IACS rules was found to increase as plate slenderness decreased and the amount of that overestimation was approximately constant as the strain increased beyond the strain at ultimate load. For example, the IACS common structural rules predicted a post-ultimate capacity 148% higher than the numerical value for Model F7 at $\varepsilon/\varepsilon_y = 2$, for which both methods predicted failure by lateral buckling of the stiffener as shown in Figure 4.15. For the other flat-bar stiffened panels, the common structural rules over predicted the post-ultimate capacity by 11-26% at $\varepsilon/\varepsilon_y = 2$.

The pronounced overestimation of post-ultimate capacity by the IACS rules is attributed to the assumption that after the ultimate stress is reached, one of three failure mechanism governs the stress-strain relationship. It is possible that the effective cross-section in the post-ultimate region is, in reality, less than that assumed in the IACS analytical formulation due to interaction of failure modes, leading to the discrepancy in load carrying capacity after the ultimate strength has been reached. This type of behaviour is demonstrated in Figure 4.19 for model F1 where the displaced shape has been magnified by a factor of 2. The non-conservative post-ultimate capacity of stiffened plates predicted by the IACS rules may lead to overestimates of hull girder ultimate strength in ship structural design, causing a delay in load-shedding from one stiffened plate element to another in a progressive collapse analysis. The influence of changing the slope of the load-shedding portion of stiffened plate load shortening curves on hull girder ultimate strength was evaluated by Rutherford and Caldwell (1965). They found that reducing the post-collapse slope of the curves, and hence the post-collapse load carrying capacity, has the potential to reduce hull girder ultimate strength by as much as 10%.

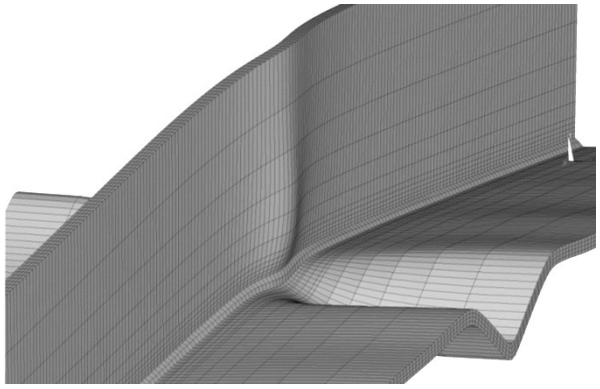

Figure 4.19, Local buckling of stiffener in post-ultimate load state (F1)

4.8 Conclusions

Residual stresses and distortions due to welding were predicted by 3D nonlinear finite element analysis for flat-bar stiffened steel plates. The welding simulation consisted of sequential nonlinear thermal and structural analyses. Seven stiffened plates with various combinations of plate slenderness and column slenderness were considered in this study. Following the welding simulation, load versus end-shortening curves were generated with and without including welding-induced residual stresses. The influence of welding residual stress on the strength and behaviour of stiffened plates under axial compressive load was evaluated and the load shortening curves determined by finite element analysis were compared with curves calculated using analytical methods prescribed in the IACS Common Structural Rules for Oil Tankers. The following conclusions are drawn from the results of the study:

1. Idealized welding residual stress distributions used in the design of stiffened plates should consider equilibrium of residual stresses in the plate and stiffener together. The residual stress distribution in the stiffener is sensitive to the shape of the tensile residual stress zone in the plate which can be represented more accurately by a trapezoidal shape than a uniform region over which the tensile stress is equal to yield.
2. The maximum reduction in ultimate strength of flat-bar stiffened plates due to welding-induced residual stress was 16.5%.

3. The ultimate strength of stiffened plates was found to decrease with increasing plate slenderness β_0. Column slenderness λ, of the stiffened plates was found to have little influence on ultimate strength for constant plate slenderness.
4. The ultimate strengths of stiffened plates predicted using the IACS common structural rules agreed with values predicted by finite element analysis within acceptable limits.
5. In comparison to load shortening curves produced by finite element analysis, the IACS common structural rules overestimate the capacity of stiffened plates in the post-collapse region by a significant amount. This may lead to non-conservative structural design of ship hull girders with regards to ultimate strength.

Chapter 5 - Effect of Simulated 3D Welding-Induced Residual Stress and Distortion Fields on Strength and Behaviour of Angle and Tee-Stiffened Plates

Liam Gannon, Yi Liu, Neil Pegg, Malcolm J. Smith

Submitted to Engineering Structures journal

5.1 Abstract

Numerical simulation based on finite element modeling is used to study the influence of welding-induced residual stress and distortion on the behaviour of angle and tee-stiffened plates under axial compression. 3D thermo-elasto-plastic finite element analysis is used to simulate residual stress and distortion caused by welding. Several stiffened plate geometries with two types of stiffener are considered in the study. The behaviour of stiffened plates under compressive axial loads is evaluated both with and without welding-induced residual stress and the results are compared with IACS design equations. The numerical results reveal that the ultimate strength of angle and tee-stiffened plates may be reduced by as much as 15% due to the presence of welding-induced residual stresses. Comparison of load-shortening curves generated by finite element analysis with those derived from IACS design equations for both types of stiffener shows that for ultimate strength, the two methods compare well in some cases while they differ significantly in other cases. In the post-ultimate portion of the load-shortening curves, there is a considerable difference between the two methods. The IACS

design equations are found to overestimate the post-ultimate capacity of stiffened plates which may affect the accuracy of ultimate strength calculations for ship hull girders.

5.2 Introduction

Longitudinally stiffened plates are the primary load-carrying elements in ship hull girders subjected to wave-induced longitudinal bending. Accurate evaluation of the strength and behaviour of these stiffened plates is essential for the safe design of ship structures. However, the determination of stiffened plate ultimate strength is a complicated problem due to the various combinations of geometry, material properties and boundary conditions that may be encountered in practice. Furthermore, fabrication-related imperfections such as welding-induced residual stress and distortion in ship hull girders, are complex and difficult to estimate, so their magnitudes and distributions are often simplified, assumed or neglected in design, leading to uncertainty in predictions of stiffened plate strength and behaviour.

The behaviour of stiffened plates under axial load is typically represented by an average axial stress versus axial strain curve, also referred to as a load-shortening curve. For tensile axial loads, welding–induced residual stress and distortion reduce stiffness in the pre-ultimate strength region and the ultimate strength is reached when gross yielding occurs. For compressive axial loads, distortions change the failure type from a sudden event to a more gradual process with a less severe reduction in load-carrying capacity as the applied strain increases beyond the strain at ultimate load (ISSC, 1979). Residual stresses cause early yielding that reduces the effective cross-sectional area resisting

compressive load, leading to the possibility of premature local buckling and column buckling. The combined effects of residual stress and distortion cause a reduction in the load-carrying capacity of stiffened plates near the collapse load, smoothing the load-shortening curve in that region (Gordo & Guedes Soares, 1993).

Although it is commonly accepted that welding-induced residual stresses reduce the ultimate strength of stiffened plates under axial compression, researchers have reached different conclusions regarding the extent of their influence on ultimate strength. This disparity is evident in a benchmark study coordinated by Ohtsubo and Sumi (2000) where there is significant scatter among strength reductions due to residual stress predicted by different contributors to the study. The differences are attributed to the various assumptions and idealizations made with regards to welding-induced residual stress in stiffened plate analysis. For example, Hansen (1996) used an approximate analytical method to describe the load-shortening behaviour of stiffened plates assuming a two-dimensional longitudinal residual stress distribution, constant along the length of the plate and no residual stress in the stiffener. Other methods of stiffened plate analysis use empirical techniques such as the Johnson-Ostenfeld correction to account for inelastic effects in stiffened plates under axial compression (Gordo & Guedes Soares 1993, IACS 2009). Hansen (1996) concluded that residual stresses have the potential to decrease stiffened plate ultimate strength by as much as 25% whereas Gordo and Guedes Soares (1993) found that ultimate strength decreases by around 10% when the compressive residual stress in the plate is taken as $0.2\sigma_y$. Gannon *et al*. (2011) used the finite element method to simulate welding of flat-stiffeners to steel plates, giving the complete, three

dimensional residual stress and distortion fields that were later used in a stiffened plate ultimate strength analysis. They found that the strength of flat bar stiffened plates was reduced by as much as 16.5% due to the presence of welding residual stress. They also compared load-shortening curves produced using finite element models with design curves given by IACS (2009) and found that the IACS curves overestimated the capacity of the stiffened plates in the post-ultimate part of the curves by a significant amount.

In the design and analysis of stiffened plates, the complex, three dimensional distribution of residual stress may be simplified by assuming a two-dimensional stress distribution that is constant along the length of the stiffened plate. Figure 5.1 shows one such simplified residual stress distribution used by Smith (2008) that consists of a zone of tensile stress in the plate at the weld location equal to the yield stress σ_y, with a width of $2\eta t$ and a nearly uniform compressive residual stress across the rest of the plate, where t is the plate thickness and η is a parameter defining the width of the tensile stress zone. The value of η usually ranges from 3 to 4.5, depending on the geometry and welding conditions (Faulkner, 1975). This longitudinal residual stress distribution is consistent with measured values published by Nagaraja Rao and Tall (1961). Sometimes the distribution of residual stress is further simplified by considering only the residual stress in the plate in a stiffened plate model. Based on the assumption that the longitudinal residual stresses in the plate alone are in equilibrium, Faulkner (1975) suggests that the magnitude of compressive residual stress in the plate σ_r (Figure 5.1), be taken as:

$$\sigma_r = \frac{2\eta\sigma_y}{b/t - 2\eta} \tag{5.1}$$

where b is the plate width.

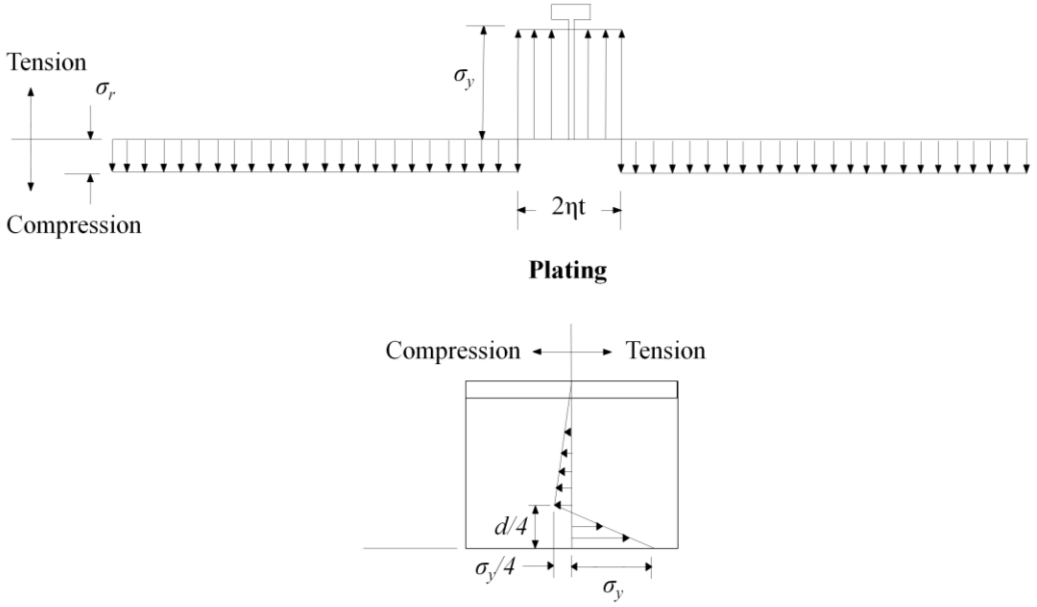

Figure 5.1, Longitudinal residual stress distribution in welded stiffened plates

Maximum out-of-plane plating imperfections δ_{o1}, measured in surveys of ship and civil engineering structures are typically expressed as a fraction of plate thickness and relate approximately to the plate slenderness β_0, given by:

$$\beta_0 = \frac{b}{t}\sqrt{\frac{\sigma_y}{E}} \tag{5.2}$$

where E is the elastic modulus. Typical values of δ_{o1} lie in the range of $0.05\,\beta_0^2\,t$ to $0.15\,\beta_0^2\,t$ with extreme values up to $0.4\,\beta_0^2\,t$ for heavily welded plates. Smith *et al.* (1992) suggest typical levels of welding-induced out-of-plane distortion of plates between

stiffeners that are the source of the familiar "hungry horse" shape seen in many welded ship hulls. They considered slight, average and severe levels of distortion defined by:

$$\frac{\delta_{01}}{t} = \begin{cases} 0.025\beta_0^2 & \text{for slight imperfections} \\ 0.1\beta_0^2 & \text{for average imperfections} \\ 0.3\beta_0^2 & \text{for severe imperfections} \end{cases} \tag{5.3}$$

Just as residual stress distributions are simplified, the complex three-dimensional distribution of welding-induced distortion is also simplified for use in design and analysis of stiffened plates. Distortions are usually idealized by assuming that they are distributed in a half sine wave along the length of a stiffened plate and across the width of the plate between stiffeners (Ohtsubo & Sumi, 2000).

The primary objective of this study is to evaluate the influence of welding-induced residual stress and distortion on the strength and behaviour of angle and tee-stiffened plates. The residual stress and distortion introduced during welding of stiffeners to the plates are determined using a three-dimensional finite element simulation. Angle and tee-stiffened plates are commonly used in ship hull girder construction and to the authors' best knowledge there is little, if any, reported literature on the three-dimensional simulation of residual stress and distortion fields in the study of strength and behaviour of angle and tee-stiffened plates. The 3D simulation of residual stress and distortion using finite element modelling has been used and validated in a previous study dealing with flat-bar stiffened plates (Gannon *et al.*, 2011). In this paper, the same methodology is adopted to study the strength and behaviour of angle and tee-stiffened plates under axial

load. Load-shortening curves are obtained to characterize the behaviour of angle and tee-stiffened plates under axial compressive load and to compare the behaviour of stiffened plates with and without welding-induced residual stress. The accuracy of design load-shortening curves, given by the International Association of Classification Societies (IACS, Common structural rules for bulk carriers, 2009) is also investigated by comparison with the curves calculated by finite element analysis.

5.3 Finite Element Modeling

5.3.1 Welding Simulation

Welding-induced three-dimensional residual stress and distortion fields in stiffened plates were simulated by nonlinear finite element analysis using ANSYS (2009) software. The finite element simulation consisted of two sequential analyses. The first of these was a nonlinear thermal analysis wherein the transient temperature field caused by the moving heat source was calculated. In a subsequent nonlinear structural analysis, the temperature field time history was applied as a series of loads where each load step corresponds to an increment in the heat source position along the weld path.

Ten millimeter long tack welds, at 250 mm intervals, were used for initial attachment of the stiffener to the plate. The stiffener was connected to the plate by 7 mm continuous fillet welds, deposited sequentially on each side of the base of the stiffener. The welding heat input and corresponding speed of welding was consistent with values recommended in the Canadian Welding Standard, CSA W59-03 (Canadian Standards Association,

2003) for the 7 mm fillet weld used in the welding simulation. The stiffened plate was allowed to cool for 30 min following the completion of the first weld and cooled to the ambient temperature of 20 °C once the second weld was completed. Both the plate and stiffener were assumed to be made from AH36 shipbuilding steel with temperature dependent material properties adopted from Michaleris and DeBaccari (1997). The yield strength and elastic modulus at room temperature were taken as 360 MPa and 210 GPa, respectively. Elasto-plastic material behaviour was assumed with von Mises failure criteria and associated flow rule. Large strains and displacements were also considered.

5.3.2 Mesh and Boundary Conditions

Figure 5.2 shows a tee-stiffened plate finite element mesh that is representative of meshes used for all tee and angle-stiffened plate models. A convergence study revealed that a relatively fine mesh with 12 elements through the thickness of the plate is required near the weld in order to accurately characterize the severe thermal gradient in that area. In regions further away from the weld location, the mesh was made coarser in order to reduce computational time. A minimum of 4 elements was used through the thickness of all parts of the stiffened plates. The 8-node Solid70 hexahedral element was used for the thermal analysis portion of the welding simulation. For the structural part of the welding simulation, and for the ultimate strength analysis, the same mesh was used as in the thermal analysis, but the element type was changed to the 8-node, Solid185. Both element types are bi-linearly interpolated isoparametric hexahedrons. For the thermal element, only the temperature degree of freedom is considered at each node, whereas the

three displacements along the Cartesian coordinate axes are used as degrees of freedom at each node for the structural element. All nodes at the two end cross-sections of the stiffened plates were connected to the node at their centroid using beam elements with high bending and axial stiffness, so that these cross-sections would remain plane during the ultimate strength analysis. These elements were inactive during the structural part of the welding simulation and then activated for the ultimate strength analysis using the ANSYS element birth and death feature.

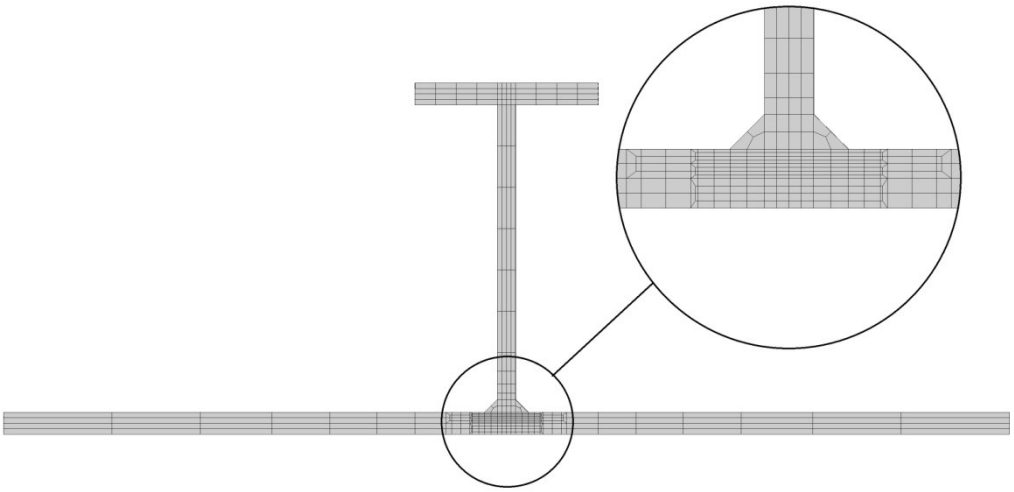

Figure 5.2, Tee-stiffened plate finite element mesh

Boundary conditions in the stiffened plates were applied in such a way that they reproduced the level of restraint observed in stiffened plates in ship hull girders. Longitudinal edges were constrained to remain straight when moving in the plane of the plating, and free to move out of the plane of the plating as suggested by Dow *et al.* (1981). The end cross-sections of the stiffened plates were simply supported, where displacements were constrained along all three coordinate axes at the centroid of one end, while vertical and transverse displacements were prevented at the opposite end. Boundary

conditions for both the welding simulation and the ultimate strength analysis were similar, except that for the ultimate strength analysis the beam elements connecting the nodes at the end cross-sections were activated, simulating the restraint provided by addition of transverse frames following welding of the longitudinal stiffener.

5.3.3 Strength Analysis Procedure

For the ultimate strength analysis, an axial displacement was applied to the centroidal node of the end cross-section where only in-plane translations were constrained. This prescribed displacement resulted in a force on the end cross-section that was evenly distributed through the stiff beam elements. The applied displacement was used instead of a force in order to track the post-ultimate, unloading part of the stiffened plate response.

5.4 Verification of the Model

In order to verify the accuracy of the welding simulation method, the results of a welding simulation were compared with experimental results given by Deng *et al.* (2007), who joined a 300 x 500 x 9 mm flat bar stiffener to a 500 x 500 x 9 mm steel plate by continuous, 6 mm fillet welds using a CO_2 gas metal arc welding process. While a detailed description of the verification can be found in Gannon *et al.* (2010), the key aspects are provided as follows for reference.

The finite element welding simulation consisted of sequential transient thermal and nonlinear structural analyses. The thermal analysis used a moving heat source to represent the welding torch, where each load step represented an increment in the position of the heat source along the weld path. As the heat source progressed along the weld path, weld elements were activated using the ANSYS element birth and death feature that deactivates elements by multiplying their stiffness or conductivity by a severe reduction factor and removes any loads applied to deactivated elements from the global load vector. Once one side of the stiffener was welded, the part was allowed to cool for 30 minutes and then the other side of the stiffener was welded to the plate and the complete stiffened plate was cooled to ambient temperature.

The transient temperature field from the thermal analysis was used as a series of loads in the subsequent structural analysis where each load step represented an increment in the welding torch position along the weld path. The ANSYS element birth and death feature was used in the structural analysis to activate weld elements behind the welding torch once their temperature fell below the solidification temperature, taken as 1450 °C. Movement of the heat source, thermal load application in the structural analysis and the element activation scheme were controlled by user-defined subroutines written in the ANSYS parametric design language. Temperature dependent material properties for the validation model were adopted from Deng *et al.* (2008).

The vertical deflection of the plate at mid-span as predicted by the welding simulation is shown in Figure 5.3 along with experimentally measured values (2007). The magnitude

and distribution of distortion predicted by the finite element analysis were in good agreement with measured values. Although residual stress measurements were not reported, the magnitude and distribution of longitudinal residual stress predicted by numerical analysis are consistent with other measurements available in literature (Nagaraja Rao & Tall 1961, Kenno *et al.* 2010). No experimental results were available for the stiffener types considered in the present study.

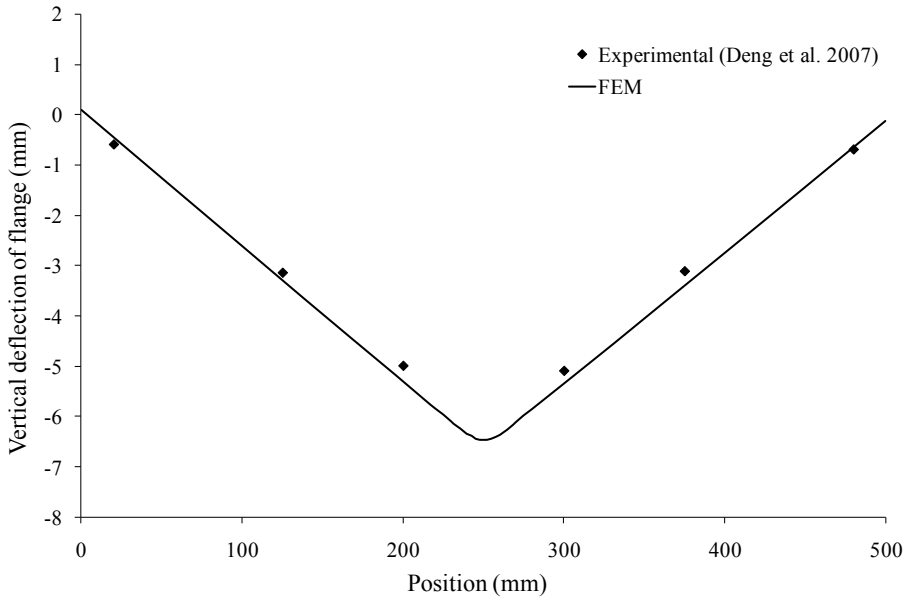

Figure 5.3, Comparison of plate vertical deflection for welding simulation validation

5.5 Parametric Study

The behaviour of angle and tee-stiffened plates under axial compressive load was studied considering 3D residual stress and distortion fields predicted using the welding simulation method described in the previous section. Load versus end-shortening curves for each stiffened plate were determined by application of an axial displacement at the centroid of one end and calculation of the reaction at the centroid of the opposite end for

each increment in the applied displacement. Table 5.1 summarizes the stiffened plate geometries used in this study where the dimensions, illustrated in Figure 5.4, were chosen to represent a range of plate slenderness β_0, and column slenderness λ, values given by:

$$\lambda = \left(\frac{a}{\pi r}\right)\sqrt{\sigma_y / E} \tag{5.4}$$

where a is the length of the stiffened plate and r is the radius of gyration. In calculating the radius of gyration, the effective width b_{em}, given by Eqn. (5.5), and the reduced effective width of the plate $b_{em'}$ at ultimate load, given by Eqn. (5.6), as derived by Faulkner (1975),were used to calculate the effective area and moment of inertia of the stiffened plates, respectively.

Table 5.1, Stiffened plate model dimensions

Section ID	a (mm)	b (mm)	t (mm)	d (mm)	w (mm)	t_w (mm)	t_f (mm)	β	λ
A1	2000	350	12	180	60	10	12	1.208	0.406
A2	2000	550	12	180	60	10	12	1.898	0.437
A3	2000	750	12	180	60	10	12	2.588	0.451
A4	2000	950	12	180	60	10	12	3.278	0.459
A5	2000	550	12	100	60	10	12	1.898	0.799
A6	2000	550	12	140	60	10	12	1.898	0.566
A7	2000	550	12	220	60	10	12	1.898	0.356
T1	2000	350	12	180	100	10	12	1.208	0.349
T2	2000	550	12	180	100	10	12	1.898	0.391
T3	2000	750	12	180	100	10	12	2.588	0.425
T4	2000	950	12	180	100	10	12	3.278	0.454
T5	2000	550	12	100	100	10	12	1.898	0.669
T6	2000	550	12	140	100	10	12	1.898	0.494
T7	2000	550	12	220	100	10	12	1.898	0.324

$$\frac{b_{em}}{b} = \begin{cases} \dfrac{2.25}{\beta_0} - \dfrac{1.25}{\beta_0^2} & \beta > 1 \\ 1 & \beta \le 1 \end{cases} \tag{5.5}$$

$$\frac{b_{em'}}{b} = \begin{cases} \dfrac{1}{\beta} & \beta_0 > 1 \\ 1 & \beta_0 \le 1 \end{cases} \tag{5.6}$$

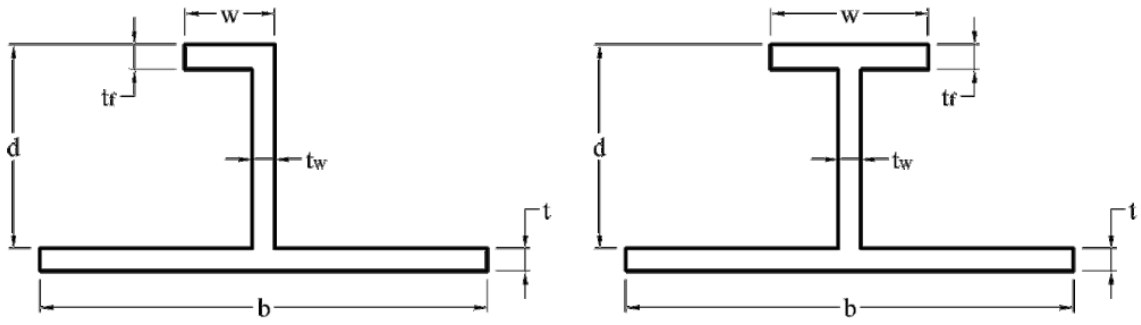

Figure 5.4, Stiffened plate model dimensions

5.6 Residual Stress and Distortion

5.6.1 Residual Stress – Angle-Stiffened Plates

Longitudinal residual stresses predicted by finite element modelling, for the plate, web and flange of angle-stiffened plates are shown in Figure 5.5, Figure 5.6 and Figure 5.7, respectively. The residual stress distributions are taken at the mid-span cross-sections of each stiffened plate and in the mid-plane of each component. The magnitude and distribution of longitudinal residual stress in the plates is consistent with experimental measurements and numerical results reported in other literature (Nagaraja Rao & Tall 1961, Yuan & Ueda 1996). Tensile stresses equal to the yield stress were present near the

weld, balanced by nearly uniform compressive residual stresses in the remainder of the plate. The magnitude of compressive residual stresses in the plates varied from -25 MPa to -75 MPa among the seven models. The width of the tensile residual stress zone η, as defined in Figure 5.1, varied from 2.6 to 3.3, similar to values suggested by Faulkner (1975). Although there was little variation in tensile residual stress in the plate among the different models, the magnitude of compressive residual stress decreased as plate slenderness β_0, increased where model A1 with the lowest β_0 value attained the highest compressive residual stress. Comparing residual stress in the plates of models A2, A5, A6 and A7 with the same plate slenderness β_0, but varying column slenderness λ, it is noted that there is little difference in the distribution of residual stress despite the fact that stiffener heights vary significantly among those models.

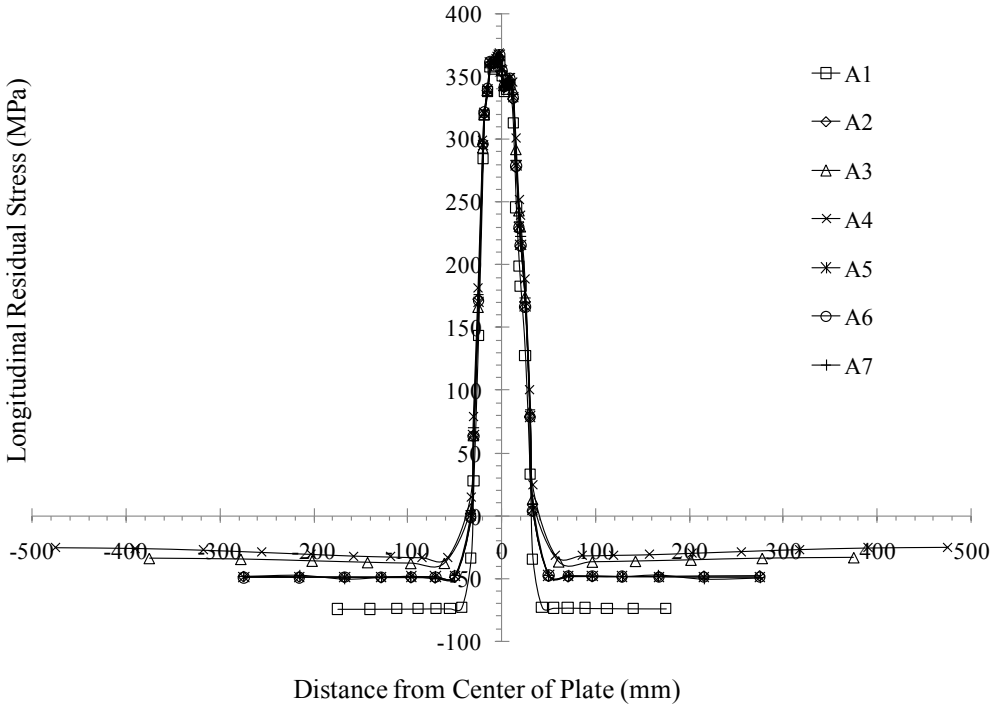

Figure 5.5, Longitudinal residual stress in the plate of angle-stiffened plates

As shown in Figure 5.6 for the webs of the angle-stiffened plates, tensile residual stresses equal to yield at the weld location quickly decreased, changing to compressive stresses for all models except A4. This decrease in residual stress, towards a state of residual compression was greater in models with low plate slenderness where model A1, with the lowest plate slenderness, showed the most pronounced residual compression. Figure 5.7 shows that longitudinal residual stresses in the stiffener flanges varied in a more or less linear manner, becoming increasingly negative towards the flange tip for most models. Residual stresses in the flanges varied in magnitude from -12 MPa to 10 MPa.

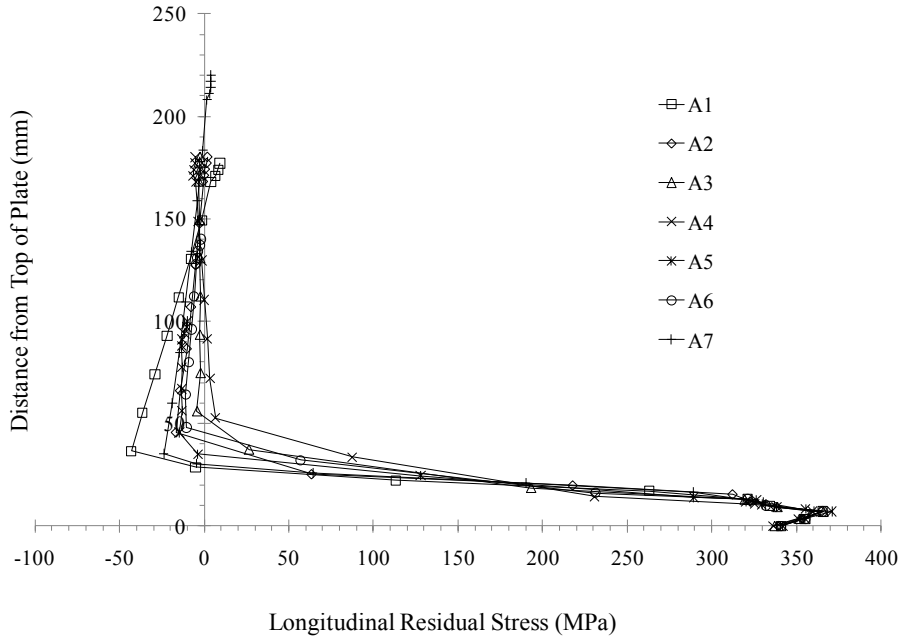

Figure 5.6, Longitudinal residual stress in the web of angle-stiffened plates

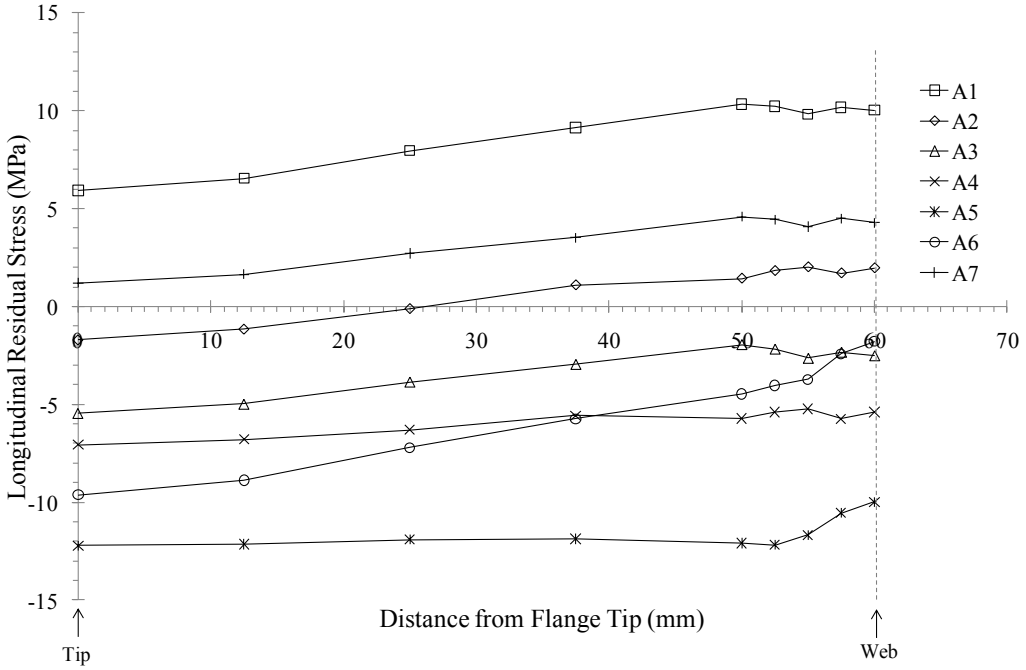

Figure 5.7, Longitudinal residual stress in the flange of angle-stiffened plates

The numerical results showed significant variations in longitudinal residual stress along the length, through the thickness and across the width of the plate. Figure 5.8 illustrates the variation of longitudinal residual stress along the length and across the width of the plate for model A4, with elements near the weld removed to allow for a finer distribution of stress contours in the compression zone. Figure 5.9 shows that there was also considerable variation in longitudinal residual stress in the angle-stiffener of model A4, where it appears that the presence of tack welds caused a repetitive pattern of longitudinal residual stress along the length of the stiffener. This variation in stress along the length was more prominent at the surface of the web than at the mid-plane. Substantial through-thickness variations in longitudinal residual stress were observed in all of the components making up the angle-stiffened plates. Figure 5.10 illustrates the variation in longitudinal residual stress through the thickness of the stiffened plate components, for model A4 at

mid-span. These figures exemplify the complex, three-dimensional characteristics of welding-induced residual stress fields in stiffened plates, that are often not considered in simplified distributions used in many stiffened plate strength analyses.

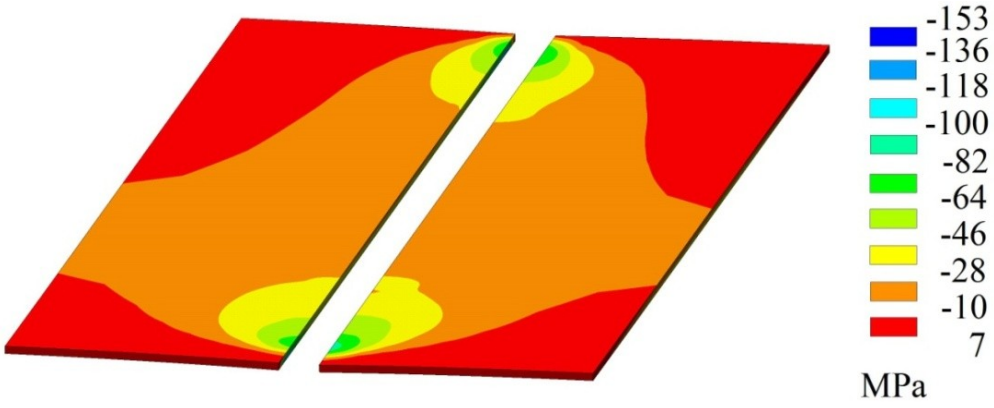

Figure 5.8, Longitudinal residual stress in the plate (A4)

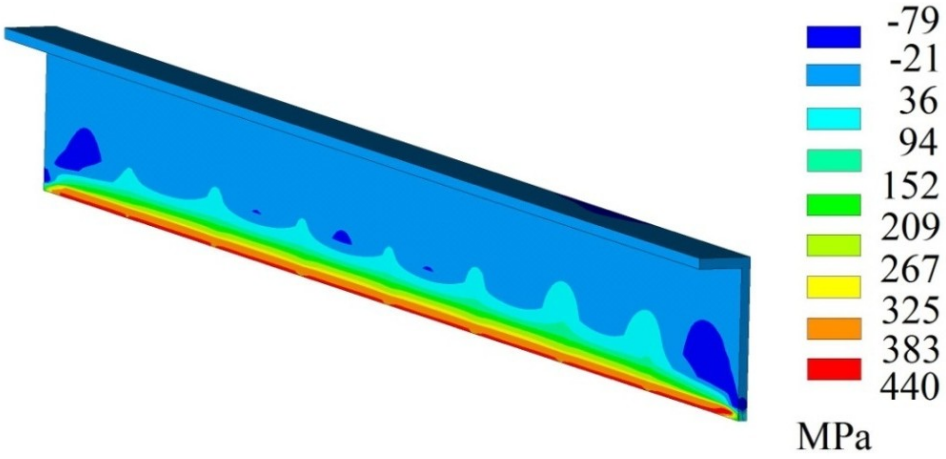

Figure 5.9, Longitudinal residual stress in an angle-stiffener (A4)

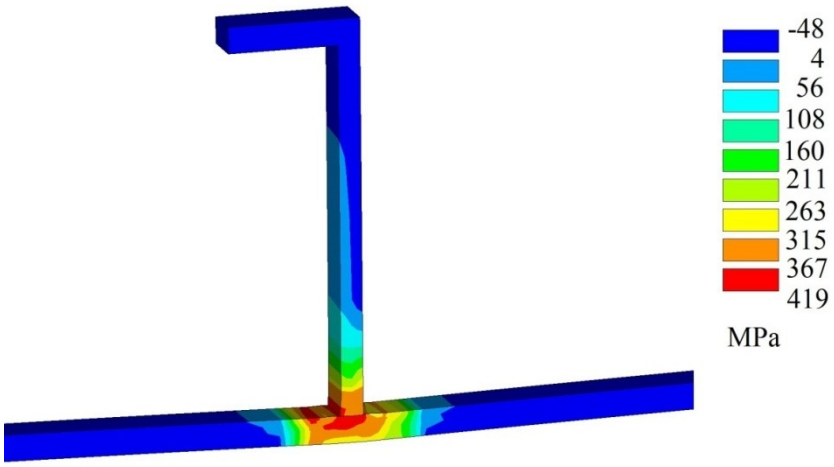

Figure 5.10, Longitudinal residual stress distribution at mid-span (A4)

5.6.2 Residual Stress – Tee-Stiffened Plates

The distributions of welding-induced longitudinal residual stresses in mid-planes of plates, webs and flanges at mid-span of the tee-stiffened plates, predicted by finite element analysis are shown in Figure 5.11, Figure 5.12 and Figure 5.13, respectively. As shown in Figure 5.11, tensile stresses equal to the yield stress are present at the weld location, where the width of the tensile stress zone η, varies from 2.6 to 3.3. In the remainder of the plate, nearly uniform compressive residual stresses were introduced with magnitudes varying from -29 MPa to -74 MPa. Similar to angle-stiffened plates, the magnitude of compressive residual stress in the tee-stiffened plates increased with decreasing plate slenderness.

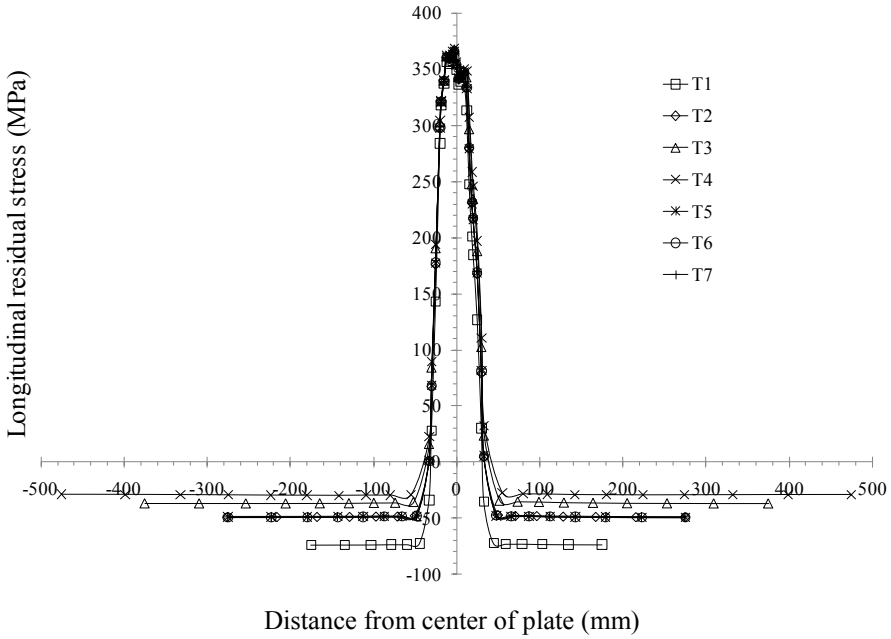

Figure 5.11, Longitudinal residual stress in the plate of tee-stiffened plates

Figure 5.12 shows that the webs of the tee-stiffened plates were subjected to tensile residual stresses equal to the yield stress near the weld. These quickly reduced to low tensile or compressive stresses approximately 30 mm from the base of the web, after which the residual stresses reduced significantly towards the top of the web. Figure 5.13 shows that the residual stresses in the flanges of the tee-stiffeners varied from -10 MPa to 7 MPa. For models T2, T5, T6 and T7 that have the same plate slenderness β_0, residual stresses in the flange became increasingly compressive as the column slenderness λ increased. The residual stress distribution in the flanges was nearly uniform for all models except for T5 and T6. Noting that models T5 and T6 have the relatively short stiffeners, the asymmetrical nature of the welding process may have a more pronounced effect on the longitudinal residual stress distribution, resulting in an asymmetric stress pattern. Significant variations in longitudinal residual stress were also found to exist

through the thickness, across the width and along the length for tee-stiffened plates. The three-dimensional distribution of residual stresses were similar to those shown in Figures 8 through 10 for angle-stiffened plates.

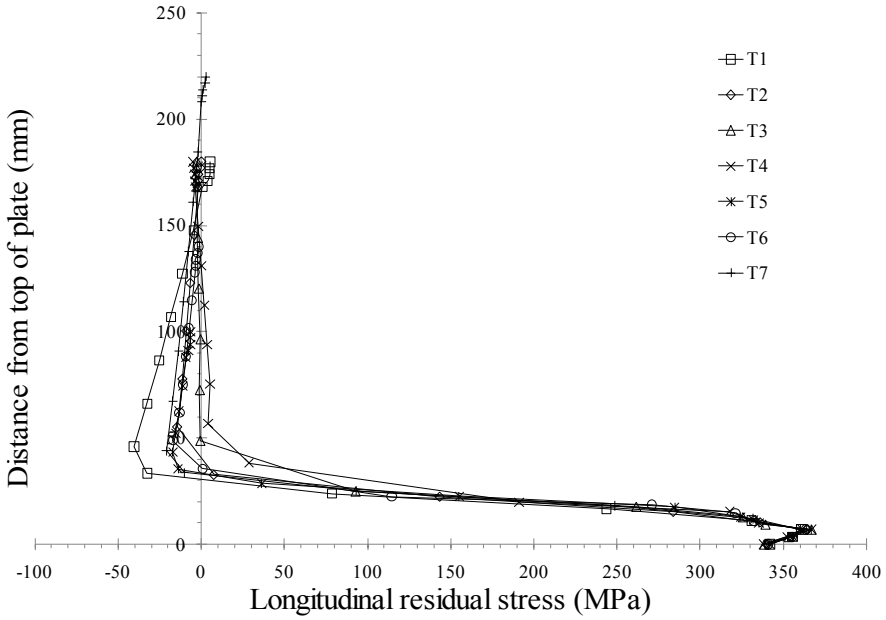

Figure 5.12, Longitudinal residual stress in the web of tee-stiffened plates

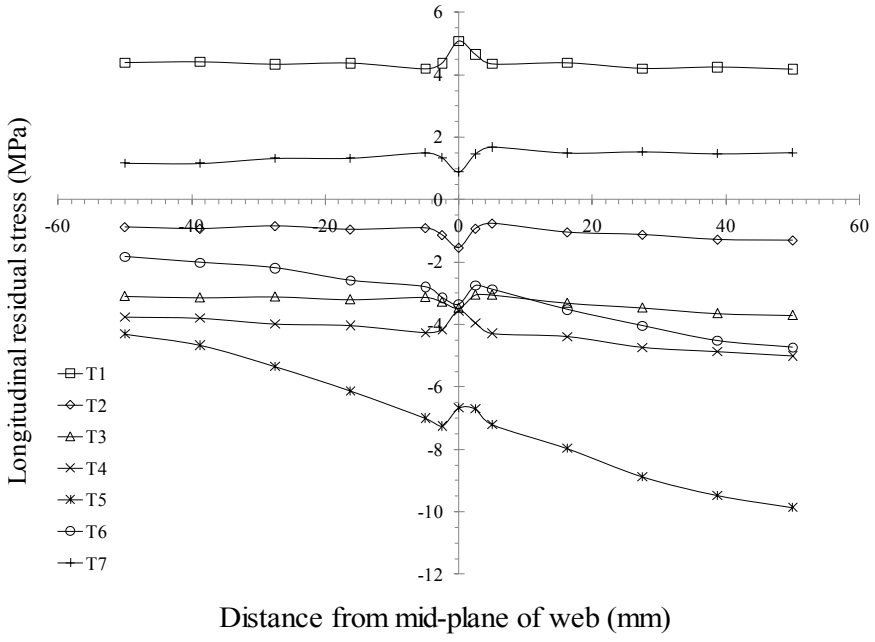

Figure 5.13, Longitudinal residual stress in flange of tee-stiffened plates

5.6.3 Distortion – Angle-Stiffened Plates

In the following discussion of welding-induced distortions, references to coordinate axes refer to the coordinate system shown in Figure 5.14. Figure 5.15 shows out-of-plane distortions predicted by finite element analysis at the mid-plane of the angle-stiffened plates. The distortion in all plates assumed the "hungry horse" shape often seen in welded ship structures. Comparison of models A1 to A4 shows that the distortion became more pronounced as the plate slenderness β_0, increased. For a given plate slenderness, the increase of column slenderness resulted in an increase in distortion but the extent is not as significant as in the case of plate slenderness. For all models except A1, the vertical distortion at the longitudinal edges of the plates, relative to the middle of the plate fell between the slight and average levels of imperfection defined by Smith *et al.* (1992) as in Eqn. (5.3). In most cases, the imperfections were closer to slight than average. Model A4, for example had δ_{01}/t = 0.475, bounded by 0.268 for slight imperfections, and 1.075 for average imperfections.

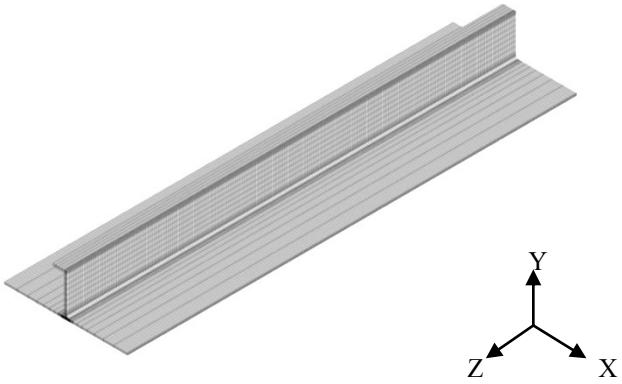

Figure 5.14, Stiffened plate coordinate system

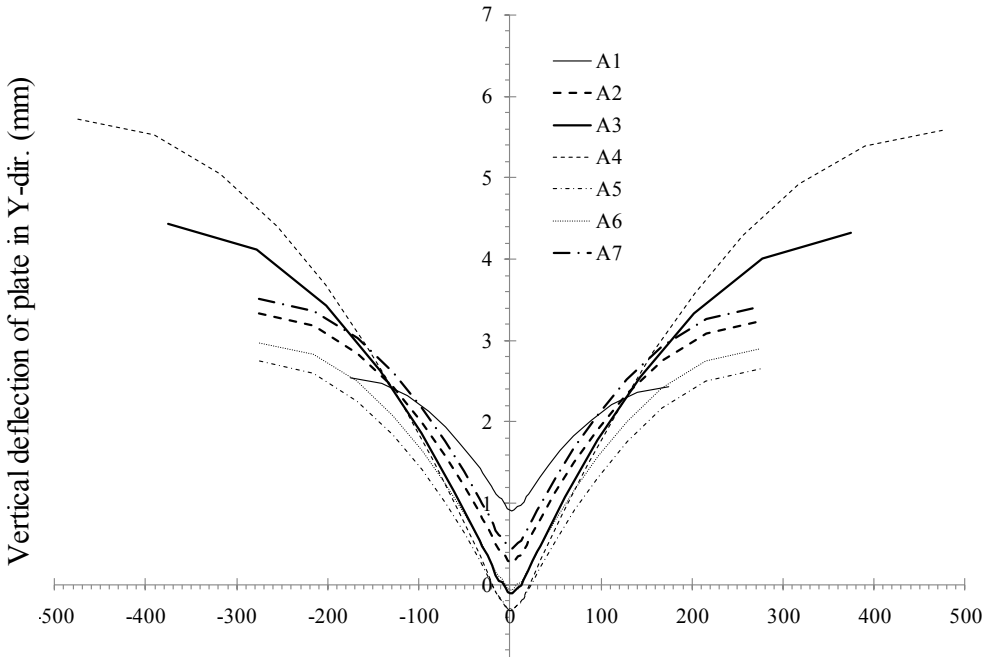

Figure 5.15, Vertical distortion of angle-stiffened plate

Distortions of the angle-bar stiffened plates in the direction of the Y-axis, along the length of the stiffener are shown in Figure 5.16. The simulated longitudinal distortions show a half-sine wave pattern for all models, which is consistent with experimental results reported by Dow (1991). In stiffened plate design and analysis, values of maximum longitudinal distortion are often taken as directly proportional to the plate length, *a* (Ohtsubo & Sumi 2000, Dow 1991). The results in Figure 5.16 however, indicate that there is some correlation between the neutral axis position, and the magnitude and direction of longitudinal distortion. For those models that had the same β_0 (A2, A5, A6, and A7), the direction of longitudinal distortion changed from the positive to negative Y-direction as the distance from the bottom of the plate to the neutral axis

decreased. This is attributed to a change in sign of the net moment of the longitudinal residual stresses about the neutral axis.

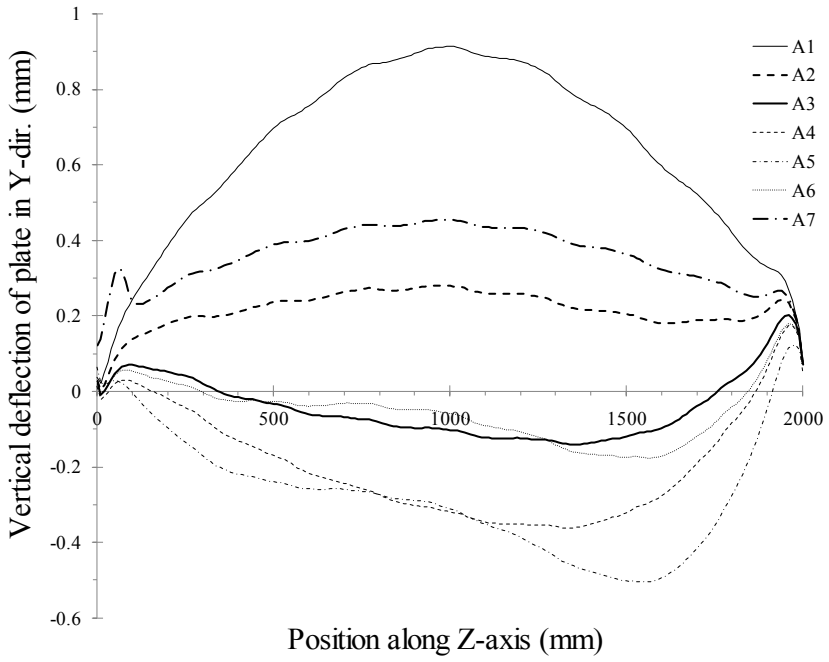

Figure 5.16, Distortion along the stiffener axis of angle-stiffened plates

Lateral distortions at the top of the web of the angle-stiffeners, predicted by the numerical models are shown in Figure 5.17. The magnitudes of maximum lateral distortion in the x-direction varied from -0.3 mm to 0.35 mm. These are smaller than typical values used in stiffened plate analysis, such as 0.001a (Ohtsubo & Sumi, 2000). Furthermore, it is often assumed in stiffened plate analysis that lateral distortions along the length of stiffeners are distributed in a half-sine wave (Ohtsubo & Sumi, 2000). The results of the numerical analyses however, show that the distribution of lateral distortion is more complex than this idealized shape in most cases. It should be noted however, that in reality the total length of stiffener being welded to the plate may be longer than a single frame space, so

that there may be some lateral restraint at the ends of the stiffener that could affect the pattern of lateral distortion.

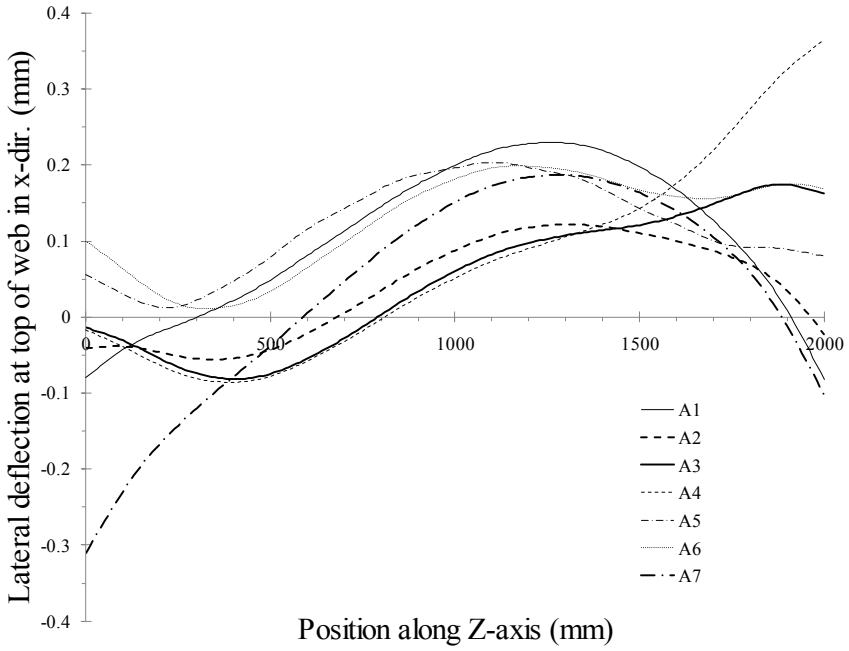

Figure 5.17, Lateral distortion at top of angle-stiffeners

5.6.4 Distortion – Tee-Stiffened Plates

Welding-induced distortions predicted by finite element analysis at the mid-plane of tee-stiffened plates are shown in Figure 5.18, Figure 5.19 and Figure 5.20. Out-of-plane distortions of the plates, shown in Figure 5.18, took on a "hungry horse" type of distribution, and with the exception of model T1, the magnitudes of maximum deflections fell between the slight and average levels defined by Smith *et al.* (1992). Figure 5.19 shows the Y-direction distribution of distortion along the length of the stiffener. Similar to the angle-stiffened plates, the magnitudes of maximum distortions were less than typical values used for stiffened plate strength analysis. Also, the direction of distortion

changed from the positive to negative y-direction as λ increased for those models with constant β_0 (T7, T2, T6 and T5).

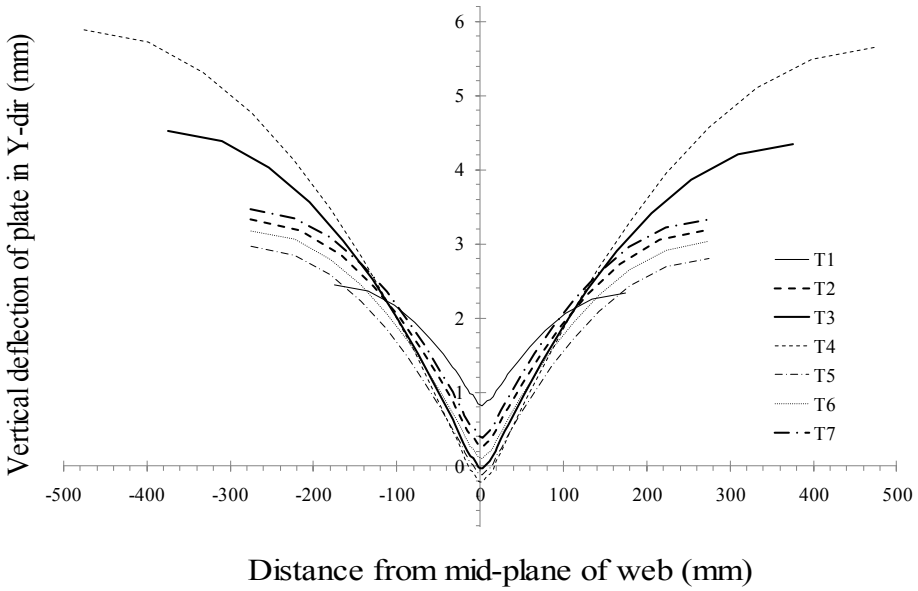

Figure 5.18, Vertical distortion of tee-stiffened plate

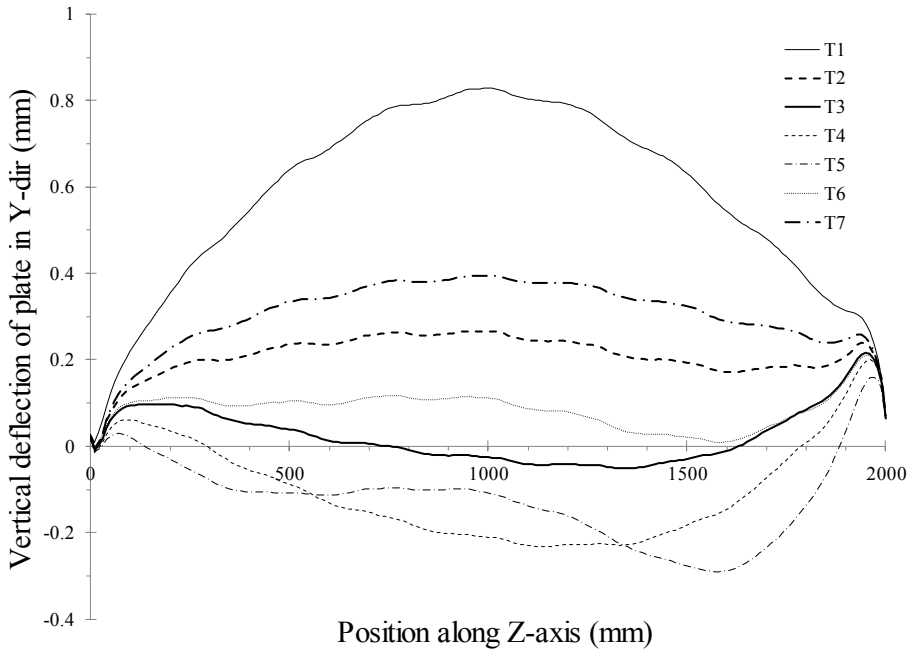

Figure 5.19, Distortion along the length of the stiffener for tee-stiffened plates

Figure 5.20 shows the lateral distortions of the tee-stiffeners at the top of the web. The magnitude of maximum lateral distortions varied from -0.15 mm to 0.38 mm. The lateral distortions showed a similar trend for all models and they were not distributed in a half-sine wave as is often assumed in stiffened plate strength analysis (Ohtsubo & Sumi, 2000). A half-cosine wave appears to be a more accurate idealization of the stiffener lateral distortions for the models considered in this study. Once again, similar to the angle-stiffened plates, if the length of stiffener were long enough to span several frame spaces, lateral distortions of the stiffeners could take on a different shape due to the lateral restraint provided by the part of the stiffener that extends into adjacent bays.

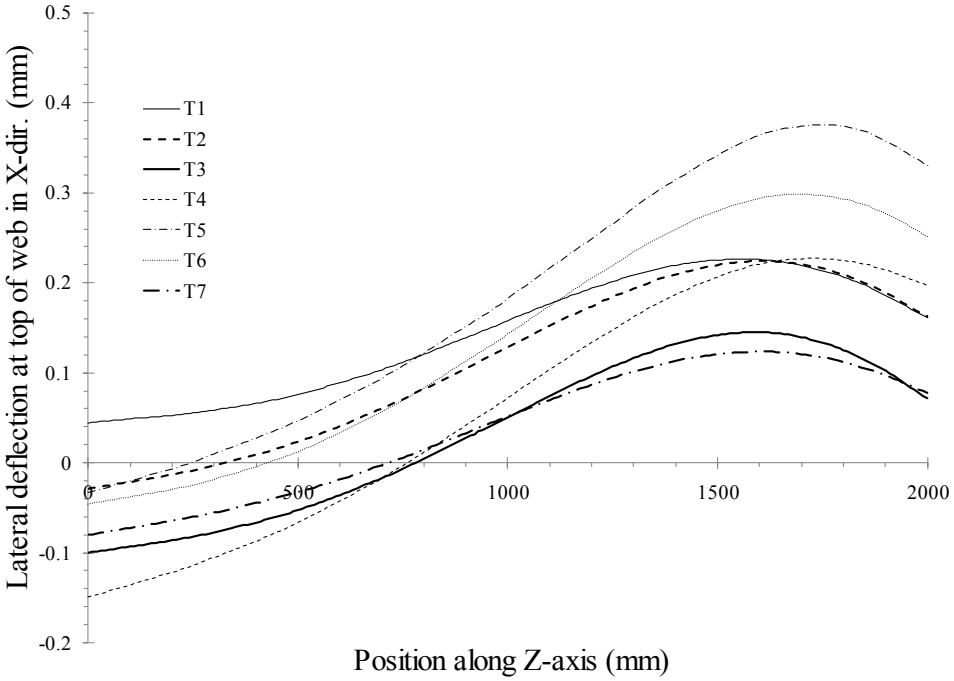

Figure 5.20, Lateral distortion at top of tee-stiffeners

5.7 Behaviour Under Axial Compressive Load

Following the welding simulation, with residual stress and distortion included in the model, a displacement controlled analysis was conducted to obtain the load-shortening curves of the stiffened plates listed in Table 5.1. Each stiffened plate analysis was then run a second time with the same welding-induced distortion, but with no residual stress in order to assess the influence of welding-induced residual stress on the stiffened plate behaviour. Table 5.2 provides ultimate stress values, normalized with respect to the yield stress, along with buckling directions for each model. Also included in the table are normalized ultimate stress values predicted using analytical methods prescribed in the IACS Common Structural Rules for Bulk Carriers (IACS, Common structural rules for bulk carriers, 2009) where an empirical method is used to account for the influence of residual stress.

5.7.1 Ultimate Strength

Table 5.2 shows that the reduction in ultimate strength due to residual stress was as high as 15.1% and 13.5% for angle and tee-stiffened plates respectively. Most models failed by flexural buckling towards the stiffener (mode S) when residual stresses were considered. Examples of both failure modes are shown in Figure 5.21. For both angle and tee-stiffened plates, ultimate strength decreased with increasing plate slenderness as shown in Figure 5.22 and Figure 5.23, respectively. The ultimate strength values

calculated using the IACS Common Structural Rules for Bulk Carriers (IACS, Common structural rules for bulk carriers, 2009) are also included in the figures for comparison.

Table 5.2, Ultimate strength predictions

Model	1) FEM σ_u/σ_y without residual stress	Buckling direction of 1)	2) FEM σ_u/σ_y with residual stress	Buckling direction of 2)	% Strength reduction from 1) to 2)	3) IACS σ_u/σ_y	% Diffence between 3) and 2)
A1	1.006	P	1.005	S	0.1	0.958	4.7
A2	1.011	P	0.858	S	15.1	0.837	2.4
A3	0.773	S	0.702	S	9.2	0.705	-0.4
A4	0.634	S	0.590	S	6.9	0.608	-3.1
A5	0.944	S	0.841	P	10.9	0.720	14.4
A6	0.991	S	0.862	S	13.0	0.802	7.0
A7	0.974	S	0.859	S	11.8	0.857	0.2
T1	1.000	P	1.000	P	0.0	0.965	3.5
T2	0.999	P	0.870	S	12.9	0.850	2.3
T3	0.733	S	0.648	S	11.6	0.725	-11.9
T4	0.630	S	0.579	S	8.1	0.623	-7.6
T5	0.997	S	0.862	S	13.5	0.760	11.8
T6	0.995	P	0.861	S	13.5	0.822	4.5
T7	0.997	P	0.864	S	13.3	0.866	-0.2

P: Buckling towards the plate

S: Buckling towards the stiffener

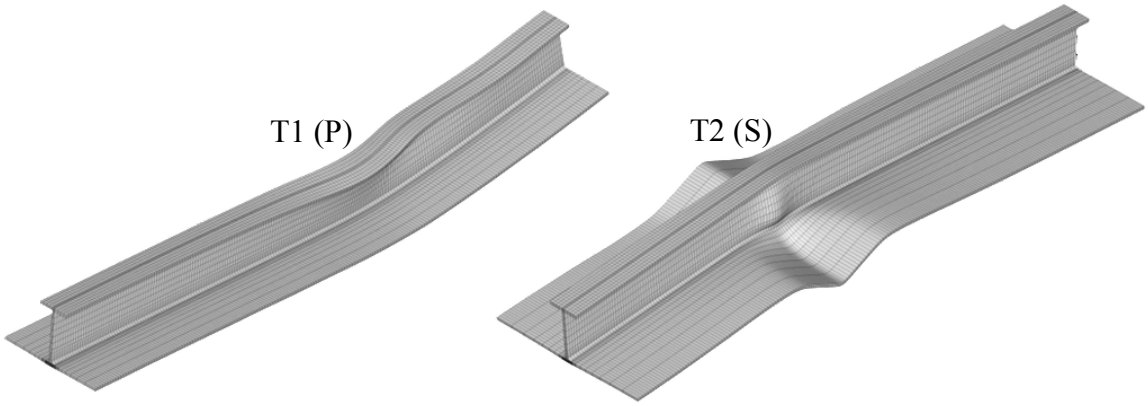

Figure 5.21, Post ultimate deformed shapes (scaled 1.5x)

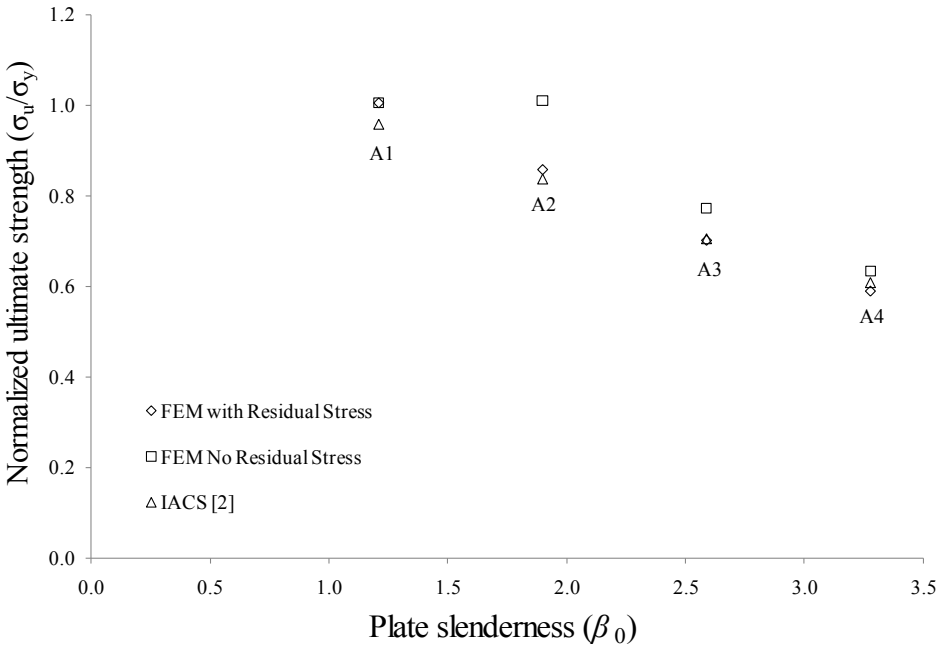

Figure 5.22, Variation in ultimate strength with plate slenderness - angle-stiffened plates

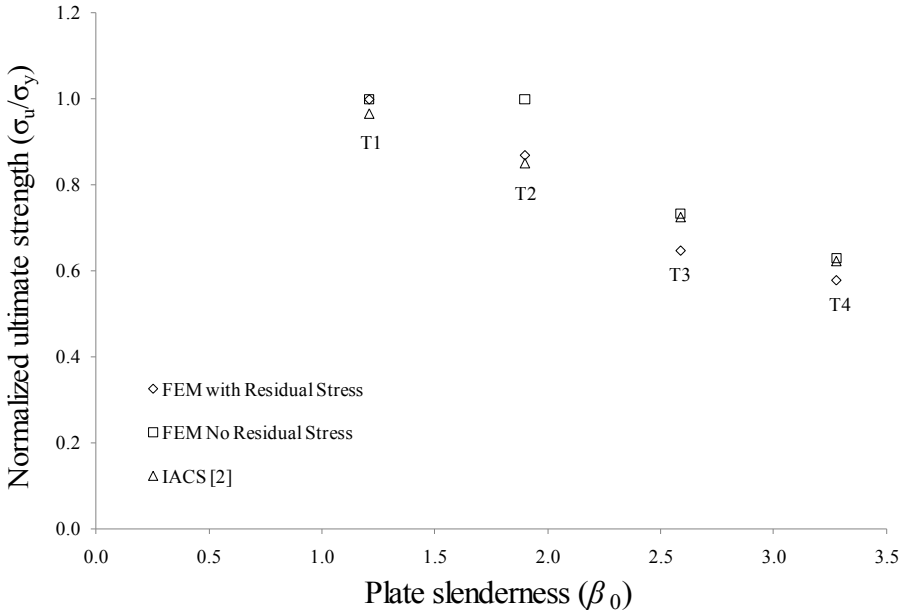

Figure 5.23, Variation in ultimate strength with plate slenderness - tee-stiffened plates

Ultimate strength values predicted using the IACS analytical formulae agreed well with those predicted by finite element analysis where welding-induced residual stresses were considered in most cases. In a few situations however, the difference between ultimate strengths predicted by the two methods were greater than 10%. For both types of stiffened plate, residual stresses had the greatest influence on ultimate strength at a plate slenderness value of 1.9. The results shown in the figures are consistent with observations made by Faulkner (1975), who found that the influence of residual stress on welded, simply supported plates increases until $\beta_0 = 2.5$, after which the degradation in strength remains relatively constant. However, there was no clear relationship between ultimate strength and column slenderness, λ. Referring to Table 2, the IACS predictions of ultimate strength for models A5, T3, and T5 were the least accurate of the IACS predictions compared to the numerical model results.

5.7.2 Load - Shortening Curves

Load-shortening curves are shown in Figure 5.24 and Figure 5.25 for the angle-stiffened plates and in Figure 5.26 and Figure 5.27 for the tee-stiffened plates. The load-shortening curves determined using the analytical methods prescribed in the IACS Common Structural Rules (IACS, Common structural rules for bulk carriers, 2009) are also shown in these figures. In comparison with numerical curves, the IACS curves predict a reduced stiffness in the pre-collapse region and this reduction in stiffness is increasingly pronounced as the plate slenderness increases. This is a result of the Johnson-Ostenfeld correction for plasticity which is an empirical method used in the IACS formulae to

account for the effects of plastic deformation in the ultimate strength analysis of beam-columns. In the numerical load-shortening curves, the onset of nonlinear behaviour generally occurs at a higher strain than in the IACS curves. In model A3 for example, nonlinearity in the IACS curves occurred at around 25% of the strain at ultimate load, whereas in the numerical model, only a small amount of nonlinear behaviour was observed at approximately 90% of the ultimate load.

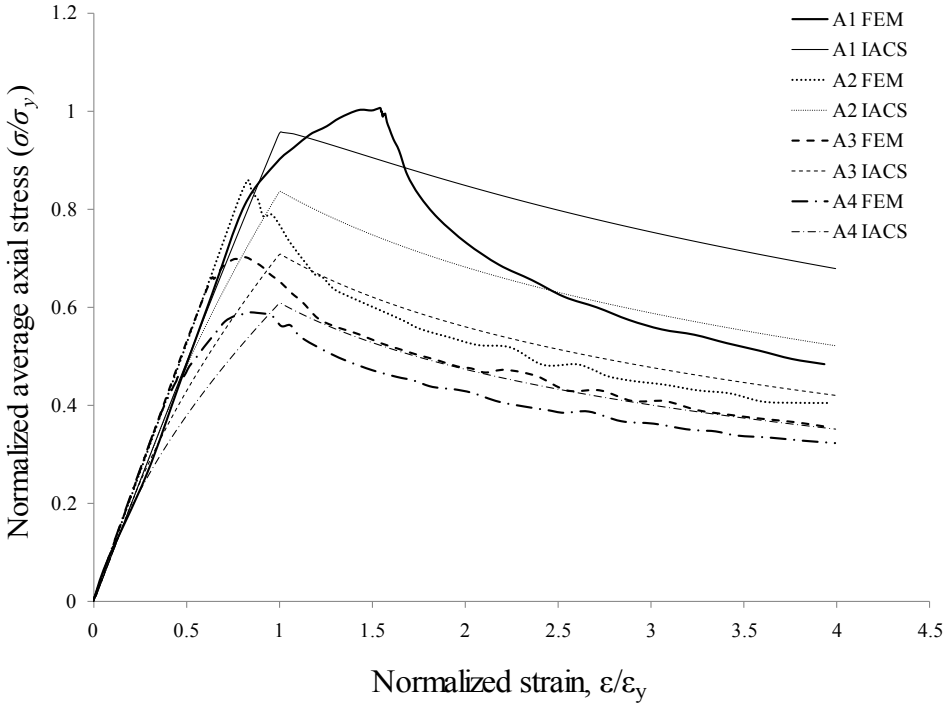

Figure 5.24, Angle-stiffened plate load shortening curves (A1-A4)

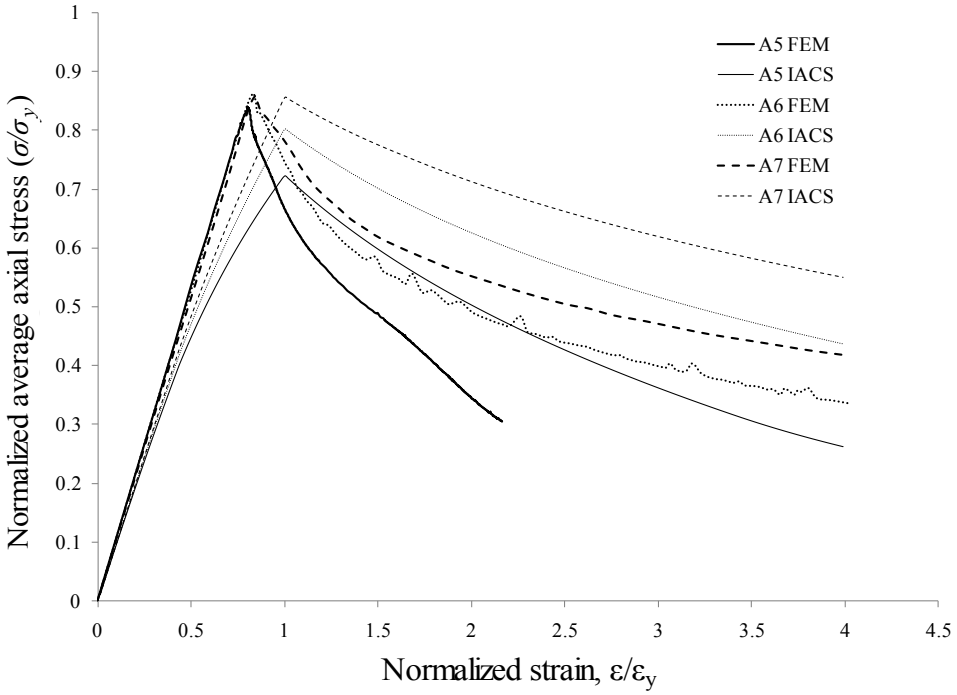

Figure 5.25, Angle-stiffened plate load shortening curves (A5-A7)

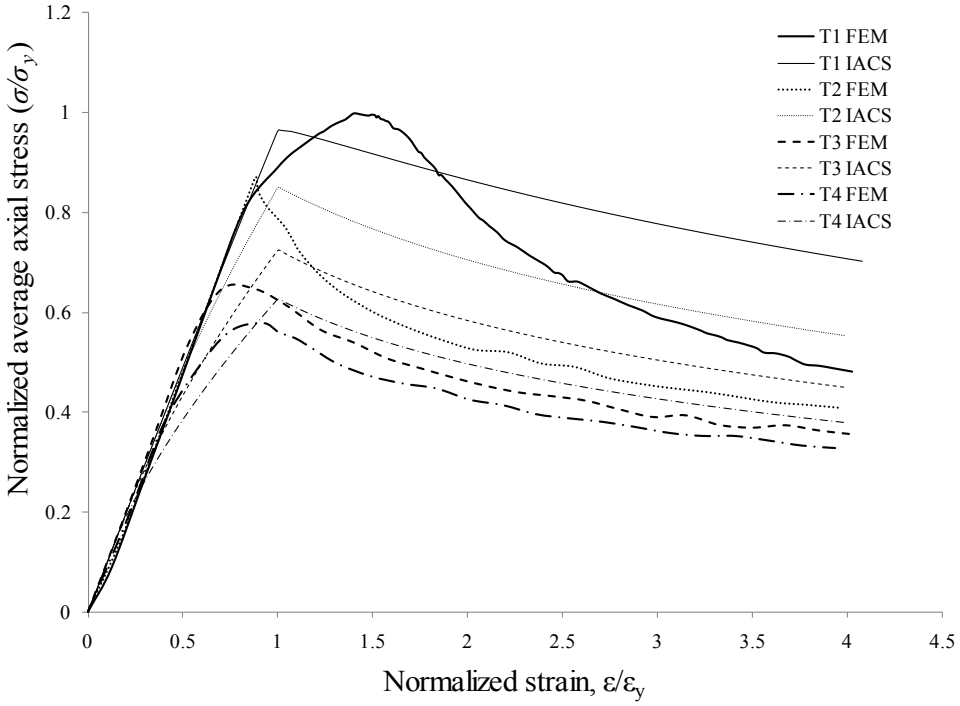

Figure 5.26, Tee-stiffened plate load shortening curves (T1-T4)

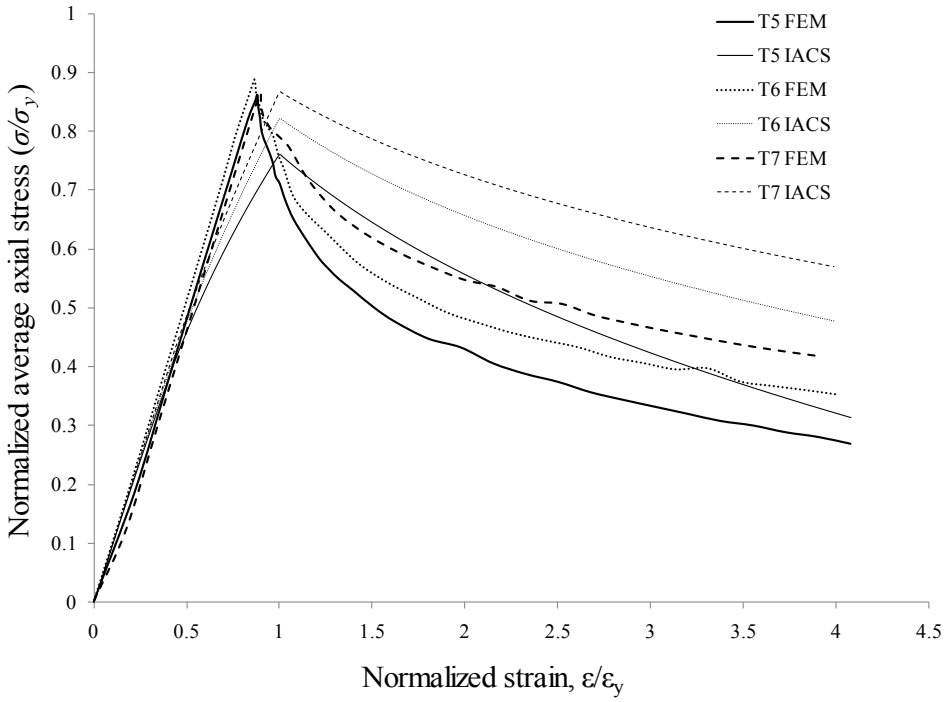

Figure 5.27, Tee-stiffened plate load shortening curves (T5-T7)

Although the IACS values of ultimate strength are generally in good agreement with those predicted by the numerical models, the IACS curves over-estimate the post-ultimate strength of both angle and tee-stiffened plates by a significant margin. For example, referring to Figure 5.24 and Figure 5.25, at a normalized strain of 1.5, the IACS curves overestimate post-ultimate capacity of angle-stiffened plates by as little as 13% for model A4 and as much as 25% for model A2. The exception was model A1, where the IACS curves underestimate the post-ultimate capacity by 9%, however as the strain increases, this difference becomes smaller until the IACS curve overestimates the strength of model A1 as well. For the tee-bar stiffened plates, the IACS load-shortening curves in Figure 5.26 and Figure 5.27 overestimate the post-ultimate capacity at a normalized strain of 1.5 by as little as 17% for model T4 to as much as 28% for models T2, T5, T6, and T7. The

exception in this case was model T1 for which the IACS curves underestimate the strength by 8%, however as the strain increases, the IACS curves overestimate the post-ultimate capacity of this model as well. With the exception of models A1 and T1, the extent of this overestimation remains relatively constant through the post-ultimate region.

The difference in post-ultimate capacity is attributed to the IACS method assumption that once the ultimate load has been reached, a single failure mechanism controls the post-buckling behaviour of the stiffened plate. For example, for beam-column type failure, IACS curves account for the reduced effective width of the plate in the post-ultimate region, however no allowance is made for the possibility of failure mode interaction such as beam-column buckling accompanied by local buckling of the web or flange of the stiffener. This may lead to an overestimate of the post-ultimate load-carrying capacity of stiffened plates analyzed by IACS rules. This argument is supported by the behaviour exhibited by the numerical models after the ultimate load was reached. Following attainment of the ultimate load in the numerical models, beam-column type buckling of the stiffened plates was often accompanied by local buckling of the plate elements making up the cross-section, as seen in the web of model T2, show in Figure 5.21. This local buckling, along with premature yielding due to the presence of residual stress may be the cause of the discrepancy between the post-ultimate capacities determined by the two methods of analysis.

The non-conservative post-ultimate capacity of stiffened plates predicted by the IACS rules may lead to overestimates of hull girder ultimate strength in ship structural design.

Rutherford and Caldwell (1990) assessed the influence of changing the slope of the load-shedding portion of stiffened plate load-shortening curves on hull girder ultimate strength. They found that varying the post-collapse slope of the curves and hence the post-collapse load carrying capacity has the potential to reduce hull girder ultimate strength by as much as 10%.

The presence of welding-induced residual stresses in the numerical models caused a reduction in ultimate load and the strain at which the ultimate load was reached. Welding-induced residual stresses only influenced the pre-collapse behaviour of the stiffened panels near the ultimate load. In the post-ultimate part of the analysis, most models showed little difference whether or not residual stresses were included. Figure 5.28 shows a typical example of the influence of welding-induced residual stress on load-shortening behaviour of stiffened plates. In the case of models A3, A4, T1 and T3, residual stress caused the onset of nonlinear behaviour at a lower strain than models with no residual stress. For the other models, there was little difference in the shape of the curve whether residual stresses were included or not. Furthermore, when those models were run with no residual stress, the failure was more sudden and accompanied by a sharper drop in post-ultimate load-carrying capacity than when residual stresses were included. These results are consistent with the behaviour of stiffened plates observed by Gordo and Guedes Soares (1993).

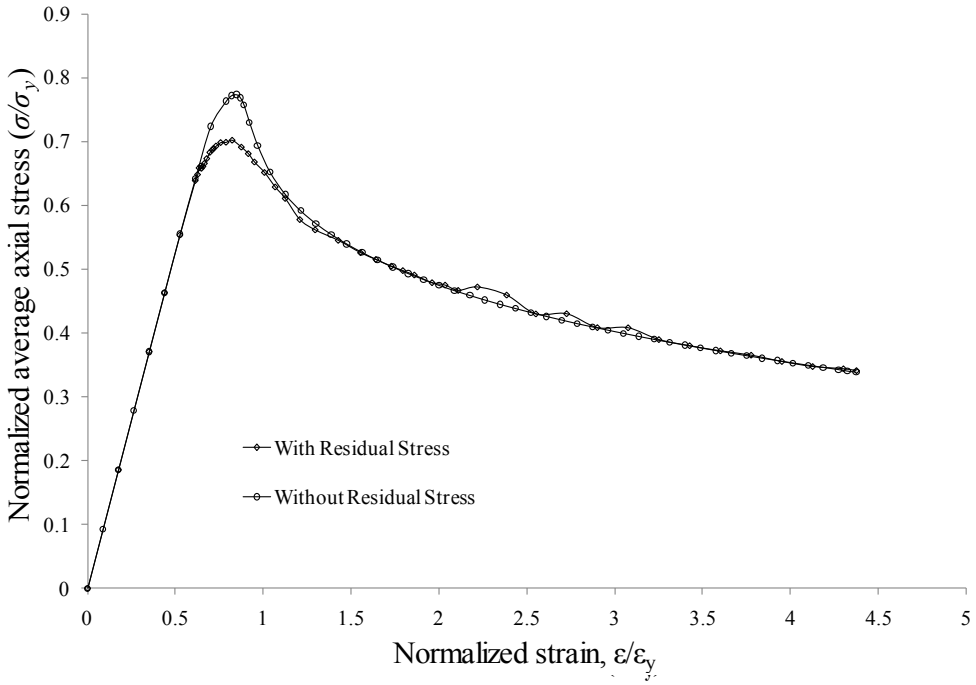

Figure 5.28, Effect of residual stress on load-shortening curve (A3)

5.8 Conclusions

Residual stresses and distortions introduced by welding in angle and tee-stiffened plates were simulated using 3D finite element analysis. The welding simulation consisted of sequential transient thermal and nonlinear structural analyses in which the transient temperature field introduced by the moving heat source and the resulting strain field were predicted. A nonlinear structural analysis was consequently carried out to evaluate the behaviour of the stiffened plates under compressive axial load incorporating 3D residual stress and distortion fields. Load-shortening curves were generated using numerical models and compared with load-shortening curves calculated using the IACS Common Structural rules that are currently used in ship structural design. The following conclusions were drawn from the results of this study:

1. There is little variation in tensile residual stress in the plate for different stiffened plate geometries, however the magnitude of compressive residual stress decreases as plate slenderness β, increases.

2. The "hungry horse" type of distortion in welded plates increases with the plate slenderness, β_0.

3. The magnitude and direction of longitudinal distortion depend to some degree on the position of the neutral axis. For stiffened plates with the same plate slenderness, the direction of vertical distortion along the axis if the stiffener changes from being towards the stiffener to towards the plate as the distance from the bottom of the plate to the neutral axis decreases.

4. Although it is often assumed in stiffened plate analysis that lateral distortions along the length of stiffeners are distributed in a half-sine wave, the results of the numerical analyses show that the distribution of lateral distortions is more complex than this idealized shape. Lateral distortion of the stiffener will vary with welding sequence and also with the amount of lateral restraint provided by the stiffener extension into adjacent bays.

5. Welding-induced residual stresses reduced the ultimate strength of angle-stiffened panels by as much as 15%, and by as much as 13.5% for tee-stiffened panels.

6. Ultimate strength values calculated using the IACS analytical agreed well with the results of the numerical analysis in most cases, however there were a few where the difference in ultimate strength was greater than 10%.

7. The IACS load-shortening curves underestimate the stiffness of angle and tee-stiffened plates in the pre-ultimate load region of the curves.

8. Load shortening curves calculated using the IACS common structural rules overestimate the post-ultimate capacity of beam columns by a significant margin. This may result in un-conservative values for hull girder ultimate strength in design.

9. There is very little difference between tee and angle stiffened plates; where the distributions and effects of residual stress and distortion are concerned, for the stiffened plate geometries considered in this study.

Chapter 6 - Shakedown of Welding-Induced Residual Stress and Effect on Stiffened Plate Strength and Behaviour

L.G. Gannon, Y. Liu, N.G. Pegg & M.J. Smith

Accepted for publication in: Proceedings, MARSTRUCT 2011 3rd International Conference on Marine Structures. Hamburg, Germany: A.A. Balkema Publishers.

6.1 Abstract

Numerical simulation is used to study the influence of welding-induced residual stress in welded, tee-stiffened plates focusing on the effect of shakedown. Residual stresses are simulated using 3D thermo-elasto-plastic finite element analysis. The influence of strain hardening and number of load cycles on residual stress shakedown is then investigated. Load versus end-shortening curves are used to characterize the strength and behaviour of stiffened plates under axial compression both before and after shakedown. Results show that the reduction in residual stress due to shakedown occurs entirely during the first load cycle provided that the magnitude of that load is not subsequently exceeded. Both the tensile and compressive welding residual stresses are reduced by as much as 40% when the applied load causes an average stress equal to 50% of the yield stress. This level of shakedown increased the ultimate strength of tee-stiffened plates by as much as 6%.

6.2 Introduction

The primary load for which ship hull girders are designed is wave-induced longitudinal bending. The bending stresses are resisted by longitudinally stiffened plates that make up the hull girder. These plates are also subjected to residual stresses caused by welding during fabrication of the structure. Several studies (Faulkner 1975, Guedes Soares 1988, Gordo & Guedes Soares 1993) have shown that residual stresses can have a detrimental effect on the ultimate strength of stiffened plates and consequently on the strength of a hull.

Welding-induced residual stresses may be relieved to some degree by stretching of stiffened plates under cyclic loads during service. This process is commonly referred to as shakedown. Abdel-Karim (2005) identifies three types of shakedown that occur when the magnitude of the cyclic load lies between the first yield and plastic collapse loads. Elastic shakedown occurs when a finite amount of plastic deformation occurs during the first few load cycles, after which any further deformation is purely elastic. In plastic shakedown, the structure experiences equal and alternating plastic strains during each load cycle and continues to experience shakedown in the form of non-cumulative cyclic plastic straining which eventually leads to failure by low-cycle fatigue. If the alternating plastic strains are asymmetric and the structure accumulates plastic strain with each load cycle, incremental plastic collapse of the structure will occur. This incremental accumulation of plastic strain during cyclic loading is called ratcheting.

Shakedown in ship structures has been investigated both experimentally and numerically; however most research has focused on the effects of shakedown on fatigue behavior in welded structures. Latrou *et al.* (2005) studied the behavior of welded joints accounting for residual stress and shakedown using numerical models. A rectangular plate was modelled assuming plane stress and residual stresses were simulated by application of a non-uniform displacement on one side of the plate. They found that after a low number of load cycles, the behavior of the joint became elastic. Similar results were reported by Liangbi *et al.* (2007). They also studied the effect of residual stress relaxation on the fatigue behavior of welded joints and found that under constant amplitude cyclic loads, residual stress relaxation was limited to the first load cycle.

In an experimental study of shakedown in butt-welded aluminum plates subjected to 3-point bending, Paik *et al.* (2005) found that measured longitudinal residual stresses were reduced by 36% and 21% in tension and compression respectively. The load in that experiment was applied for three cycles, producing extreme fiber stresses equal to 88% of the yield stress.

In the analysis of stiffened plates, simplified residual stress distributions are sometimes assumed based on measurements available in literature. In design, fabrication related imperfections are typically accounted for using an empirical method such as the Johnson-Ostenfeld correction for plasticity in beam columns. In some cases however, residual stresses are neglected under the assumption that they are relieved by shakedown.

A welding-induced residual stress distribution commonly used in stiffened plate analysis assumes a two dimensional distribution of stress over a cross-section that is constant along the length of the stiffened plate. Based on experimental data and assuming that the residual stresses acting over the cross-section of the plate in a welded stiffened plate are in equilibrium, Faulkner (1975) proposed the idealized longitudinal residual stress distribution shown in Figure 6.1, where b is the plate width, σ_y is the yield stress, t is the plate thickness and η is a parameter describing the width of the tensile stress block at the weld in the middle of the plate. Faulkner (1975) suggested initial values for η in the range of 4.5 - 6 and lower values ranging from 3 - 4.5 to allow for some shakedown at sea. Based on equilibrium requirements, the compressive residual stress σ_r is given by:

$$\sigma_r = \frac{2\eta\sigma_y}{b/t - 2\eta} \tag{5.7}$$

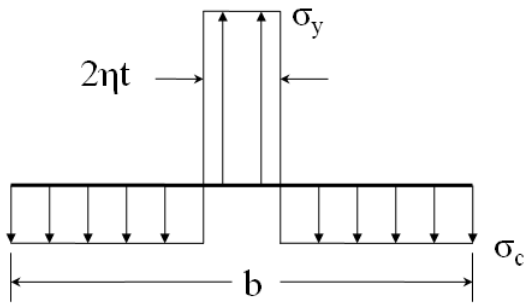

Figure 6.1, Idealized longitudinal residual stress distribution in a welded plate

Although some studies on shakedown are available in literature, the geometries considered in these studies were limited and simplified residual stress distributions were often assumed. The primary objective of this study is to investigate the influence of residual stress shakedown on the strength and behaviour of longitudinally stiffened plates

typical of ship hull girders. The application of the finite element method, described herein is unique in that it considers the complete, complex three-dimensional characteristics of welding-induced residual stress and distortion fields throughout the analysis.

Welding-induced residual stress and distortion in the stiffened plates were determined using sequential 3D, nonlinear thermal and mechanical finite element analyses. Assuming that the stiffened plates are not subjected to any type of stress relief such as annealing, a cyclic axial load was then applied, causing shakedown of the residual stress. An ultimate strength analysis was then conducted and load-shortening curves that characterize the behaviour of the stiffened plates under axial load were obtained. The finite element method was also used to determine the effect that strain hardening of the material and variable amplitudes of loading have on the shakedown of welding-induced residual stresses.

6.3 Finite Element Modelling

6.3.1 Welding Simulation

A finite element simulation was used to predict welding-induced residual stress and distortion in tee-stiffened plates. The simulation consisted of sequentially coupled nonlinear thermal and structural analyses. The model made use of two element types; 8-node, linearly interpolated hexahedrons to mesh the solid volume, and 2-node nonlinear springs to model contact between the stiffener base and the plate. The material used for the stiffened plates was AH36 shipbuilding steel with a nominal yield stress of 360 MPa

and elastic modulus of 210 GPA. An elastic, perfectly plastic material model was used with temperature dependent properties adopted from Michaleris and DeBiccari (1997).

Twelve elements were required through the thickness of the plate in the vicinity of the weld in order to accurately characterize the severe thermal gradient in that region. The mesh density was decreased in regions further away from the weld where the thermal gradient was small so that the analysis could be run in a reasonable amount of time with the computational resources available. A minimum of 4 elements was used through the thickness of all components of the stiffened plate model. Figure 6.2 shows a finite element mesh typical of those used for the tee-stiffened plates in this study.

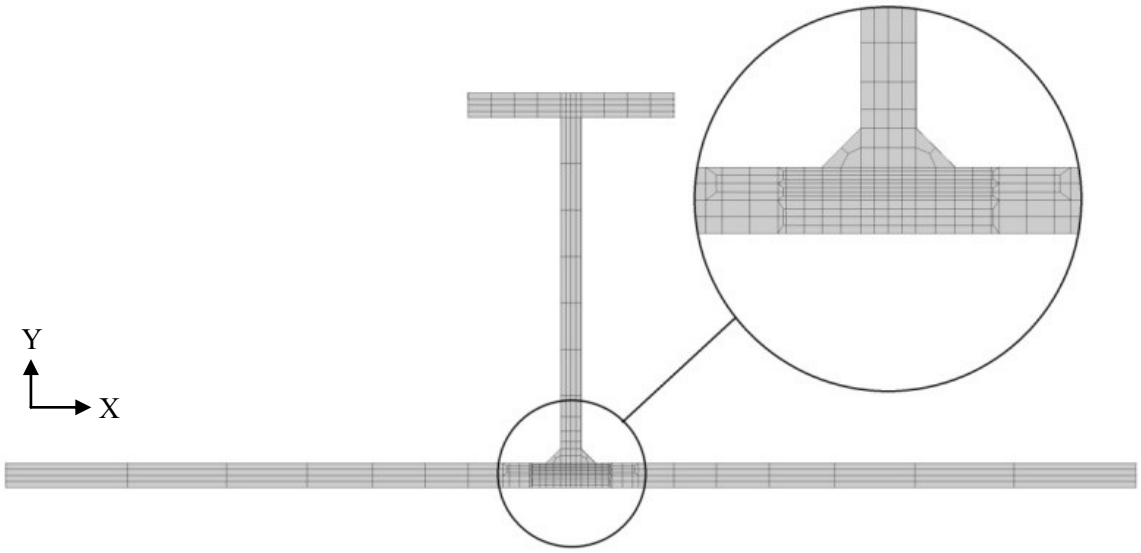

Figure 6.2, Finite element mesh of tee-stiffened plate

A nonlinear thermal analysis was used to predict the transient temperature field produced by the moving heat source. A circular heat source with a Gaussian energy distribution representing the heat from a welding torch, was moved along the weld path in 10 mm

increments. After the continuous fillet weld on one side was finished, the model was allowed to cool for 30 minutes before the weld on the other side of the stiffener web was started. The thermal analysis considered temperature dependent material properties including thermal conductivity, specific heat and density. Heat loss due to convection and radiation was accounted for using a film coefficient given by Goldak *et al.* (1984) to account for heat loss by both mechanisms. Latent heats of melting and fusion were also accounted for. User-defined subroutines were created using the ANSYS® parametric design language to model the moving heat source and to control the activation of weld elements as the heat source progressed.

For the second stage of the analysis, the transient temperature field from the thermal analysis was used as a series of load steps in a structural analysis. Each load step consisted of an incremental progression of the heat source along the weld path. As the heat source advanced along the weld path, the ANSYS® element birth and death feature was used to activate the weld elements behind the heat source once their temperature fell below the solidification temperature, taken as 1450 °C. This enabled the model to simulate the dynamic coupling of the stiffener to the plate as the weld progressed. The application of sequential thermal loads, and the element activation scheme were controlled via user-defined subroutines.

Boundary conditions in the structural analysis were representative of the level of restraint in stiffened panels in ship hull girders where a panel with multiple evenly spaced stiffeners can be divided into several individually stiffened plates. Longitudinal edges

were constrained to remain straight, but free to move in the plane of the plating. This produced a level of restraint similar to that provided by adjacent panels in ship hulls (Dow *et al.*, 1981). Simple supports were applied at the end cross-sections by constraining displacements along all three coordinate axes at the centroid of one end and the vertical and transverse displacements at the centroid of the opposite end. An elastic-plastic material model was used with von Mises failure criteria and associated flow rule. Nonlinearities due to large strain and displacement were considered.

The accuracy of the simulation was verified using the methods described above to simulate a welding experiment carried out by Deng *et al.* (2007). In the experiment, a steel flat-bar stiffener was connected to a steel plate by sequential, 6 mm fillet welds. Figure 6.3 shows the weld sequence and direction along with the test specimen dimensions. The material used in the experiment was SM400A shipbuilding steel with a yield stress of 300 MPa. Temperature dependent material data necessary for numerical modelling was adopted from Deng *et al.* (2008). Figure 6.4 shows that the vertical deflection of the plate predicted by the welding simulation method is in good agreement with experimental measurements provided by Deng *et al.* (2007). Figure 6.5 shows the longitudinal residual stress distribution at the mid-length, mid-plane of the plate. Although residual stress measurements from the experiment were not available, the residual stress distribution determined by finite element analysis is consistent with measured values available in literature (Michaleris & DeBiccari 1997, Nagaraja Rao & Tall 1961, Kenno *et al.* 2010). For a more comprehensive description of the welding simulation method, the reader is referred to Gannon *et al.* (2010).

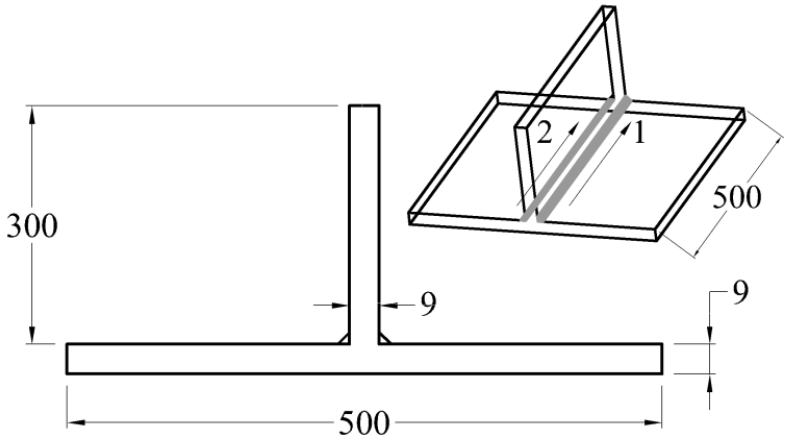

Figure 6.3, Test specimen used by Deng et al. (2006). Dimensions in mm

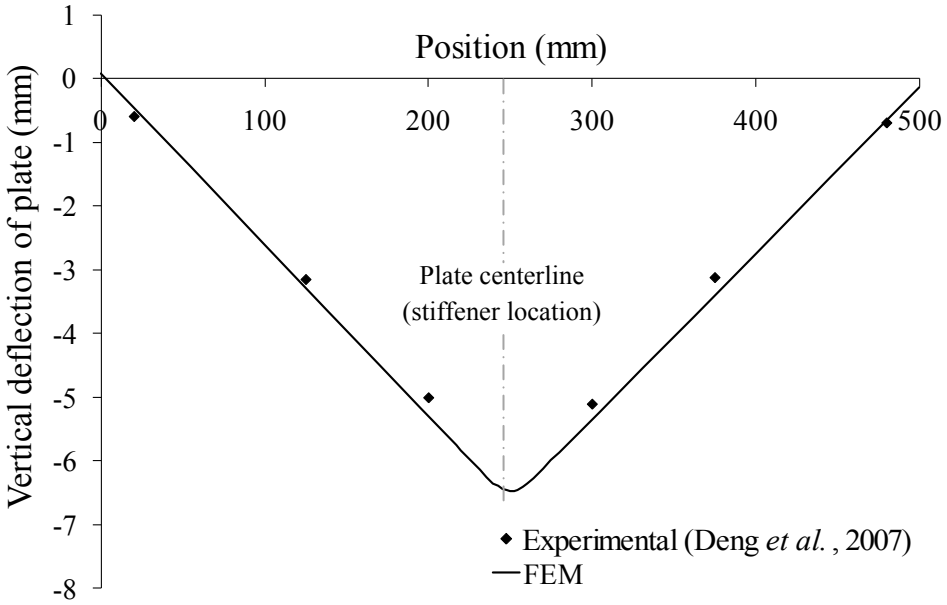

Figure 6.4, Comparison of vertical deflection of plate with measured values

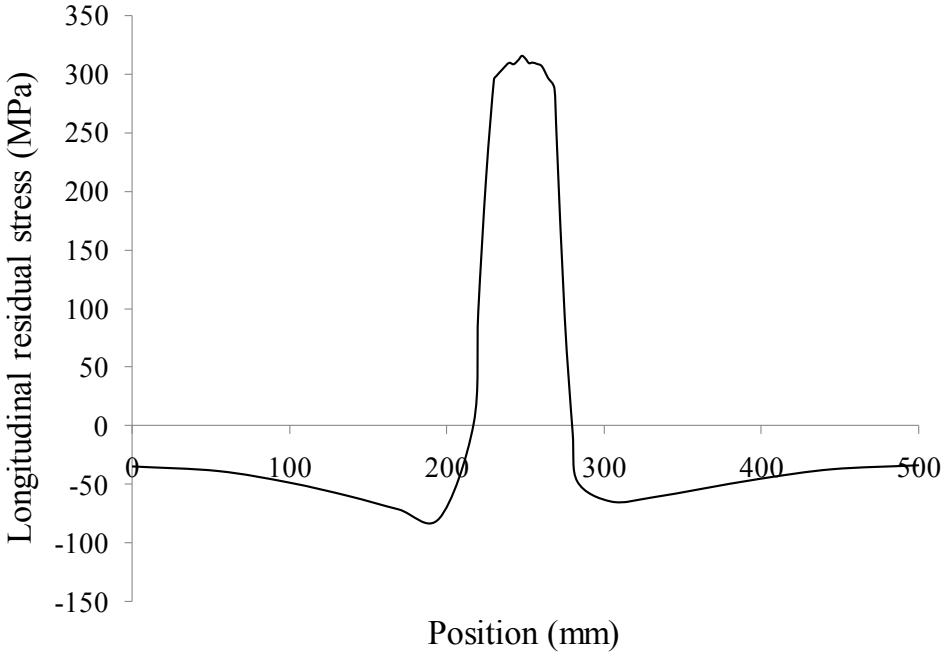

Figure 6.5, Longitudinal residual stress at mid-span from welding simulation

6.3.2 Shakedown Analysis

At the end cross-sections of the stiffened plate, every node in the section was connected to a single node at the cross-section centroid using stiff beam elements. These beam elements were deactivated during the welding simulation using the ANSYS® element birth and death feature which multiplies the stiffness of inactive elements by a severe reduction factor and removes any loads applied to those elements from the global load matrix. For the subsequent shakedown analysis, the beam elements were re-activated so that they forced the end cross-section nodes to remain planar during the shakedown and ultimate strength analyses. This constraint represents the support that would be provided by transverse frames added after the stiffeners are welded to the plate. For the shakedown analysis, an axial load was applied to the centroidal node of one cross-section while the

other end cross-section remained pin supported at its centroid. The stiff beam elements at the loaded end facilitated the even distribution of load from the centroidal node over the rest of the cross-section.

6.4 Parametric Study

6.4.1 Geometry

The study considered tee-stiffened plates with geometries chosen to cover a range of values of two non-dimensional parameters commonly used to characterize stiffened plate geometry. These are the plate slenderness β_0, and column slenderness λ, given by:

$$\beta_0 = \frac{b}{t}\sqrt{\sigma_y / E} \tag{5.8}$$

$$\lambda = \left(\frac{a}{\pi r}\right)\sqrt{\sigma_y / E} \tag{5.9}$$

where b is the plate width, t is the plate thickness, σ_y is the yield stress, E is the elastic modulus, a is the plate length and r is the radius of gyration. A summary of the stiffened plate geometries is given in Table 6.1 with dimensions defined as shown in Figure 6.6. All stiffened plates were 2000 mm long with 7 mm, continuous fillet welds on each side of the stiffener base, connecting it to the plate. Welds were deposited in the sequence shown in Figure 6.3.

Table 6.1, Stiffened plate dimensions

Model	b	t	d	w	t_w	t_f	B_0	λ
T1	350	12	180	100	10	12	1.21	0.34
T2	550	12	180	100	10	12	1.90	0.37
T3	750	12	180	100	10	12	2.59	0.40
T4	950	12	180	100	10	12	3.28	0.43
T5	550	12	100	100	10	12	1.90	0.64
T6	550	12	140	100	10	12	1.90	0.47
T7	550	12	220	100	10	12	1.90	0.31

* All dimensions in mm

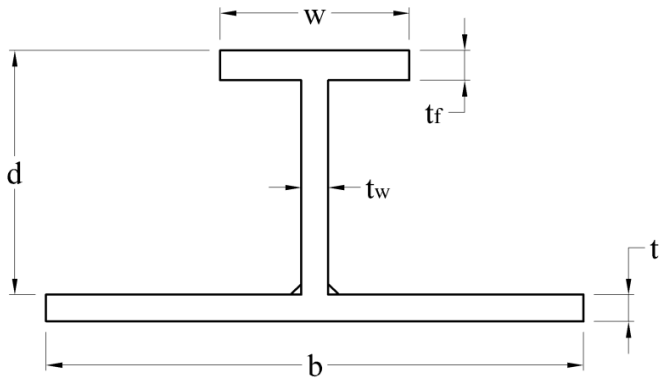

Figure 6.6, Stiffened plate dimensions

6.4.2 Shakedown

Shakedown of residual stress in the tee-stiffened plates was facilitated by application of a single cycle of axial load at the centroid of the simply supported stiffened plates. For each model, two load amplitudes were considered; one producing an average stress in the stiffened plate equal to $0.25\sigma_y$, and the other producing an average stress of $0.5\sigma_y$. The load cycles began with a compressive load increasing linearly from zero to the specified

amplitude. This was followed by a linear transition to the same amplitude in tension, after which the load was reduced linearly back to zero.

Table 6.2 contains a summary of normalized maximum tensile and compressive residual stresses in the plates of the finite element models before and after shakedown. These are denoted $\bar{\sigma}_t$ and $\bar{\sigma}_c$, respectively. To exemplify the change in the longitudinal residual stress distribution due to shakedown, Figure 6.7, Figure 6.8 and Figure 6.9 show the residual stress distributions in the plate, web and flange respectively, of model T2. The results indicate that residual stresses are reduced significantly by shakedown. Where the applied load produced a stress equal to $0.25\sigma_y$, tensile and compressive residual stresses were reduced by approximately 20% and 15%, respectively. When the applied load produced a stress equal to $0.5\sigma_y$, welding-induced residual stresses were reduced by around 43% in tension and 40% in compression.

Table 6.2. Normalized maximum longitudinal residual stresses

Model	Initial		$0.25\sigma_y$		$0.5\sigma_y$	
	$\bar{\sigma}_t$	$\bar{\sigma}_c$	$\bar{\sigma}_t$	$\bar{\sigma}_c$	$\bar{\sigma}_t$	$\bar{\sigma}_c$
T1	1.00	0.20	0.79	0.17	0.57	0.13
T2	1.01	0.14	0.79	0.12	0.57	0.09
T3	1.02	0.10	0.79	0.08	0.57	0.06
T4	1.02	0.08	0.79	0.07	0.57	0.05
T5	1.01	0.13	0.79	0.11	0.57	0.08
T6	1.02	0.14	0.79	0.11	0.56	0.08
T7	1.01	0.13	0.79	0.11	0.56	0.09

*Normalized with respect to yield stress of 360 MPa

It is evident from the results in Table 6.2 that the geometry of the stiffened plates had little influence on the effects of shakedown. It is also noted that due to the low magnitude of compressive residual stress and the amplitude of the applied load, no plastic straining occurred during the compressive portion of the load cycle. The shakedown of residual stress in these cases occurred during the tensile part of the load only.

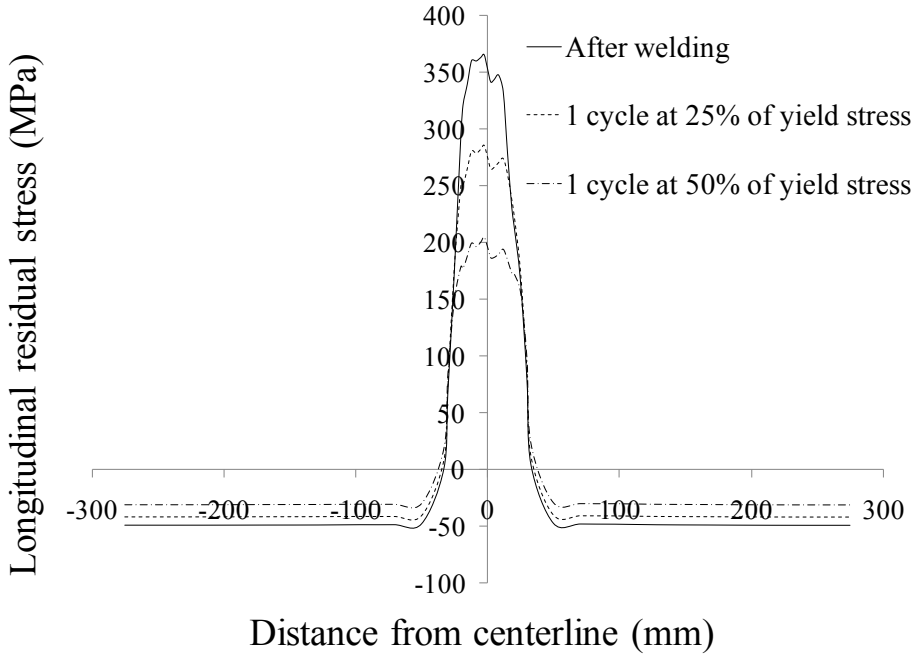

Figure 6.7, Longitudinal residual stress in plate of model T2

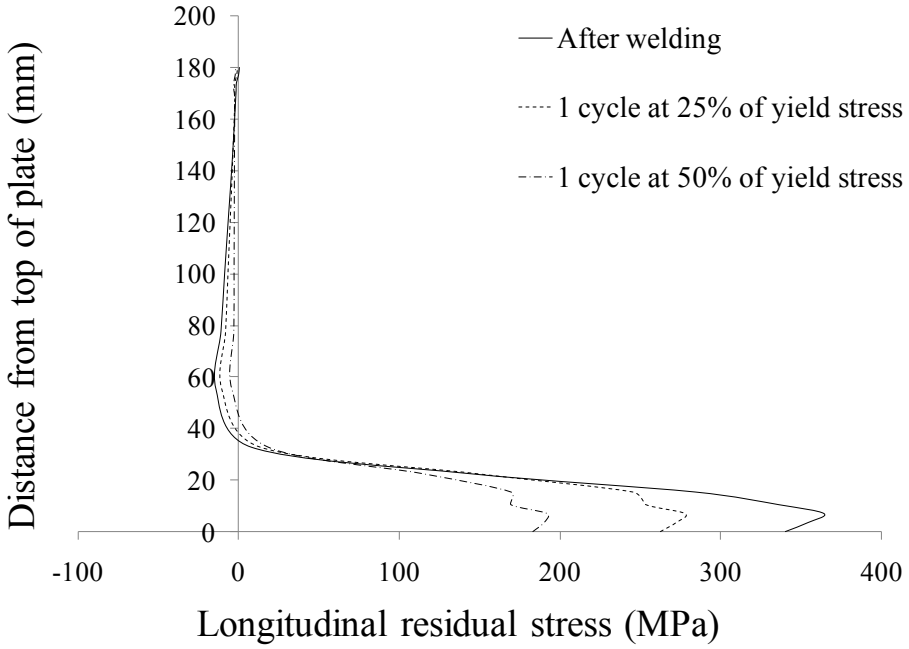

Figure 6.8, Longitudinal residual stress in web of model T2

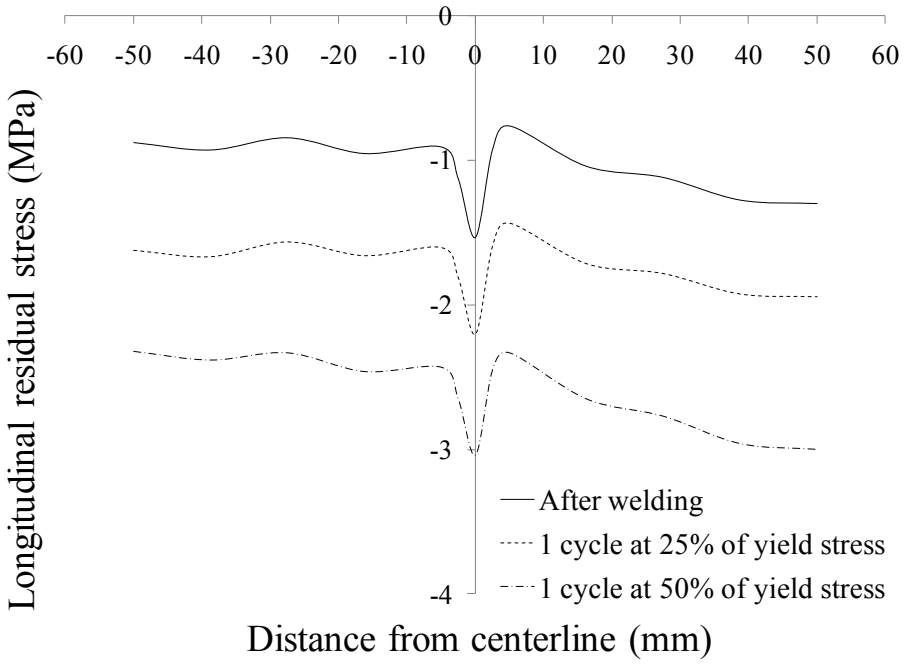

Figure 6.9, Longitudinal residual stress in flange of model T2

The residual stress distribution in the plate of model T2 before shakedown is shown in Figure 6.7 has a tensile stress zone approximately 66 mm wide, so that the tensile stress block parameter η (Figure 6.1) is equal to 2.75. After welding, the width of the equivalent tensile stress block decreased so that η = 2.17 and η = 1.57 for shakedown stresses of $0.25\sigma_y$ and $0.5\sigma_y$, respectively. This is consistent with Faulkner's (1975) statement that the range of η decreases from 4.5 - 6 to 3 - 4.5 after shakedown, however in this case η values were lower than Faulkner's suggestion.

Examination of welding-induced distortions before and after shakedown revealed that the shakedown also causes a change in distortions in stiffened plates. Figure 6.10 and Figure 6.11 show changes in distortion in model T2 following one load cycle at $0.5\sigma_y$. These changes in distortions, along with the reduced state of residual stress shown in Figures 6.7 through 6.9 indicate that there are significant changes in fabrication-related imperfections once a hull girder has been in subjected to longitudinal bending moments during service.

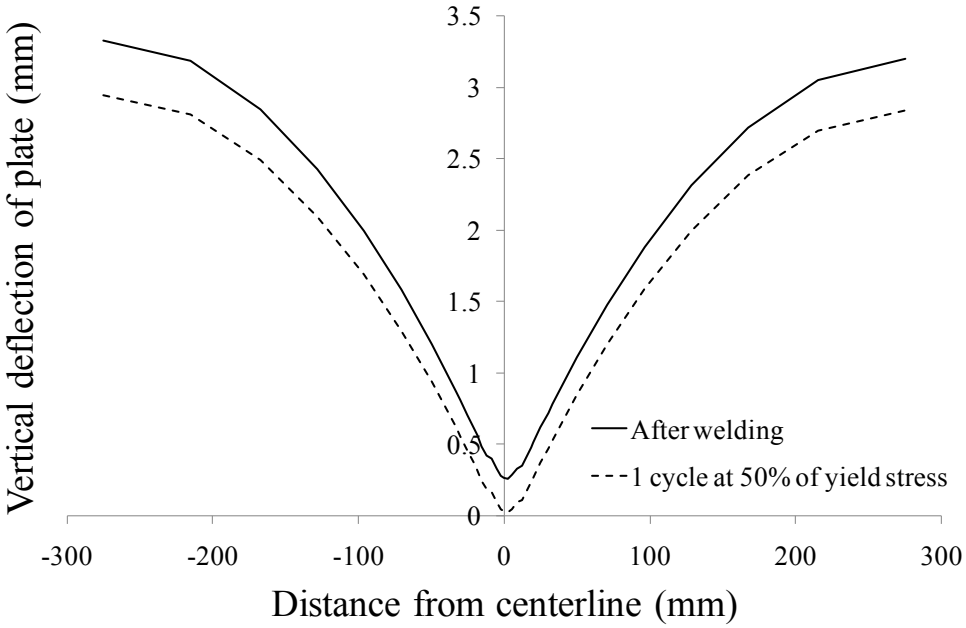

Figure 6.10, Vertical distortion of plate at mid-span

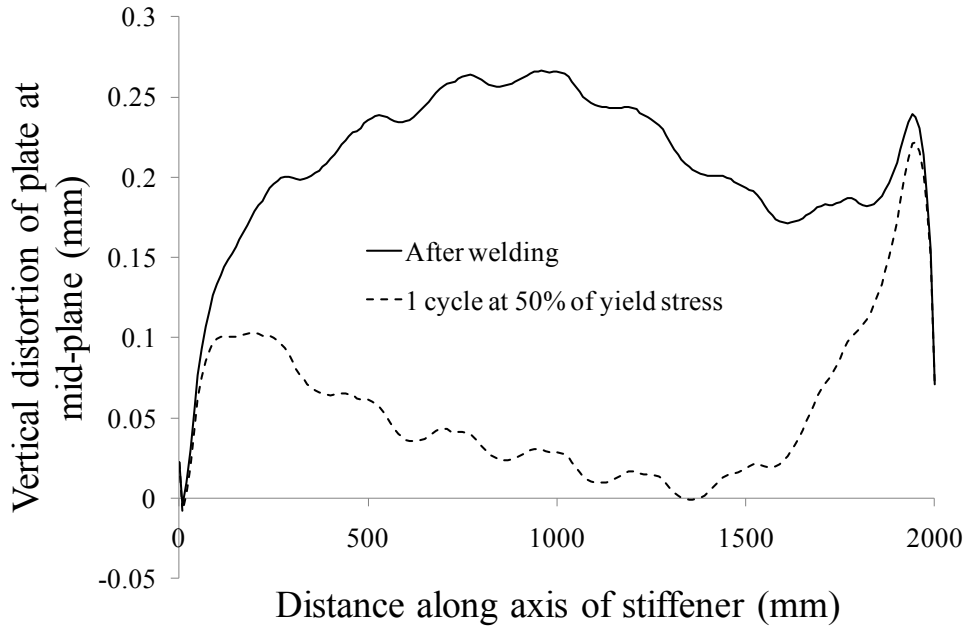

Figure 6.11, Vertical distortion of plate along axis of stiffener

6.4.3 Ultimate Strength

The strength and behaviour of the stiffened plates is characterized by plots of average axial strain versus average axial stress, known as load-shortening curves. An axial displacement was applied at the centroidal node of one end cross-section while the opposite end remained pin-supported at its centroid, producing a compressive load on the stiffened plate that was uniformly distributed over the cross-section through stiff beam elements connecting the nodes of each end cross-section. An applied displacement was used in order to allow the post-ultimate portion of the load-shortening curve to be calculated.

Load-shortening curves were also calculated for each stiffened plate considering welding-induced distortions, but no residual stresses. This was done to evaluate the ultimate strength when it is assumed that residual stresses have been completely relieved by shakedown. The ultimate strength analyses considered large strains and displacements through the finite element formulation, and used the same material properties as the welding simulation and shakedown analysis described previously.

Table 6.3 provides a summary of normalized ultimate stress values for the stiffened plates calculated by finite element analysis. Ultimate stress values are given before shakedown $\left(\bar{\sigma}_{u,0}\right)$, after one load cycle at $0.25\sigma_y$ $\left(\bar{\sigma}_{u,25}\right)$, after one load cycle at $0.5\sigma_y$ $\left(\bar{\sigma}_{u,50}\right)$, and with no residual stress $\left(\bar{\sigma}_{0RS}\right)$. An example of load-shortening curves before and after shakedown is given in Figure 6.12 for model T5, and the deformed shape of the model in

the post-ultimate stage is shown in Figure 6.13. This overall column type of buckling failure is typical of the stiffened plates considered in this study where the effective width of the plate is reduced until the cross-section can no longer sustain the applied load.

Table 6.3, Normalized ultimate strengths

Model	$\bar{\sigma}_{u,0}$	$\bar{\sigma}_{u,25}$	$\bar{\sigma}_{u,50}$	$\bar{\sigma}_{0RS}$
T1	1.00	0.99	0.99	1.00
T2	0.87	0.89	0.92	1.00
T3	0.65	0.67	0.68	0.73
T4	0.58	0.59	0.61	0.63
T5	0.86	0.89	0.92	1.00
T6	0.86	0.89	0.92	1.00
T7	0.86	0.88	0.91	1.00

Shakedown of residual stress increased the ultimate strength of the stiffened plates by a maximum of 3.4% for an applied stress of $0.25\sigma_y$ and 6.5% for an applied stress of $0.5\sigma_y$ (models T5 and T6). Results of the ultimate strength analyses indicate that the percentage change in ultimate strength due to shakedown is more pronounced in stiffened plates with plates of intermediate values of slenderness (β_0 = 1.0 - 2.5). This is consistent with Faulkner's (1975) statement that plates within this slenderness range are most susceptible to loss of strength caused by residual stress. Figure 6.12 shows that although shakedown increased the ultimate load of model T5, it had little influence on the shape of the load-shortening curve. The shape of load-shortening curves calculated for the other stiffened plates were also similar before and after shakedown. A comparison of ultimate strengths after shakedown at a stress of $0.5\sigma_y$ against values calculated without considering residual stress reveals that the remaining residual stresses may still decrease the ultimate strength

by as much as 10%. This shows that a potentially unsafe design may result if it is assumed that residual stresses are completely relieved by shakedown in order to simplify an ultimate strength analysis.

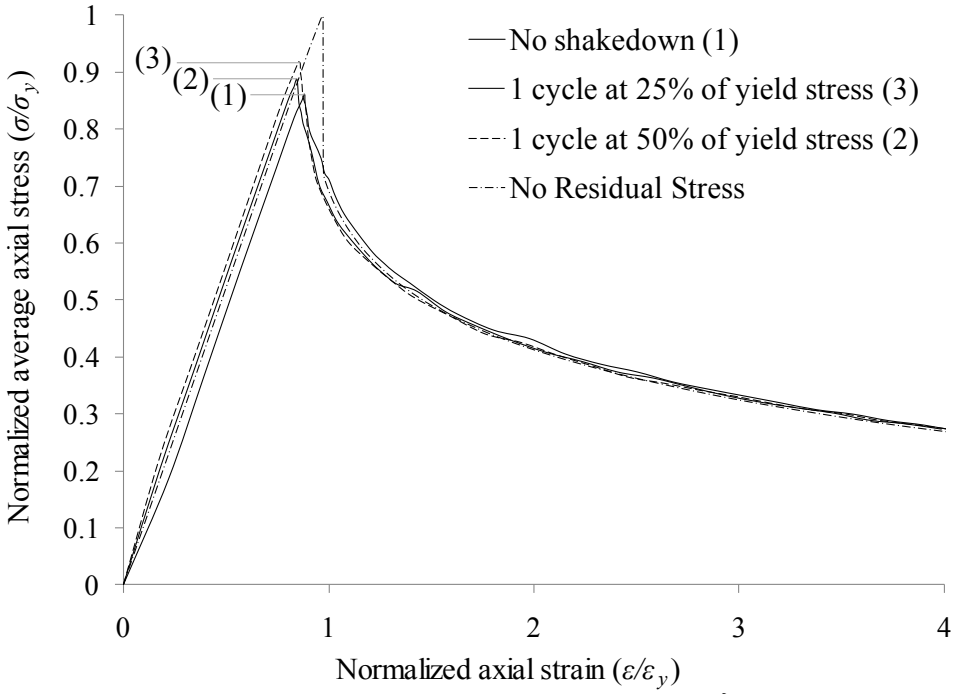

Figure 6.12, Load-shortening curves for model T5

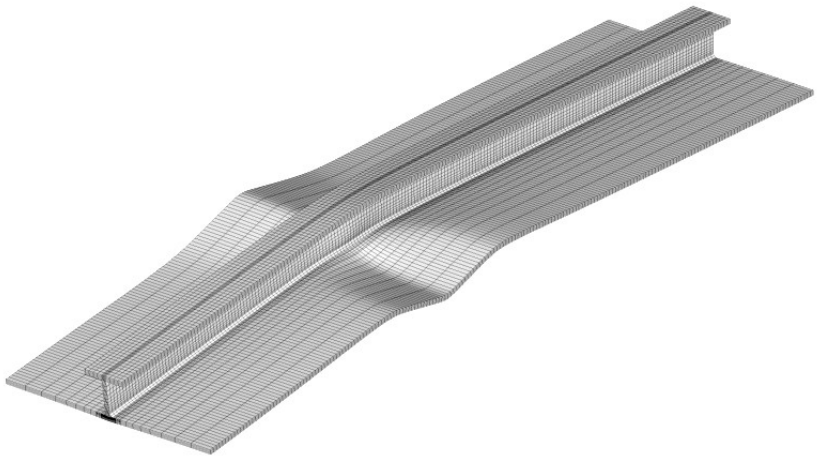

Figure 6.13, Deformed shape of Model T5 after ultimate load

6.5 Effect of Hardening and Number of Load Cycles

The shakedown analyses in Section 6.3 assumed an elastic perfectly plastic material so that it would be consistent with the material behaviour used in the welding simulation. In order to understand how those results might differ from those of a shakedown analysis where kinematic strain hardening is considered, shakedown analyses of a stiffened plate considering both no strain hardening and a kinematic hardening material behaviour were run and results are compared below.

Model T5 (Table 6.1) was chosen for the analysis and the initial residual stress was similar to that show in Figures 6.7 through 6.9. A notional hardening modulus of 5 GPa (Andersen 2000) was used, which is typical of mild steels used in ship structures. The difference in shakedown behaviour between the two analyses with different plastic material properties is shown by comparing the strain histories at two nodes located at the mid-plane and at the mid-length of the model. Node 1 is located at the mid-width of the plate in the tensile stress zone, and node 2 is located near the edge of the plate where the residual stress is compressive. The node locations are shown in Figure 6.14. Figure 6.15 shows the strain history at these points over 3 load cycles represented by 8 steps with a stress amplitude of $0.25\sigma_y$. Figure 6.16 shows the same for the case where the material is perfectly plastic. A summary of residual stresses at node 1 and node 2 at the points indicated in Figure 6.15 and Figure 6.16, is provided in Table 6.4.

Table 6.4, Stress history comparison considering perfect plasticity and kinematic hardening

Step	Kinematic hardening		Perfectly plastic	
	Node 1	Node 2	Node 1	Node 2
1	350	-50	350	-50
2	269	-132	269	-132
3	365	38	363	38
4	204	-126	202	-126
5	365	38	363	38
6	204	-126	202	-126
7	365	38	363	38
8	285	-44	283	-44

*All values in MPa

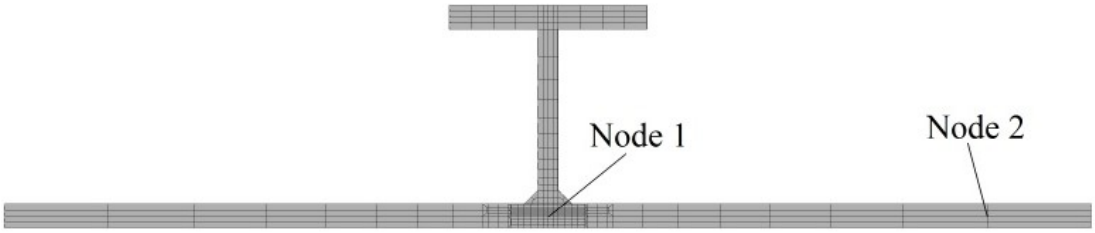

Figure 6.14, Location of nodes for results comparison.

The results in Table 6.4 indicate that there is little difference (0.7%) in the tensile residual stress after shakedown between the two models considering perfectly plastic and kinematic hardening materials. The change in compressive residual stress due to shakedown was virtually the same for both models. Furthermore, examination of Figure 6.16 and Figure 6.17 reveals that for both the perfectly plastic and kinematic hardening models, all plastic straining and thus, residual stress shakedown occurred entirely during the first load cycle.

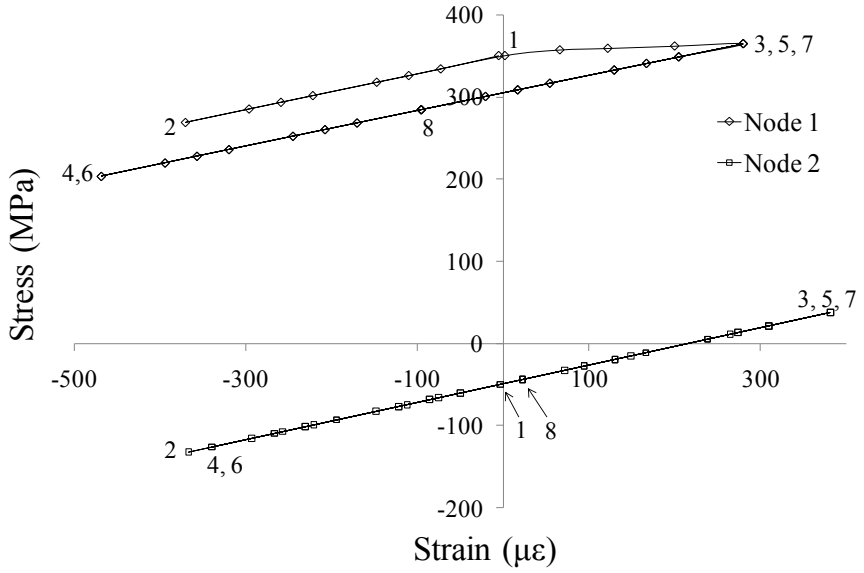

Figure 6.15, Stress-strain history during shakedown with kinematic hardening

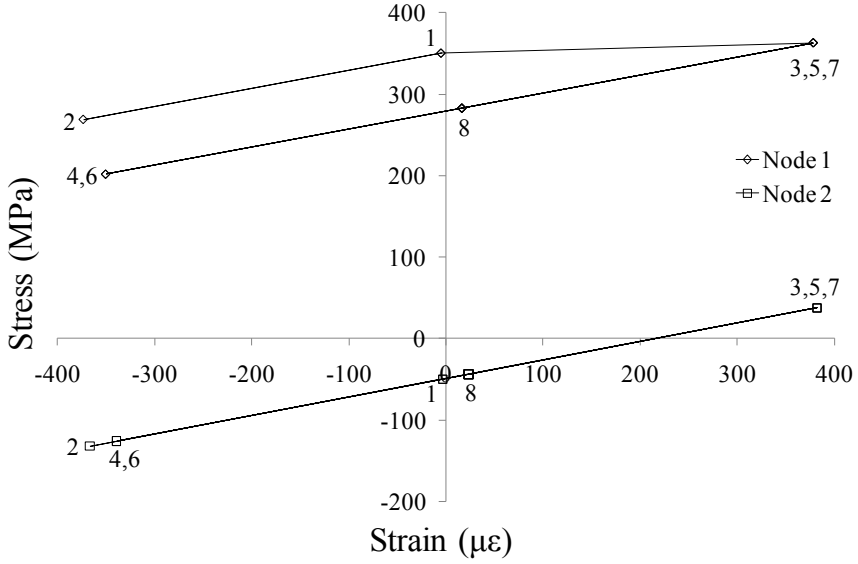

Figure 6.16, Stress-strain history during shakedown with no hardening

6.6 Variable amplitude load cycles

In order to determine whether residual stress relief by elastic shakedown is controlled only by the maximum applied load and not by the load history, model T5 was subjected to 3 variable amplitude load cycles. The complete load history is illustrated in Figure 6.17 and the strain histories at nodes 1 and 2 (Figure 6.14) are plotted in Figure 6.18. The maximum applied stress was $0.25\sigma_y$ and the material model used for the analysis assumed perfectly plastic behaviour.

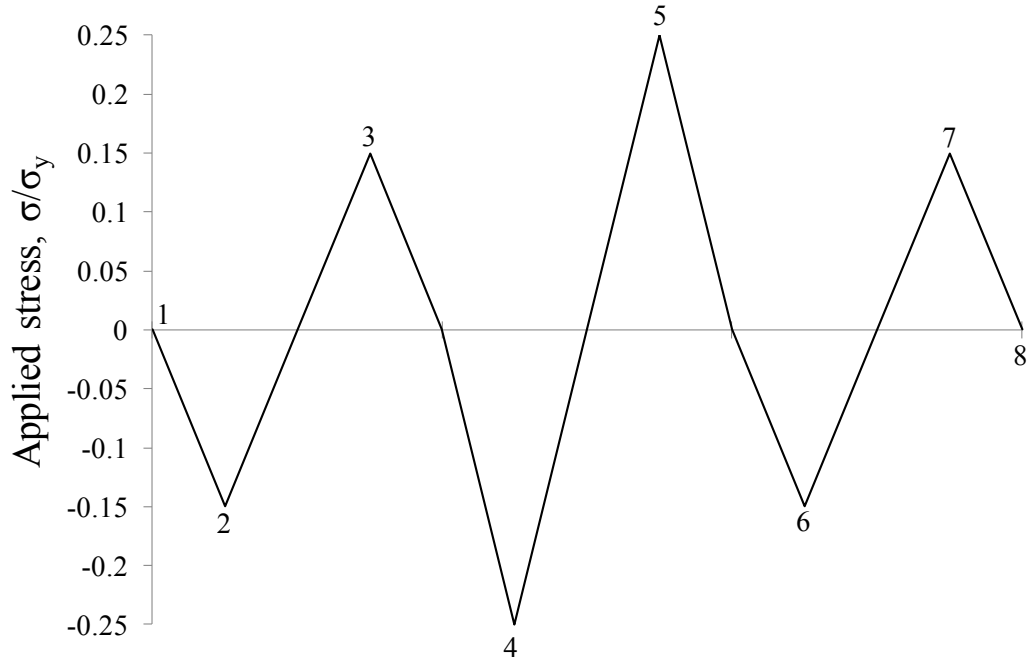

Figure 6.17, Variable amplitude load history

After application of the variable amplitude cyclic load, the tensile stress at node 1 and the compressive stress at node 2 were reduced to 283 MPa and -44 MPa, respectively. Referring to Table 6.4, where shakedown occurred entirely during the first cycle at a

stress of $0.25\sigma_y$, it is evident that the maximum applied stress governs the final magnitude of residual stress and that the sequence of loads is not relevant.

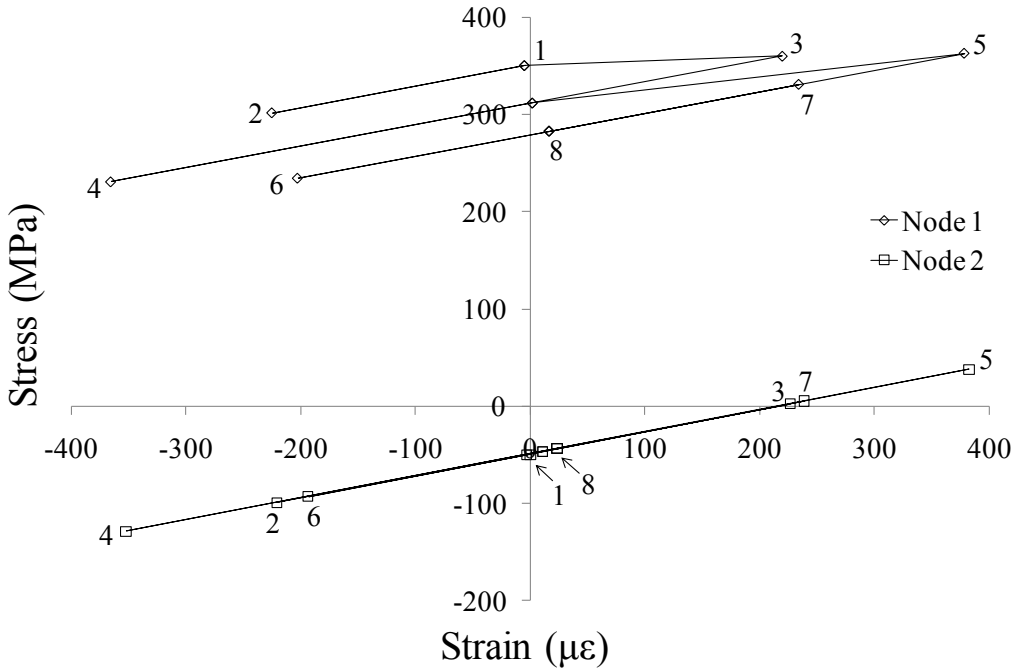

Figure 6.18, Stress-strain history for variable amplitude loading

6.7 Conclusions

Welding-induced three-dimensional residual stress and distortion fields in tee-stiffened plates were simulated using finite element analysis. Cyclic axial loads were applied to the stiffened plates and the resulting reduction in residual stress due to elastic shakedown was studied. Following the shakedown analysis, a compressive axial load was applied to the stiffened plates and their strength and behavior was characterized by load-shortening curves. The effects of strain hardening and variable amplitude loads on shakedown were also investigated. The following summarizes key conclusions drawn from this study.

1. Welding-induced residual stresses in stiffened plates typical of ship hull girders may be significantly reduced when subjected to axial loads while in service. For applied axial stresses of $0.25\sigma_y$ and $0.5\sigma_y$, longitudinal residual stresses were decreased by around 20% and 40%, respectively. Relief of residual stress occurs entirely during the first load cycle of a constant amplitude cyclic load. When the load amplitude is varied, the magnitude of the highest load is the primary factor controlling the amount of residual stress shakedown achieved.
2. After partial stress relief by shakedown under average axial stresses of $0.25\sigma_y$ and $0.5\sigma_y$, the ultimate strengths of tee-stiffened plates increased by 1.5 – 3.5% and 4.5 – 7%, respectively. When welding-induced residual stresses were neglected and only distortions included, the ultimate strengths of the stiffened plates increased by 8 – 16%. This suggests that although residual stress relief by shakedown in stiffened panels is beneficial, it should not be assumed in a hull girder analysis that residual stresses are entirely removed due to shakedown while in service, as this may lead to overly optimistic estimates of hull girder ultimate strength.
3. A comparison of strain hardening models demonstrated that for hardening moduli typical of shipbuilding steels, kinematic hardening has little influence on shakedown of welding-induced residual stress.

Chapter 7 - Effect of Welding-Induced Residual Stress and Distortion on Hull Girder Ultimate Strength

Liam Gannon, Yi Liu, Neil Pegg, Malcolm Smith

7.1 Abstract

Nonlinear finite element analysis is used to simulate welding of stiffened plates so that the complete three-dimensional distribution of welding-induced residual stress and distortion is determined. The potential reduction in residual stress due to shakedown is examined and load-shortening curves are generated for the welded stiffened plates under axial compression both before and after shakedown. These curves are used as input to a hull girder ultimate strength analysis by Smith's method and results are compared with published experimental data. The ultimate strength is also calculated using load-shortening curves derived from analytical methods prescribed in the IACS common structural rules. Results from the ultimate strength analysis using the different methods are compared and the influence of welding-induced residual stress and distortion on hull girder ultimate strength is examined.

7.2 Introduction

Accurate evaluation of the longitudinal bending moment capacity of a hull girder is a fundamental aspect of safe ship structural design. The first formal use of analytical methods to calculate hull girder ultimate strength was by John (1874), who used classical

linear beam theory to calculate the bending moment and shear caused by a wave of length equal to the length of the ship. The first known attempt to account nonlinearities such as yielding and buckling in an ultimate strength analysis was made by Caldwell (1965). Caldwell's method considered plate buckling in longitudinally stiffened hulls before the ultimate strength is reached, allowing for the fact that buckled plates shed some load to the longitudinal stiffeners that continue to carry load until they buckle between transverse supports. At the time of publication, little was known about post-buckling behaviour and the ultimate strength of complete deck and side shell panels, so Caldwell was not able to account for the post-buckling strength of the structural members which can have a significant influence on ultimate strength.

Following a period of significant advances in the understanding of stiffened plate behaviour, Smith (1977) introduced a method of determining the complete moment-curvature relationship of a hull girder subjected to longitudinal bending. His method accounted for both the progressive failure and the post-buckling capacity of stiffened plates in the cross-section. In Smith's method, each stiffened panel in the hull girder cross-section is divided into individually stiffened plates. The behaviour of these stiffened plates under axial load is defined by a curve relating average axial stress and average axial strain, known as a load-shortening curve. The moment-curvature relationship for the hull can be determined by imposing a sequence of incremental curvatures and calculating the resulting strains and stresses in the stiffened plates making up the cross-section using the predefined load-shortening curves.

Thus, a key component of Smith's method in the determination of hull girder ultimate strength is the determination of load-shortening curves of stiffened plates. Much research has been conducted in the past 30 years on this subject. Dow *et al.* (1981) divided stiffened plates into a number of horizontal fibers to account for the reduction in the effective cross-section as yielding progressed through the section. Plates consisted of a single fiber and experimental curves were used to describe their behaviour under axial compression. A computer program was used for the nonlinear analysis of the stiffened panels to calculate load-shortening curves including the effects of residual stress and geometric imperfection. Other researchers (Billingsley 1980, Gordo & Guedes Soares 1993) used approximate analytical expressions to describe the behaviour of stiffened plates under axial compression. Gordo *et al.* (1996) used Smith's method to calculate the ultimate strength of the VLCC Energy Concentration. The hull of that vessel suffered failure under longitudinal bending while discharging cargo at Rotterdam in 1980. The ultimate bending moment calculated by Gordo *et al.* (1996) agreed well with the true value determined from the known loading condition at failure. Gordo *et al.* (1996) calculated load-shortening curves using analytical methods, accounting for the effective width of the plate elements using Faulkner's (1975) approach which accounts for loss of plating effectiveness due to both buckling and shear lag effects. The authors also studied the effects of residual stress, corrosion and biaxial bending on ultimate strength, using the Johnson-Ostenfeld correction to account for inelastic effects during buckling of stiffened plates. Residual stresses were accounted for by modifying the material properties.

An alternative method used for ultimate strength analysis of hull girders is the idealized structural unit method (ISUM) introduced by Ueda and Rashad (1984). This method uses specially formulated finite elements to represent plates with multiple stiffeners. The use of single elements to represent large portions of the structure greatly reduces analysis time. The ISUM continues to be developed by researchers including Paik *et al.* (1993, 1996) and Fujikubo *et al*. (2000) who have added new functionality to the elements including the ability to account for residual stress and initial distortion. At present ISUM elements do not have the capability to represent localization of plastic deformation or stiffener tripping.

For design purposes, a closed form analytical method of calculating hull girder ultimate strength is preferred because the calculations are relatively simple in comparison to numerical modelling. The International Association of Classification Societies (IACS, Common structural rules for bulk carriers, 2009) provides a single step procedure for estimating hull girder ultimate moment capacity. The method is based on the assumption that the hull girder ultimate capacity is attained when the ultimate strength of the stiffened deck panels is reached. The method used to determine the buckling strength of the deck panels is outlined in the Appendices of the IACS (2009) common structural rules.

In a benchmark study published by the International Ship Structures Congress (Ohtsubo & Sumi, 2000), stiffened plate behaviour and hull girder ultimate strength values were evaluated by different contributors to the study using various analytical and numerical

methods. The results of the study show that there is significant scatter among the ultimate strength values computed using the different methods of analysis. This discrepancy may be attributed in part to the various assumptions and idealizations made with regard to fabrication related imperfections such as welding-induced residual stress and distortion. With tensile axial loads, residual stress and distortion reduce stiffness of stiffened plates in the pre-ultimate strength region and the ultimate strength is reached when gross yielding occurs. For compressive axial loads, the combined effects of residual stress and distortion cause a reduction in the load-carrying capacity of stiffened plates but suppress the sudden drop in load-carrying capacity after the ultimate load is reached in nearly perfect plates (Gordo & Guedes Soares, 1993).

In the design and analysis of stiffened plates, the complex distribution of residual stress may be simplified by assuming a two-dimensional stress distribution that is constant along the length of the stiffened plate. Figure 7.1 shows one such residual stress distribution used by Smith (2008) that consists of a zone of tensile stress in the plate near the weld equal to the yield stress σ_y, of width of $2\eta t$ and a nearly uniform compressive residual stress across the rest of the plate, where t is the plate thickness and η defines the width of the tensile stress zone. The value of η usually ranges from 3 to 4.5, depending on the geometry and welding conditions (Faulkner, 1975).

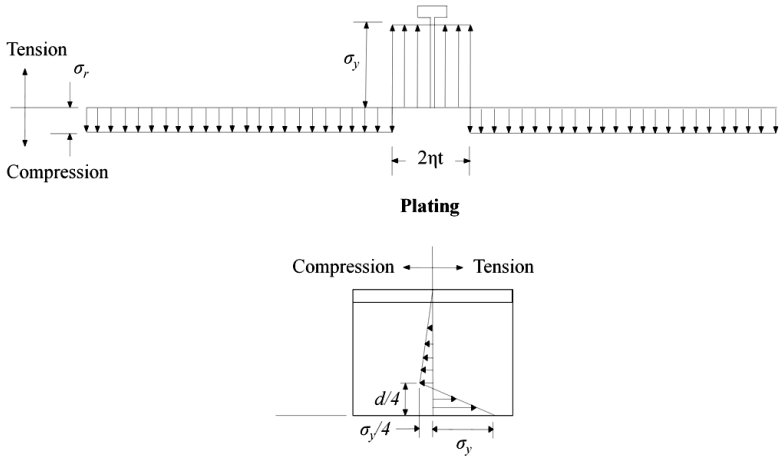

Figure 7.1, Longitudinal residual stress distribution in welded stiffened plates

Maximum out-of-plane plating imperfections δ_{o1}, measured in surveys of ship and civil engineering structures are typically expressed as a fraction of plate thickness and relate approximately to the plate slenderness β_0, given by:

$$\beta_0 = \frac{b}{t}\sqrt{\frac{\sigma_y}{E}} \tag{7.1}$$

where E is the elastic modulus. Typical values of δ_{o1} lie in the range of $0.05\,\beta_0^2\,t$ to $0.15\,\beta_0^2\,t$ with extreme values up to $0.4\,\beta_0^2\,t$ for heavily welded plates. Smith *et al.* (1992) suggest typical levels of welding-induced out-of-plane distortion of plates between stiffeners that are the source of the familiar "hungry horse" shape seen in many welded ship hulls. They considered slight, average and severe levels of distortion defined by:

$$\frac{\delta_{01}}{t} = \begin{cases} 0.025\beta_0^2 & \text{for slight imperfections} \\ 0.1\beta_0^2 & \text{for average imperfections} \\ 0.3\beta_0^2 & \text{for severe imperfections} \end{cases} \tag{7.2}$$

Based on surveys of imperfections in warship hulls, Smith *et al.* (1992) also classify the magnitude of column-type vertical distortion δ_0, along the axis of the stiffener as slight, average or severe. The magnitude of these distortions depends on both the length of the stiffened plate a, and the column slenderness λ, according to Table 7.1.

Table 7.1, Levels of stiffener distortion

	δ_0/a		
λ	Slight	Average	Severe
0.2	0.00025	0.0008	0.002
0.4	0.00025	0.0012	0.0038
≥ 0.6	0.00025	0.0015	0.0046

Where,

$$\lambda = \left(\frac{a}{\pi r}\right)\sqrt{\sigma_y / E} \tag{7.3}$$

The influence of residual stress on hull girder ultimate strength was examined by Gordo and Guedes Soares (1996), who used an approximate method to generate load-shortening curves that were used in ultimate strength analyses of several box girder tests using Smith's method. For the plate-induced failure mode, residual stresses were considered using the approach of Crisfield (1975), whereas for flexural buckling, the Johnson-Ostenfeld formulation was used to account for inelastic effects. Residual stress was not considered in the stiffener tripping failure mode calculations. In simulating a box girder test performed by Dowling *et al.* (1973), Gordo and Guedes Soares found that increasing the compressive residual stress level in the stiffened plates from $0.089\sigma_y$ to $0.192\sigma_y$ reduced the ultimate strength of the box girder by 5%. The measured average value of

compressive residual stress in the test specimen was $0.176\sigma_y$. In an analysis of the structural failure of the VLCC Energy Concentration, Gordo *et al.* (1996) found that ultimate strength values determined using approximate analytical methods agreed well with the true ultimate moment capacity of the hull girder calculated from the known loading condition at failure. The authors found that the relation between ultimate bending moment and the tensile stress block parameter η (Figure 7.1), is nearly linear. They found that for $\eta = 3$, corresponding to a compressive residual stress in the plate (with a width to thickness ratio of 40) of $0.167\sigma_y$, the reduction in ultimate strength due to residual stress was 5.1% for hogging and 4.7% for sagging.

Welding-induced residual stresses may be relieved to some degree by plastic deformation of stiffened plates under cyclic loads during service. This process is commonly referred to as shakedown. Shakedown in ship structures has been investigated both experimentally and numerically; however most research has focused on the effects of shakedown on fatigue behavior in welded structures. Studies of shakedown in welded structures by Latrou *et al.* (2005) and Liangbi *et al.* (2007) revealed that under constant amplitude cyclic loads, residual stress relaxation was limited to the first load cycle. Gannon *et al.* (2011) found similar results by numerical analysis of stiffened plates. Following a three-dimensional nonlinear finite element analysis modeling the welding of stiffened plates, they applied cyclic axial loads to the numerical models to simulate residual stress shakedown. They found that applied axial stresses of $0.25\sigma_y$ and $0.5\sigma_y$ caused reductions in the magnitude of residual stress of approximately 20% and 40%, respectively. In a subsequent compressive strength analyses of the stiffened plates, shakedown-induced

reductions in residual stress were found to increase the ultimate strength of the stiffened plates by as much as 6.5%.

The objective of this study is to evaluate the influence of welding-induced residual stress and distortion on hull girder strength and behaviour, also considering the effects of shakedown. The method used is novel in that residual stresses and distortions are predicted by sequentially coupled, three-dimensional transient thermal and nonlinear structural analyses. These residual stresses and distortions are included in subsequent analyses wherein shakedown loads are applied and load-shortening curves are generated for use in ultimate strength analysis by Smith's method. The hull girder ultimate strength determined using the present finite element analysis techniques is compared with ultimate strength values determined using load-shortening curves generated using the IACS (2009) common structural rules and an approximate analytical method proposed by Gordo and Guedes Soares (1993). The hull girder test specimen on which the geometry of the finite element model, and input to the analytical methods are based was built and tested by Akhras *et al.* (1998).

7.3 Description of Hull Girder Model

The hull girder cross-section used in the present research was tested by Akhras *et al.* (1998). The scantlings (plate, frame and stiffener dimensions), shown in Figure 7.2, were approximately half of those in a Canadian warship, while the overall cross-section was approximately 1/15 the size of the hull of a full-scale Canadian Patrol Frigate. The length of the test section was 2850 mm, consisting of three bays, 950 mm long each. From

tensile coupon tests, the average yield stress and elastic modulus of the plate material (SAE 1010) were found to be 294 MPa and 212 GPa, respectively. The yield stress and elastic modulus of the stiffener material (ASTM A-36) were 318 MPa and 205 GPa, respectively. Welding was carried out in accordance with procedures specified in the Department of National Defence of Canada Welding Specification of HMC Ships (Department of National Defence, 1981), where the minimum fillet weld size is specified as a function of plate thickness. The heat input and corresponding welding speed for the 4 mm fillet weld was consistent with values recommended in the Canadian Standards Association welding specification W59-03 (Canadian Standards Association, 2003). Longitudinal stiffeners were attached to the plating using a back-step welding sequence as illustrated in Figure 7.3.

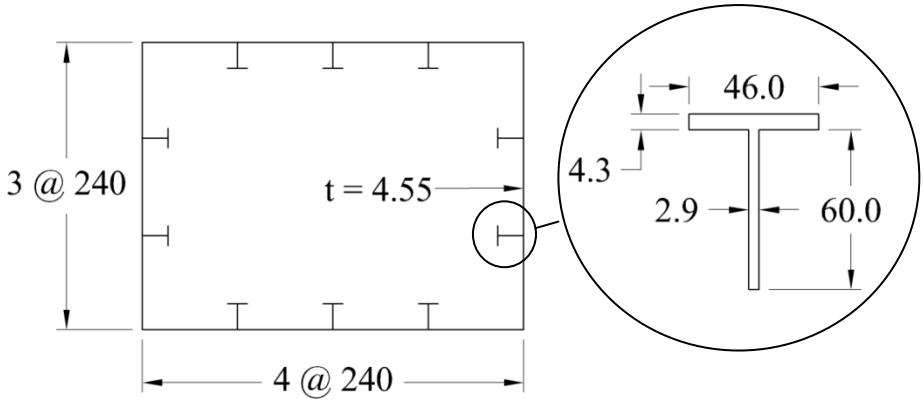

Figure 7.2, Test specimen cross-section scantlings (mm)

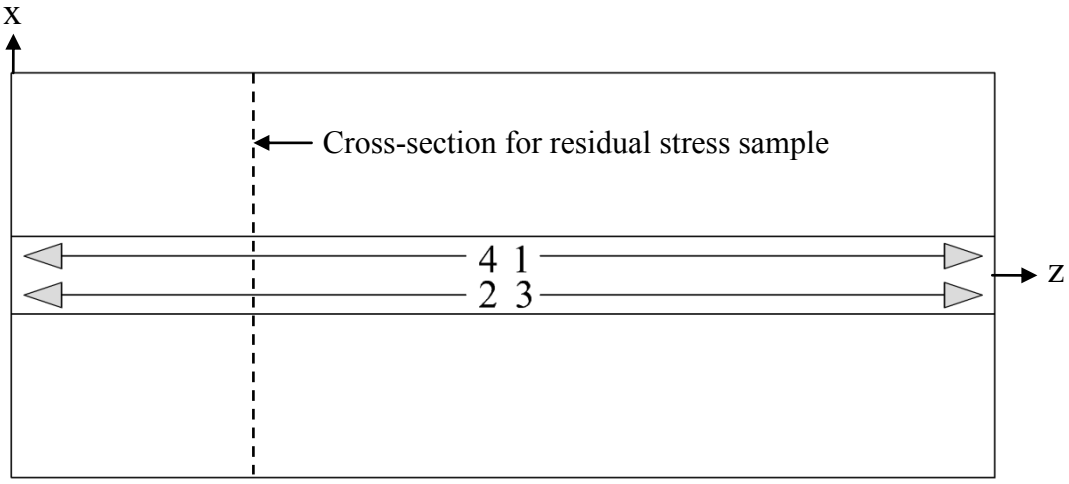

Figure 7.3, Back-step welding sequence for tee-stiffened plates

7.4 Finite Element Modelling

Two different types of finite element model were used to investigate the effects of residual stress and distortion on stiffened plate behaviour and subsequently on hull girder ultimate strength. One is a detailed finite element model meshed with hexahedral solid elements. This detailed mesh allowed the complex, three-dimensional distribution of welding-induced residual stress to be accounted for in ultimate strength analyses. The other type of model was meshed with shell elements to facilitate a faster solution time compared with the solid element models. These models were used to study the effects of distortion on stiffened plate behaviour and on hull girder ultimate strength.

7.4.1 Welding Simulation

A finite element simulation was used to predict welding-induced residual stress and distortion caused by welding the stiffeners to the plates during construction of the hull

girder model. The simulation consisted of sequentially coupled nonlinear thermal and structural analyses, both of which used the same model meshed with 8-node, linearly interpolated hexahedral elements. Two-node nonlinear spring elements were also used to model contact between the stiffener base and the plate. Temperature dependent material properties given by Deng and Murkawa (2008) for a Korean mild shipbuilding steel (SM400A) were used for both the plate and stiffener material. To account for the difference in material properties between SM400A and those measured by Ahkras *et al.* (1998), the temperature-dependent yield stress and elastic modulus of SM400A were adjusted for the plate and stiffener separately. The properties were adjusted over the entire temperature range in proportion to the difference between the measured values and nominal values of SM400A at 0 °C.

In the finite element mesh, twelve elements were used through the thickness of the plate in the vicinity of the weld in order to accurately characterize the severe thermal gradient in that region. The mesh density was decreased in regions further away from the weld where the thermal gradient was small so that the analysis could be run in a reasonable amount of time with the computational resources available. A minimum of 4 elements was used through the thickness of all components of the stiffened plate model. Figure 7.4 shows the finite element mesh used for the tee-stiffened plate in this study. For the thermal analysis, the Solid70 hexahedral element was used whereas the structural equivalent Solid185 element was used in the ultimate strength analysis. Both element types are 8-node, bi-linearly interpolated isoparametric hexahedrons. For the thermal element, only the temperature degree of freedom is considered at each node, whereas the

three displacements along the Cartesian coordinate axes are used as degrees of freedom at each node for the structural element.

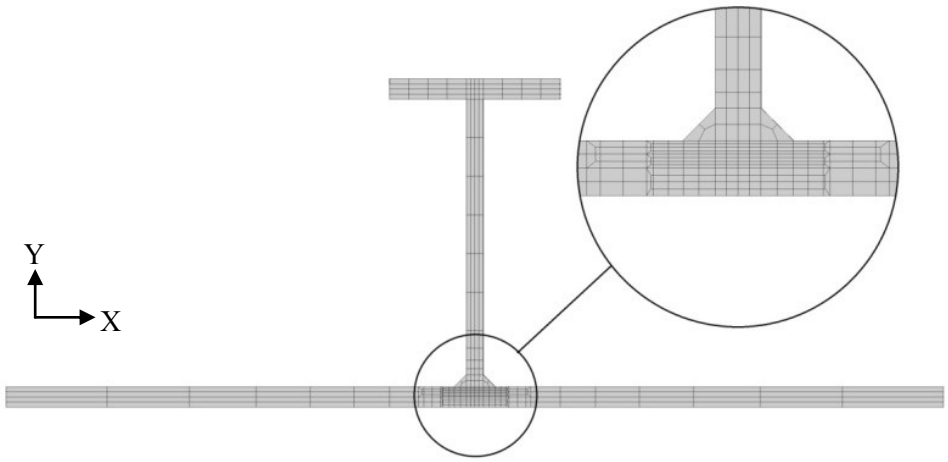

Figure 7.4, Finite element mesh of tee-stiffened plate.

A nonlinear thermal analysis was used to predict the transient temperature field produced by the moving heat source. A circular heat source with a Gaussian energy distribution representing the heat from a welding torch, was moved along the weld path in 10 mm increments. Continuous, 4 mm fillet welds were deposited using the back-step welding sequence described previously. Although the weld size and heat input were not provided by Akhras *et al.* (1998), the referenced document (Department of National Defence, 1981) for the welding procedures they used was used to size the welds and determine the heat input (453 J/mm). When welding was completed, sufficient time was allowed for the stiffened plate to return to the ambient temperature (20°C). The thermal analysis considered temperature dependent material properties including thermal conductivity, specific heat and density (Deng & Murakawa, 2008). Heat loss due to convection and radiation was accounted for using a film coefficient given by Goldak *et al.* (1984) to

account for heat loss by both mechanisms. Latent heats of melting and fusion were also considered. User-defined subroutines were created using the ANSYS® parametric design language to model the moving heat source and to control activation of weld elements as the heat source progressed.

For the second stage of the analysis, the transient temperature field from the thermal analysis was used as a series of load steps in a structural analysis. Each load step consisted of an incremental progression of the heat source along the weld path. As the heat source advanced along the weld path, the ANSYS® element birth and death feature was used to activate the weld elements behind the heat source once their temperature fell below the solidification temperature, taken as 1450°C. This enabled the model to simulate the dynamic coupling of the stiffener to the plate as the weld progressed. The application of sequential thermal loads, and the element activation scheme were controlled via user-defined subroutines.

For the structural analysis, longitudinal edges were constrained to remain straight, but free to move in the plane of the plating. This produced a level of restraint similar to that provided by adjacent panels in typical ship hulls (Dow *et al.*, 1981). At the end cross-sections, displacements were constrained along all three coordinate axes at the centroid of one end and in the vertical (y-axis) and transverse (x-axis) directions at the centroid of the opposite end. An elastic, perfectly plastic material model was used with von Mises failure criteria and associated flow rule was used, and nonlinearities due to large strain and displacement were also considered.

The accuracy of the welding simulation was verified using the methods described above to simulate a welding experiment carried out by Deng *et al.* (2007). In the experiment, a steel flat-bar stiffener was connected to a steel plate by sequential, 6 mm fillet welds. Figure 7.5 shows the weld sequence and direction along with the test specimen dimensions. The material used in the experiment was SM400A shipbuilding steel with a yield stress of 300 MPa. Temperature dependent material data for numerical modelling was adopted from Deng *et al.* (2008). Figure 7.6 shows that the vertical deflection of the plate predicted by the welding simulation is in good agreement with experimental measurements provided by Deng *et al.* (2007). Figure 7.7 shows the longitudinal residual stress distribution at the mid-length, mid-plane of the plate. Although residual stress measurements from the experiment were not available, the residual stress distribution determined by finite element analysis is consistent with measured values available in literature (Michaleris & DeBiccari 1997, Nagaraja Rao & Tall 1961, Kenno *et al.* 2010). For a more comprehensive description of the welding simulation method, the reader is referred to Gannon *et al.* (2010).

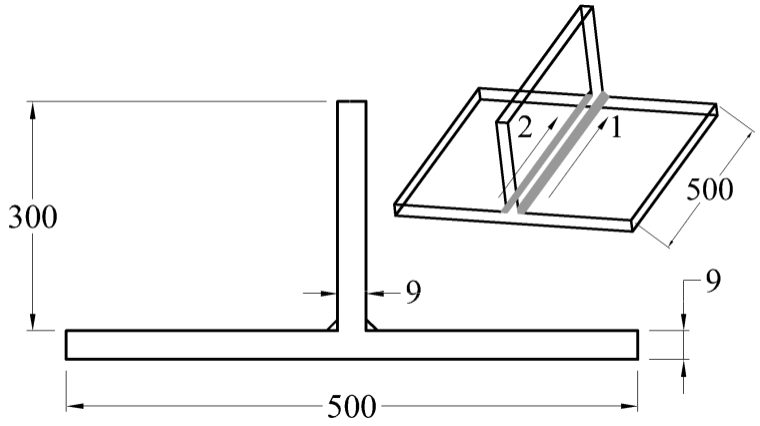

Figure 7.5, Test specimen used by Deng et al. (2006). Dimensions in mm.

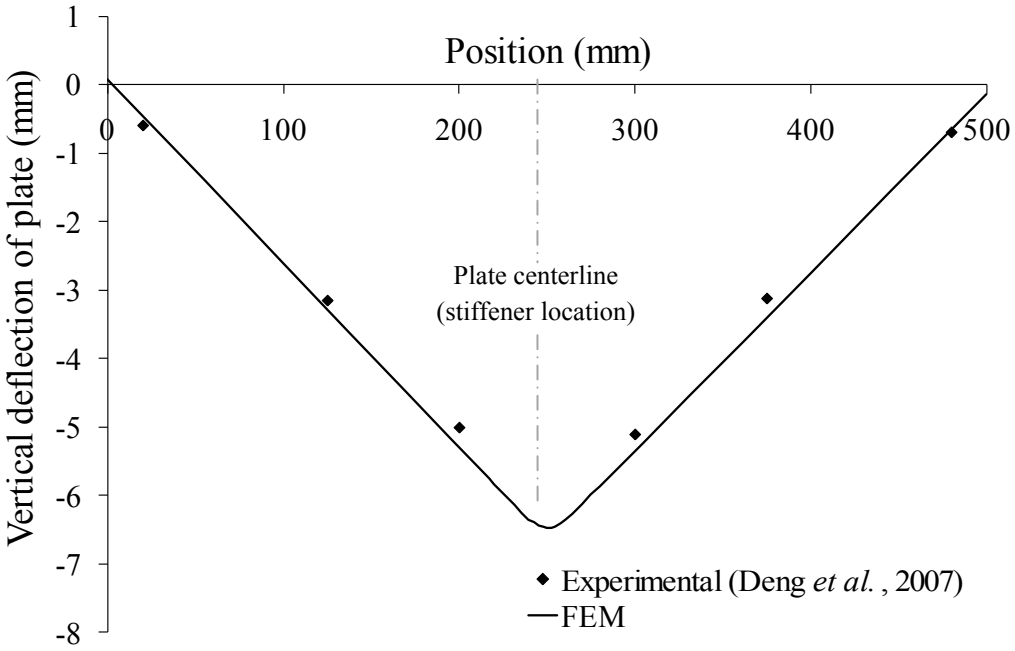

Figure 7.6, Comparison of vertical deflection of plate with measured values.

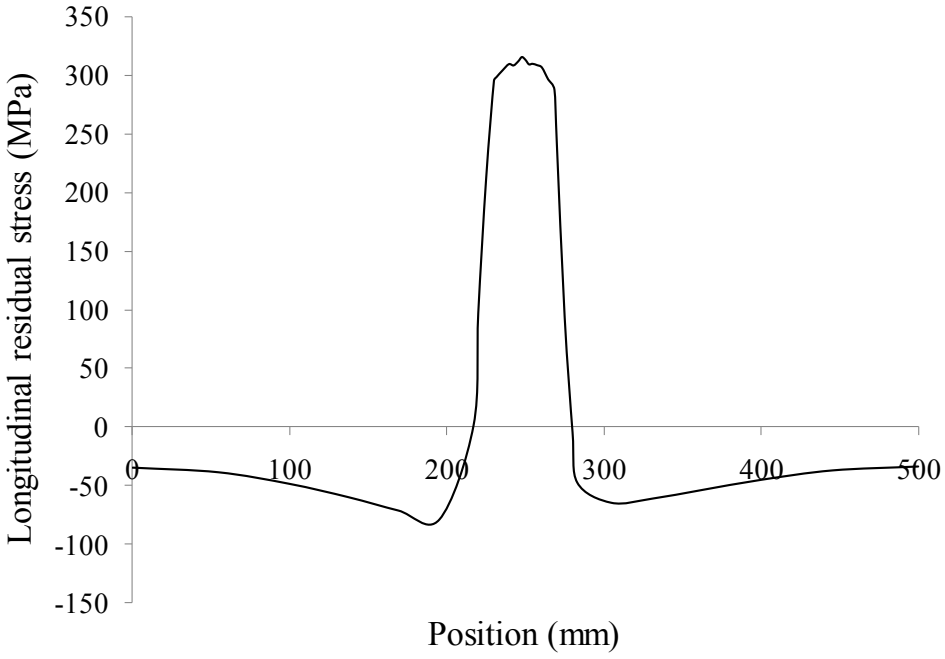

Figure 7.7, Longitudinal residual stress at mid-span from welding simulation.

7.4.2 Load-Shortening Curve Calculation

The behaviour of stiffened plates under axial compressive load was determined by application of an axial displacement to the centroid of one end of the finite element model, while translation at the centroid of the opposite end was constrained along all three Cartesian coordinate axes. For each increment in displacement, the average axial strain and stress were determined and normalized with respect to the yield strain and stress, giving the load-shortening curves for each stiffened plate geometry in the cross-section. Load-shortening curves were generated using finite element models meshed with both solid and shell elements. The solid model described in the previous section included three-dimensional residual stresses and distortions predicted by welding simulation. Where shell element models were used to generate load-shortening curves, the longitudinal residual stresses predicted by weld simulation using solid elements were mapped onto the shell elements for the analysis.

Figure 7.8 shows an exaggerated view of initial distortions that were used in the shell element models including the first elastic buckling mode; a small amount of which was included in the initial distortion to allow for local buckling. The amplitude of plate (δ_{01}) and stiffener (δ_0) distortions for slight, average and severe imperfections given in Eqn. 7.2 and Table 7.1 were considered in the study. The amplitude of the elastic buckling mode distortion δ_{02}, was taken as 1/32 of the plate distortion amplitude with minimum and maximum limits of 0.05t and 0.08t, respectively (Smith, 2008).

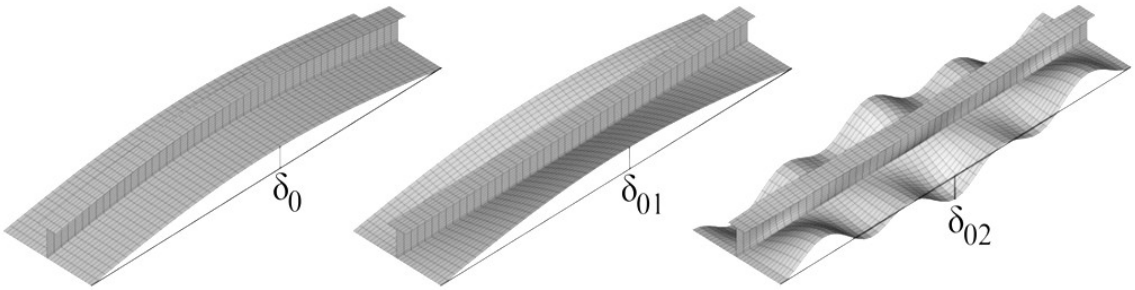

Figure 7.8, Initial distortions in shell element models

7.4.3 Shakedown Analysis

A shakedown analysis was conducted to assess the potential reduction in welding-induced residual stress due to loads applied while a ship is in service. For the shakedown analysis, an axial load was applied to the centroidal node of one cross-section while the other end cross-section remained pin supported at its centroid. The axial load was of sufficient magnitude to cause an average axial stress of $0.25\sigma_y$. In both the solid and shell element models, stiff beam elements were used to connect each node of each end cross-section to a node at the centroid of the respective cross-section. This was done to constrain those cross-sections in such a way that they remained plane during the strength analysis following the welding simulation. This constraint represents the support that would be provided by transverse frames added after the stiffeners were welded to the plate. During the welding simulation, those beam elements were deactivated using the ANSYS® element birth and death feature which multiplies the stiffness of inactive elements by a severe reduction factor and removes any loads applied to those elements from the global load matrix.

It has been shown by Gannon *et al.* (2011) that if the average applied stress is less than the yield stress, shakedown of residual stress depends only on the magnitude of the highest applied load, and not on the number of load cycles. Therefore, a single load cycle was applied where a compressive axial load was applied and removed followed by application and removal of a tensile axial load.

7.5 Hull Girder Ultimate Strength Analysis

The hull girder ultimate strength was evaluated using Smith's method, also known as the beam-column method. Smith's method is a simplified method of hull girder analysis wherein the progressive collapse and post-buckling behaviour of structural elements making up a cross-section is accounted for. The hull cross-section is subdivided into a number of individually stiffened plate elements and the moment-curvature relationship is determined by imposing incremental curvatures on the cross-section. For each curvature, the average strain in each longitudinally stiffened plate element is calculated based on its position relative to the neutral axis after which the associated stress is determined from a predefined load-shortening curve. The bending moment carried by the cross-section is calculated by summation of the moments of the forces in each individual element about the neutral axis of the cross-section. The main assumptions of the method are (Gordo *et al.*, 1996).

1. The elements into which the cross-section is divided act independently.
2. Plane sections remain plane after bending.
3. Overall grillage failure is prevented by sufficiently stiff transverse frames

The initial position of the neutral axis passes through the centroid of the cross-section at the point $(\bar{x},\bar{y})$ given by:

$$\bar{x} = \frac{\sum x_i A_i}{\sum A_i}$$
$$\bar{y} = \frac{\sum y_i A_i}{\sum A_i} \tag{7.4}$$

where A_i is the cross-sectional area of the i^{th} element and x_i and y_i are the distances along the x and y axes respectively of the i^{th} element from the origin. For the general case of a singly symmetric hull girder cross-section subjected to an unsymmetric bending moment represented by the vector **M**, the concomitant curvature vector **C**, can be resolved into its components about the major and minor principle axes (x and y axes, respectively) with corresponding curvatures $\mathbf{C}_x$ and $\mathbf{C}_y$, given by:

$$\mathbf{C}_x = \mathbf{C}\cos\theta$$
$$\mathbf{C}_y = \mathbf{C}\sin\theta \tag{7.5}$$

where θ is the angle between the curvature **C**, and the x-axis, shown in Figure 7.9.

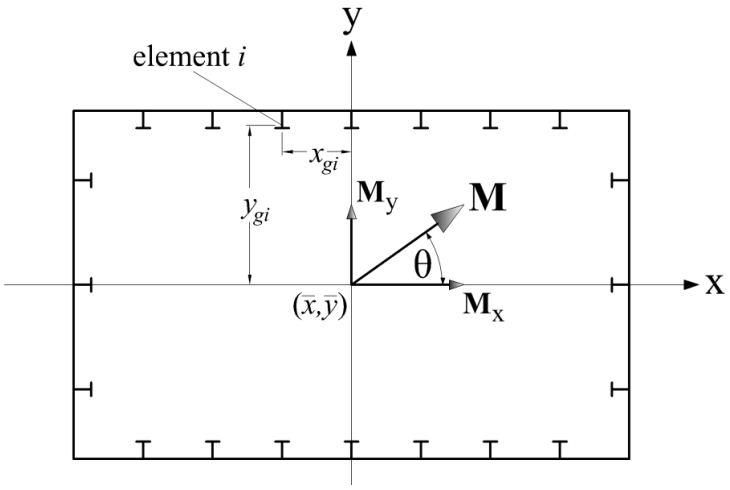

Figure 7.9, Hull girder biaxial bending

The strain ε_i, at the centroid of element i is then:

$$\varepsilon_i = y_{gi}\mathbf{C}_x - x_{gi}\mathbf{C}y \tag{7.6}$$

where $\langle x_{gi}, y_{gi} \rangle$ is the vector from the centroid of the cross-section to the centroid of the i^{th} element. With the strain in each element known, the corresponding stresses are determined from the load-shortening curves for the elements. and the components of the total bending moment about the principle axes, $\mathbf{M}_x$ and $\mathbf{M}_y$, are given by:

$$\begin{aligned} \mathbf{M}_x &= \sum y_{gi}\Phi\left(\bar{\varepsilon}_i\right)\sigma_y A_i \\ \mathbf{M}_y &= \sum x_{gi}\Phi\left(\bar{\varepsilon}_i\right)\sigma_y A_i \end{aligned} \tag{7.7}$$

where $\Phi\left(\bar{\varepsilon}_i\right)$ is the average stress in element i at a normalized strain of $\bar{\varepsilon}_i$, normalized by the yield stress, σ_y. The bending moment $\mathbf{M}$, on the cross-section about the instantaneous center of gravity is then:

$$\mathbf{M} = \sqrt{\mathbf{M}_x^2 + \mathbf{M}_y^2} \tag{7.8}$$

As the curvature increases and the response of the hull girder becomes nonlinear, the location of the centroid changes, making it necessary to calculate the shift in the centroid position between successive curvatures. The new position of the centroid is calculated using the effective area of each element given by:

$$A_{ei} = \eta A_i \tag{7.9}$$

where η, represents the deviation of the element from perfectly elastic behaviour, given by:

$$\eta = \bar{\sigma} / \bar{\varepsilon} = \frac{\left(\sigma / \sigma_y \right)}{\left(\varepsilon / \varepsilon_y \right)} \tag{7.10}$$

The position of the neutral axis is then given by:

$$\begin{aligned} \bar{x} &= \frac{\sum x_i A_{ei}}{\sum A_{ei}} \\ \bar{y} &= \frac{\sum y_i A_{ei}}{\sum A_{ei}} \end{aligned} \tag{7.11}$$

Due to the dependence of A_{ei} on the position of the centroid, Eqns. 7.9 through 7.11 must be applied repeatedly to determine the position of the neutral axis until convergence criteria is achieved. The complete iterative process for ultimate strength analysis was conducted using the ULTMAT software developed by Defence Research and Development Canada (ULTMAT User's Manual, V2.1)

The hull girder in the current study was subdivided into structural elements as shown in Figure 7.10. Top and bottom corners of the cross-section were assumed to act as hard corners, being fully effective through the complete ultimate strength analysis. Hard corners consist of a width of plating on each side equal to half of the distance to the adjacent stiffener (IACS, 2009). The length of the stiffened plates was taken the spacing between transverse frames (950 mm) giving β_0 and λ values of 1.99 and 0.45, respectively Load-shortening curves were not generated for elements in tension because

it was assumed that these members are fully effective up to the ultimate load, so that they fail by gross section yielding.

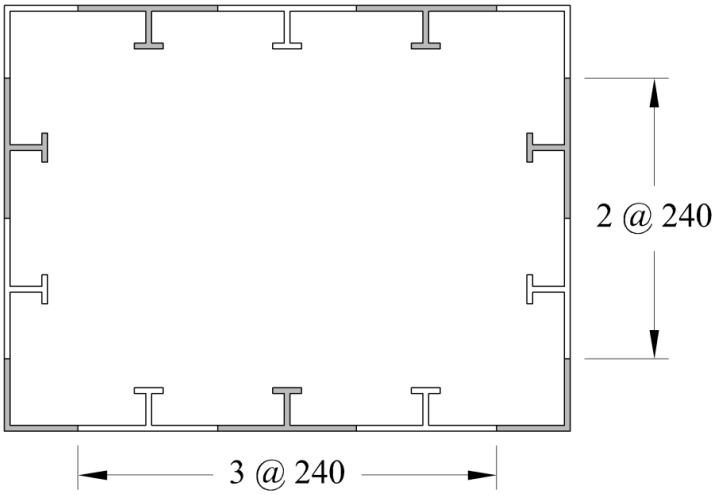

Figure 7.10, Division of hull cross-section into stiffened plate elements

7.6 Results of Residual Stress and Distortion

7.6.1 Initial Values

Longitudinal residual stresses in the plate, web and flange of the tee-stiffened plate, calculated by finite element welding simulation, are shown in Figure 7.11, Figure 7.12, and Figure 7.13 respectively. The stresses are reported at a cross-section located 240 mm along the z-axis (Figure 7.3). As shown in Figure 7.11 for the plate, tensile residual stresses equal to the yield stress were present in the vicinity of the weld, balanced by nearly uniform compressive residual stress in the rest of the plate. This is consistent with measured residual stress distributions reported in the literature (Nagaraja Rao *et al.*, 1964). The tensile stress block parameter is approximated at $\eta = 6.7$, larger than typical

values (3.5 - 4.5) recommended for stiffened plate analysis (Faulkner, 1975). This larger value of η, is attributed to the fact that the weld leg length (4 mm) is nearly equal to the plate thickness, and is larger than the stiffener web thickness. Although this weld size is consistent with the welding standard (Department of National Defence, 1981) that was adhered to for fabrication of the test specimen, in a full-scale ship structure it is not common practice for a fillet weld leg size to exceed the thickness of the thinnest plate component being joined. Longitudinal residual stresses in the stiffener web (Figure 7.12) were largely tensile with stress equal to yield from the base of the web up to 12 mm from the base. From 12 mm above the base of the stiffener, there is a linear decrease in residual stress to approximately 25 MPa in compression at the bottom of the flange. Residual stresses in the stiffener flange (Figure 7.13) were compressive, varying linearly from -43 MPa to -53 MPa.

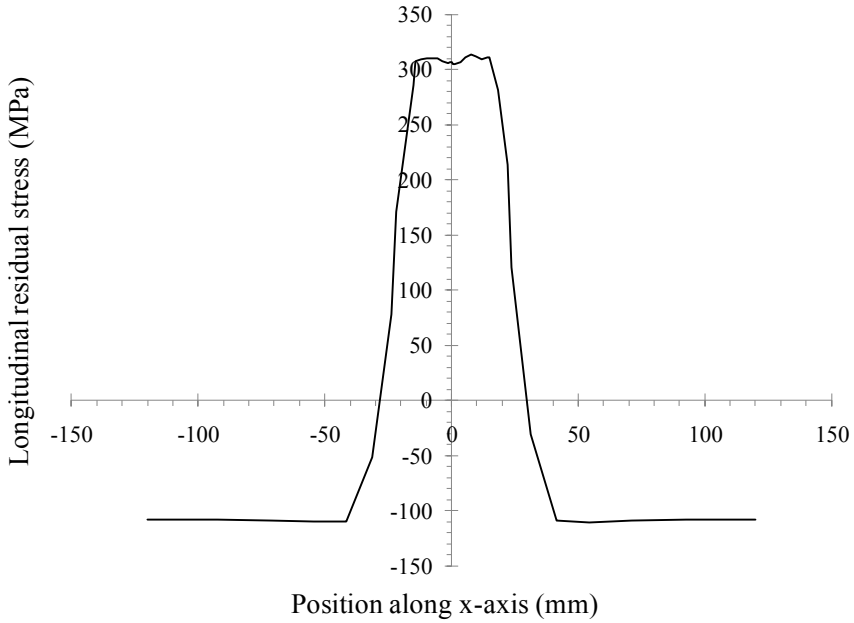

Figure 7.11, Longitudinal residual stress in the plate

Out-of-plane distortion (y-direction) of the plate at the same location where residual stresses were shown is illustrated in Figure 7.14, where the typical 'hungry horse' type of distortion seen in many ship structures is evident. Maximum plate imperfections generated by the welding simulation correspond to the slight level defined by Smith *et al.* (1992). The plate distortion falls within the range of measured values provided by Akhras *et al.* (1998). Figure 7.15 shows the column-type vertical distortion (δ_0, Figure 7.8) of the stiffened plate along the axis of the stiffener. The maximum value of this type of distortion (δ_0 = 3.6 mm) falls between the average and severe categories, and is also within the range of experimentally measured values (Smith *et al.*, 1992).

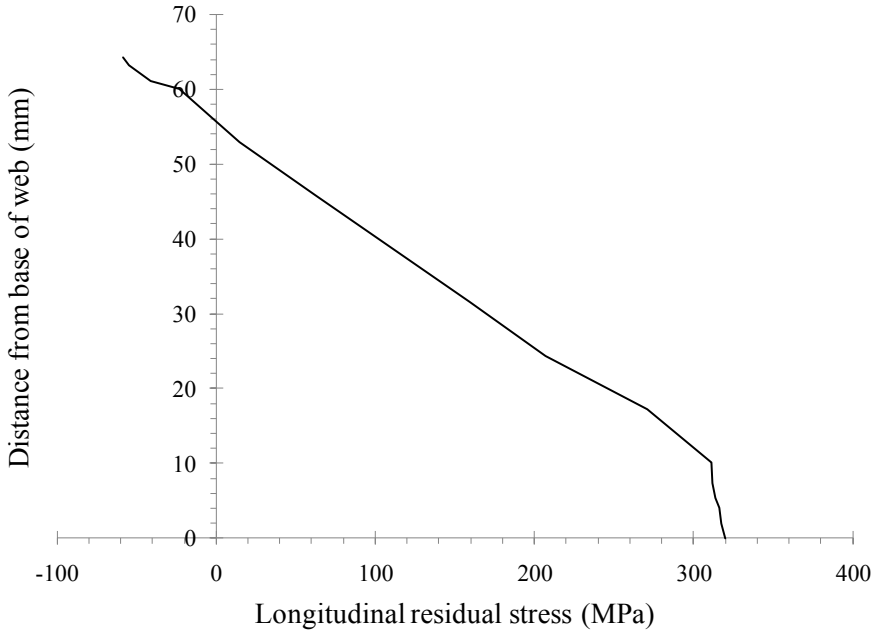

Figure 7.12, Longitudinal residual stress in the stiffener web

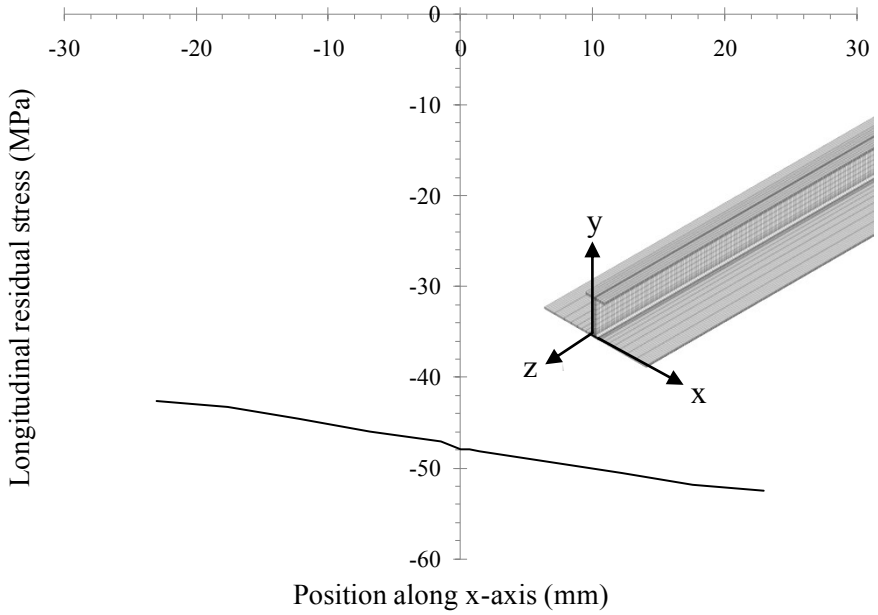

Figure 7.13, Longitudinal residual stress in the stiffener flange

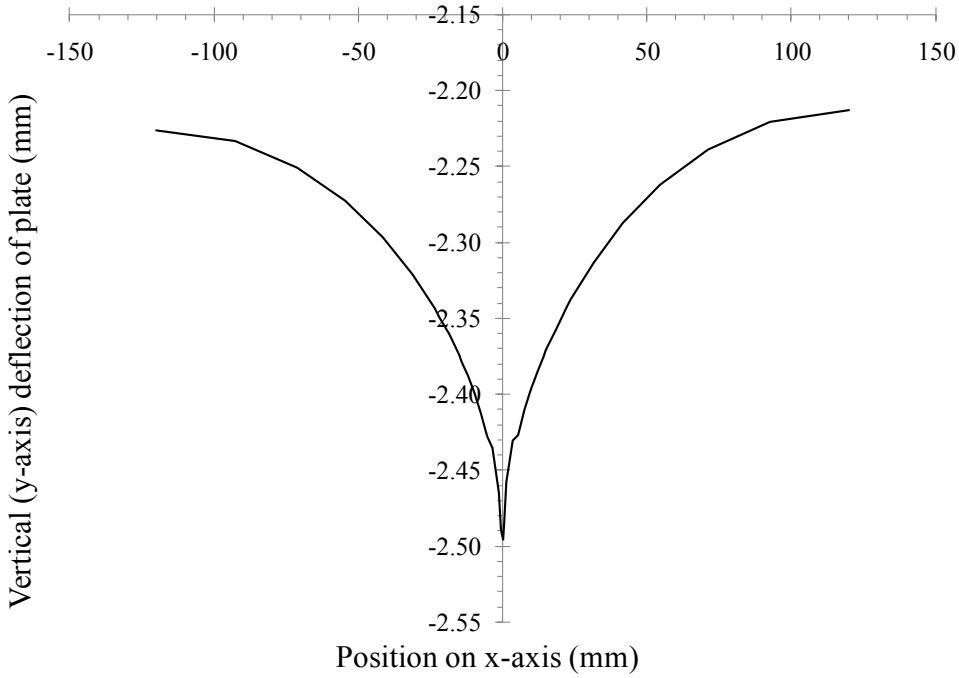

Figure 7.14, Typical out-of-plane plate distortion

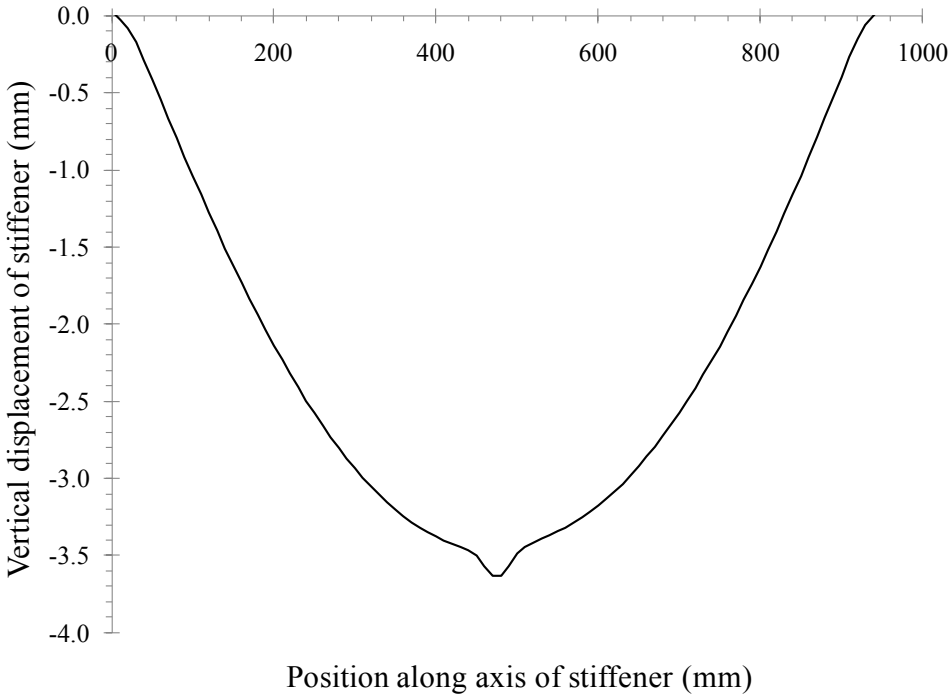

Figure 7.15, Column-type vertical distortion along axis of stiffener

7.6.2 Residual Stress and Distortion after Shakedown

One cycle of an average axial stress of $0.25\sigma_y$ was applied to the stiffened plate to determine to what extent in-service loads affect the distribution of residual stress and distortion. Figure 7.16, Figure 7.17 and Figure 7.19, respectively compare the distribution of longitudinal residual stress in the plate, web and flange of the stiffened plate before and after shakedown. Figure 7.16 shows that maximum tensile and compressive residual stresses in the plate were reduced by approximately 18% and 11%, respectively after shakedown. In the web as seen in Figure 7.17, peak tensile residual stresses were reduced by around 12.5%. The change in residual stress in the web was negligible in areas where the sum of the residual stress, and the stress due to the applied load, was less than yield.

In the case of the flange shown in Figure 7.18, residual stress was reduced by a constant 3% across the width after shakedown.

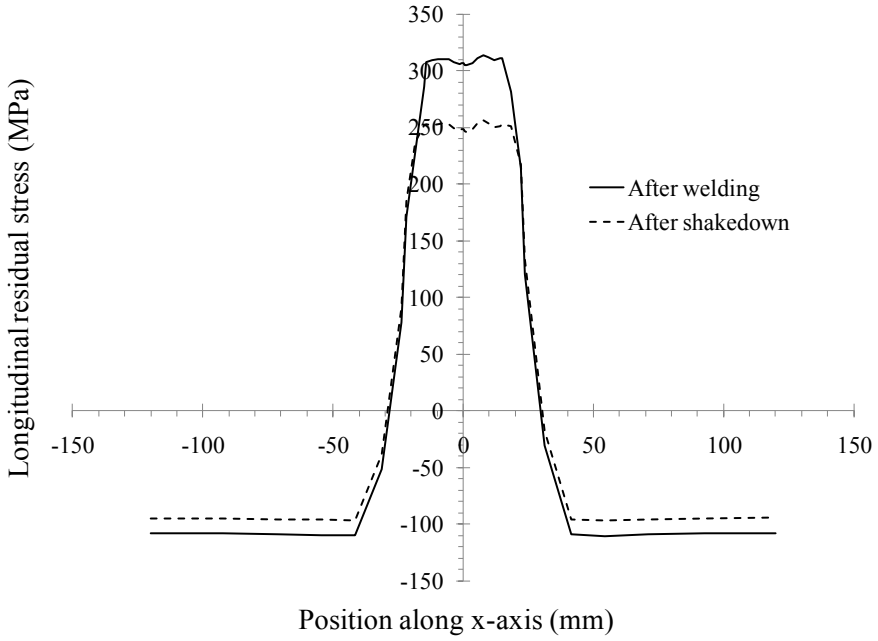

Figure 7.16, Longitudinal residual stress in the plate

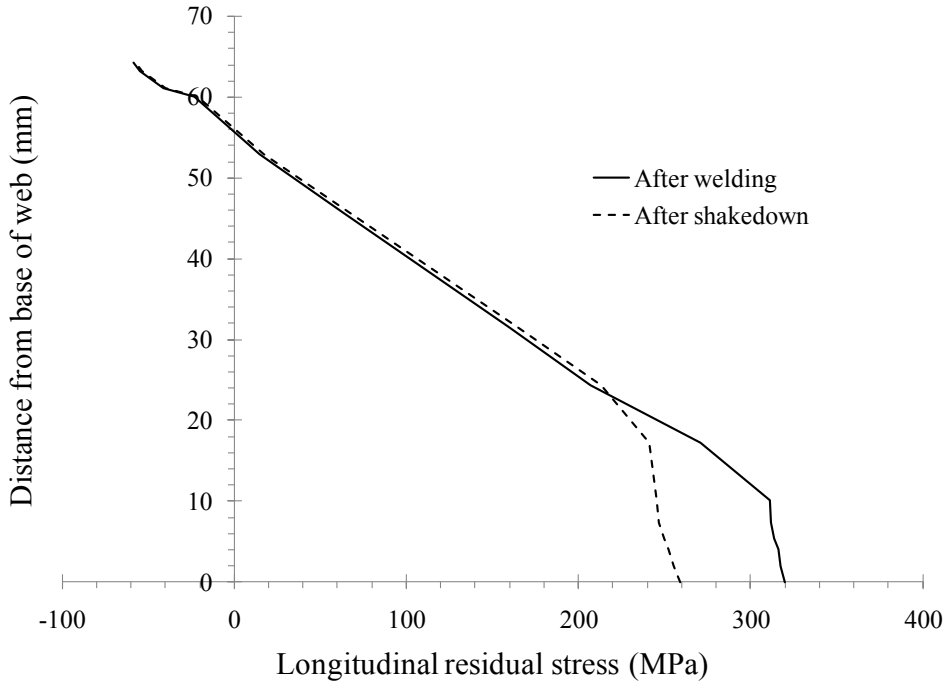

Figure 7.17, Longitudinal residual stress in the stiffener web

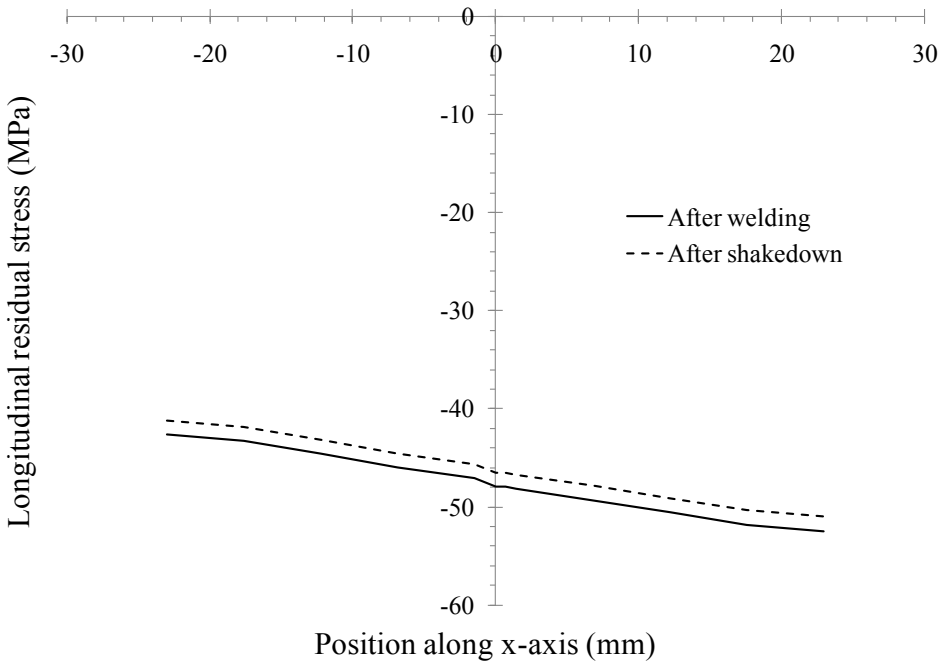

Figure 7.18, Longitudinal residual stress in the stiffener flange

The redistribution of residual stress during shakedown resulted in a change in the distortions in the stiffened plate. Figure 7.19 and Figure 7.20 show the change in plate distortion at mid-length and the change in column-type distortion along the axis of the stiffener, respectively. While distortion of the plate at mid-span relative to the stiffener decreased by around 5%, there was a slight increase (2.5%) in the peak vertical deflection of the stiffened plate along the axis of the stiffener from 3.63 mm to 3.72 mm at the mid-length.

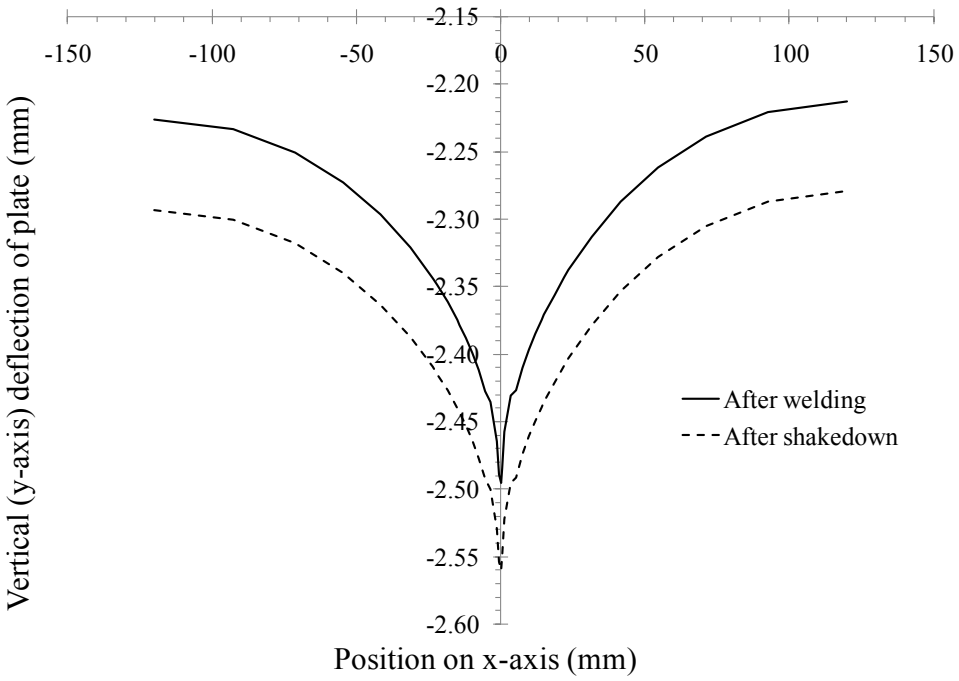

Figure 7.19, Plate distortion before and after shakedown

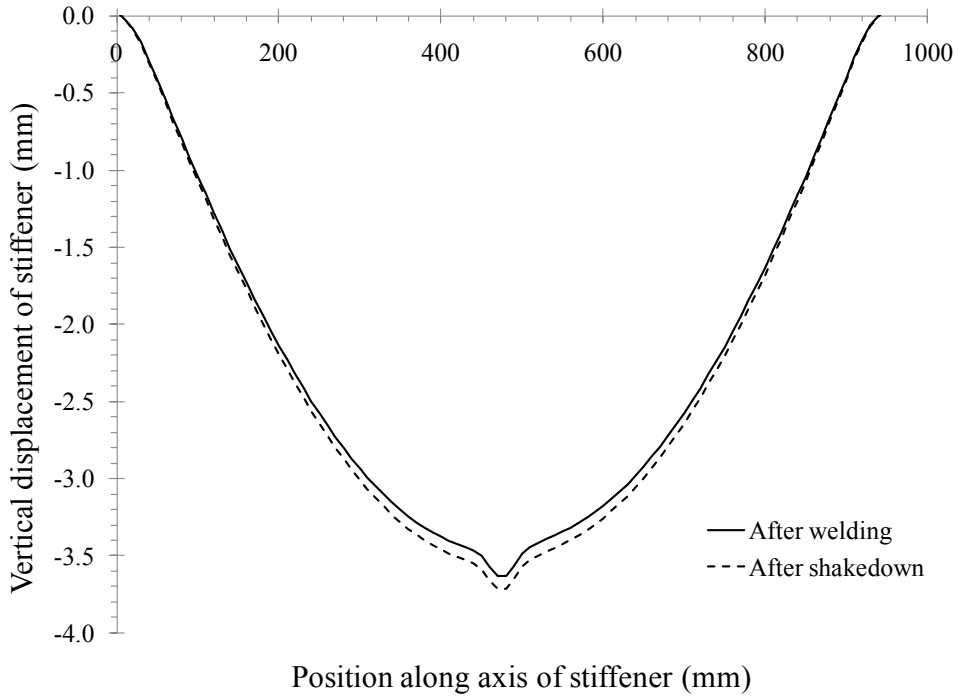

Figure 7.20, Column type distortion before and after shakedown

7.7 Results of Load-Shortening Curves

7.7.1 Comparison with Analytical Methods

Three different methods were used to generate load-shortening curves defining the behaviour of the stiffened plate shown in Figure 7.2 under axial compressive load. The first was finite element models using solid elements including residual stress and distortions predicted by welding simulation. The other two are analytical methods including an approximate analytical method formulated by Gordo *et al.* (1993), and the IACS (2009) Common Structural Rules for Bulk Carriers. For the method of Gordo *et al.* (1993), the tensile residual stress block parameter η, was taken as 3.75.

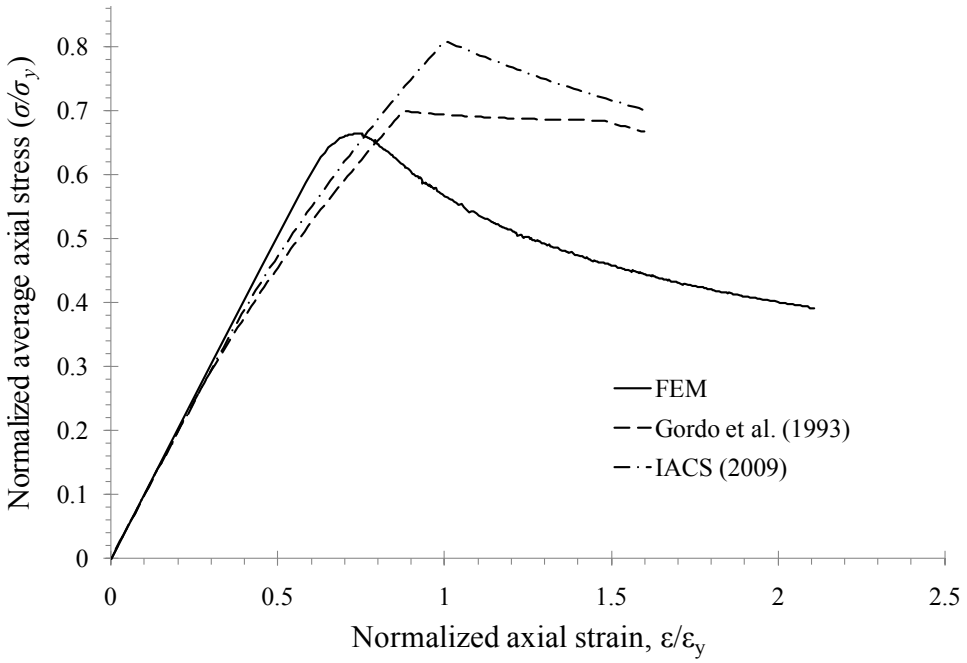

Figure 7.21, Load-shortening curves from numerical and analytical methods

The comparison of load-shortening curves obtained using respective methods is presented in Figure 7.21. Two analytical methods yield load-shortening curves that are less stiff than that derived from the finite element model. Of the two analytical methods, the IACS (2009) curve is slightly stiffer than the curve of Gordo *et al.* (1993). This is due to the difference in plate effective width used in the two methods. IACS uses the U.S. Navy plate strength (Eqn. 7.12) equation which gives a higher effective width than the expression used by Gordo *et al.* (1993) (Eqn. 7.13).

$$\frac{b_e}{b} = \frac{2.25}{\beta_0} - \frac{1.25}{\beta_0^2} \tag{7.12}$$

$$\frac{b_e}{b} = \frac{2}{\beta_0} - \frac{1}{\beta_0^2} \tag{7.13}$$

Compared with the numerical model, the IACS common structural rules overestimate the stiffened plate ultimate strength by 23.4%, and the method proposed by Gordo *et al.* (1993) gives an ultimate strength 6.4% greater than the numerical model. The discrepancy among ultimate strength values predicted by the different methods may be a consequence of the level of compressive residual stress in the plate that is assumed in the analytical methods. In the IACS (2009) method, inelastic effects due to early yielding are accounted for using the Johnson-Ostenfeld correction, which is based on empirical data and so only accounts for residual stresses within the range of those present in the plates from which the empirical relation was derived. In the method of Gordo *et al.* (1993), the value of η, was taken as 3.75, which is considered appropriate for most naval ships (Akhras *et al.*, 1998). However, from the welding simulation, the compressive residual

stress in the plate was approximately 108 MPa, giving η = 6.7, which is considerably higher than typical values. This could be a consequence of the relatively close stiffener spacing compared with full-scale ship structures, meaning that the tensile stress block parameter η, also depends on this spacing. Considering the important influence that the level of compressive residual stress may have on the ultimate strength of stiffened plates, this relationship should be investigated further in future research.

7.7.2 Effect of Residual Stress

The effect of welding-induced residual stresses is evaluated using finite element load-shortening curves obtained with and without residual stress. Figure 7.22 shows that residual stresses decreased load-carrying capacity and smoothed the load-shortening curve as the ultimate load was approached. The reduction in ultimate capacity of the stiffened plate as a result of residual stress is around 11%. This is a result of premature yielding under the sum of residual stress and stress due to the applied load, causing a reduction in the effective cross-section and stiffness.

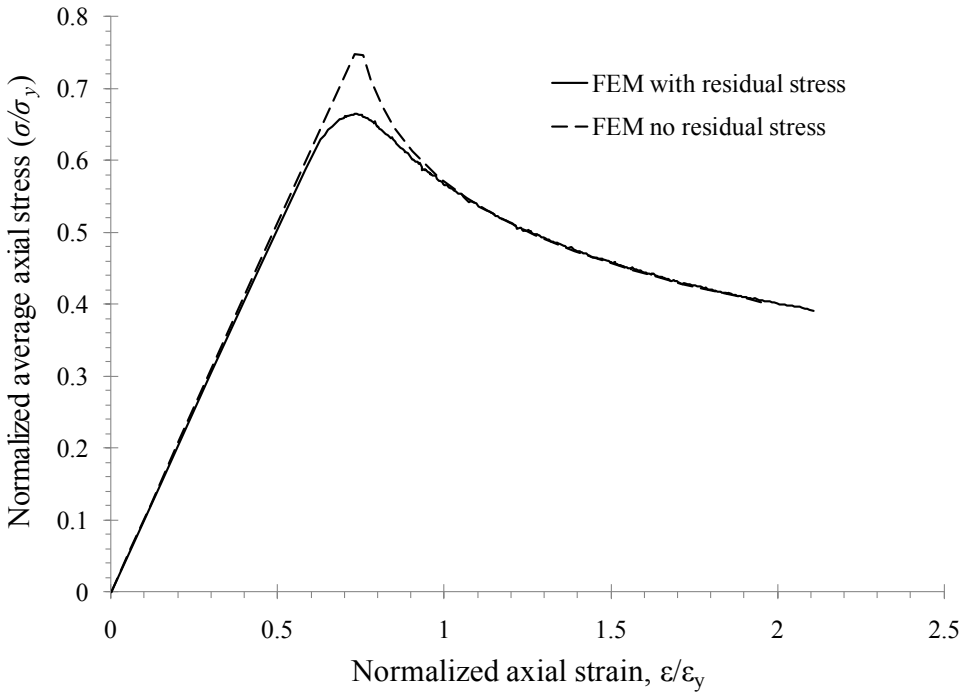

Figure 7.22, Effect of residual stress on stiffened plate behaviour

7.7.3 Effect of Shakedown

Figure 7.23 shows that shakedown of residual stress and the associated change in distortion due to a single load cycle of an average axial stress of $0.25\sigma_y$ had negligible effect on the behaviour of the stiffened plate under axial compression. Although this contradicts previous findings (Gannon *et al.*, 2011), it should be noted that the stiffened plate finite element model considered presently failed by flexural buckling of the stiffened plate toward the plate accompanied by lateral buckilng of the stiffener. Buckling of the plate did not occur, and for this reason, the change in compressive residual stress in the plate due to shakedown had little effect on the ultimate strength of the stiffened plate. Considering that failure mode resulted in compression in the stiffener flange, it is not

unexpected that the small change in compressive residual stress in the stiffener flange due to shakedown, shown in Figure 7.18, had little influence on the ultimate load of the stiffened plate. This important result indicates that although shakedown may increase stiffened plate ultimate strength in some cases, the potential increase in strength is dependent on the failure mode of the stiffened plate.

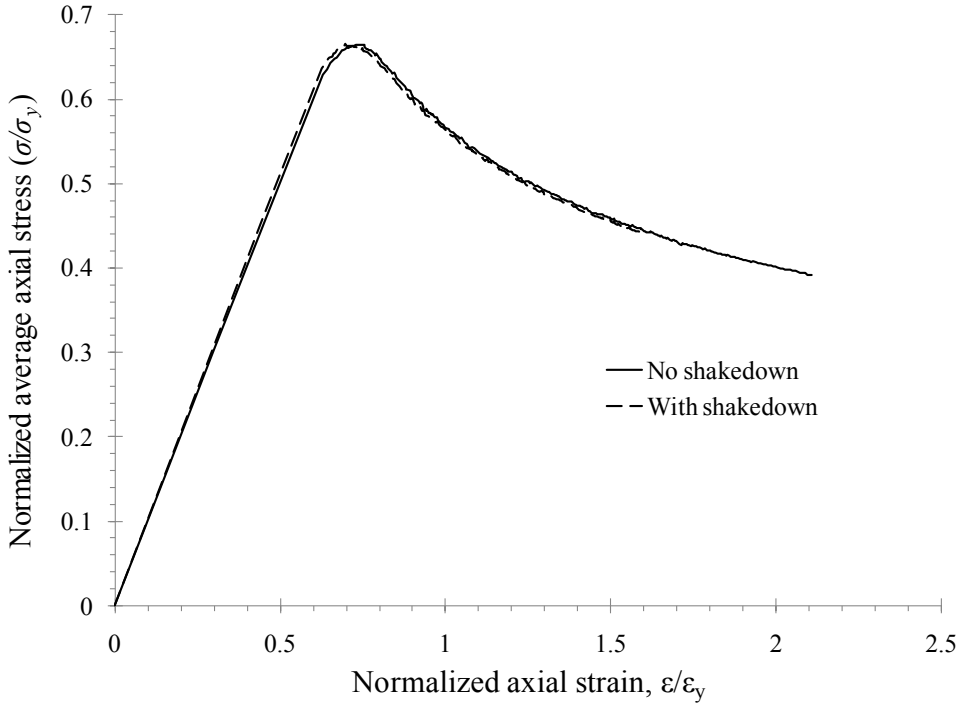

Figure 7.23, Effect of shakedown on load-shortening curve

7.7.4 Effect of Distortion

Load-shortening curves generated using shell element models with slight, average and severe distortions (Table 7.1, Eqns. 7.2) are shown in Figure 7.24. For each level of distortion, the analysis was performed with the stiffener vertical distortion δ_0, being toward the plate (P) as well as toward the stiffener (S). Each model included longitudinal

residual stresses predicted by the welding simulation, from the mid-plane of the plate components at a cross-section located 240 mm along the z-axis. Residual stresses were mapped directly onto the integration points of the shell elements using a user-defined subroutine.

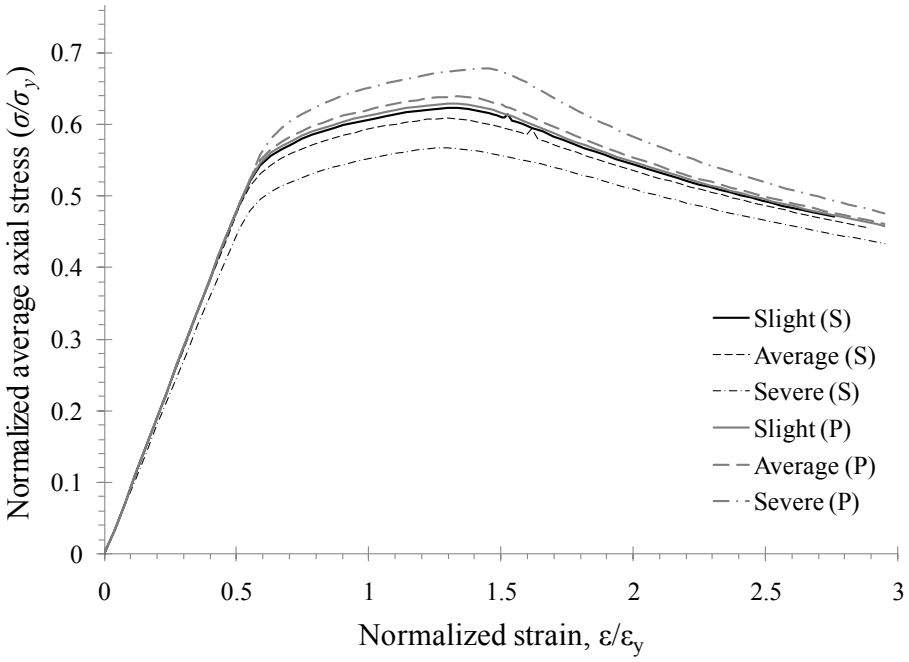

Figure 7.24, Load-shortening curves for various levels of distortion

As the level of distortion increased from slight to average with δ_0 being toward the stiffener, the ultimate strength was reduced by 3.3%, whereas severe imperfections reduced the ultimate strength by 10% compared with slight imperfections. Where the vertical distortion of the stiffened plate δ_0, was toward the plate, the ultimate strength increased as the level of distortion increased. The increases in ultimate strength from slight to average and slight to severe distortions were 1.6% and 7.8%, respectively. The increase in ultimate strength as distortion toward the plate increased can be explained

using the following rationale. The distortion of the plate results in an effective eccentricity of the applied end load relative to the centroid of the stiffened plate along its length, which in turn results in a bending moment. This moment introduced a tensile stress in the plate and this stress became larger as the magnitude of δ_0, increased. As a result, plate compressive stress was relieved by the bending stresses within the plate and this effect became increasingly pronounced as the distortion increased. The effective width of the plate and thus the ultimate capacity became increasingly greater with the increase in the distortion. In the case where the distortion is toward the stiffener, the direction of moment as a result of distortion was reversed and the resulting stress in the plate was compressive. Combined with compressive stress caused by the axial load, this decreased the effective width of the plate and thus the ultimate capacity.

7.8 Results of Hull Girder Ultimate Strength

7.8.1 Effect of Residual Stress

A hull girder ultimate strength analysis was carried out using Smith's method incorporating load-shortening curves generated using the stiffened plate finite element model both with and without welding-induced residual stress. Figure 7.25 shows the resulting moment-curvature relationships for each case. The presence of residual stress resulted in earlier onset of nonlinear behaviour and a decrease in the ultimate moment capacity when compared with the case with no residual stress. The ultimate moment capacity with residual stress was 1206 kNm, which represented a 3.3% reduction from

the moment capacity of 1245 kNm obtained without residual stress. The change in slope of the curve of no residual stress, at a curvature of approximately 3.1 x 10^{-6} coincides with the peak of the load-shortening curve for the stiffened plate with no residual stress (Figure 7.22). This is followed by a slight decrease in moment capacity as the neutral axis shifts toward the bottom. This shift in the neutral axis is a result of the reduction in load-carrying capacity of the deck elements after they have reached their ultimate load-carrying capacity, while the bottom elements in tension are able to resist additional load. Failure occurs once the bottom elements have failed by gross-section yielding.

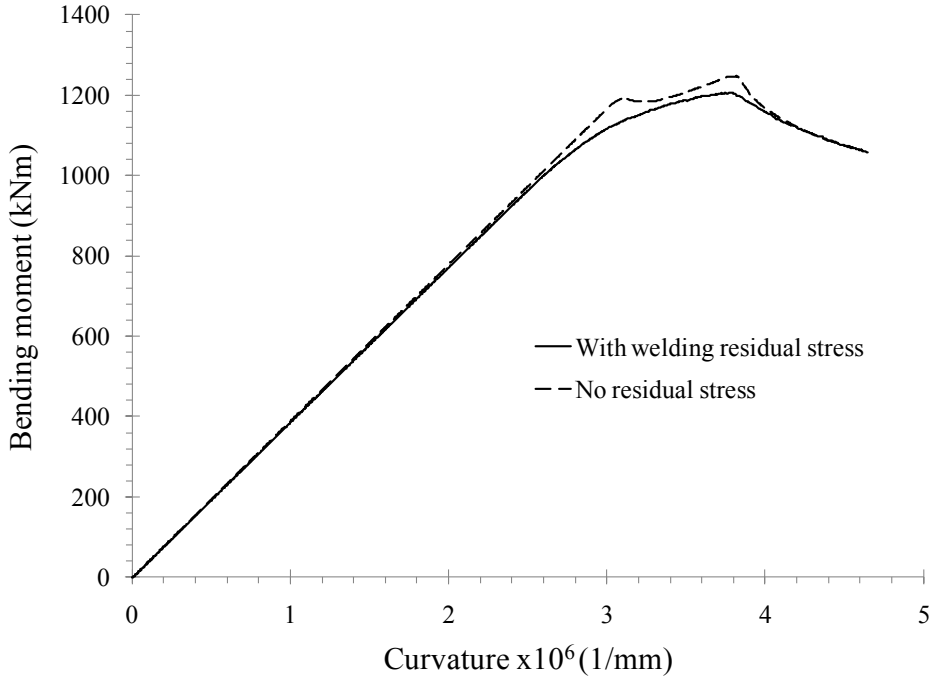

Figure 7.25, Effect of residual stress on hull girder behaviour

7.8.2 Effect of Distortion

Figure 7.26 shows moment-curvature curves calculated by Smith's method using load-shortening curves from shell element models with various levels of distortion, and including longitudinal residual stresses as determined by welding simulation. Consistent with the effect of distortion shown in load-shortening behaviour, where vertical distortion along the axis of the stiffener δ_0, was toward the stiffener, the change from slight to average and slight to severe imperfections reduced the moment capacity of the hull girder by 1.6% and 6%, respectively. For the case of vertical distortion toward the plate, the ultimate moment capacity increased as distortion increased from slight to average and slight to severe by 1% and 5.2%, respectively. These results emphasize the importance of controlling distortion throughout the shipbuilding process in that the load-carrying capacity of the structure may be unnecessarily diminished if welding sequences and heat inputs are not optimized to minimize the effects of distortion. In the case of the current tee-stiffened plate for example, if specified welding procedures cause distortion toward the plate rather than toward the stiffener, then an increase in ultimate strength may be realized.

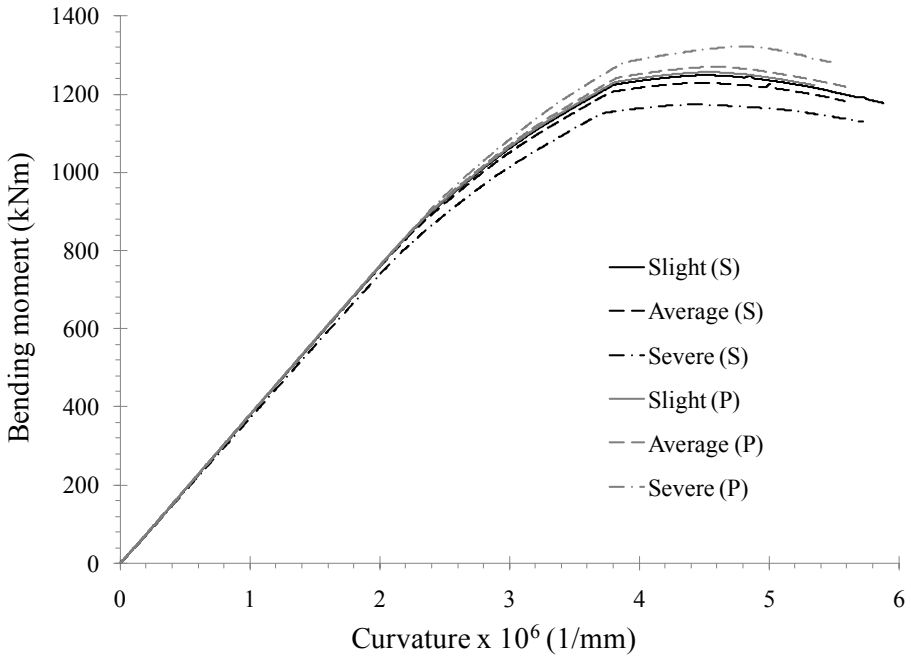

Figure 7.26, Effect of distortion on hull girder behaviour

7.8.3 Shakedown

Considering that there was little difference in the load-shortening curves shown in Figure 7.23 before and after shakedown, there would also be a negligible change in the hull girder ultimate moment capacity as a result of shakedown. As mentioned previously, Dowling and Frieze (Dowling & Frieze, 1977) found that there is little difference in stiffened plate ultimate strength for compressive residual stress in the plate above 10% of the yield stress. This explains the negligible effects of shakedown in the present case considering that the compressive residual stresses in the plate were significantly higher than 10% of the yield stress both before and after shakedown. This is an important result because it shows that in some cases, it may be un-conservative to assume in-service loads reduce residual stress to the point that it no longer affects ultimate strength. In the present

case for example, neglecting residual stress would result in overestimates of stiffened plate and hull girder ultimate strength by 11% and 3.3%, respectively.

7.8.4 Comparison with Analytical Methods

Load-shortening curves generated using the solid element finite element model, and the analytical methods provided by Gordo *et al.* (1993) and IACS (2009), were used in a Smith's method ultimate strength analysis of the box girder tested by Akhras *et al.* (1998). The moment-curvature curves from these analyses are compared in Figure 7.27, and ultimate moment capacities are summarized in Table 7.2.

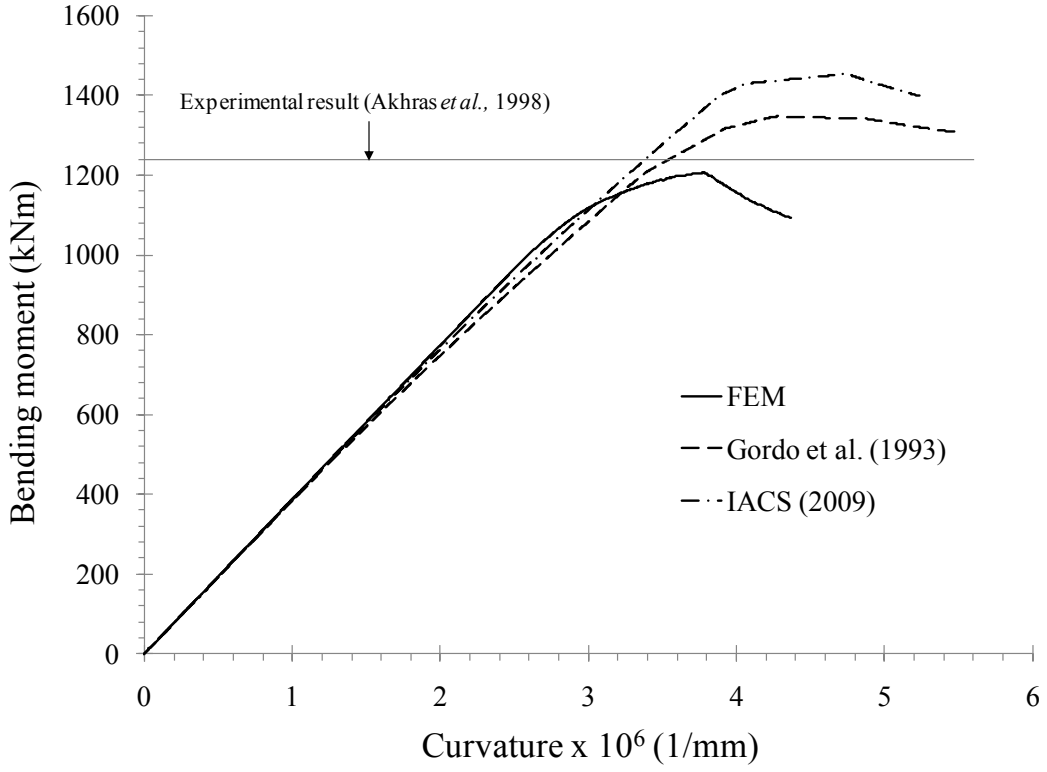

Figure 7.27, Comparison of hull girder behaviour from different analysis methods

Table 7.2, Ultimate bending moment comparison

Method	Ultimate moment (kNm)	Difference from exp. (%)
Experiment (Akhras, 1998)	1238	-
FEM	1205	-2.7
Gordo *et al.* (1998)	1345	8.6
IACS (2009)	1452	17.3

The ultimate moment capacity calculated using finite element load-shortening curves including residual stress and distortion was in good agreement with the experimentally measured value. Using load-shortening curves calculated by the analytical methods of Gordo *et al.* (1993), and IACS (2009), the ultimate strength was overestimated. This may be partly due to the fact that the dimensions of the test specimen were not full-scale and as a result, welding stresses were higher than those that might exist in a full-scale ship hull. The IACS method in particular, is not well suited to dealing with this situation because residual stress and distortion are accounted for implicitly in the load-shortening curve formulations. Consequently, their values cannot be changed in situations where the hull girder scantlings and welding conditions do not fall within the range of those used to derive the empirical effective width expressions in the IACS rules. Although residual stresses and distortions may reduce the ultimate moment capacity of a hull girder by as much as 3% and 6%, respectively, the IACS method leads to a value of ultimate strength outside the bounds of these two sources of uncertainty. This overestimate of ultimate strength may lead to the structural design of unsafe hull girders. Furthermore, since the scantlings of the tee-stiffened plates in the box girder were all the same, all of the

stiffened plates in the compression flange reached their ultimate load at the same time. This indicates that in the present case, the overestimate of ultimate strength using the IACS method is not a result of the IACS overestimate of post-ultimate strength of stiffened plates in the load-shortening curves, demonstrated in Chapters 4 and 5. Therefore, the overestimate in hull girder ultimate strength in this particular case is attributed solely to the difference in stiffened plate ultimate strength calculated using the IACS load-shortening curves and by finite element analysis.

7.9 Conclusions

The finite element method was used to simulate welding of a stiffened plate, giving the complete three-dimensional residual stress and distortion fields. These imperfections were included in an ultimate strength analysis of an experimental box girder test specimen. Results were compared with an approximate analytical method from literature and with the IACS common structural rules. The effects of residual stress, distortion and shakedown, on both the load-shortening behaviour of stiffened plates and the overall hull girder ultimate moment capacity were also investigated. The results of the study are summarized in the following.

1. Residual stresses reduced the ultimate strength of the stiffened plate by 11% with a consequent reduction in hull girder ultimate moment of 3.3%.
2. A single applied stress cycle of $0.25\sigma_y$ caused reductions in tensile and compressive residual stress of 18% and 11%, respectively. The change in residual stress had little effect on the load-shortening behavior of the stiffened plate and

thus did not affect the hull girder ultimate strength. It is noted that the influence of residual stress shakedown on stiffened plate ultimate strength appears to depend on the failure mode, and so should not be relied upon in design of stiffened plates.

3. The ultimate strength of the box girder determined using a load-shortening curve generated by finite element analysis, and using residual stress and distortion predicted by welding simulation, was within 2.7% of the experimentally measured value.
4. Load-shortening curves generated by analytical methods resulted in overestimates of the box girder ultimate strength. In particular, the methods prescribed in the IACS common structural rules resulted in an ultimate moment capacity 17% higher than the experimental value. This indicates that the current rules used for ship structural design may, in some cases, lead to overestimates of the ultimate longitudinal bending moment capacity of ship hulls.

Chapter 8 - Conclusions

8.1 General

A review of literature on the calculation of ship hull ultimate strength showed that welding-induced residual stress and distortion have the potential to reduce the maximum longitudinal bending moment that the hull girder can withstand. However; there is some uncertainty in the magnitude of this reduction, which may be a result of differing assumptions and simplifications made with regard to the magnitude and distribution of welding-induced residual stress and distortion fields in ship structures.

In the current research, the complex distribution of welding-induced residual stress and distortion in stiffened plates was determined by simulating the welding process through nonlinear finite element analysis. The products of this simulation were the complete, three-dimensional residual stress and distortion fields caused by plastic deformation and uneven cooling during welding. The first application of the welding simulation was to determine to what extent the sequence of welding affects residual stress and distortion in stiffened plates. The welding simulation also facilitated the inclusion of complete, three-dimensional residual stress and distortion fields in stiffened plate ultimate strength analyses; the end result being load-shortening curves describing the behaviour of stiffened plates under axial compressive load.

The stiffened plate models discussed above were used to quantify the reduction in residual stress and distortion due to in-service loads, commonly referred to as shakedown.

The shakedown analysis provided useful insight on the validity of an assumption sometimes made in hull girder ultimate strength analysis, that residual stresses are partially or completely relieved by wave-induced longitudinal bending.

The analysis of welding-induced stress and distortion, and stiffened plate strength and behaviour culminated in a hull girder ultimate strength analysis to evaluate the potential effects of those imperfections on the ultimate longitudinal bending capacity of a ship hull. Results of both the stiffened plate strength analysis and the hull girder ultimate strength analysis were compared with values determined using analytical methods prescribed in the IACS common structural rules, and using an approximate analytical method from a related journal paper. Conclusions drawn from the results of this research are summarized in the following.

8.2 Residual Stress and Distortion

- Longitudinal residual stress distributions predicted by numerical modelling techniques were similar in magnitude and distribution to measured and idealized values reported in the literature. Maximum tensile residual stresses exist in the plate near the weld with a magnitude equal to the material yield stress. These are balanced by nearly uniform compressive residual stresses across the rest of the plate.
- The sequence of welding does not have a significant influence on the distribution of residual stress in flat-bar stiffened plates, however it may affect peak values.

- Two welding sequences, identified as A and C in Chapter 3, caused notably higher compressive residual stresses in the plate than welding sequences B and D. This indicates that the welding sequence has the potential to influence plate effectiveness under axial compressive load.
- Considering both residual stress and distortion, welding sequence D produced the lowest residual stress and distortion, and was identified as the preferred welding sequence for flat-bar stiffened plates.
- The magnitude and direction of longitudinal, column-type distortion depend to some degree on column slenderness. Where plate slenderness is the same, the direction of longitudinal distortion along the axis of the stiffener changes from being towards the plate to towards the stiffener as column slenderness decreases.
- Distortions predicted by the welding simulation were generally lower than values typically used in design and analysis of stiffened plates. Column-type vertical distortions of the stiffeners were slight, while plate distortions were closer to average, with a few cases having above average distortions. It should be noted that the definitions of the different levels of distortion are based on data from ships that were built over 35 years ago, when welding and handling practices were not as well controlled as they are with contemporary equipment and procedures. Moreover, out-of-straightness caused by hot rolling and other fabrication steps aside from welding the stiffener to the plate were not considered in this study.

8.3 Shakedown

- Welding-induced residual stresses in stiffened plates may be significantly reduced by application of axial loads. For applied axial stresses of $0.25\sigma_y$ and $0.5\sigma_y$, longitudinal residual stresses were decreased by around 20% and 40%, respectively.
- For the level of compressive residual stress typically found in ship hull stiffened plating, the reduction of residual stress due to shakedown only occurs during the tensile part of the load cycle.
- The magnitude of the residual stress reduction following shakedown depends only on the magnitude of the highest load cycle, and not the number of cycles applied.
- Although shakedown may reduce residual stresses in stiffened plates, this does not always lead to an increase in load-carrying capacity of the stiffened plate or of the hull girder. This is because stiffened plates may fail in a mode that does not take advantage of the decrease in compressive residual stress due to shakedown. Furthermore, reducing or neglecting residual stresses in a stiffened plate analysis under the assumption that they are relieved by in-service loads may result in overestimates of stiffened plate and consequently hull girder ultimate strength.

8.4 Strength and Behaviour of Stiffened Plates

- The maximum reduction in ultimate strength of flat-bar stiffened plates due to welding-induced residual stress was 16.5%. In angle and tee-stiffened plates,

residual stresses caused maximum ultimate strength reductions of 15.0% and 13.5%, respectively.

- The ultimate strength of stiffened plates decreases with increasing plate slenderness, β_0.
- For the stiffened plate geometries considered in this research, no clear relationship between ultimate strength and column slenderness λ, was observed.
- The ultimate strengths of flat-bar stiffened plates calculated by the IACS common structural rules were within 5% of those determined by finite element analysis. The IACS common structural rules generally overestimated ultimate strength, compared with the finite element models.
- The ultimate strength of angle and tee-stiffened plates predicted by the IACS common structural rules agrees well with values calculated by finite element analysis in most cases, however there were a few cases where the difference between the two was greater than 10%.
- In comparison to load-shortening curves calculated by finite element analysis, the IACS common structural rules overestimate the capacity of stiffened plates in the post-collapse region by a significant margin.

8.5 Hull Girder Ultimate Strength

- Residual stresses and distortions were found to reduce hull girder ultimate strength by 3.3% and 6%, respectively.

- An ultimate strength analysis of a box girder using a load-shortening curve generated by finite element analysis, including residual stress and distortion calculated by welding simulation, predicted the ultimate moment capacity of the box girder within 2.7% of the experimentally measured value. This shows that using the finite element method to predict residual stress and distortion in stiffened plates by simulating the welding process is a valuable means of reducing uncertainty in hull girder strength analysis. Although it is complex and time-consuming, as high speed computing technology improves in the future, this type of analysis may facilitate more reliable and efficient ship structural design.
- The IACS analytical method for generating load-shortening curves for ultimate strength analysis may lead to significant overestimates of hull girder ultimate moment capacity.

8.6 Recommendations for Future Research

Welding simulation by finite element modeling allows various aspects of the ship fabrication process to be analyzed without the need of costly physical parametric studies. The following identifies a few areas where welding simulation could be used to improve the efficiency of the shipbuilding process.

- The effects of welding conditions such as heat input and welding sequence on residual stress and distortion might be further investigated to optimize these parameters for various stiffened plate geometries.

- Tack welds influence the distortion pattern in stiffened plates. The effects of tack weld spacing and sequence on distortion could be investigated.
- Pre and post-heating times and temperatures could be studied to determine their influence on the final state of residual stress and distortion in stiffened plates.
- The effects of failure mode interaction on the post-ultimate load-carrying capacity of stiffened plates, and consequently on hull girder ultimate strength should be investigated.
- Numerical models and analytical methods are often validated by comparison of results with experiments on scale models of hull girders. The results of this research indicate that residual stresses and distortion in scale models may not be representative of imperfections in full-scale ship structures. Although it would be expensive, an experimental test of a test section with full-scale scantlings would be valuable in ensuring that validation of ultimate strength analysis methods by comparison with reduced-scale hull girder test results is legitimate.
- The welding simulation technique may also be used to simulate weld overlay repair, which is commonly performed on submarine pressure hulls to reclaim material lost due to corrosion. This may be useful in predicting the levels of residual stress and distortion induced by welding so that their effects on the structural capacity of the pressure hull may be evaluated.

References

Abdel-Karim, M. (2005). Shakedown of complex structures according to various hardening rules. *International Journal of Pressure Vessels and Piping , 82*, 427-458.

Adamchack, J. C. (1984). An approximate method for estimating the collapse of a ship's hull in preliminary design. *SNAME Ship Structure Symposium*, (pp. 37-61).

Akhras, G., Gibson, S., Yang, S. & Morchat, R. (1998). Ultimate strength of a box girder simulating the hull of a ship. *Canadian Journal of Civil Engineering, 25,* 829-843.

Allum, C., & Quintino, L. (1985). Control of fusion characteristics in pulsed current MIG welding, Part 2 - simple model of fusion characteristics. *Metal Construction , 17* (5), 314r-317r.

Andersen, L. F. (2000). Residual stresses and deformations in steel structures. *PhD Thesis* . Denmark: Department of Naval Architecture and Offshore Engineering, Technical University of Denmark.

Antoniou, A. C. (1980). On the maximum deflection of plating in newly built ships. *Journal of Ship Research , 24* (1), 31-39.

Bhatti, M. A. (2005). *Fundamental Finite Element Analysis and Applications.* Hoboken, New Jersey: John Wiley & Sons, Inc.

Billingsley, D. W. (1980). Hull girder response to extreme bending moments. *5th Star Symposium* (pp. 51-63). SNAME.

Caldwell, J. B. (1965). Ultimate longitudinal strength. *Trans. RINA* (107), 411-430.

Canadian Standards Association (2003). CSA W59-03, Welded steel construction (metal arc welding).

Carlsen, C. A. (1977). Simplified collapse analysis of stiffened plates. *Norwegian Maritime Research , 4*, 20-36.

Carlsen, C. A., & Czujko, J. (1978). The specification o post-welding distortion tolerance for stiffened plates in compression. *The Structural Engineer , 53(A)* (5), 133-141.

Chrisfield, M. A. (1975). Full-range analysis of steel plates and stiffened plating under uniaxial compression. *Proceedings of the Institute of Civil Engineers , 59* (2), 595-624.

Cronje, M. (2005). *Finite element modelling of shielded metal arc welding.* Department of Mechanical Engineering. Matieland South Africa: Stellenbosch University.

Cui, W., Yongjun, W., & Pedersen, P. T. (2002). Strength of ship plates under combined loading. *Marine Structures , 15* (1), 75-97.

Deng, D. (2009). FEM prediction of welding residual stress and distortion in carbon steel considering phase transformation effects. *Materials and Design , 30*, 359-366.

Deng, D., & Murakawa, H. (2008). Prediction of welding distortion and residual stress in a thin plate butt-welded joint. *Computational Materials Science , 43*, 353-365.

Deng, D., Liang, W., & Murakawa, H. (2007). Determination of welding deformation in fillet-welded joint by means of numerical simulation and comparison with experimental results. *Journal of Materials Processiing Technology , 183*, 219-225.

Dow, R. S. (1991). Testing and analysis of a 1/3 scale welded steel frigate model. In C. S. Smith, & R. S. Dow (Ed.), *Advances in Marine Structures 2*, (pp. 749-773).

Dow, R., Hugill, R., Clark, J., & Smith, C. (1981). Evaluation of ultimate ship hull strength. *SNAME Extreme Loads and Response Symposium.* Arlington VA: SNAME.

Dowling, J. P., Chatterjee, S., Frieze, P. A., & Moolani, F. M. (1973). Experimental and predicted collapse behaviour of rectangular steel box girders. *Proceedings of the International Conference on Steel Box Girder Bridges.* London.

Dwight, J. B., & Little, G. H. (1976). Stiffened steel compression flanges - a simpler approach. *The Structural Engineer , 54* (12), 501-509.

Dwight, J. B., & Ratcliffe, A. T. (1969). The strength of thin plates in compression. *Thin-Walled Structures* .

Eager, T. W., & Tsai, N. S. (1983). Temperature fields produced by traveling distributed heat sources. *Welding Journal , 62* (12), 346s-355s.

Fanous, I. F., Younan, M. Y., & Wifi, A. S. (2003). 3D Finite element modelling of the welding process using element birth and element movement techniques. *ASME Journal of Pressure Vessel Technology , 125* (2), 144-150.

Fanous, I. F., Younan, M. Y., & Wifi, A. S. (2005). Introduction of the element interaction technique for welding analysis and simulation. *ASME Journal of Pressure Vessel Technology , 127* (4), 487-494.

Fanous, I. F., Younan, M. Y., & Wifi, A. S. (2003). Study of the effect of boundary conditions on residual stresses in welding using element birth and element movement techniques. *ASME Journal of Pressure Vessel Technology , 125* (4), 432-439.

Faulkner, D. (1975). A review of effective plating for use in the analysis of stiffened plating in bending and compression. *Journal of Ship Research , 19* (1), 1-17.

Faulkner, D. (1977). Compression tests on welded eccentrically stiffened plate panels. (P. J. Dowling, Ed.) *Steel Plated Structures* , 130-139.

Faulkner, D., Adamchack, J. C., Snyder, J. G., & Vetter, M. F. (1973). Synthesis of welded grillages to withstand compression and normal loads. *Computers and Structures , 6*, 221-246.

Frankland, J. M. (1940). *The strength of ship plating under edge compression.*

Friedman, E. (1975). Thermomechanical analyssi of the welding process usign the finite element method. *ASME Journal of Pressure Vessel Technology , 97* (3), 206-213.

Fujikubo, M., & Kaeding, P. (2000). ISUM rectancular plate element with new lateral shape function (1st report) - Longitudinal and transverse thrust. *Japan Society of Naval Architects , 187*, 479-487.

Fujikubo, M., & Kaeding, P. (2000). ISUM rectangular plate element with new lateral shape function (2nd report) - Stiffened plates under biaxial thrust. *Japan Society of Naval Architects , 188*, 507-515.

Fujita, Y., Takeshi, Y., Kitamura, M., & Nomoto, T. (1972). *Welding stresses with special reference to cracking. IIW Doc X-655-72.*

Galambos, T. V. (1998). *Guide to stability design criteria for metal structures* (Vol. 5). New York: John Wiley.

Gannon, L. G., Liu, Y., Pegg, N. G., & Smith, M. J. (2011). Effect of 3D welding-induced residual stress and distortion fields on strength and behaviour of flat-bar stiffened plates. *Under review, Marine Structures* .

Gannon, L. G., Liu, Y., Pegg, N. G., & Smith, M. J. (2010). Effect of welding sequence on residual stress and distortion in flat-bar stiffened plates. *Marine Structures*, 23(3), 385-404.

Gannon, L. G., Liu, Y., Pegg, N. G., & Smith, M. J. (2011). Shakedown of welding-induced residual stress and effect on stiffened plate strength and behaviour. *Proceedings, MARSTRUCT 2011 3rd International Conference on Marine Structures.* Hamburg, Germany: A.A. Balkema Publishers.

Goldak, J., Chakravarti, A., & Bibby, M. (1984). A new finite element model for welding heat sources. *Metallurgical Transactions B , 15B*, 229-305.

Gordo, J. M., & Guedes Soares, C. (1993). *Approximate load shortening curves for stiffened plates under uniaxial comression.* Technical University of Lisbon, Department of Naval Architecture and Ocean Engineering. Lisbon: Integrity of Offshore Structures.

Gordo, J. M., & Guedes Soares, C. (1996). Approximate method to evaluate the hull girder collapse strength. *Marine Structures , 9*, 449-470.

Gordo, J. M., Guedes Soares, C., & Faulkner, D. (1996). Approximate assessment of the ultimate strength of the hull girder. *Journal of Constructional Steel Research , 40* (1), 60-69.

Guedes Soares, C. (1988). Design equation for compressive strength of unstiffened plate elements with initial imperfections. *Journal of Constructional Steel Research, 9*, 287-310.

Guedes Soares, C., & Gordo, J. M. (1997). Design methods for stiffened plates under predominantly uniaxial compression. *Marine Structures , 10*, 465-497.

Hansen, A. M. (1996). Strength of midship sections. *Marine Structures , 9*, 471-494.

Hibbitt, H., & Marcal, P. (1973). A numerical thermo-mechanical model for the welding and subsequent loading of a fabricated structure. *Computers and Structures, 97* (3), 206-213.

Horne, M. R., Montague, P., & Narayanan, R. (1977). Influence of strength of compression panels of stiffener section, spacing and welded connection. *Proceedings of the Institute of Civil Engineers, 63* (2), 1-20.

Hughes, O. F. (1983). *Ship Structural Design.* Wiley-Interscience.

IACS. (2009). *Common structural rules for bulk carriers.* London: International Association of Classification Societies. (IACS, Common structural rules for double hull oil tankers, 2009)

ISSC. (1979). *Report by Committee II.2 on nonlinear structural response.* Paris: Institut de Recherches de la Construction Navale.

Iwaki, T., & Masubuchi, K. (1971). Thermo-elastic analysis of metals with temperature dependant material properties. *Journal of the Society of Naval Architects of Japan , 130*, 195-204.

John, W. G. (1874). The strength of iron ships. *Transactions, RINA* .

Karlsson, R., & Josefson, B. (1990). Three-dimensional finite elemnt analysis of temperatures and stresses in a single-pass butt-welded pip. *ASME Journal of Pressure Vessel Technology , 112*, 76-84.

Kenno, S. Y., Das, S., Kennedy, J. B., Rogge, R. B., & Gharghouri, M. (2010). Residual stress distributions in ship hull specimens. *Marine Structures* , 263-273.

Kmiecik, M., Jastrzebski, T., & Kuzniar, J. (1995). Statistics of ship plating distortions. *Marine Structures , 8* (2), 119-132.

Krutz, G. W., & Segerlind, L. J. (1978). Finite element analysis of welded structures. *Welding Journal , 57* (7), 211s-216s.

Kutt, L. M., Piaszczyk, C. M., Chen, Y. K., & Lin, D. (1985). Evaluation of the longitudinal ultimate strength of various ship hull configurations. *Transactions, SNAME , 93*, 33-53.

Latrou, N., Thevenet, D., & Cognard, J. Y. (2005). A novel crack initiation approach for naval welded joints. *Oceans 2005 - Europe, Proc. IEEE. 2*, pp. 20-23. Brest France: IEEE.

Lee, C. H., & Chang, K. H. (2007). Numerical analyssi of residual stresses of similar or dissimilar steel weldments under superimposed tensile loads. *Computational Materials Science , 40*, 548-556.

Liangbi, L., Moan, T., & Zhang, B. (2007). Residual stress shakedown in typical weld joints and its effect on fatigue of FPSOs. *Proceedings of the International Conference on Offshore Mechanics and Arctic Engineering - OMAE*, (pp. 193-201). San Diego, California.

Lindgren, L. E. (2001). Finite element modeling and simulation of welding part 1: Increased complexity. *Journal of Thermal Stresses , 24* (2), 141-192.

Lindgren, L. E. (2001). Finite element modeling and simulation of welding part 2: Improved material modeling. *Journal of Thermal Stresses , 24* (33), 195-231.

Lindgren, L. E. (2001). Finite element modeling and simulation of welding part 3: Efficiency and integration. *Journal of Thermal Stresses , 24* (44), 305-334.

Lindgren, L. E. (2001). Finite element modelling and simulation of welding part 1: Increased complexity. *Journal of Thermal Stresses , 24* (2), 141-192.

Lindgren, L., & Karlsson, L. (1988). Deformations and stresses in welding of shell structures. *International Journal for Numerical Methods in Engineering , 25*, 635-55.

Mahapatra, M., Datta, G., & Pradhan, B. (2006). Three-dimensional finite element analysis to predict the effects fo shielded metal arc welding process parameters on temperature distributions and weldment zones in butt and one-sided fillet welds. *Proceedings of the Institute of Mechanical Engineers Part B: Journal of Engineering Manufacture*, *220*, pp. 837-845.

Mansour, A., Yang, J. M., & Thayamballi, A. (1990). An experimental investigation of ship hull ultimate strength. *Transactions, SNAME* .

Michaleris, P., & DeBiccari, A. (1997). Prediction of welding distortion. *Welding Research Supplement to the Welding Journal* , 172-181.

Moxham, K. G. (1971). *Theoretical prediction of the Strength of welded steel plates in compression.* Cambridge University.

Murray, N. W. (1973). Buckling of stiffened panels laoded axially and in bending. *The Structural Engineer , 51* (8), 285-301.

Nagaraja Rao, N. R., & Tall, L. (1961, October). Residual stresses in welded plates. *Welding Journal* , 468s-480s.

Nagaraja Rao, N. R., Estuar, F. R., & Tall, L. (1964). Residual stresses in welded shapes. *The Welding Journal , 43*, 295s-305s.

Nasstrom, L., Wikander, L., Karlsson, L., Lindgren, L., & Goldak, J. (1992). Combined 3D solid and shell modelling of welding. *IUTAM Symposium on the Mechanical Effects of Welding*, (p. 197).

Nguyen, N. T., Ohta, A., Matsuoaka, K., Suzuki, N., & Maeda, Y. (1999, August). Analytical solutions for transient temperature of semi-infinite body subjected to 3-D moving heat sources. *Welding Journal* , 265s-274s.

Nickerson, J., & Smith, M.J. (2007). *User's manual for the ultimate strength application.* Defence Research and Development Canada - Atlantic: Dartmouth, Nova Scotia. DRDC Atlantic TM 2007-291.

Ohtsubo, H., & Sumi, Y. (2000). Report of special task committee VI.2 - Ultimate hull girder strength. In H. Ohtsubo, & Y. Sumi (Ed.), *Procedings of the 14th International Ship and Offshore Structures Congress.* Nagasaki: ISSC.

Paik, J. K. (1993). *Advanced idealized structural elements considering both ductile collapse and excessive tension deformation.* Technical Report n. PNUNA-SE-30, Pusan National University, Department of Naval Architecture.

Paik, J. K., & Thayamballi, A. K. (2003). A concise introduction to the idealized structural unit method for nonlinear analysis of large plated structures and its application. *Thin-Walled Structures , 41* (4), 329-355.

Paik, J. K., & Thayamballi, A. K. (2006). Some recent developments on ultimate limit state design technology for ships and offshore structures. *Ships and Offshore Structures , 1* (2), 99-116.

Paik, J. K., & Thayamballi, A. K. (2006). Some recent developments on ultimate limit state design technology for ships and offshore structures. *Ships and Offshore Structures , 1* (2), 99-116.

Paik, J. K., & Thayamballi, A. K. (2003). *Ultimate Limit State Design of Steel-Plated Structures.* West Sussex, England: John Wiley & Sons Ltd.

Paik, J. K., Hughes, O. F., Hess, P. E., & Renaud, C. (2005). Ultimate limit state design technology for aluminum multi-hull ship structures. *Transactions, SNAME , 113*, 270-305.

Paik, J. K., Thayamballi, A. K., & Che, J. S. (1996). Ultimate strength of ship hulls under combined vertical bending, horizontal bending and shearing forces. *Transactions, SNAME , 104*, 31-59.

Paley, Z., & Hibbert, P. D. (1975). Computation of temperatures in actual weld designs. *Welding Journal , 54*, 385s-392s.

Pavelic, V., Tanbakuchi, R., Uyehara, O. A., & Myers. (1969). Experimental and computed temperature histories in gas tungsten arc welding of thin plate. *Welding Journal , 48*, 259s-305s.

Rosenthal, D. (1946). The theory of moving heat source and its application to metal transfer. *Transactions, ASME , 43* (11), 849-866.

Rutherford, S. E. (1982). *Stiffened compression panels: The analytical approach.* Loyd's Register. Lloyd's Register.

Rutherford, S. E., & Caldwell, J. B. (1990). Ultimate longitudinal strength of ships: A case study. *Transactions, SNAME , 98*, 441-471.

Rykalin, R. R. (1974). Energy sources for welding. *Welding in the World , 12*, 227-248.

Smith, C. S. (1975). Compressive strength of welded steel ship grillages. *Transactions of RINA* (117), 325-359.

Smith, C. S. (1977). Influence of local compressive failure on ultimate longitudinal strength of a ship's hull. *Proceedings of the first PRADS*, (pp. 73-79). Tokyo.

Smith, C. S. (1986). *Ultimate strength of a ship's hull under biaxial bending.* Admiralty Research Establishment, Dunfermline, Scotland.

Smith, C. S., & Kirkwood, W. (1977). Influence of initial deformations and residual stresses on inelastic flexural buckling of stiffened paltes ans shells. *Steel Plated Structures* (pp. 838-864). London: Crosby Lockwood Staples.

Smith, C. S., Anderson, N., Chapman, J. C., Davidson, P. C., & Dowling, P. J. (1992). Strength of stiffened plating under combined compression and lateral pressure. *Transactions, RINA , 134*, 131-147.

Smith, C. S., Davidson, P. C., Chapman, J. C., & Dowling, P. J. (1988). Strength and stiffness of ships' plating under in-plane compression and tension. *Transactions, RINA , 130*, 277-296.

Smith, M. J. (2008). *Ultimate strength assessment of naval and commercial ships.* Halifax: Defence Research and Development Canada.

Tall, L. (1964). Residual stresses in welded plates - a theoretical study. *Welding Journal Supplement , 43* (1), 10s-23s.

Totten, G., Howes, M., & Inoue, T. (. (2002). *Handbook of Residual Stress nad Deformation of Steel.* ASM International.

Tupper, E. C. (2004). *Introduction to naval architecture* (4th ed.). Elsevier Ltd.

Ueda, Y., & Rashad, S. M. (1984). The idealized structural unit method and its application to deep girder structures. *Computers and Structures , 18* (2), 227-293.

Ueda, Y., & Yamakawa, T. (1971). Analysis of thermal elastic-plastic stress and strain during welding by finite element method. *Japan Welding Society Tranactions , 2* (2), 90-100.

Ueda, Y., & Yamakawa, T. (1971). Mechanical cracking characteristics of cracking of welded joints. *Proceedings of the 1st International Symposium on Precaution of Cracking in Welded Structures Based on Recent Theoretical and Practical Knowledge. IC5.1.* Tokyo: The Japan Welding Society.

Ueda, Y., & Yamakawa, T. (1971). Themal stress analysis of metals with temperature dependent mechanical properties. *Proceedings of the International Conference on Mechanical Behavior of Materials.*

Wells, A. A. (1952). Heat flow in welding. *Welding Journal , 31* (5), 263s-267s.

Westby, O. (1968). *Temperature distribution in the workpiece by welding.* Department of Metallurgy and Metals Working. Trondheim Norway: The Technical University.

Yao, T. (1999). Ultimate longitudinal strength of ship hull girder: Historical review and state of the art. *International Journal of Offshore and Polar Engineering , 9* (1).

Yuan, M. G., & Ueda, Y. (1996). Prediction of residual stresses in T - and I - joints using inherent strains. *Journal of Engineering Materials and Technology* , 229-234.